UNIVERSIDADE FEDERAL DO PARANÁ

SHER ALI

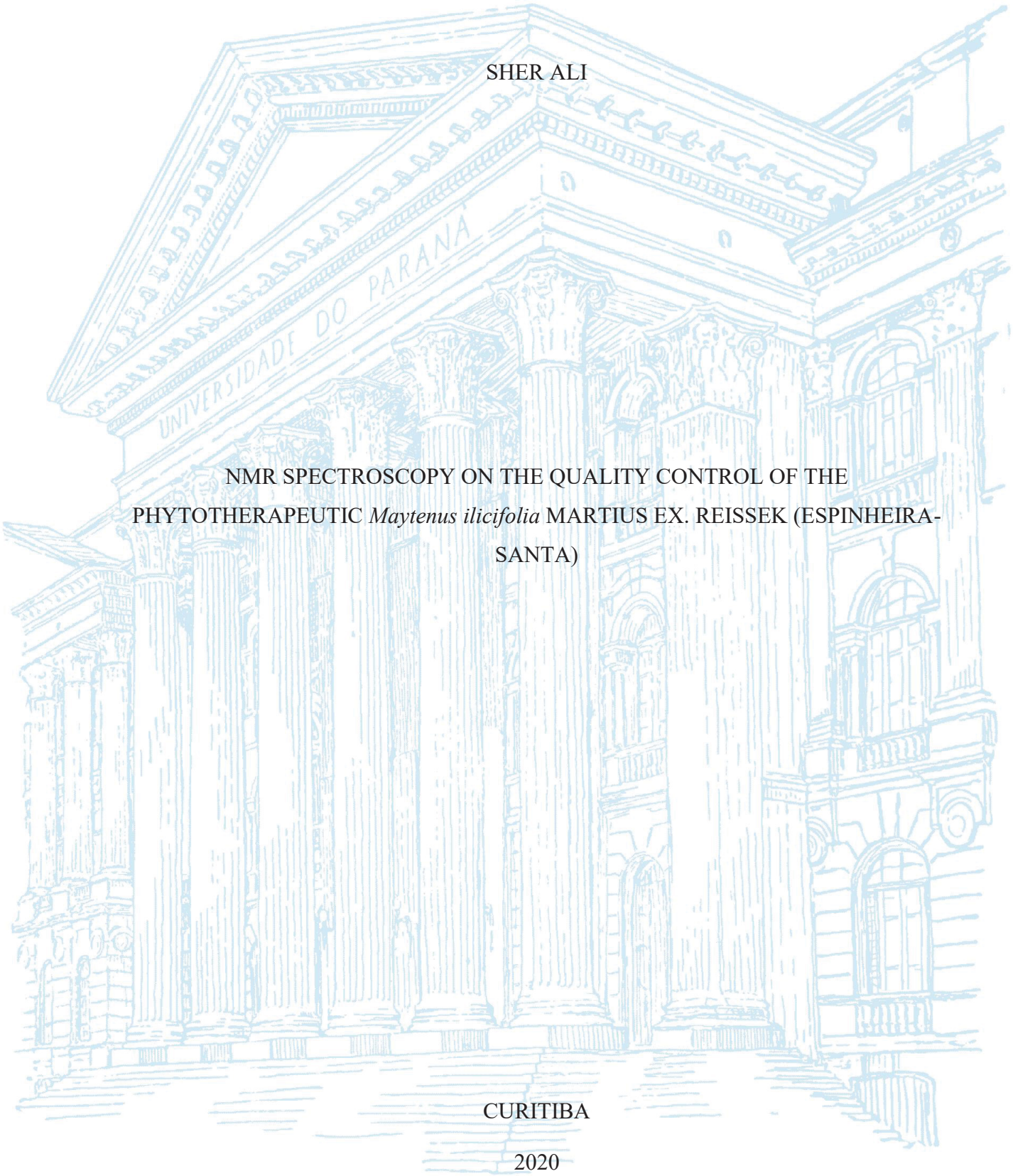

NMR SPECTROSCOPY ON THE QUALITY CONTROL OF THE PHYTOTHERAPEUTIC *Maytenus ilicifolia* MARTIUS EX. REISSEK (ESPINHEIRA-SANTA)

CURITIBA

2020

SHER ALI

NMR SPECTROSCOPY ON THE QUALITY CONTROL OF THE PHYTOTHERAPEUTIC *Maytenus ilicifolia* MARTIUS EX. REISSEK (ESPINHEIRA-SANTA)

Tese apresentada ao curso de Pós-Graduação em Química, Departamento de Química, Setor de Ciências Exatas, Universidade Federal do Paraná, como requisito parcial à obtenção do título de Doutor em Química, área de concentração Química Orgânica.

Orientador: Prof. Dr. Andersson Barison

Coorientador: Prof. Dr. Guilherme Lanzi Sassaki

CURITIBA

2020

Catalogação na Fonte: Sistema de Bibliotecas, UFPR
Biblioteca de Ciência e Tecnologia

A398n Ali, Sher
NMR spectroscopy on the quality control of the phytotherapeutic *Maytenus ilicifolia* martius ex. reissek (espinheira-santa) [recurso eletrônico] Sher Ali. – Curitiba, 2020.

Tese - Universidade Federal do Paraná, Setor de Ciências Exatas, Programa de Pós-Graduação em Química, 2020.

Orientador: Andersson Barison.
Coorientador: Guilherme Lanzi Sassaki.

1. Espectroscopia de ressonância magnética nuclear. 2. Espinheira Santa. 3. Controle de qualidade. I. Universidade Federal do Paraná. II. Barison, Andersson. III. Sassaki, Guilherme Lanzi. IV. Título.

CDD: 543.0877

Bibliotecária: Vanusa Maciel CRB- 9/1928

MINISTÉRIO DA EDUCAÇÃO
SETOR DE CIENCIAS EXATAS
UNIVERSIDADE FEDERAL DO PARANÁ
PRÓ-REITORIA DE PESQUISA E PÓS-GRADUAÇÃO
PROGRAMA DE PÓS-GRADUAÇÃO QUÍMICA - 40001016026P2

TERMO DE APROVAÇÃO

Os membros da Banca Examinadora designada pelo Colegiado do Programa de Pós-Graduação em QUÍMICA da Universidade Federal do Paraná foram convocados para realizar a arguição da tese de Doutorado de **SHER ALI** intitulada: **NMR spectroscopy on the quality control of the phytotherapeutic *Maytenus ilicifolia* martius ex. reissek (espinheira-santa)**, sob orientação do Prof. Dr. ANDERSSON BARISON, que após terem inquirido o aluno e realizada a avaliação do trabalho, são de parecer pela sua APROVAÇÃO no rito de defesa.

A outorga do título de doutor está sujeita à homologação pelo colegiado, ao atendimento de todas as indicações e correções solicitadas pela banca e ao pleno atendimento das demandas regimentais do Programa de Pós-Graduação.

CURITIBA, 30 de Abril de 2020.

Andersson Barison

ANDERSSON BARISON
Presidente da Banca Examinadora

FREDERICO LUIS FELIPE SOARES
Avaliador Interno (UNIVERSIDADE FEDERAL DO PARANÁ)

CAROLINE DA ROS MONTES D`OCA
Avaliador Interno (UNIVERSIDADE FEDERAL DO PARANÁ)

LUCIANO MORAIS LIÃO
Avaliador Externo (UNIVERSIDADE FEDERAL DE GOIÁS)

FERNANDO MOLIN
Avaliador Externo (UNIVERSIDADE TECNOLÓGICA FEDERAL DO

Dedication

I dedicate this work to my family, my dearest (Late) father Fatih Muhammad and mother, brother Umar Ali and sisters for entire love, encouragement and support from start till to date.

ACKNOWLEDGEMENT

First and foremost, I would like to thank God for his never-ending grace, mercy, and provision during what ended up being one of the toughest times of my life.

I sincerely very much thankful to both CNPq (National Council for Scientific and Technological Development) and TWAS (The World Academy of Sciences) for the undistinguished financial support under TWAS-CNPq Fellowship 2015 program.

The Post-Graduate Program in Chemistry (PPGQ), UFPR is highly acknowledged for providing me the facilities with open and creative working environment for my research. I thank all my colleagues and whole teaching and non-teaching staff for support.

Special and incomparable thanksgivings to my respectable mentor, Prof. Dr. Andersson Barison for accepting me as doctoral student, who always encouraged, supported me like a friend in scientific accomplishments, knowledge and enabled me how to be a researcher.

I would like to thank my cosupervisor Prof. Dr. Guilherme Lanzi Sassaki for his kind mentorship with proper support throughout the studies.

I convey my distinct thanks to Prof. Dr. Noemi Nagata for all time support in scientific learning especially statistical tool. Her special and friendly support will always be remembered.

I feel great pleasure to express my deep and sincere gratitude to Prof. Dr. Caroline Da Ros Montes D'Oca, for friendly support, knowledge, ethical support and as a committee memeber in my doctoral thesis evaluation.

I feel great pleasure to express my deep and sincere gratitude to Prof. Dr. Luciano Morais Liao for participating and evaluation my PhD thesis, as well as unexceptional thanks to him once again for initial support and acceptance, he is key role in my Ph.D.

I feel great pleasure to express my deep and honest gratitude to Prof. Dr. Fernando Molin for participation and evaluation my PhD thesis.

Equal and undistinguished thanks to Prof. Dr. Frederico Luiz Felipe Soares for participation and evaluation my PhD thesis.

Very much thank you Prof. Dr. Jaisa F. Soares, Prof. Dr. Daniel da Silveira Rampom, and Prof. Dr. Ronilson V. Barbosa for all supports, help and forever appreciations.

In addition, special and honest thanks to my school teachers, college and university professors from past to present in particular, Prof. Dr. Abdul Majeed Khan (MSc. mentor) and

Prof. Dr. Jamshed Hashim (Ex-project mentor), whom played central roles in my academic career, a wish of thanks is ordinary for them.

My special gratitude to the taxonomists Tadeu Jose, Marcelo Brutto, and their whole staff from Herbarium of Curitiba, whom supported me in overall collections and taxonomic identification of the plant species, anticipated in my PhD thesis.

Special thanks to my friends and colleagues from both NMR centers (Chemistry and Biochemistry) Dr. Maria de Fátima Costa Santos, MSc. Leice Milla Ribeiro de Novais, MSc. Ana Caroline Qualis, Raquel, Tatiane K. Mathias, Dr. Leociley Rocha Alencar Menezes, Dr. Lívia Macedo Dutra, Dr. Alan Diego da Conceição Santos, Dr. Arquimedes Paixão de Santana Filho, and other friends.

I immensely appreciative to the people very close to me whom always accompanied, appreciated, and fully supported me, M.Phil. Umar Ali, Ali Akbar, Hazrat Umar, MSc. Kelly Mara Seronato, Dr. Ajmir Ali Khan, Dr. Anwar Shamim, MSc. Gul Badshah, MSc. Evaldir Damião Aparecido Lopes, Umar Gul, M.Phil. Ghaus-Ur-Rehman, MSc. Katlin Suellen Rech, Dr. Miguel Jorge Saldaña Jimenez, and Dr. Otavio Fuganti.

Last but not least, I deeply wish my undistinguishable thanks to my family members specifically my dearest (late) **father**, **mother**, **brother** Umar Ali, and **sisters** for supporting me spiritually, morally and financially throughout educational career and my life in general.

“I walk slowly, but I never walk backward”

(Abraham Lincoln, 1809-1865)

RESUMO

Maytenus ilicifolia Mart. ex Reissek, popularmente conhecida como "Espinheira-Santa", é uma planta utilizada terapeuticamente no tratamento de diversas doenças como úlceras intestinais e de estômago, entre outras. Esse fitoterápico é consumido como infusão (chá), extrato, cápsulas de gelatina e/ou planta seca, no Brasil e em outros países. Devido à ampla distribuição, consumo e natureza terapêutica, *Maytenus ilicifolia* (e *Maytenus aquifolium*) e outras 70 plantas medicinais fazem parte da lista de plantas de interesse do Sistema Único de Saúde (SUS)–RENISUS. Além disso, *Maytenus ilicifolia* também foi citada no Formulário de Fitoterápicos Farmacopeia Brasileira, 1ª edição – 2018. Devido à morfologia foliar semelhante, *Maytenus ilicifolia* é confundida com outras espécies (como *Zollernia ilicifolia*, *Sorocea bomplandii*, *Citronella gongonha*, *Berberis laurina*), as quais são difíceis de diferenciar de modo simples. Para superar esse problema, medidas de controle de qualidade utilizando métodos analíticos integrados são frequentemente necessárias. Nesse trabalho, a espectroscopia de RMN de ^{1}H HR-MAS, juntamente com a análise não supervisionada de componentes principais (PCA), distinguiu todas as espécies com base em seu *fingerprint* químico. Essa técnica possibilitou a identificação de vários metabólitos (flavonoides, flavanois, carboidratos, ácidos orgânicos) em estado inalterado nas folhas de Espinheira-Santa. Essa abordagem permitiu uma distinção ambígua, e avaliação do padrão químico das folhas nas duas espécies de *Maytenus*, que eram completamente diferentes das outras espécies analisadas. A topologia baseada em RMN possivelmente descreveu os sinais dos principais metabólitos; epicatequina, sacarose e ácidos graxos foram mais intensos nas folhas superiores de *Maytenus ilicifolia* durante o meio do outono e inverno (junho-agosto) de 2019. Enquanto, *Maytenus aquifolium* foi mais dominada por teores de açúcar, com sinais mais intensos em todas as quatro estações do ano. A PCA expôs que a (-)-epicatequina era o principal biomarcador de diferenciação de *Maytenus ilicifolia* de *Maytenus aquifolium*. Essa variação pode ser devida a composição química (teores mais baixos e/ou elevados de determinado composto) das espécies. Além disso, os padrões químicos topológicos das folhas nas espécies correlacionadas de *Maytenus* foram investigadas de acordo com a variação sazonal ou interações ecológicas. Em *Maytenus ilicifolia* a maioria das folhas superiores acumulou (-)-epicatequina durante o meio do verão e inverno, e no final do outono; as folhas do meio acumularam açúcar no meio da primavera e no final do outono; e as folhas inferiores, ácidos graxos no meio do verão, inverno e outono. Além do meio do inverno (agosto) que foi eficaz para o acúmulo de açúcar, (-)-epicatequina e ácidos graxos nas folhas de *Maytenus aquifolium,* embora tenha sido dominada por açúcares durante todas as estações. Essa quantidade elevada de açúcar pode estar associada com outros fatores (bioma, sombras, patógenos etc.) em *Maytenus aquifolium* spp. De modo geral, o final do outono (junho) e o meio do inverno (agosto) foram períodos mais críticos para os fingerprints químicos em espécies de *Maytenus*. Além disso, foram estudados materiais comerciais (folhas picadas, sachés de chá e plantas em pó em cápsulas). No entanto, a maioria dos produtos fitoterápicos foram encontrada diferente da verdadeira Espinheira-Santa (*M. ilicifolia*). Esses resultados podem ser úteis e adotáveis em outras pesquisas relacionadas à saúde, controle de qualidade, produtos agronômicos, alimentos e outrasrelacionadas a plantas.

Palavras-chave: Autenticidade; RMN HR-MAS; *Maytenus ilicifolia*; Principal; Análise de Componentes Principais (PCA); Controle de Qualidade.

ABSTRACT

Maytenus ilicifolia Mart. ex Reissek, popularly known as "Espinheira-Santa", is a plant used therapeutically in the treatment of multiple diseases as intestinal and stomach ulcers, and others. This phytotherapeutic is consumed as infusion (tea), extract, gelatin capsules and/or as dried leaves in Brazil and further countries. On account of wide distribution, consumption, and therapeutic nature, the *Maytenus ilicifolia* (and *Maytenus aquifolium*) and additional 70 herbal plants are part of the list of interest to the Brazilian Unified Health System (SUS)-RENISUS. Moreover, *Maytenus ilicifolia* has also been cited in the "Brazilian Pharmacopoeia" Phytotherapeutic Form, 1st edition-2018". Due to similar leaf morphology, *Maytenus ilicifolia* is confused among further species (e.g. *Zollernia ilicifolia*, *Sorocea bomplandii*, *Citronella gongonha*, *Berberis laurina*) which is challenging to differentiate by simple ways. To overcome this problematic issue, quality control measures using integrated analytical methods are necessary. In this work, ^{1}H HR-MAS NMR spectroscopy together with unsupervised principal component analysis (PCA) distinguished all species based on their chemical fingerprints. HR-MAS NMR enabled the identification of several metabolites (flavonoids, flavanols, carbohydrates, organic acids) in unaltered state of leaves from Espinheira-Santa. This approach permitted an ambiguous distinction, and leaf chemical pattern evaluation in both *Maytenus* species, which were completely different from other plants. NMR-based topology possibly described that signals from major metabolites; epicatechin, sucrose and fatty acids were more intense in upper leaves from *Maytenus ilicifolia* during middle autumn and winter (June-August) 2019. While, *Maytenus aquifolium* was completely dominated by sugar contents appeared with most intense signals in all four seasons. PCA exposed that (-) epicatechin was main biomarker of differentiating *Maytenus ilicifolia* from *Maytenus aquifolium*. This variation may be due to the chemical compositions (lower and/or higher level of certain compounds) of species. Moreover, the topological leaf chemical patterns in the correlated *Maytenus* species were investigated according to seasonal variation or ecological interactions. In *Maytenus ilicifolia* most of the upper leaves accumulated (-)-epicatechin during the middle of summer and winter, and in late autumn; the middle leaves accumulated sugar in the middle of spring, and late autumn; and the lower leaves accumulated fatty acids in the middle of summer, winter, and autumn. Beyond middle of winter (August) which was effective to the accumulation of sugar, (-)-epicatechin, and fatty acids in several leaves although *Maytenus aquifolium* was over dominated by sugar during all seasons. This high amount of sugar may be associated to other factors (biome, shades, pathogens, etc.) to *Maytenus aquifolium* spp. In general view the end-autumn (June) and mid-winter (August) were more critical periods to the chemical fingerprints in *Maytenus* species. In addition, commercial materials (chopped leaves, tea sachets and plant powdered in capsules) were studied. However, most of the herbal products were found different from real Espinheira-Santa (*M. ilicifolia*). These results can be useful and adoptable in other research related to health, quality control, agronomic products, food and other related to plants.

Keywords: Authenticity; HR-MAS NMR; *Maytenus ilicifolia*; Principal Component Analysis (PCA); Quality control.

LIST OF FIGURES

List of tables

LIST OF ABREVIATIONS OR ACRONYMS

ANVISA- Agência Nacional de Vigilância Sanitária (National Sanitary Surveillance Agency)

AQ- Acquisition time in seconds (FIDs collection time)

AMIX- Analysis of Mixture

BBI- Broad Band Inverse detection (NMR probe)

br- Broad

CE- Capillary Electrophoresis

COSY- Correlation Spectroscopy

COW- Correlation Optimized Warping

CZE- Capillary Zone Electrophoresis

d- Doublet

dd- doublet of doublet

ddd- doublet of doublet of doublet

dB- Decibel (Unit of power level)

D1- Relaxation delay\ Delay time (prior to acquisitions)

D8- Saturation time in milliseconds in *noesypr1d* experiment

ds- Number of dummy scans

DTW- Dynamic Time Warping

FFT- Fast Fourier Transformation

FHW- Full Half Width (used for the broadening of TMS signal)

FID- Free Induction Decay

FT- Fourier Transformation

Gal- Galactose

GC- Gas Chromatography

GC-MSD- Gas Chromatography- Mass Selective Detector

HMBC- Heteronuclear Multiple Bond Coherence (or Correlation)

HPLC- High Performance Liquid Chromatography

HPTLC- High Performance Thin Layer Chromatography

HPLC-DAD- High Performance Liquid Chromatography-Diode Array Detector

HR-MAS- High-Resolution Magic Angle Spinning

HSQC- Heteronuclear Single Quantum Coherence (or Correlation)

Hz- Hertz

***J*-** Coupling constants in Hertz (Hz)

kHz- Kilohertz

LB- Line Broadening (an exponential multiplication function to FIDs)

LC- Liquid Chromatography

LC-UV- Liquid Chromatography with Ultra Violet detection

LCMS- Liquid Chromatography coupled to Mass Spectrometry

***m*-** Multiplet

MAPA- Ministério da Agricultura, Pecuária e Abastecimento (Ministry of Agriculture, Livestock and Food supply)

MAS- Magic Angle Spinning

MRI- Magnetic Resonance Imaging

MS- Mass Spectrometry

ms- Milliseconds

MHz- Megahertz

NMR- Nuclear Magnetic Resonance

***noesy1d*-** Nuclear Overhauser Spycotroscopy, a 1D experimental notation in NMR that uses for solvent suppression

NS- Number of Scan

P1- Duration of Pulse angle (in microseconds)

PCA- Principal Component Analysis

pl9- Pre-saturation power level

ppm- part per million

qPCR- quantitative Polymerase Chain Reaction

RENISUS- Relação Nacional de Plantas Medicinais de Interesse ao SUS (National List of Medicinal Plants of Interest to the Unified Health System)

RF- Radio Frequency

RG- Receiver Gain

***s*-** Singlet

SSBs- Spinning Side Bands

***S/N*-** Signal to Noise ratio

SUS- Sistema Único de Saúde (Unified Health System)

SW- Spectral width/ Spectral Window

***t*-** Triplet

t1- Increments interval in *noesypr1d* experiment

T_1- Spin-lattice (or longitudinal) relaxation time

T_2- Spin-spin (or transverse) relaxation time

TLC- Thin Layer Chromatography

TD- Size of FID (number of points implemented to digitize and form FIDs)

t_{mix}- Mixing time in *noesypr1d* experiment

TMS- Tetramethyl silane

TOCSY- TOtal Correlation SpectroscopY

TPPI- Time-Proportional Phase Incrementation

WHO- World Health Organization

zg- Basic notation to represent 1D sequence in NMR

zgpr- Basic notation to represent 1D sequence in NMR for solvent suppression

zgcppr- Basic notation to represent 1D sequence in NMR for solvent suppression

LIST OF SYMBOLS

B_0 - Main magnetic field of spectrometer

B1 - Radio frequency field (or RF-pulse)

δ - Chemical shift

θ - Theta

ΔX - Difference in magnetic susceptibility

μ - Micro

β - Beta

α - Alpha

K - Kelvin

°C - Degree Celsius

± - Plus, Minus

ω - Omega

ω_o - Larmor precessional frequency

≥ - Greater or equal

> - Greater

< - Smaller

Π/2 - Tip angle of 90°

SUMMARY

INTRODUCTION

1 INTRODUCTION

1.1 PHYTOTHERAPEUTICS

In agreement to National Health Surveillance Agency (ANVISA) (RDC no. 18, April 3, 2013-article 3), phytotherapeutics (*Phyto*, plant; *therapeutic*, healer) are the products obtained from medicinal plant, except isolated substances, to healing purposes (BRASIL., 2013). In accordance to the literature (KHAN et al., 2019; FREIRE et al., 2018; ALAMGIR, 2017; PALHARES et al., 2015), World Health Organization (WHO) estimated total use of herbal products consumption by population around the world-wide (60%), and in developing countries (80-85%) such as Asia, Africa, South America, and others. Amongst developing countries, Brazil offers a huge collection of medicinal plants, which are vastly used in research as well as by the public in the form of infusion (tea), extracts, herbal remedies (FREIRE et al., 2018) and or as raw materials to cure various diseases (AGRA et al., 2007).

Frequently, herbal materials can be found in common stores, market, and pharmacies in the cities, towns etc., that are easily accessible to public. As per demand of consumers, herbal products on market must be real, free of adulteration, labeled with authentic certification (SPANAKIS et al., 2019, CARVALHO et al., 2014), and or with prescription of active chemical ingredients (ALAMGIR, 2017). The direct use of unauthentic, mixed-up with (toxic) plant materials or any other unwanted substances may be drastic to human. In fact, plants are natural producers of large range of various (non)harmful metabolites of several classes. In literature, manifold toxic chemical substances are reported such as catechol hydroquinone and resorcinol that are genotoxic; gossypol, a pigment present in cotton seed (*Gossypium* spp.) is highly toxic to livestock causing dyspnea, anorexia, thriftiness, and diarrhea (CHEN et al., 2010), neurotoxin; rotenoids in plant legumes inhibits cell respiration and phenolic cucurbitacin blocks cell development (MBAVENG et al., 2014; WINK, 2010). Human metabolism dysfunction is reported from certain plants belongs to Fabaceae, Solanaceae, Lamiaceae, and Rutaceae families (MAHOMOODALLY et al., 2018). Some additional side-effects such as hepatotoxicity, damage in the kidney and nervous systems, and heart diseases from the leaf extract of *Pistacia palaestina*, *Juglans regia*, and *Quercus ithaburensis* (SAAD et al., 2006). *Maytenus ilicifolia* (Espinheira-Santa) has been reported for teratogenic (cause growth abnormalities) effect due to maytansine constituent (SEUKEP et al., 2014). In addition, *Maytenus robusta* (Celastraceae) has been described for genotoxicity

(RAYMUNDO et al., 2012). Acute toxicity effect was reported from aqueous methanolic extracts leaf from *Zollernia ilicifolia* species (GONZALEZ et al., 2001).

In this regard, public health treatments by plants formulation, are pre-supervised and controlled by national health associates and legislatives in a country for example, National Health Surveillance Agency (ANVISA) and Ministry of Agriculture, Livestock and Food Supply (MAPA) in Brazil (CARVALHO et al., 2014). The Brazilian Unified Public Health System (SUS) produced a list of 71 herbal plant species of interest (RENISUS), which had been made available to population (BRASIL, 2009).

The "RENISUS" incorporated the therapeutic *Maytenus ilicifola* Mart. (Espinheira-Santa), highlighted also in the "Brazilian Pharmacopoeia of Phytotherapeutic Form, Ed. 1st–2018", showing total tannins as active chemical ingredients with additional details (ANVISA, 2018). Tannins are the polymeric flavanols and or flavan-3-ol (skeleton; C6-C3-C6) natural polyphenolic compounds of numerous catechin (e.g. epicatechin) monomers (units) chemically arranged into large size polymer (QIAN et al., 2015; TSAO, 2010). The tannin polymers are formed by *n*-number of epicatechin units, chemically combined at position-4,8 in C- and A-ring in the basic structure (Figure 1.1). The hydroxylation at position-3 permits two chiral centers (C2, C3) in flavanols with four stereoisomers such as (±)-epicatechin with 2,3-*cis*-isomer and (±)-catechin of 2,3-*trans*-configuration, in a diastereomeric relationship. The chiral or stereo center (C2, C3 with different atoms or groups of atoms) basically differentiate two epimers (of opposite configurations) in a diastereomer (two stereoisomers). For example, (-)-catechin and (-)-epicatechin are mutually epimers, due to the configuration (*S, R* → *R, R*) at substituted chiral carbons (C2, C3) simultaneously equal rule applies to (+)-catechin and (+)-epicatechin of rather different type of configuration (*R, S* → *S, S*). The (-\+)-catechins are in diastereomeric relationship to (-\+)-epicatechins because they are neither mirror images nor superimposable to each other (configuration changes only in one chiral center in a pair). The (-)-catechin and (+)-catechins or (-)-epicatechin and (+)-epicatechins are mirror images and enantiomer to each other (see Figure 1.1). These diastereomers, the catechin and epicatechin are widely distributed in vascular plants (TSAO, 2010). Tannins may be commonly small procyanidins ($n > 0$) and or large sized oligomeric procyanidins ($n = 1$-7) or condensed tannins (TSAO, 2010).

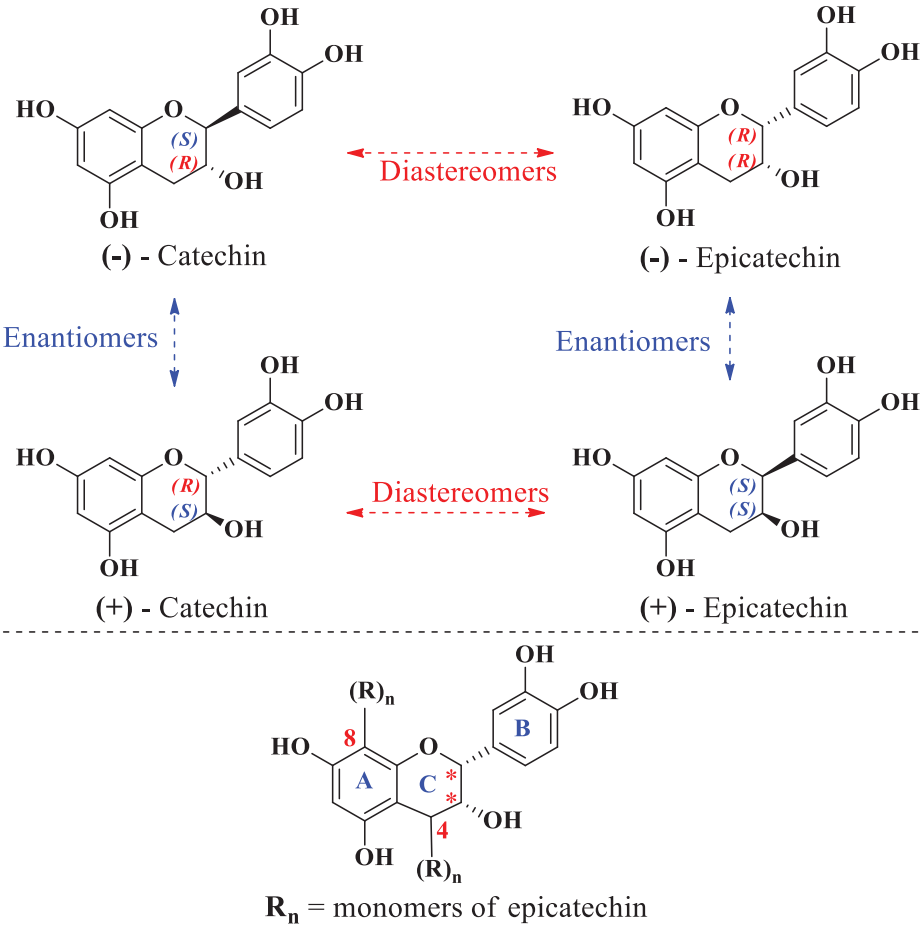

Figure 1.1. Chemical structures showing different configuration of (±)-catechin and (±)-epicatechin with tannins. **Source:** TSAO, 2010.

The phenylpropanoid is main route for the biogenesis of phenolic tannins and additional flavonoids, which are efficient in plant defense mechanisms, antioxidations, and more biological activities (HARDING, 2019; QIAO, et al., 2019; KUMAR et al., 2013). The thorny leaves of Espinheira-Santa are well-known sources fro the production of polyphenolic compounds, thus they are considered best healing agent in several health issues and largely used in Brazil and other countries (CALDAS et al., 2019; PÉRICO et al., 2018; KUJAWSKA, 2018; SÁ et al., 2017). Based on similar dentated leaves, a major challenge arise to differentiate *Maytenus ilicifolia* from other species of *Maytenus aquifolium*, *Sorocea bomplandii*, *Zollernia ilicifolia* etc. (CALDAS et al., 2019; PÉRICO et al., 2018; JESUS et al., 2012), which thus, need deep understanding and quality control measurements. Other than finding real herbal spp., the quality control moreover delivers pre-knowledge associated to healthcare and novel findings (PELKONEN et al., 2014). Strict quality control measurements must be carried out to consider, for instance, plant identity (taxonomy), source (e.g. part of

plant), harvest time, handling (washing, drying, grinding, storage etc.) (ALAMGIR, 2017) and followed by investigations through some of integrated analytical approaches.

1.2 QUALITY CONTROL OF PHYTOTHERAPEUTICS

Since last decades, quality control of *Maytenus ilicifolia* Mart. has been evaluated on the basis of multiple flavonoids that were investigated by means of various methods. Such as; High-Performance Thin layer Chromatography (HPTLC) (VILEGAS et al., 1998), High-Performance Liquid Chromatography (HPLC), Thin Layer Chromatography (TLC), Capillary Zone Electrophoresis (CZE), Gas Chromatography\Mass Selective Detector (GC-MSD) (MOSSI et al., 2009), High-Performance Liquid Chromatography-Diode Array Detector (HPLC-DAD) (SÁ et al., 2017), and others (DIAGONE et al., 2012). These analytical tools were technically used extraction, separation, purification, and derivatization of the samples. Such procedures supposed to be effective to the reliability in biological activities of chemical compounds e.g. some affect to the antioxidant activities was observed for polyphenol content in the vine tea (MUHAMMAD et al., 2018). In fact, samples tissue needs to study in intact state (without extractions) to acquire metabolites rich profile and to preserve reliability in molecular biological activities. In this regard, the intact sample tissue can be investigated by High-Resolution Magic Angle Spinning (HR-MAS) NMR that offer great advantages over extraction, separation, or even conventional liquid-state NMR (TAKISTAKISTAKIS et al., 2017). HR-MAS NMR technique can be directly used to the non-altered physical state of plant tissue or other type natural sample. In non-altered sample or material in original state include unwanted multidirectional anisotropic interactions of several (hundreds-thousands) hertz magnitudes, which causes signal shape and spectral resolution. To devastate these interactions, better line shape and spectral resolution could be achieved in HR-MAS NMR. This technique permits acquisition(s) in definite orientation, the so-called magic angle ($\theta = 54.74°$) direction to the main magnetic field ($\mathbf{B_0}$) by providing a spinning speed of several (hundred-thousands) hertz, equal or greater magnitude to the anisotropic interactions. Usually, NMR spectroscopy has large contributions in assessing quality control of herbal products (SIMMLER et al., 2018; RIACHI et al., 2018; LI et al., 2017).

To preserve intact state, the ^{1}H HR-MAS NMR fingerprinting method was applied to discriminate *Maytenus ilicifolia* Mart. from additional adulterants and or similar plants species (PÉRICO et al., 2018; JESUS et al., 2012). The NMR spectra contain maximum potential information which are tragic to obtain by visually inspecting the spectra. In order to

obtain these information, further analytical methods such as unsupervised multivariate principal component analysis (PCA) (JAHANGIR et al., 2018; SIMMLER et al., 2018) was used.

OBJECTIVES

2 OBJECTIVES

2.1 GENERAL OBJECTIVES

The goal of this work was to develop and implement ^{1}H HR-MAS NMR-based metabolomics together with chemometric (PCA) approach to carry out the authentication of *Maytenus ilicifolia* Mart. ex. Reissek (Espinheira-Santa) which have similar marginal spiny and leathery leaf to *Maytenus aquifolium*, *Zollernia ilicifolia*, *Sorocea bomplandii*, *Berberis laurina* Bilb. and *Citronella gongonha*.

2.2 SPECIFIC OBJECTIVES

Specific objectives were intended to:

* Evaluate ^{1}H HR-MAS NMR methodology and its application to the plant materials (*Maytenus* spp. and other);
* Investigate initial distinction among morphologically similar plants through ^{1}H HR-MAS NMR spectroscopy;
* Discriminate real *Maytenus ilicifolia* on the basis of biomarker by considering maximum chemical fingerprints from the species;
* Investigate topologically leaf (upper to lower) chemical patterns in correlated plants with respect to seasonal variation and ecological interactions;
* Correlate and confirm NMR-based results by unsupervised principal component analysis (PCA) method;
* Discriminate authenticity for commercial products (chopped leaves, tea sachets, capsules) from *Maytenus ilicifolia* (Espinheira-Santa) of different places and vendors;

JUSTIFICATION

3 JUSTIFICATION

According to previous studies, therapeutic *Maytenus ilicifolia* has been used to cure several disorders, for example stomach and liver ulcers. This plant is being confused among the consumers and challenging to differentiate from other species (especially *Maytenus aquifolium*, *Zollernia ilicifolia*, *Sorocea bomplandii,* in addition *Citronella gongonha*, and *Berberis laurina*) due to comparable spiny leaf texture. Based on such confusion, several plant species (e.g. *S. bomplandii*) with additional adulteration have been found under same name (Espinheira-Santa) on various commercial points in Brazil (CALDAS et al., 2019; PÉRICO et al., 2018; JESUS et al., 2012). It is notable that low quality of less regulated herbal products supposed to be critical issue among customers, by considering only products batch, thus it may contain impurities, adulterants and misidentified toxic products. In this regard a strict quality control procedure is highly recommended to manipulate falsification, misrepresentation and to furthermore suggest real herbal plant which guaranteeing welfare and public safety.

Thus, quality control assessment for herbal products needs several basic steps, and are important to carry out as mentioned by Alamgir (2017), for example, the plant identity (taxonomy), source (e.g. part of plant), harvest time, handling (washing, drying, grinding, storage, etc.). The significant steps of prescribed protocol, can also be implemented to the commercially available materials, including the herbal products, with precise and non-variable labeling, correct name(s) and additional prescriptions need to be sustained under health regulatory legislation guidelines.

Thus, the differentiation among similar plant species, demanding powerful integrated analytical approaches e.g. HR-MAS NMR. This approach is helpful to investigate herbal samples in original states, and establishes authenticity considering chemical composition or fingerprints. The HR-MAS NMR spectroscopy attained great attention due to the fact that it collects a set of information related to molecules detection, preservation, and correct connectivities in the chemical structure, quantification, integrity, and reproducibility of the material under study.

LITERATURE REVISION

4 LITERATURE REVISION

There exist large number of medicinal plants in Brazil, including therapeutic *Maytenus ilicifolia* Mart. ex Reissek that has been famous by its common name, “Espinheira-Santa”. Based on therapeutic attributes, Espinheira-Santa is generally used as extracts, infusion, gelatin capsuls, and or dried leaves to cure ulcers in the stomach and liver, etc.

Espinheira-Santa has common spiny leaf that raised confusion to differentiate it from other plants (*Maytenus aquifolium*, *Zollernia ilicifolia*, and *Sorocea bomplandii,* in addition with *Berberis laurina*, and *Citronella gongonha*). It is challenging to the users, venders and or investigaters to distinguish one plant from other on merely observing (similar) leaves.

In accordance to literature (CALDAS et al., 2019; PÉRICO et al., 2018; JESUS et al., 2012) as well as current work, different plant species (e.g. *S. bomplandii*) have been found under batch name “Espinheira-Santa and *Maytenus ilicifolia*” from various commercial points in Brazil. In this regard a strict quality control procedure was highly recommended to differentiate original Espinheira-Santa from improper false ones. Thus, it deemed that the differentiation between similar plants could be assessed through analytical approach (e.g. HR-MAS NMR) to establish authenticity based on their chemical compositions (fingerprints).

4.1 *Maytenus ilicifolia* MARTIUS (MART.) EX REISSEK

The *Maytenus* genus comprised almost 300 species including a five-meter taller *Maytenus ilicifolia* Mart. ex Reissek (Figure 4.1. A; p. 30) belongs to the Celastraceae family. It is commonly known as Espinheira-Santa, but also *Celastrus spinifolius* Larannaga; *M. Angustior* Briq.; *M. hassleri* Briq.; *M. muelleri* Schwacke; *M. officinalis* Mabb.; *M. pilcomayensis* Briq.; *Maytenus aquifolium* Mart., which is widely distributed in various regions of Brazil (PÉRICO et al., 2018). This species is found in Amazonian forest, Atlantic Rainforest, “Caatinga” and “Cerrado” (PÉRICO et al., 2018), in Paraná, São Paulo, Mato Grosso do Sul, Rio Grande do Sul, Santa Catarina State, Paraguay, Uruguay and accordingly Eastern Argentina (CALDAS et al., 2019; MAZZA et al., 2011).

This herbal plant is an woody, shrubby of branched physiognomic texture, with dark green and spiny leathery leaves, light-yellow and clustered flowers (PÉRICO et al., 2018; FISCHER et al., 2015). The leaves from this species are used domestically as infusion (tea) or dried leaves, and commercially in folk medicines in the Latin American countries including Brazil (CALDAS et al., 2019; PÉRICO et al., 2018; SÁ et al., 2017; CIPRIANI et al., 2006).

It is believed that the leaves infusion (tea) is therapeutically important in stomach, gastritis, nausea, and ulcers however, folk medicines (gelatin capsules) are useful in contraceptive, abortifacient, liver disease, blood disorder whereas, pharmacologically as anti-inflammatory, antispasmodic, antacids and healers e.g. antioxidant activities and antidiabetics, blood cleansing, cholesterol control (CALDAS et al., 2019; PÉRICO et al., 2018; KUJAWSKA., 2018; SÁ et al., 2017). The relative plant is specified for the presence of numerous molecular components, several among them are mentioned in Table 4.1; p. 31 and in Figure 4.2; p. 33.

4.2 *Maytenus aquifolium* MARTIUS (MART.)

The *Maytenus aquifolium* Mart. (Figure 4.1. B; p. 30) is commonly known as "Espinheira-Santa" which is distributed in various regions of Brazil (PINTO et al., 2018) such as in the state of Paraná. Both the *Maytenus ilicifolia* and *Maytenus aquifolium* species are almost equal due to similar thorny leaves, and belonging to the same Celastraceae.

As reported in Leite et al. (2001), the leaves of *Maytenus aquifolium* are also used as infusion and beverages, foodstuffs and folk medicines. Moreover, the leaves of this plant species are reported as phytotherapeutic remedies, playing important role in the treatment of multiple chronic ulcers (PINTO et al., 2018). The leaves are rich sources fro the presence of many metabolites, several are given in Table 4.1; p. 31 and Figure 4.2; p. 33 .

4.3 *Sorocea bomplandii* BAILON (BAIL.) W. C. BURGER, LANJOUW & BOER

The genus, *Sorocea* belongs to Moraceae family that contain almost 1,180 species in addition of *S. bomplandii* (Bail.) W. C. Burger, Lanjouw & Boer, also known as *Sorocea ilicifolia* (Figure 4.1. C; p. 30). This plant is approximately 20 meters tall, woody, shrubby and branched tree, with elongated dark green spiny leaves, and are edible with therapeutic importance (GARCIA et al., 2011; RUSCHEL et al., 2007).

The *Sorocea bomplandii* is broadly distributed in various temperate and subtemperate regions, and Atlantic forests biomes, including several Brazilian states as Paraná, Rio Grande do Sul and Pernambuco, similarly Paraguay and Northern Argentina (TURCHETTO et al., 2018; RUSCHEL et al., 2007). This species has communal morphology with *M. ilicifolia*, *M. aquifolium* and *Zollernia ilicifolia* (VINICIUS et al., 2018; LEITE et al., 2001). The leaves of this species are medicinally valuable and therapeutically important in blood cleansing and cholesterol level regulations (KUJAWSKA, 2018; VINICIUS et al., 2018).

4.4 *Zollernia ilicifolia* (BRONGN.) VOGEL

A well-known large family, Fabaceae comprised 751 genera and 19,000 known species. In accordance to Mansano et al. (2002), the genus *Zollernia* comprises about 11 species including *Zollernia ilicifolia* (Figure 4.1. D; p. 30). This species is known by several names of *Coquebertia ilicifolia* (Brongn.) and *Zollernia houlletiana* Vog.; *Zollernia ilicifolia* (Brongn.) Tul.; *Zollernia securidacifolia* Benth.; *Zollernia vogelii* Tul.; and *Zollernia splendens.* The *Z. ilicifolia* is commonly famous as Espinheira-Santa and Espinheira-divine; *Coquebertia ilicifolia* Brongn. Tul and respectively *Zollernia houlletiana* Tul.

Zollernia ilicifolia is woody tree ranges up to 15-meter in height with marginal spiny green leaves, white scented and bunched flowers (5 petals), and somewhat elongated fruits (CORADIN et al., 2011). It has common leaf morphology with *Maytenus ilicifolia*, *Maytenus aquifolium*, and *Sorocea bomplandii* or *ilicifolia* (VINICIUS et al., 2018; LEITE et al., 2001). Such therapeutically important plant and can be found in Tropical Atlantic Rain Forest (COELHO et al., 2003) with additional Brazilian states such as Paraná.

Other than the aforementioned four plants, according to the similar leaf structures as well as plant taxonomists from Herbarium of Curitiba-PR, Brazil some more plants also contribute similar leathery and spiny leaves. Due to the lack of reported data, these two plants are discussed briefly in the following sections and were investigated in the current work.

4.5 *Berberis laurina* BILBERG (BILB.)

Globally, the genus *Berberis* fits into a large family, Berberidaceae, that contain approximately 13 genera and 600 species, where *Berberis laurina* Bilb. (Figure 4.1. E; p. 30) is considered one of main parts among 500 species. The *B. laurina* is deciduous, shrub or small woody tree with spiny leaves, characteristic yellow flowers (BHARDWAJ et al., 2012). In accordance to the current investigation, *Berberis laurina* is about one and half meter taller in height and possesses highly stronger spines (~3 cm) on its trunk.

The *Berberis laurina* Bilb. is distributed in Northern hemisphere and Latin American countries including various regions of Southern Brazil, such as Paraná, Minas Gerais, São Paulo, Rio de Janeiro, Santa Catarina, Rio Grande do Sul and also in Argentina, Uruguay and Paraguay, commonly known as, Espinho-de-São-João, Espinho-de-São-João-Simão, São-João, Berbéris-da-terra, Quina-cruzeiro, Uva-de-espinho, Espina-amarilla and Palo-amarillo (LANDRUM, 1999).

The study from Bhardwaj et al (2012), resumed that roots, stem, and leaves of this plant contain multiple chemical compounds, for example, terpenoids, alkaloids including a characteristic Berberine and some further metabolites.

4.6 *Citronella gongonha* MARTIUS R. A. HOWARD

The genus, *Citronella* is main part of Cardiopteridaceae family that contain almost 20 species together with *Citronella gongonha* Mart. (VIANI et al., 2007), Figure 4.1. F; p. 30. It reaches up to eight meters in height and is woody, shrubby, and deciduous non-flexible plant (RODRIGUES et al., 2008). Similarly, it keeps characteristically flattened, harder and marginal spiny leaves, whitish-purple flowers with fragrance and slightly elongated oval brownish fruits (LORENZI 2009).

Citronella gongonha is commonly known as *Congonha*, Orange-plum, *Villaresia cuspidata* Miers.; *Cassine gongonha* Mart.; *Laranjeira-do-banhado*. The *Citronella gongonha* is broadly distributed and can be found in Southern Brazil such as Curitiba-Paraná, Irati, and Alto Rio Grande-Minas Gerais (RODRIGUES et al., 2008), in addition in Northern Argentina and Northern Uruguay. The phytochemicals investigation for this plant species are very restricted.

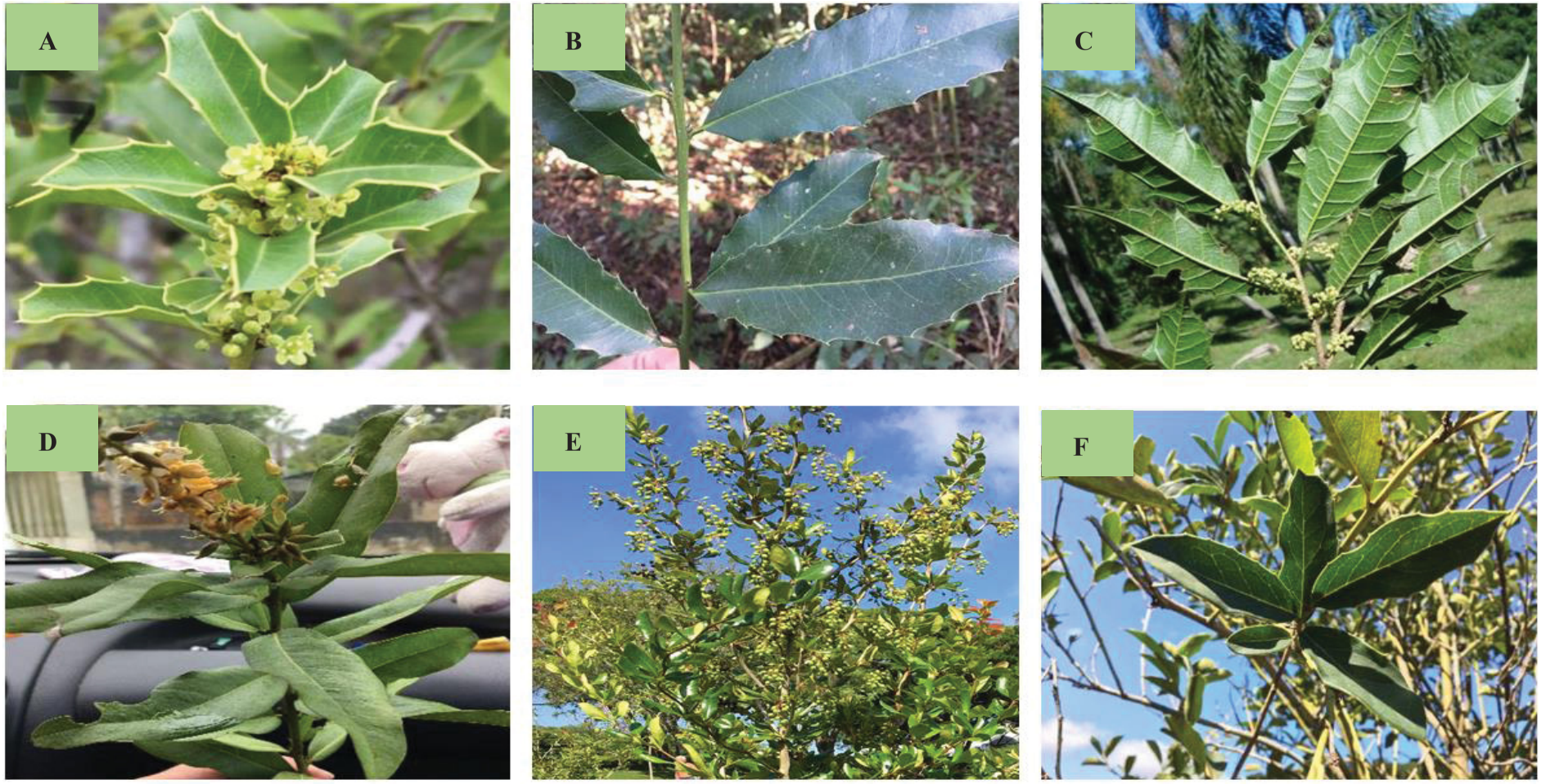

Figure 4.1. The plants species (**A**) *Maytenus ilicifolia* Mart. ex Reissek (**B**) *Maytenus aquifolium* Mart. (**C**) *Sorocea bomplandii* Bailon (bail.) W. C. Burger, Lanjouw & Boer (**D**) *Zollernia ilicifolia* (Brongn.) Vogel (**E**) *Berberis laurina* Bilb. (**F**) *Citronella gongonha* Martius R. A. Howard. All photos were taken by the auther (Sher Ali) and confirmed in herbarium of Curitiba (MBM in Table 5.1; p. 51), and accessible also in the given link; http://www.ufrgs.br/fitoecologia/florars/open_sp.php?img=1390.

Table 4.1. Chemical compounds, previously identified in the leaves from both *Maytenus ilicifolia* and *Maytenus aquifolium* (Celastraceae).

Plant	Class	Compounds	No.	Therapeutic use	Reference
Maytenus ilicifolia and *Maytenus aquifolium* **(Leaves)**	**Flavonoids & Flavanols**	3,5,7-trihydroxy-2-(4-hydroxyphenyl)-4H-chromen-4-one (**Kaempferol**)	**1**	Brain disorders Gastroprotective Antioxidant Anticancer Anti-inflammatory Diabetes Heart diseases Anti-obesity Anti-asthma Antiaging Antiallergic Antibacterial Anti-rhombogenic Antiatherosclerosis Hepato-protective Bone protective Antioxidant Antilisterial Antimicrobial	PÉRICO et al., 2018; VELOSO et al., 2017; IMRAN et al., 2018; **Error! Reference source not found.** et al., 2016; PREMALATHA et al., 2018; BAKOYANNIS et al., 2019
		5,7-Dihydroxy-2-(4-hydroxyphenyl)-4-oxo-4H-chromen-3-yl β-D-galactopyranoside **(Trifolin)**	**2**		
		2-(3,4-Dihydroxyphenyl)-5,7-dihydroxy-4-oxo-4H-chromen-3-yl β-D-galactopyranoside **(Hyperin)**	**3**		
		(2*S*,3*R*)-2-(3,4-Dihydroxyphenyl)-3,5,7-chromanetriol **(Catechin)**	**4**		
		(-)-Epigallocatechin-3-o-gallate **(epigallocatechin-3-gallate)**	**5**		
		(2*R*,2'*R*,3*R*,3'*R*,4*R*)-2-(3,4-Dihydroxyphenyl)-2'-(4-hydroxyphenyl)-3,3',4,4'-tetrahydro-2H, 2'H-4,8'-bichromene-3,3',5,5',7,7'-hexol **(Condensed tannin)**	**6**		
		2-(3,4-Dihydroxyphenyl)-5,7-dihydroxy-4-oxo-4H-chromen-3-yl6-O-(6-deoxy-α-L-mannopyranosyl)-β-D-glucopyranoside **(Rutin)**	**7**		
		3'-Methylquercetin 3-O-rutinoside **(Rutinosoid)**	**8**		
		Quercetin-3-O-rhamnoside **(Quercitrin)**	**9**		
		Quercetin 3-O-rhamnosyl-galactoside	**10**		
		Kaempferol 3-O-(2,6-di-O-α-L-rhamnopyranosyl)-β-D-galactopyranoside (**Mauritianin**)	**11**		
		Quercetin-3-O-α-L-rhamnopyranosyl-(1-->6)-β-D-galactopyranoside (**Mauritianin**)	**12**		
		Kaempferol tetrasaccaride	**13**		
		4'-O-methyl-(-)-epigallocatechin (**4-methylepigallocatechin**)	**14**		
	Steroids & Triterpenes	(4*R*,4a*S*,6a*S*,6b*R*,8a*R*,12a*R*,12b*S*,14a*S*,14b*S*)-4,4a,6b,8a,11,11,12b,14a-octamethylicosahydropicen-3(2H)-one (**Friedelin**)	**15**	Antitumor, anti-inflammatory	PÉRICO et al., 2018; ALVES et al., 2018; VELOSO et al., 2018; SINGH et al., 2019
		(3*R*,4R,5*S*,6a*S*,6b*R*,8a*R*,12a*R*,12b*S*,14a*S*,14b*R*)-4,5,6b,8a,11,11,12b,14a-octamethyldocosahydropicen-3-ol (**Friedelan-3-ol**)	**16**	-	
		(4*R*,4a*S*,6a*S*,6b*R*,8a*R*,12a*R*,12b*S*,14a*S*,14b*S*)-4,4a,6b,8a,11,11,12b,14a-Octamethylicosahydro-3(2H)-picenone (**Friedelan-3-one**)	**17**	-	
		(2*R*,6a*S*,14a*S*)-methyl 10-hydroxy-2,4a,6a,9,12b,14a-hexamethyl-11-oxo-1,2,3,4,4a,5,6,6a,11,12b,13,14,14a,14b-tetradecahydropicene-2-carboxylate (**Pristimerin**)	**18**	Antimicrobial, anti-leishmaniasis,	

				Anti-Chagas	
		(6a*S*,6b*S*,8a*S*,11*R*,12a*R*,14a*R*)-3-hydroxy-4, 6a,6b,8a,11,14a-hexamethyl-7,8,9,11,12,12*a*,13,14-octahydropicene-2,10-dione (**Tingenone**)	**19**	Antinociceptive stimulation	
		(3β,20*R*,22*E*,24*S*)-Stigmasta-5,22-dien-3-ol **(Stigmasterol)**	**20**	Antidiabetic, Immune modulatory	
		4-[6-[(3,5-dihydroxy-4-methoxyoxan-2-yl) oxymethyl]-3,5-dihydroxy-4-methoxyoxan-2-yl] oxy-2-(hydroxymethyl)-6-methyloxane-3,5-diol (**Arabinogalactose**)	**21**	-	PÉRICO et al., 2018
		(2*S*,3*R*,4*S*,5*R*)-2,3,4,5-tetrahydroxy-6-oxohexanoic acid (**Galacturonicacid**)	**22**	Anti-gastric ulcer	
		(*E*)-3,7,11,15-tetramethylhexadec-2-en-1-ol (**Phytol**)	**23**	-	
		(6*E*,10*E*,14E,18*E*)-2,6,10,15,19,23-hexamethyltetracosa-2,6,10,14,18,22-hexaene (**Squalene**)	**24**	-	
		(*R*)-2,5,7,8-tetramethyl-2-((4*R*,8*R*)-4,8,12-trimethyltridecyl)chroman-6-ol (**Vitamin-E**)	**25**	-	
		1-methyl-4-(prop-1-en-2-yl) cyclohex-1-ene (**Limonene**)	**26**	-	
		Palmitic acid	**27**	-	
		Lauric acid (Dodecanoic acid)	**28**	-	
		(2*E*)-3,7-Dimethyl-2,6-octadien-1-yl acetate **(Geranyl acetate)**	**29**	-	

Figure 4.2. Several chemical compounds, previously identified in the leaves of both *Maytenus ilicifolia* and *M. aquifolium*, each chemical compound is numbered that corresponds to table 4.1.

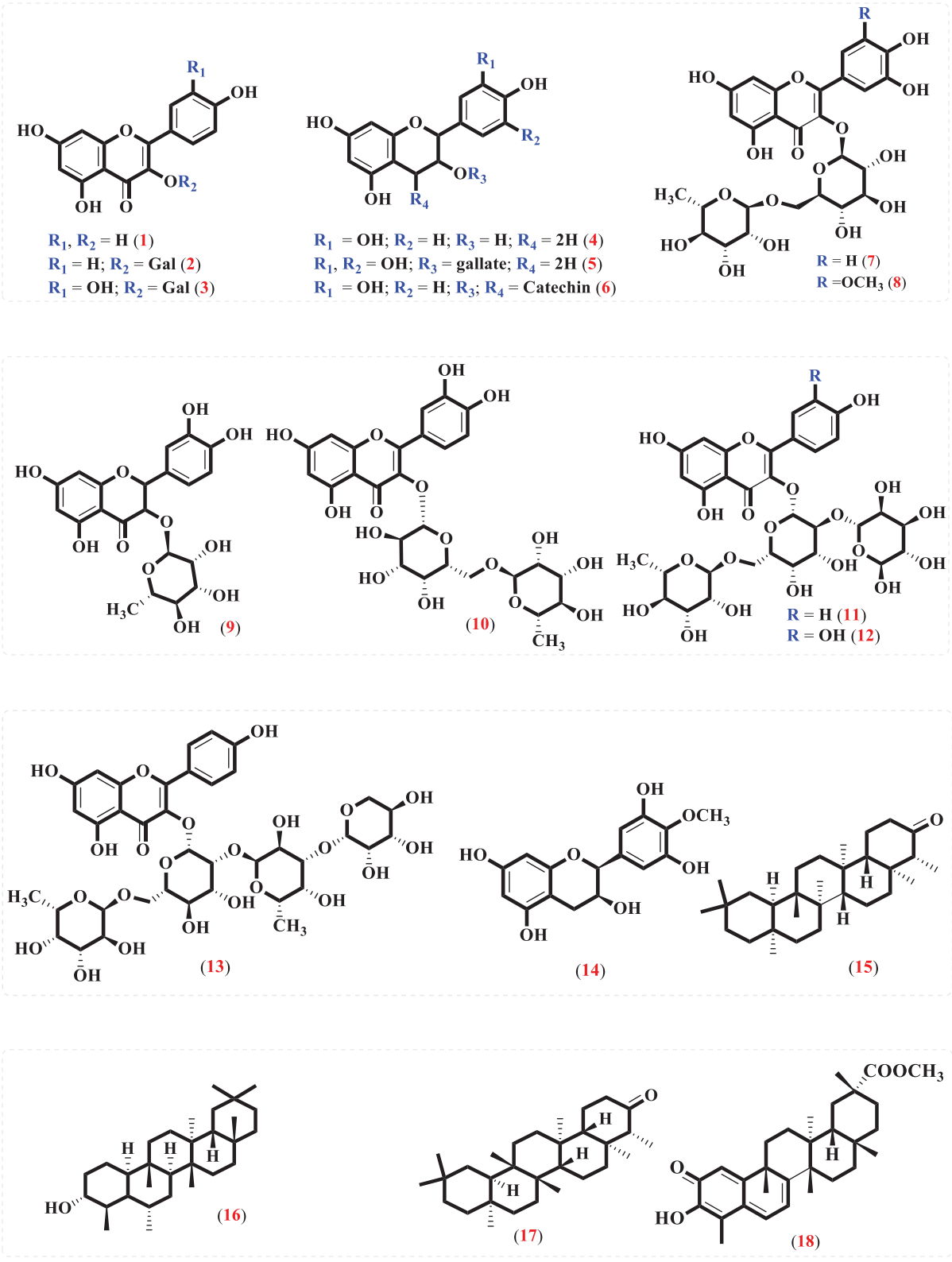

Figure 4.2. *Continued...*

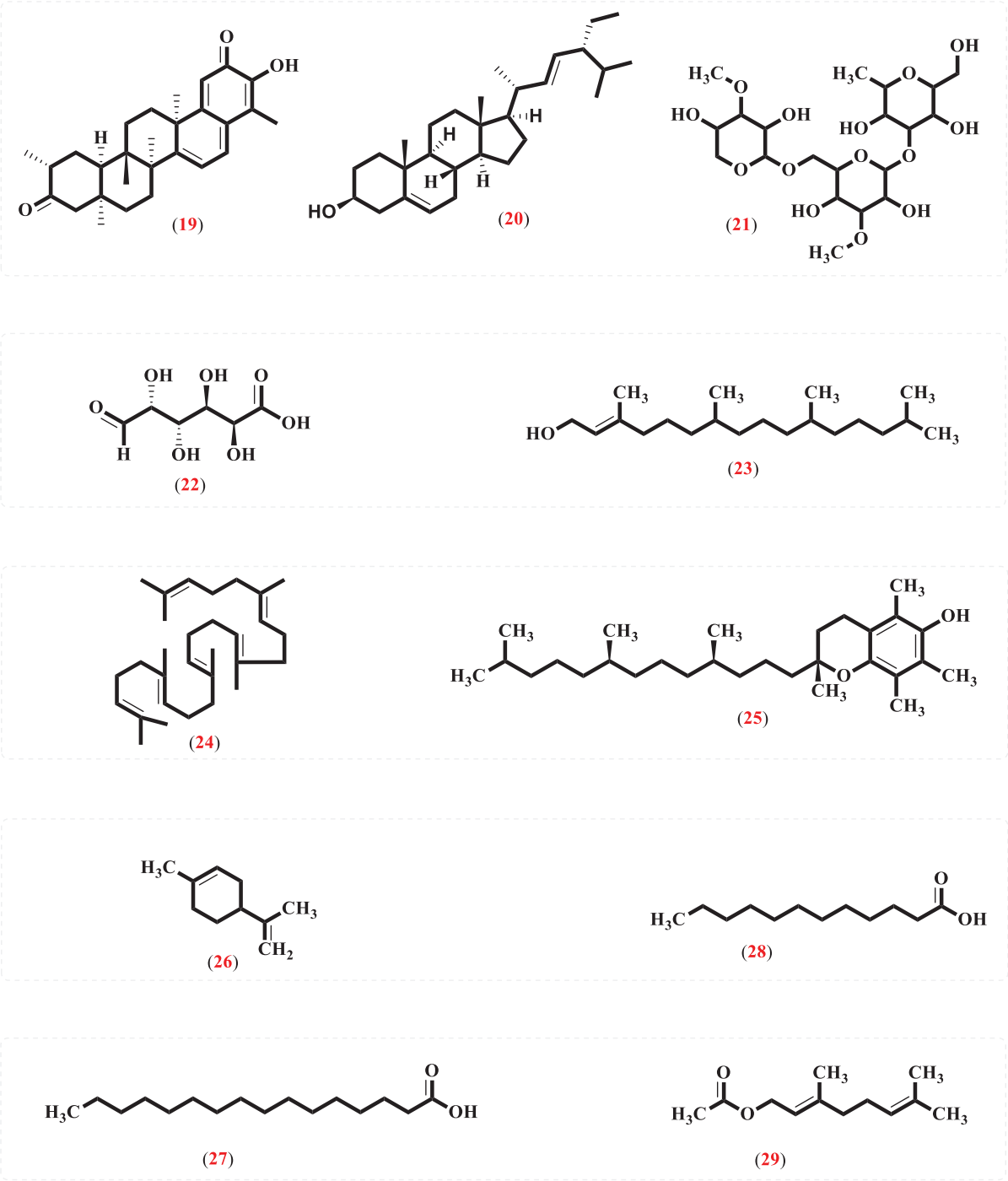

4.7 NUCLEAR MAGNETIC RESONANCE (NMR) SPECTROSCOPY

Nuclear Magnetic Resonance (NMR) spectroscopy is powerful analytical method generally applied in different laboratorial and large-scale industrial investigations. NMR phenomena was first presented in 1945-1946, when paraffin wax and water were studied by Edward Mills Purcell and Felix Bloch, and their groups, respectively. The pioneers of modern NMR spectroscopy, Felix Bloch and Edward Mills Purcell described the nuclear magnetic precision measurements and were awarded the Noble Prize in 1952. The physical chemist, Richards Ernst was awarded Noble Prize in 1991 for his great contributions in the field of high-resolution NMR methodology. In 2002, the chemist/biophysicist Kurt Wüthrich was awarded the Noble Prize, on discovering NMR-based three-dimensional structure of macromolecules in solution. While recently, the physiology or medicine Noble Prize in 2003 was jointly awarded to Sir Paul Christian Lauterbur and Peter Mansfield with a discovery associated to Magnetic Resonance Imaging (MRI).

NMR spectroscopy is a versatile non-destructive and commanding analytical tool, used in the characterization of multiple products in manifold researches. Broadly, all types of NMR approaches focus to study the resonance states of magnetized atomic nuclei (e.g. ^{1}H, ^{13}C, etc.) in both homogenous and heterogenous states, by exposing the material(s) into applied large magnetic field ($\mathbf{B_0}$) (KOKOVA et al., 2019). In other words, NMR relies on the bulk magnetization (total sum of all microscopic magnetic moments) of NMR active atomic isotopes in the material(s) (LEVITT, 2015).

NMR is an ideal approach, which can be applied in different ways to solid-, semi-solid and liquid-state, depending on the state of materials. Except other type of materials and methods, here the semisolid materials were studied by ^{1}H high-resolution magic angle spinning (HR-MAS) NMR spectroscopy that is briefly described with additional applications.

4.7.1 High-Resolution Magic Angle Spinning (HR-MAS) NMR spectroscopy

The solid-, semi-solid and liquid-state NMR spectroscopic methods uses different probe heads with multiple frequency channels e.g. cross polarization magic angle spinning (CP-MAS), high-resolution magic angle spinning (HR-MAS) and Liquid state (BBI, BBO, and so on). These methods entail different matter states with and without NMR solvent(s).

In solid-state NMR experiments, a minute quantity of pure solid (crystalline powder) material (without solvent) is packed in MAS rotor (e.g. 4-mm) to perform acquistion.

Although, in HR-MAS NMR, a small amount of semi-solid sample and locking solvent are packed in the MAS rotor (e.g. 4-mm), and measuements are performed on gel-like state of sample. However, in liquid-state experiment, sample is extracted or solubilized in several hundred microliters of deuterated solvent (~600 µL), followed by NMR measurements. In liquid-state NMR based plants studies, the sample is prepared in various steps of extraction and purification, possible information loss such as partial extraction of metabolites can happen, dependent on extraction protocol. Other than incomplete extraction, longer preparation procedure can offer spectral artifacts, as detected in the plant metabolomics (SAUERSCHNIG et al., 2018). In plant metabolomics, it is optimal to perform acquistions as soon as possible to investigate complete profile without changes in the chemical state in targeted material(s). The complete information is possibly obtained under more controlled experimental protocols and or to study the target sample in its original state with little efforts. The complete chemical compositions can be completed, alterantively by High-Resolution Magic Angle Spinning (HR-MAS) NMR spectroscopy.

High-Resolution Magic Angle Spinning (HR-MAS) NMR requires minimal sample quantity in its natural, or gel-like state which can be achieved by adding minute quantity of deuterated solvent that is useful to (provide molecular mobilities and) lock the magnetic field. The small amounts of material and locking solvent are prepared and tightly packed in MAS (4-mm) rotor using fundamental accessories (Figure 4.3) to perform the experiments.

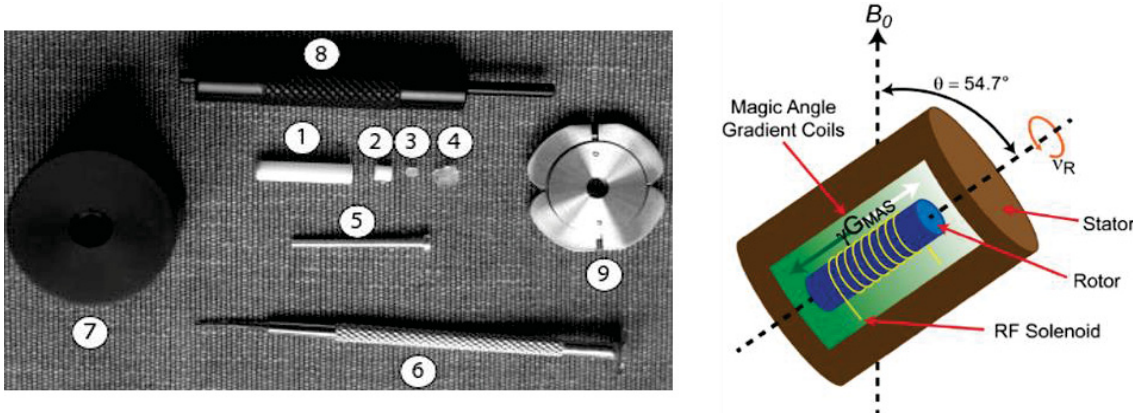

Figure 4.3. Schematic presentation of all accessories used as HR-MAS 4 mm rotor (1), spacer (2), thead pin (3), cap (4), screw (5), screw driver (6), rotor packer (7), depth gauge (8), cap remover (9) and stator part showing magic angle gradient along the rotor spinning axis (ALAM et al., 2012).

The HR-MAS NMR technique perform experiments of complex heterogenous samples to obtain similar high-resolution spectra as those acquired from homogeneous ones. As an example, a comparative general demonstration is given (Figure 4.4) that shows two spectra

recorded with same spectrometer from same material in its extracted homogenous (liquid-state) and original heterogenous (semi-solid) state.

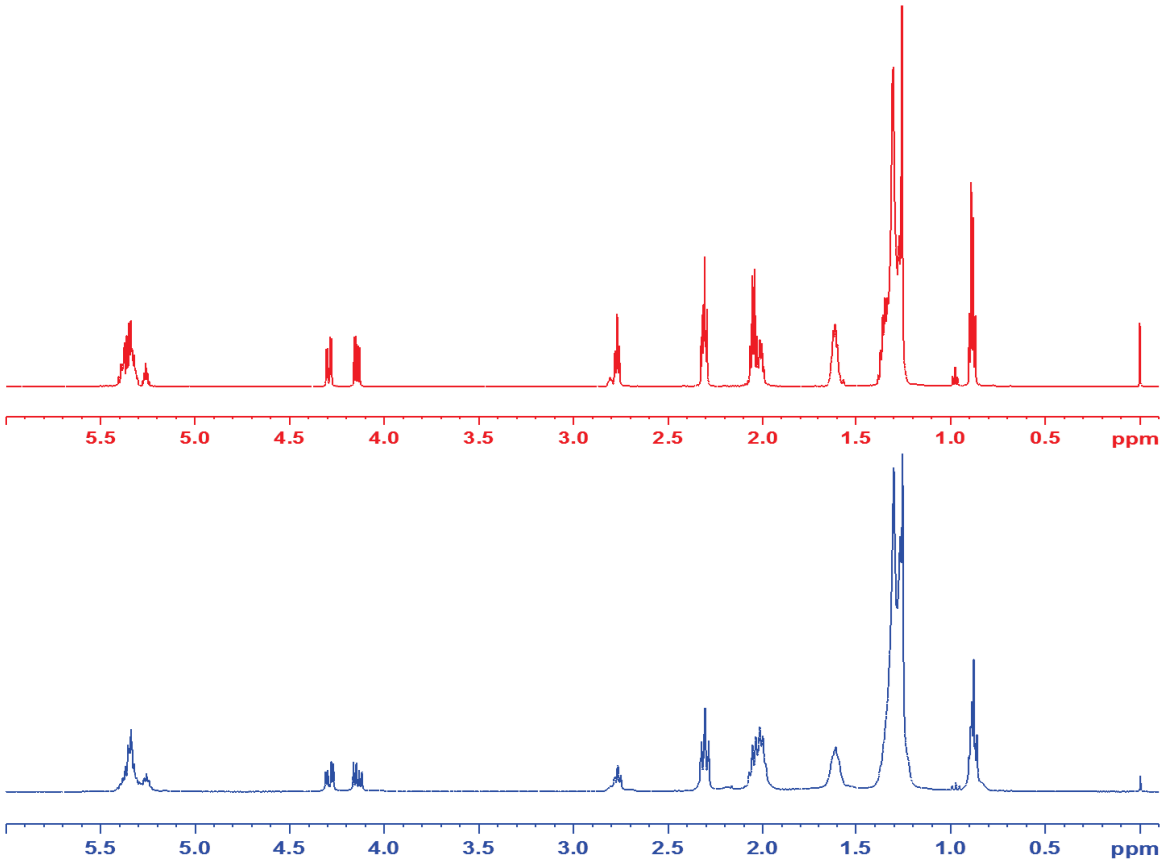

Figure 4.4. The comparative spectra (^1H = 400.13 MHz; $CDCl_3$) from soybean in homogenous or oily extract (red spectrum: liquid-state) and heterogenous or semisolid pwdered grains (blue: HR-MAS).

Moreover, HR-MAS NMR tool provides direct insight into the molecular system to locate approximately all detectable magnetic spins (e.g. ^1H) in original state of sample. To imagine an internal microscopic environment in semi-solid (anisotropic) samples, several unwanted factors are potentially present that make spectral interpretation difficult. These small microscopic components are dipole-dipole interaction between closed spins, chemical shift anisotropy, and the magnetic susceptibility differences. Prior to describe these typical trends in the sample lets briefly overview relaxation time constants affecting from the anisotropic medium, for example spin-lattice (or longitudinal) T_1, and the spin-spin (or transverse) T_2 relaxation.

Phenomenologically, once the applied B_1 (or RF-pulse) field is switched off, magnetization does not precess finitely in the transverse plane, since, it returns back to the equilibrium state with respect to time. The bulk or net magnetization vector of all detectable microscopic spins in sample, re-establishes equilibrium state longitudinally (*z*-axis), governed

by T_1, simultaneously, depashing or coherence loss along *x,y*-plane of transverse component take place during T_2 relaxation (CLARIDGE, 2016; BAKHMUTOV, 2005) as shown in Figure 4.5. In T_2 mechanism, the magnetic vectors in *x,y*-plane generate oscillating field tracked by the electronic receiver coil as FIDs, followed by Fourier transformation into signals (SILVA et al., 2012). Small amounts of undetectable energies are lost within the sample surrounding during T_1 while T_2 relaxation characterizes the dephasing (or decaying) of signals in receiver coil in the probehead. Analogously, the T_1 and T_2 are termed as spin-lattic (or longitudinal) as well as spin-spin (or transverse) relaxation time constants.

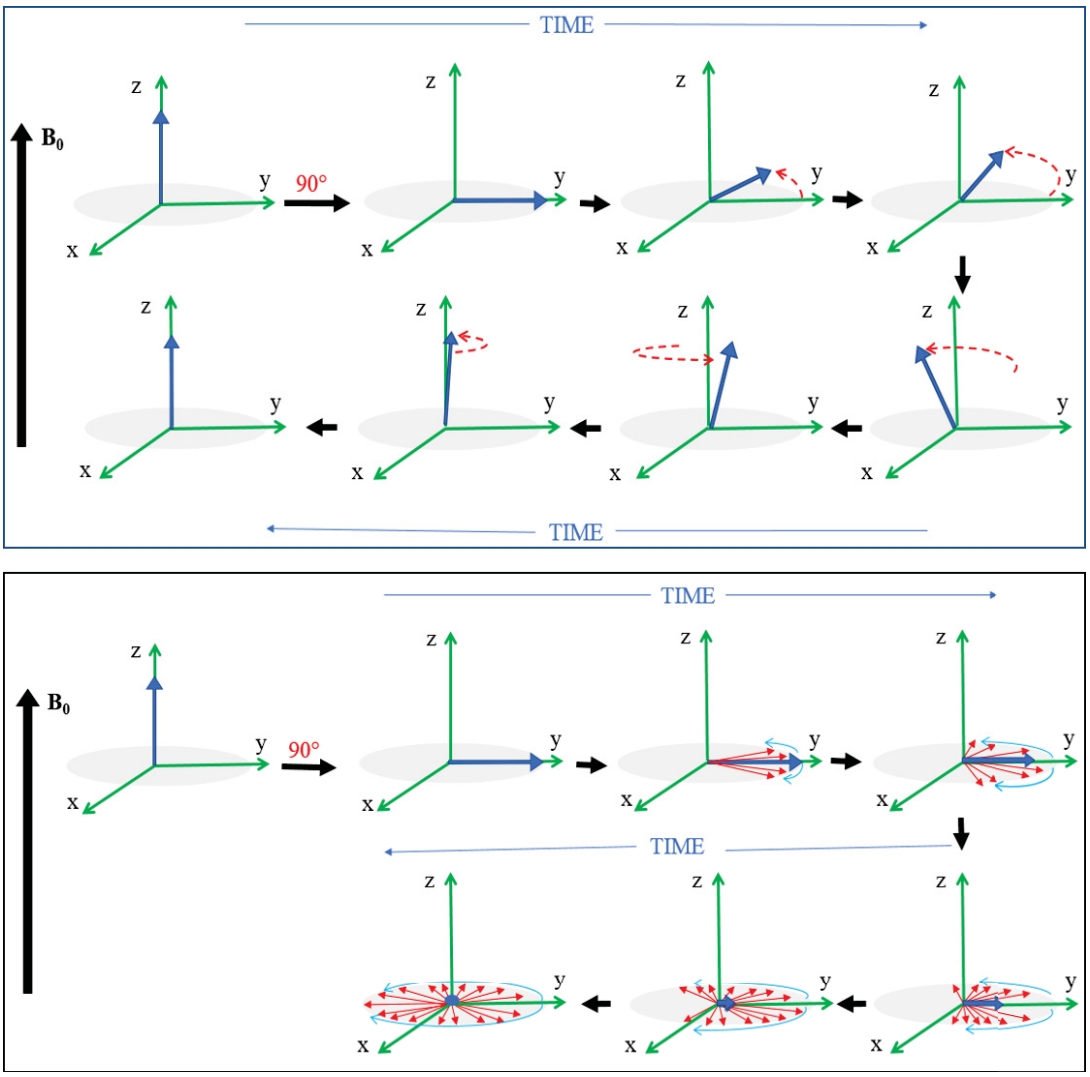

Figure 4.5. Vectorial representation of spin-lattice (or longitudinal) T_1 relxation (upper) and the spin-spin (or transverse) T_2 relxation (downward image). At first the net magnetization (blue bold-faced arrow) along $\mathbf{B_0}$ in both cases is followed by 90° tip angle applied for short time (µsec), in intitial mechanism the net magnetization fall on the *x,y*-plane, after switching off B_1 (RF) the net magnetization vector returns its original state in a spiral way (shown by red dotted arrows) with a specific time (T_1). However, in the second case the resultant vector along *x, y*-plane starts dephasing (decaying) with respect to T_2, where the vector slightly decreasing with time and finally zero ($Mxy = 0$).

Generally speaking, relaxation times have substantial contribution to signal resolution and sensitivity in NMR experiments. The relaxation time constants (i.e. T_1, T_2) are strongly affected by molecular mobililities and static (or restricted) condition in materials (liquid, semi-solid and or solids). In liquids, owing to rapid molecular motions (tumbling, rotation, and so on) usually the $T_1 \geq T_2$, where motional frequencies of spins get closer to the Larmor precessional frequency ($\boldsymbol{\omega_0}$) that result highly sharp NMR signals (CLARIDGE, 2016; BAKHMUTOV, 2005). Contrarily, in semi-solid (and or solid) materials, molecules literally present in constrained environment with limited molecular motion. The restricted conditions do not permit mobile situation and reduced in T_2 relaxation time of the spins due to very close proximities. Molecular limited mobilities decrease spectral resolution causes line broadening, and poor sensitivities (lower intensities) in (HR-MAS) NMR spectra (TENG, 2013).

As stated previously, the obstructive trends hinder molecular movements and its NMR frequency in comparison to isotropic medium when exposed to external magnetic field ($\mathbf{B_0}$) (JENSEN et al., 2019; WONG et al., 2018). Indeed unwanted dipolar interactions (between proximal nuclei), fluctuating magnetic susceptibility and chemical shift anisotropic (Figure 4.6) are leading factors causing poor resolution and signals broadening (FLORES et al., 2018; WONG et al., 2018; MAZZEI et al., 2018; FAROOQ et al., 2013; ALAM et al., 2012).

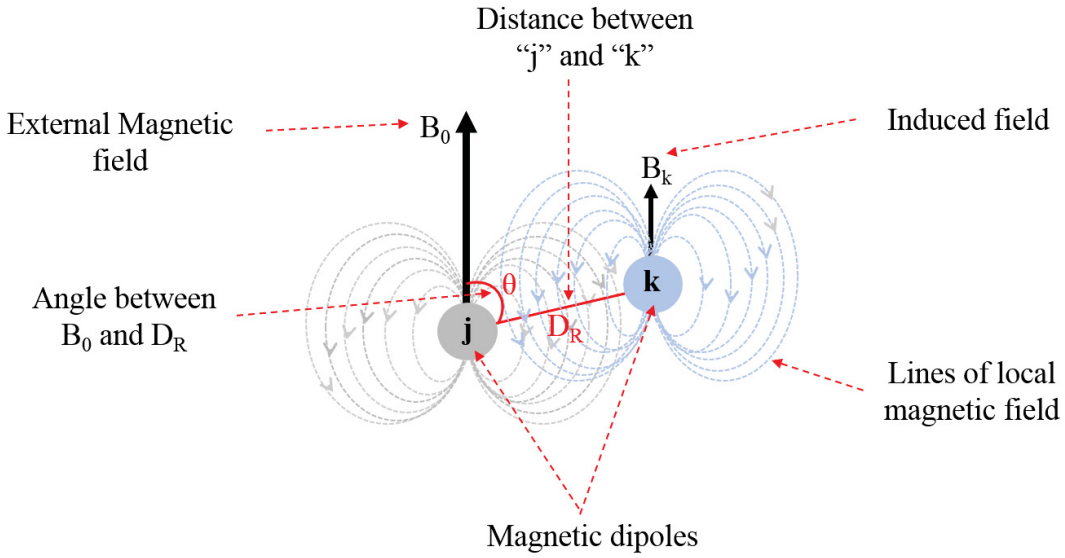

Figure 4.6. The illustration of "$3cos^2\ \theta$-1" effect between two (j and k) imaginary magnetic dipoles and their influences on each other in the presence of an external applied magnetic field ($\mathbf{B_0}$). **Source**: WONG et al., 2018; JENSEN et al., 2019; FAROOQ et al., 2013.

This ideal picture could be imagined in plant matrices, where molecules present in bound conditions surrounded by distinct boundaries in the cell (e.g. cell wall and cell

membrane) which do not allow atoms to be fully magnetized inside "**B_0**", thus fluctuation in magnetic susceptibility arises. The imbalance in magnetic susceptibility furthermore affects locally induced magnetic field of other nearby spins (j, k) separated at certain distances (D_R) (Figure 4.6), thus, unwanted shift and signal-broadening arise. Magnetic susceptibility, is a measure (higher/lower state) of magnetization produced in a spin in the presence of applied magnetic field (**B_0**) "or" the response of spins to the applied magnetic field (if, $X > 0$; spins alignment; or $X < 0$; opposition to **B_0**). HR-MAS NMR technique can minimize such effects by positioning sample at the so-called magic angle providing spinning along **B_0**, such as $\theta_{MAS} = 54.74°$ (WONG et al., 2018; FAROOQ et al., 2013) shown in Figure 4.7.

The broadening effect can be lessened more, if magic angle spinning condition is implemented to the sample swollen in appropriate NMR solvent to support internal motions of magnetic dipoles and additional gain in signal resolution (FAROOQ et al., 2013; ALAM et al., 2012). However, this mechanism can be realized when the MAS rotor is packed with swollen sample, and positioned it at the magic angle spinning ($\theta_{MAS} = 54.74°$) in the HR-MAS probehead (GOGIASHVILI et al., 2019; SERKOVA et al., 2019; FLORES et al., 2018; WONG et al., 2018; MAZZEI et al., 2018; ALAM et al., 2012; FAROOQ et al., 2013) as given in Figure 4.7.

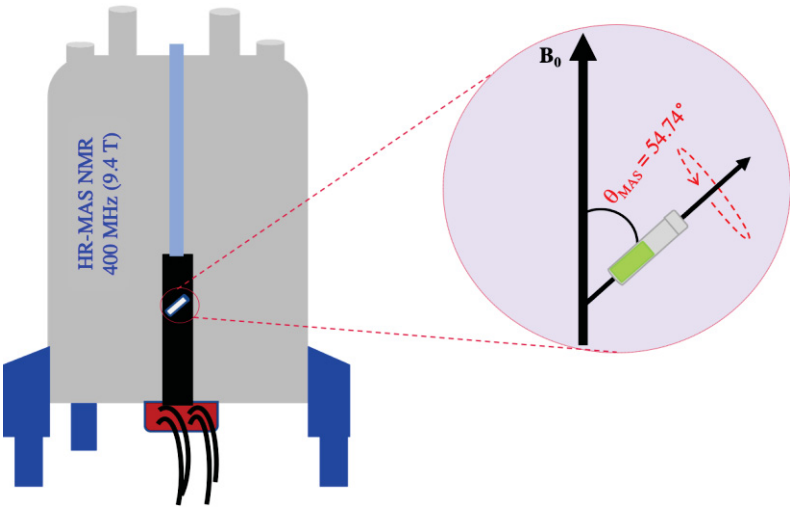

Figure 4.7. Overview of NMR spectrometer (400 MHz) equipped with a 4-mm HR-MAS probehead and magnified picture showing Magic Angle Spinning ($\theta_{MAS} = 54.74°$) around the direction of externally applied magnetic field **B_0** (right). **Source**: JENSEN et al., 2019; WONG et al., 2018; FAROOQ et al., 2013.

Notably special care is neccessary (to avoid increase in sample temperature, molecular degradation as well as rotor disruption) to provide high magnitude of spinning speed (ALAM et al., 2012). Finally, all broadening factors, dependent on second-order Legendre polynomial,

"P_2 (cosθ) = ½ (3cos^2 -1)" can be removed or reduced when θ = 54.74°, thus "P_2 (cosθ) = 0" (FAROOQ et al. (2013). HR-MAS NMR spectroscopy has achieved great attention in multiple disciplines. There are several applications such as fingerprints based floral sequences characterization in *Ribes nigrum* (PAGTER et al., 2017), passion fruit (*Passiflora alata* Curtis), cherry (*Eugenia uniflora* L.), and acerola (*Malpighia emarginata* DC.) (FLORES et al., 2018). NMR in foodomics, meat, fish, cereals, dairy products, fruits and vegetables (MAZZEI et al., 2017), maize seed (MAZZEI et al., 2018), lemon juice characterization (CICERO et al., 2015). Characterization of Illicit drugs and its identification in tablets and in blotter papers (SOUZA et al., 2016). NMR applications in human studies (GOGIASHVILI et al., 2019; SERKOVA et al., 2019; ALAM et al., 2012) and many more can be found elsewhere (JENSEN et al., 2019).

4.8 METABOLOMICS AND ANALYTICAL METHODS

Prior to describe analytical procedures, it is desired to briefly discuss "metabolomics". In the 1940s, Roger Williams suggested, "metabolic profile", the biological components in every individual, and was continued to investigate since paper chromatography was used and led the identification of body fluids (urine, saliva). Pauling and coworkers suggested several proposals that the quantitative measure of metabolites in biofluids may define functional status of biological system (PAULING et al., 1971). This newborn concept of "metabolic profiling" was reported for the first time by Horning and his team in 1971, using gass chromatography-mass spectrometry (GC-MS) (HORNING et al., 1971). Later on, the term "metabolome", used for the first time by Oliver et al. (1998), and was furthermore elaborated into "metabolomics", in a study conducted by NMR spectroscopy coupled to multivariate statistical analysis (NICHOLSON et al., 1999).

As powerful approach, metabolomics is supportive in the diagnosis of diseases as cancer, metabolic mechanisms, drugs, nutrition, and agronomy (YANG et al., 2019). In plant research, metabolomics can extensively summarize plants phenotypical, morphological, protein, and metabolites information, utilizing functional genomics (XIA et al., 2020; WANG et al., 2020), and system biology (PATHAK et al., 2019; KHALID et al., 2019; MOSCHEN et al., 2019).

Metabolomics, the wide-ranging scientific examination of all small organic molecules in "metabolome". Metabolome, is a composite assembly of various small organic primary and secondary metabolites, considered to be the intermediate and or end products of multiple

(bio)chemical processes taking place within cell, tissue, and or organ of a plant and or human organism linked to its environment (MATICH et al., 2019; SIMMLER et al., 2018; SAMPAIO et al., 2016).

Metabolomic studies involve several fundamental segments (JAHANGIR et al., 2018): initially the pre-analytical treatment or sample handling which is vital to stop chemical pattern variations by quenching biochemical process followed by drying, storage and so on. In second step, the pre-handled samples are submitted to the analytical methods such as NMR, MS, chromatographic, or other corresponding technique. Similarly, the final stage intitiate by the interpretation of raw data (from NMR, MS, etc.) through multivariate statistical approaches, e.g. principal component analysis (PCA) (JAHANGIR et al., 2018) to obtain further details.

Metabolomics have been indispensable role in several field of researches like quality control of botanicals, and dietary supplements (CAGLIANI et al., 2017; BAZAZ et al., 2017), environmental (QIAO, et al., 2019), and identification of biomarkers responsible to various diseases (LUAN et al., 2017). The quality control, adulteration management and authenticity are extensively covered by molecular separation alone and or coupled to detection methods. For example, High Performance Thin Layer Chromatography (HPTLC), Liquid Chromatography (LC), Liquid Chromatography-Ultra Violet (LC-UV), Liquid Chromatography-Mass Spectrometry (LC-MS), Gas Chromatography-Mass Spectrometry (GC-MS), Nuclear Magnetic Resonance (NMR) (SIMMLER et al., 2018; LEE et al., 2017), and many other analytical approaches (BALLIN et al., 2019; ABBAS et al., 2018). Every analytical technique has different application encompassed (dis)advantages, since NMR and MS are two complementary and widely used approaches in metabolomic investigations.

Throughout analytical methods, NMR provides main advantages over spectrometries and chromatographies, such as simple sample preparation, whithout derivatization and or separation as require in HPLC or HPTLC, MS or GC-MS, or CE (LIEBEKE et al., 2019; ZHOU et al., 2019; AGATONOVIC-KUSTRIN et al., 2019). NMR advantages can be noted by sample recovery, simultaneous detection of multiple metabolites of various classes even in different concentrations, quantitative nature, high reproducibility and repeatability, and precise structural information (VERHOEVEN et al., 2017; WISHART, 2008).

In the case of sensitivity, MS is more sensitive (picomolar range detection) in comparison to NMR (molecular traces detection up to micromolar range), but the use of NMR can be boosted by attaining accurate structural information from chemical compounds (YUN et al., 2018; LEE et al., 2017). In metabolomic, metabolic fingerprinting and profiling

techniques are mostly assessed through both NMR and MS platforms (KOOY et al., 2009), so far chemometric methods are coupled to similfy results obtained via fingerprinting approach (SIMMLER et al., 2018). In order to realize quality control, instead targeted approach it is necessary to execute global fingerprinting to achieve maximum molecular information from the system under study (TRIMIGNO et al., 2015).

4.8.1 Metabolic fingerprinting and NMR spectroscopy

Plants are biological machineries that produce varieties of molecular fingerprints (sugars, organic acids, phenylpropanoids, alkaloids, terpenoids), participating in multiple endogenous (biochemical processes) and exogenous ((a)biotic) mechansims along lifespan. The endogenous mechansims are metabolic pathways associated to the biogenesis of primary and secondary metabolites that are responsible for plant growth and environmental adaptation (FANG et al., 2019) against exogenous (a)biotic interactions as temperature, sunlight, shade, humidity, herbivores, and others (SAIJO et al., 2020). These (a)biotic interactions persuade quantitative shift in normal metabolic states, reflecting variations in the chemical substances and their properties, and plant growth. This means that, environmental trends crucially affect genotype associated to plant morphology (AKILAN et al., 2019), and molecular biogenesis (SHEN et al., 2019). Quantitative variations in flavonoids, flavanols (catechins) organic and phenolic acids, and carbohydrates have been reported from intense sunlight (LI et al., 2020), shady conditions (XU et al., 2020), temperature variabilities, rain fall, humidity, seasonal and geographical orientations (WEN et al., 2020), and herbivores interactions (LI et al., 2020).

In addition to plant nourishment, coloring, scent, and defense, the primary and secondary metabolites possess characteristic dietary, neutraceutical and therapeutic standards (KHAN et al., 2019; BAKOYANNIS et al., 2019; FREIRE et al., 2018; PREMALATHA et al., 2018; IMRAN et al., 2018; ALAMGIR., 2017), which are changeable in inconvenient ecological conditions. Several studies underpinned quantitative and qualitative metabolic variations due to high CO_2 flux to the leaves from *Camellia sinensis* L, studied by quantitative Polymerase Chain Reaction (qPCR) and statistical analysis (LI et al., 2017). Soni et al. (2015), perceived manifold decrease in several metabolites and their biological activities, caused by season, temperature, water, and sunlight. In a GC-MSD-based study by Mossi et al. (2009) revealed that temperature, geomorphology, altitude and latitude highly affected the leaf polyphenol profile in *Maytenus ilicifolia* and *Maytenus aquifolium* Mart. (Celastraceae). This demonstrates that plants undergo through several growing stages; however, time to time

molecular variations are possible (RIACHI et al., 2018). Resuming environmental impacts to chemical pattern, it is essential to monitor plant system along its development (KIM et al., 2011), which is useful to trigger-out further proposals to quality measurements.

To gather and use such information in plants quality control establishment, needs metabolomics studies by integrated analytical approaches e.g. spectrometry, spectroscopy and or coupled them to multivariate analytical tools. Metabolomics based diagnosis are mostly completed by metabolic profiling (targeted) and fingerprinting (non-targeted) methods. Metabolic profiling measures the qualitative and quantitative nature of particular up to a range of targeted compounds, however, fingerprinting can outline global (whole) chemical status in the samples (PATTI et al., 2012). These approaches are useful in complex systems, such as to discriminate quality of botanicals products (LEE et al., 2017), although fngerprinting is more preferred method (KHARBACH et al., 2020; XIE et al., 2006). Metabolomics fingerprinting is usually carried out by integrated analytical methods of NMR (and MS) coupled to (un)supervised multivariate methods (KRISHNAN et al., 2004).

NMR-based metabolic fingerprinting, is believed to be suitable method to distinguish between correlated samples (KRISHNAN et al., 2004) based on all measurable endogenous metabolites in the matrices by considering associated (a)biotic features. In addition to environmental toxicity and pollution, NMR fingerprinting can describe, genotype allied to phenotypes, origin-based classification, and comparison between smaller lichens, mosses, and higher plants of *Taraxacum officinalis* and *Populus nigra* (DJINGOVA et al., 2004). NMR spectroscopy has prompted to characterize Brazilian roasted coffee (TOCI et al., 2018; CONSONNI et al., 2012), plants authenticity (SIMMLER et al., 2018), leaves and flowers metabolome in *Tussilago farfara* L. (ZHI et al., 2012), origin-based distinction in leaf metabolome of soybean (YUN et al., 2018), banana (YUAN et al., 2017), food and drink products (KUBALLA et al., 2018).

To consider the abovementioned details related to metabolites, and their association to environment, complete molecular profile was covered by fingerprinting approach. In this study, HR-MAS NMR-based fingerprinting was adopted to establish quality control of *Maytenus ilicifolia* Mart. ex Reissek (Espinheira-Santa). *Maytenus ilicifolia* Mart. (Espinheira-Santa) is one of therapeutically important Brazilian plants. Based on therapeutic actions in chronic ulcers in stomach and intestine, Espinheira-Santa is legalized by the Brazilian Health Regulatory Agency (ANVISA), and Unified Health System (SUS) (PÉRICO et al., 2018; CARVALHO et al., 2018).

In fact, due to the therapeutic importance and official permission, this species is largely consumed in Brazil. For example, 160-ton plant materials are marketed per annum, however, ~21% of these products are found *Maytenus ilicifolia*, and or *M. aquifolium*, with further adulterantion of other plants (CALDAS et al., 2019; PÉRICO et al., 2018). This adultration might be due to the similar leaf morphology of *Maytenus ilicifolia*, which is challenging to simply distinguish it from other plants (mentioned above). The solution to figure out real *Maytenus ilicifolia* among natural similar plants, and commercial products of related plant can be achieved through chemical analysis or fingerprinting by HR-MAS NMR.

^{1}H HR-MAS NMR profiles from *Maytenus ilicifolia* may contain more information that are complex to attain simply by spectra. In this case, unsupervised principal component analysis (PCA) as one of chemometric techniques (JAHANGIR et al., 2018; SIMMLER et al., 2018) can be coupled to ^{1}H HR-MAS NMR. In statistical point of view, ^{1}H HR-MAS NMR observations should be preprocessed to remove artifacts, signals mismatch, or other errors in the spectra. There are several preprocessing methods, to correct ^{1}H HR-MAS NMR data before performing principal component analysis (PCA).

4.9 NMR DATA PRE-PROCESSING AND PRINCIPAL COMPONENT ANALYSIS (PCA)

In NMR experiment, the free induction decays (FIDs) are time-domain data that can be Fourier transformed into its readable frequency domain (spectra). Initially the spectra are zero-filled (apodization), zero-, and first-ordered phase corrected (manually\ automatically) to eliminate baseline distortions and reference to the signal from internal reference standard (e.g. TMS signal at δ 0.00). The ^{1}H HR-MAS NMR-based metabolomics data are typically made up of tens of thousands of small digital data points or variables (e.g. 131072) that typically construct spectra and tens or hundreds of objects representing botanical (natural) samples.

The botanical samples constitute multiple types of organic molecules such as the aromatic, carbohydrates, and aliphatic compounds with various functional groups. These small organic molecules in botanical material can be characterized utilizing a well-known NMR spectroscopic method. All NMR active nuclei in organic molecule can be traced by their precise signals at specific frequency positions (in ppm) in ^{1}H HR-MAS NMR spectrum.

The ^{1}H HR-MAS NMR spectra of botanical samples consist series of shifted signals from precise frequencies positions, due to differ molecular state (e.g. acidic or basic) and or possibly from other factors. There are several factors like, uncontrolled pH, ionic strength (Cu^{2+}, Mn^{2+}, Fe^{2+}, Fe^{3+}), sample different amount, molecular concentration and dilution,

unstable temperature, imperfect shimming (TMS signal at FHW > 1.0 Hz), tuning-matching, imperfect pulse sequences, acquisition and parameters (RG, NS, etc.) leads into signals misalignments and misleading spectral interpretation (DEBORDE et al., 2019; ZACHARIAS et al., 2018). To overcome unwanted spectral artifacts, observations from desired sample(s) should accomplish multiple (triplicate or more) time. Moreover, in case, if there were still present signals mismatch across the spectra, vitally NMR data ought to be preprocessed (ZACHARIAS et al., 2018) by binning, alignment, normalization, scaling, etc. to perform principal component analysis (PCA).

4.9.1 Binning (bucketing)

The binning (also called bucketing) is a process in which the whole ^{1}H HR-MAS NMR spectra are divided into equal small segments (chemical shifts), where each bin corresponds to the chemical shift (δ = ppm) values of signals in the spectrum. Basically, the bin size of a specific range (e.g. 0.03 to 0.04 ppm) justifies to capture and enclose the related small variations in peak positions and furthermore filters out signal noises across NMR data prior to performing the multivariate analyses.

4.9.2 Alignment

Alignment is additional method to adjust shifted signals in the NMR spectra. There are different alignment methods such as; dynamic time warping (DTW) and correlation optimized warping (COW). These alignment methods are generally used to chromatographic spectra and this is not a good option to use in NMR, because it stretches and compresses peaks and spectral baselines (EUCEDA et al., 2015). Moreover, signal misalignement corrections can be done algorithmatically using "*interval correlation shifting* (*icoshift*)", that use Fast Fourier Transformation (FFT) correlation engine to simultaneously aminupulate artifacts from entire spectral profiles (SAVORANI et al., 2010).

4.9.3 Normalization (row-wise operation)

Plant primary and secondary metabolites may vary in concentrations level according to environmental conditions, and can happen also from unequal amount measurements during sample preparation steps (EUCEDA et al., 2015). Plants generally correlated to its influential environment, which cause variations in molecular productions in different quantity ranges.

However, NMR profiles of botanicals may contain diverse siganl intensities associated to (higher or lower production of) same or different metabolites affected by seasonal varaitions, ecological contacts, and or due to samples random quantities, dilution factor, and so on. These effective characterisitis can be traced directly from signal relative intensity in NMR spectra. In statistical modeling, NMR profiles should be equivalent or without artifacts that can be removed through and normalization (and also scaling), prior to perform chemometric analyses.

In NMR profiles, the undesired regions e.g. noise, residual water, acetone, solvent should need to eliminate in the spectra, hence, to operate normalization to the total intensity (total area) (EUCEDA et al., 2015). As specified by Craig et al. (2006), normalization is a row-wise operational method that applies through the buckets table generated from NMR spectra (rows) and spectral intensities or chemical shifts (columns). Normalization can be carried out to the total intensity (area) of all signals from entire molecular components (fingerprints) in NMR measurements. Total intensity normalization to spectra (buckets), prevent artificial differences of intensities in botanical spectra due either to different factors as acquisition and processing of the spectra or to variability in concentration of metabolites. In normalization, intensities of *n*-variables (*n*-signals of *n*-digital points) in the spectrum (row-wise) in the table are initially summed to calculate the sum value and then every individual variable (signal's) intensity is divided by the calculated sum value (EUCEDA et al., 2015) to normalize the spectral data, as mentioned in a general example of several variables (Figure 4.8). In this general example are shown only few variables affected by sample(s) different amounts (mg).

Sample weight (mg)	Signals intensities			Sum
	Variable 1	Variable 2	Variable 3	
7.5	5.1	13.35	3.15	21.6
15	10.2	26.7	6.3	43.2
22.5	15.3	40.05	9.45	64.8

Intensity of each variable → divide by sum

Normalized signals intensities		
Variable 1	Variable 2	Variable 3
0.2	0.6	0.1
0.2	0.6	0.1
0.2	0.6	0.1

Figure 4.8. Generally showing normalization to the total intensity area. In order to remove the incomparablities in NMR signals intensities caused by samples different amounts (mg), can be normalized when the intensity of each signal's variables (digital data points that construct the signals) is divided by the sum of all intensities in each set (EUCEDA et al., 2015).

4.9.4 Scaling (column-wise operation)

The scaling is normally considered columns-wise approach, used in the buckets table; thus, it applies to the spectral intensities in the NMR dataset (EUCEDA et al., 2015; CRAIG

et al., 2006). Nonuniform signals intensities can be detected in NMR spectra which reflects differences in molecular amount and concentration in the samples. For instance, some metabolites are present in higher amount and concentration (e.g. sugar, fatty acids, etc.) showing intense signals with statistically maximum variation and dominante lower amount metabolites in the sample. Moreover, these differences can be adjusted in different scaling methods such as mean centering, autoscaling (or scale to unit variance), pareto scaling, range scaling, variable stability (Vast) scaling and level scaling (EMWAS et al., 2018; DEBORDE et al., 2017; EUCEDA et al., 2015; CRAIG et al., 2006). In the mean centering approach, the mean intensity in column is subtracted from the intensity value of each individual column (variable), which allows to balance the concentration differences among metabolites.

In the autoscaling (or standardization) method, each column is centered by subtracting the mean from each signal intensity and divide them by standard deviation (SD) of the related columns as a scaling factor. In this case, variances of all variables have a unit variance (that is why it is called unit variance scaling) and thus all variables become equally important, it is not a suitable choice to apply in NMR, due to the presence of baseline artifacts and random noise across the spectra (EMWAS et al., 2018; EBRAHIMI et al., 2017).

As compromise, pareto scaling on the other hand, is comparable to autoscaling method. In pareto scale, each column (or variable) is scaled and centered by subtracting the mean from each signal intensity and divide them by the square root of standard deviation, as a scaling factor. Pareto scale, is considered a good choice to apply in NMR data, because it helps to reduce noise and deliver more equivalent resultant values to the original, raw measurements, though, it is sensitive to large variance up to some limits (EMWAS et al., 2018; EBRAHIMI et al., 2017).

4.9.5 Principal Component Analysis (PCA)

Principal component analysis (PCA) was initially presented by Karl Pearson in 1901 (PEARSON, 1901), and further progressions was made by Harold Hotelling in 1933 (HORNING, 1971; HOTELLING, 1933). PCA is an unsupervised multivariate approach and handy in metabolomic researches, typically in NMR- (or MS-) based metabolomic (GIULIANI, 2017; KRISHNAN et al., 2004) complex data obtained from fingerprinting in plant quality control (SIMMLER et al., 2018).

In NMR-based fingerprinting (or profiling), PCA construct mathematical model to compare and highlight the (dis)similarities within the data based on chemical patterns such as

metabolites (SIMMLER et al., 2018). In order to apply PCA onto NMR profiles, the analysis contained an *n*-dimensional matrix (X) of several rows (*N* observations\spectra) and columns (*K* variables\chemical shifts). PCA provides *scores* and *loadings* that helps to easily observe the associated trends in the data. It transforms and spreads the complex NMR profiles onto newly formed uncorrelated variables, also called principal components in the *scores* and *loadings* plots. The principal components (PCs), describe directions of the data by means of variance, contain maximum in first few PCs (PC1, PC2, etc.) (IACCARINO et al., 2018).

Similarly, principal components (PC1, PC2, etc.) are n-dimensional in the spectral data space that displays samples outline with possible clusters and outliers (if present) in the samples. On the other hand, variables-based response of each cluster (in *scores*) will be viewed in the *loadings* graph of the same PCA model. The *loading* graph generally provides an overview of the dispersed variables along PCs. In the case of NMR, each variable (in *loadings* plot) represents or equivalent to the chemical shift (δ) values in the spectra. These variables are significant candidates which hold different chemical features (metabolites) that are helpful to discriminate botanical samples (none)grouping in the *scores*.

The ^{1}H HR-MAS NMR spectra of plant samples always contain large number of available information which are complex to obtain directly from the spectra. To acheive such information, PCA jointly support and offer tremendous advantages to enable NMR dataset into interpretable information. PCA is one of leading methods in chemometric to apply on NMR-based corroboration of botanical materials (SIMMLER et al., 2018; BAZAZ et al., 2017).

EXPERIMENTAL

5 EXPERIMENTAL

5.1 MATERIAL AND METHODS

5.1.1 Reference botanical samples collection

In this study the healthy and mature leaves were harvested from the upper, middle and lower parts in *Maytenus ilicifolia* Mart. ex. Reissek and other similar plants. The leaf collection was completed from different locations in the state of Paraná, Brazil (Table 5.1). After collection the leaves were washed with common water to remove unwanted contaminations. The samples collection was initiated in October 2018 and continued until August 2019 around four seasons (spring, summer, autumn to winter).

The leaf samples were assigned general codes with letters; “T”, “M” or “B” showing top, middle, bottom and letters O, D etc. shows collection months as October (O), December (D), etc. for example, “SA016-TO” indicates SA016 sample was harvested from top (T) portion in plant in the month of October (O). Initialy all plants were submitted for botanical identification to the taxonomists, José Tadeu Weidlich Motta and Marcelo Leandro Brotto, and their staff and deposited (Table 5.1) in the herbarium, Museu Botânico Municipal (MBM) of Curitiba, Paraná, Brazil.

Table 5.1. Leaves samples from the studied herbal plants species (families) with related information.

Sample	Reservation	Species (Family)	Location and Geographic coordinates	M\Year
SA016	MBM415084	*Maytenus ilicifolia* Mart. Ex Reissek (Celastraceae)	R. Engo. Ostaju Roguski, 690-Jardim Botânico-Curitiba-PR Brazil 25° 26' 24" S, 49° 14' 15" W, Altitude 910 m	Oct. (2018)-Aug. (2019)
SA026	MBM415127	*Maytenus aquifolium* Mart. (Celastraceae)	UFPR- Botanical Campus, Av. Prefeito Lothário Meissner, 632 - Jardim Botânico, Curitiba - PR, 80210-170, Brazil 25° 26' 57" S, 49° 14' 12" S, Altitude 920 m	Oct. (2018)-Aug. (2019)
SA027	*	*Soroceae bonplandii* (Bail.) W. Burger & Lanjouw (Moraceae)	Est. da Cruz Alta, America de Baixo, Morretes-PR, 83350-000, Brazil. 25° 28' 34" S, 48° 51' 44" W; Altitude 690 m	Oct.-Dec (2018)
SA028	MBM415142	*Zollernia ilcifolia* (Brongn.) Vogel (Fabaceae)	Rua Salvador Graciano, 505, Ponta da Pita, Antonina-PR, 83370-000, Brazil 25° 27' 07" S; 48° 41' 05" W, Altitude 01 m	Oct.-Dec (2018)
SA024	MBM415083	*Berberis laurina* Bilb. (Berberidaceae)	R. Engo. Ostaju Roguski, 690-Jardim Botânico-Curitiba-PR Brazil 25° 26' 27" S, 49° 14' 24" W; Altitude 910 m	Oct.2018-April 2019
SA025	MBM415085	*Citronella gongonha* Mart. R.A. Howard (Cardiopteridaceae)	UFPR-Polytechnic Center, Av. Cel. Francisco H. dos Santos, 100 - Jardim das Américas, Curitiba - PR, 81530-000, Brazil, 5° 27' 11" S; 49° 14' 06" W, Altitude 900 m	Oct.2018-April 2019

* based on similar spiny leaves, this plant species was recommended by taxonomists as “*Soroceae bomplandii*”, but due to lack of the presence of flowers (continuously monitored) this spp. was not reserved in the herbarium.

5.1.2 Samples handling

The drying procedure for all botanical samples was completed as shown in Figure 5.1, to evaluate the convenient drying method.

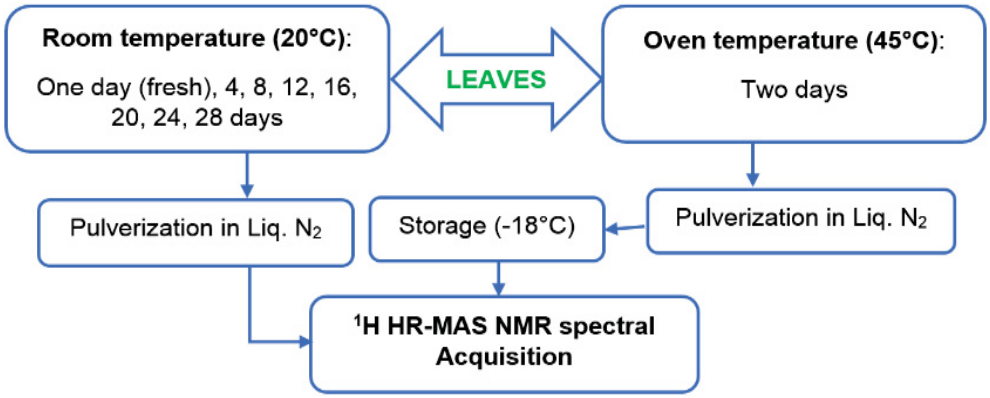

Figure 5.1. The schematic representation of samples drying evaluation in the study.

Initially three individual spectra were obtained, from fresh leaves, dried on room temperature and oven temperature (45 °C). The samples drying on room temperature was continued for one month since, seven ^{1}H HR-MAS NMR profiles were achieved from each plant species (Figure 6.2 p.63) by considering some gaps in between measurements. These optimizational analyses were performed to select appropriate drying method and also to understand microbial enzymatic effects to the molecular compositions in materials along periodic circulation of one month.

5.1.3 Commercial botanical samples collection and handling

The commercial samples were purchased from different (non)local markets, natural product stores as well as pharmacies in Brazil (Table 5.2). The commercial samples were identified by their batches, labeled as *Maytenus ilicifolia* and Espinheira-Santa. These commercial Espinheira-Santa were in different form of chopped leaves, tea sachets as well as capsules of powdered materials. After purchase, the related samples were stored under freezing temperature (-18 °C) until ^{1}H HR-MAS NMR measurements.

Table 5.2. Commercial samples from *Maytenus ilicifolia* (Espinheira-Santa) with additional information

Sample	Label	Purchase Location	M/Year
SA029	*Maytenus* spp.	Mato Grosso do Sul	Jan/2017
SA030	*Maytenus ilicifolia*	Mato Grosso do Sul	Jan/2017

SA031	Espinheira-Santa	Foz do Iguaçu	May/2017
SA032	Espinheira-Santa	Casa fiesta, Curitiba-PR	Oct/2018
SA033	*Maytenus ilicifolia* (Espinheira-Santa)	Walmart new, J. das Américas Curitiba-PR	Jan/2019
SA034	Espinheira-Santa	S. K. Natural Products, J. Das Américas, Curitiba-PR	Jan/2019
SA035	Espinheira-Santa (Capsule)	Shopping J. das Américas, Curitiba-PR, Brazil	Jan/2019
SA036	Espinheira-Santa (Capsule)	Rio de Janeiro	Nov./ 2019
SA037	Espinheira-Santa	Rio de Janeiro	Nov./ 2019
SA038	Espinheira-Santa (*Maytenus ilicifolia* Mart.)	GREENDAY Produtos Naturais, J. das Américas	Dec/2019
SA039	Espinheira-Santa (Capsules)	GREENDAY Produtos Naturais, J. das Américas	Feb/2020
SA040	Espinheira-Santa (Capsules)	Mundo das Ervas, J. das Américas	Feb/ 2020
SA041	Espinheira-Santa	Mundo das Ervas, J. das Américas	Feb/ 2020
SA042	Espinheira-Santa (Tea sachet)	Mundo das Ervas, J. das Américas	Feb/ 2020
SA043	Espinheira-Santa	Jardim das Ervas, Centro de Curitiba	Feb/ 2020

5.2 METHODOLOGY EVALUATION AND ^{1}H HR-MAS NMR MEASUREMENTS

The optimization steps to spectral acquisition was began from solvent selection, sample preparation, 1D (HR-MAS) NMR pulse sequences (*zg*, *zgpr*, *zgcppr*, *noesypr1d*) and basic parameters evaluation for example; number of scans (NS), rotor spinning velocity (kHz), mixing time (D8 of milliseconds, in *noesypr1d*), power level (pl9 in decibel or dB).

5.2.1 Solvent evaluation and selection

The solvent evaluation was carried out by taking powdered (10 ± 1.0 mg) leaf from *Maytenus ilicifolia* and deuterated solvents (40 µL) in 4-mm MAS rotor (*v.* 50 µL). In this process, three individual deuterated solvents e.g. D_2O, $CDCl_3$ and CD_3OD were considered (Figure 5.2) and followed by ^{1}H HR-MAS NMR measurements. Smilarly, the NMR spectra were recorded and mutually compared to choose appropriate deuterated solvent for further measurements.

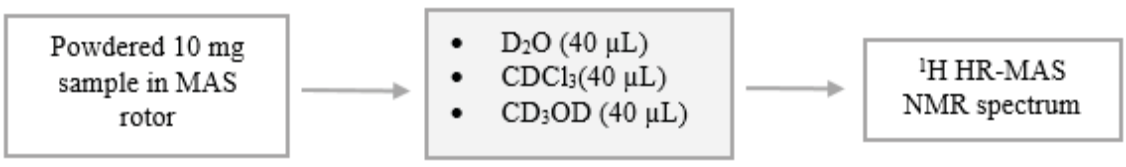

Figure 5.2. Schematic presentation for solvent evaluation.

5.2.2 Sample preparation and swelling time evaluation

In order to attain high-resolution spectra from natural materials, it is necessary to swell the related sample in appropriate solvent (FLORES et al., 2018) that helps to improve cell wall porosity, enabling metabolites diffusion (ALAMGIR., 2017), and increase molecular dynamics. In this way sample(s) preparation was performed in the powdered (10 ± 1.0 mg) leaf from *Maytenus ilicifolia* in CD_3OD (99.95% D, 0.05% TMS). Furthermore, sample swelling state was sustained in accordance to different intervals and monitored when HR-MAS NMR acquisitions were completed. In this process, 10 ± 1.0 mg sample was taken in a 4-mm MAS rotor (50 µL) and soaked in 40 µL CD_3OD with various time intermissions individually (Figure 5.3). The materials were swollen according to the literature (FLORES et al., 2018) with minor changes.

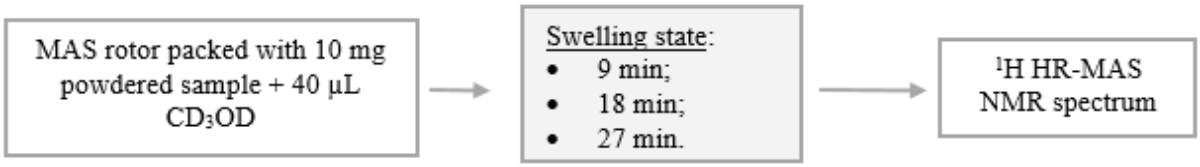

Figure 5.3. Scheme showing sample preparation, swelling state and ^{1}H HR-MAS NMR acquisition.

5.2.3 ^{1}H HR-MAS NMR pulse sequence selection with additional parameters evaluation

In this step, four NMR pulse sequences were used (Figure 5.4) in same 10 ± 1.0 mg powdered leaf materials from *Maytenus ilicifolia.* In this way, MAS rotor was packed (sample and solvent) and subjected to external magnetic field ($\mathbf{B_0}$) followed by shimming and ^{1}H-spectrum was recorded with conventional *zg* pulse sequence. The recorded ^{1}H-spectrum showed intense water signal which was complementarily removed. The saturation of intense water peak was removed through *zgpr*, *zgcppr*, and *noesypr1d* solvent pre-saturation pulse programs (Figure 5.4). Morover, experimental parameters for example; number of scans (NS), rotor spinning frequency (kHz), mixing time (D8/ t_{mix}; only in *noesypr1d*), as well as pre-saturation power level (pl9) (Figure 5.5 to Figure 5.8) were accordingly evaluated.

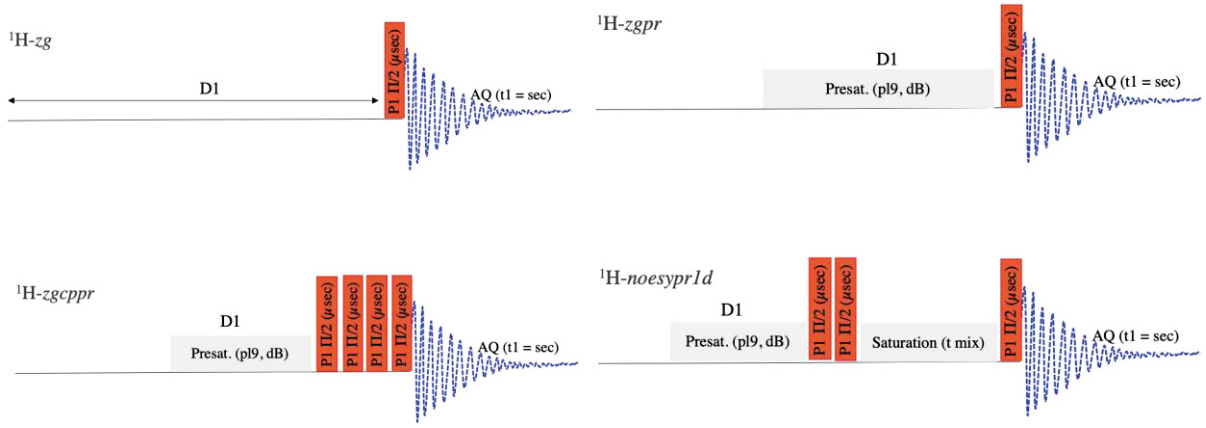

Figure 5.4. Schematic representation of four different pulse sequences evaluated during the study.

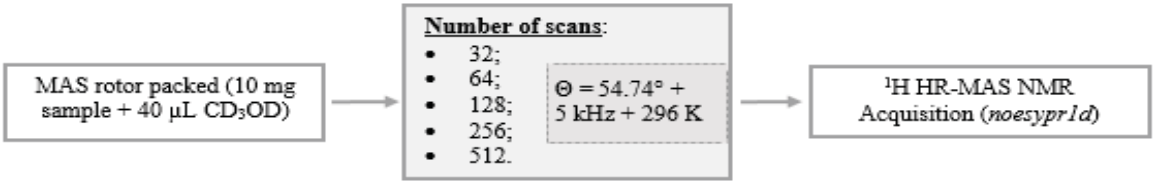

Figure 5.5. Scheme showing number of scans evaluation in ^{1}H HR-MAS NMR acquisition.

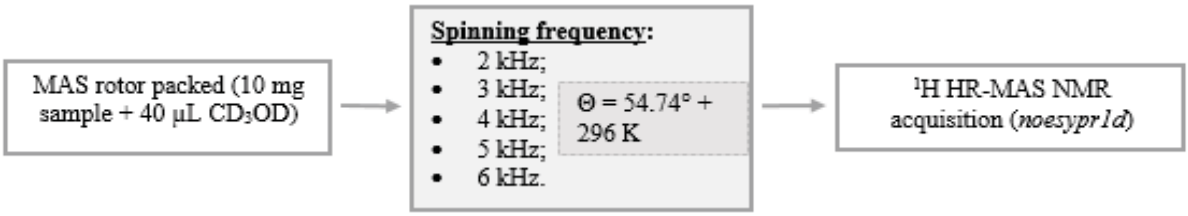

Figure 5.6. Scheme showing spinning frequency evaluation in ^{1}H HR-MAS NMR acquisition.

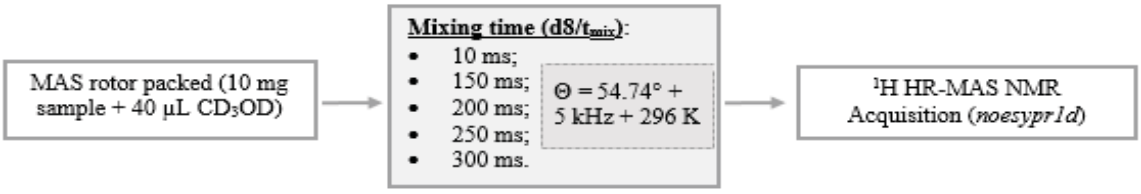

Figure 5.7. Scheme showing mixing time (t_{mix} = D8) evaluation in ^{1}H HR-MAS NMR *noesypr1d*.

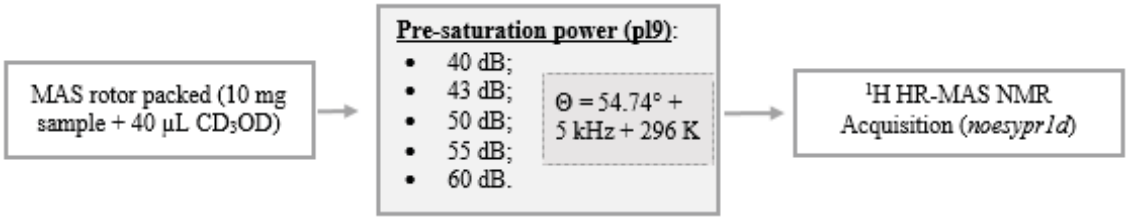

Figure 5.8. Scheme showing pre-saturation power level (pl9) evaluation in ^{1}H HR-MAS NMR acquisition.

5.3 ^{1}H HR-MAS NMR MEASUREMENTS IN SEMISOLID-STATE

The overall HR-MAS NMR acquisitions of botanical materials were carried out on Bruker AVANCE NMR spectrometer (400 MHz) with magnetic field strength of 9.4 Tesla. The equipment observed proton (^{1}H) nucleus with 400.13 MHz. The spectrometer was equipped with a 4-mm HR-MAS four channeled (^{1}H, ^{13}C, ^{15}N, and ^{2}H) probehead which allows the sample(s) analysis in the magic angle direction with respect to the main magnetic field ($\mathbf{B_0}$), a general demonstration is given in the Figure 5.9.

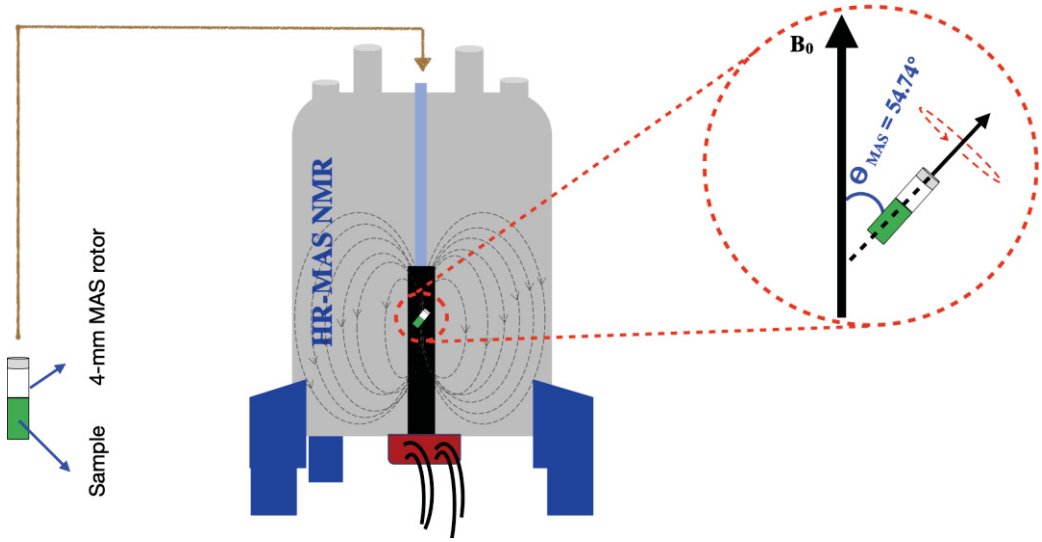

Figure 5.9. Schematic representation of spectrometer equipped with HR-MAS probe with MAS rotor direction.

5.4 TWO-DIMENSIONAL (2D) NMR MEASUREMENTS IN LIQUID-STATE

5.4.1 Sample preparation

In sample preparation, the previously stored powdered leaf materials were weighed (100 ± 1.0 mg) into a two 1000 µL microcentrifuge tube and mixed with 650 µL CD_3OD. The mixture was then subjected to sonication (30 minutes) and centrifugation (30 minutes) processes. The extraction process was followed by pipetting out deuterated methanolic supernatant (~600 µL) and transferred into a 5 mm NMR tube and finally subjected into the magnetic field ($\mathbf{B_0}$) to perform 2D NMR analyses. Overall 2D NMR analyses were completed according to the scheme shown in Figure 5.10.

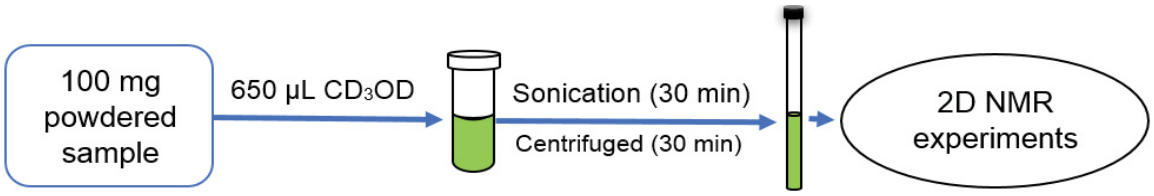

Figure 5.10. Scheme showing the methodology for liquid-state two-dimensional NMR experiments.

5.4.2 Two-dimensional (2D-) NMR measurements

The 2D NMR experiments in liquid-state were performed with a Bruker AVANCE-III NMR spectrometer (400 MHz) with magnetic field strength of 9.4 Tesla, observing frequencies of 400.13 (^{1}H) and 100.62 (^{13}C) MHz, which was equipped with multinuclear broad band inverse detection 5 mm probe with gradient field in the *z*-direction. Prior to 2D NMR acquisitions, the sample was inserted in equipment, since, temperature was regulated (296 K), probe head was tuned-matched and magnetic field (B_0) was optimized manually by shimming (Figure 5.11) and observing the full half width (≤ 1.0 Hz) of TMS signal (δ 0.00).

Figure 5.11. Schematic presentation of 2D NMR analyses in liquid-state of materials.

The entire chemical structures identified (in ^{1}H HR-MAS) in the leaves from *Maytenus ilicifolia* in comparison to other spp. were confirmed by 2D NMR correlation maps such as multiplicity edited HSQC, HMBC, TOCSY and COSY. The heteronuclear (^{1}H-^{13}C) one bond correlations were measured with multiplicity edited HSQC, a 2D version of 1D-DEPT135 experiment (GAILLOT et al., 2018) that differentiate one chemical group from other in the molecular system. Multiplicity edited HSQC experiment provides multiplicities edition and correlation information to simplify intramolecular connection utilizing distinct phases (positive and negative phases). In this work the blue (positive phase) represent CH and CH_3 since, the red color (negative phase) denoted all CH_2 groups in molecular structures.

Multiplicity edited HSQC experiment was in the phase sensitive mode using Echo/Antiecho-TPPI gradient selection, where the decoupling was achieved via trim pulses in INEPT transfer yet multiplicity edition in the selection step via shaped pulses (180° for spins refocusing) in F2-dimension with gradients in back-inept. The experiment was done with "*hsqcedetgpsisp2.2*" pulse seqeunce (Bruker library). The experimental parameters were: 128

FIDs in F1 x 2 k datapoints (TD) in F2 dimension, by providing 64 number of scans (NS), spectral width (SW) 20124.1 Hz (F1) x 5597.0 Hz (F2) with offset (O1) 9055.1 Hz (F1) x 1932.2 Hz (F2). The receiver gain (RG) was 203, recycle delay (D1) of 1.0 sec, and acquisition time (AQ) of 0.2 seconds.

Heteronuclear (^{1}H-^{13}C) long ranged correlations were measured through 2D HMBC experiment using "*hmbcgplpndqf*" pulse sequence (Bruker library). In HMBC, 200 FIDs were collected in F1 *vs* 2 k data points (TD) in F2 with spectral width (SW) of 25641 Hz of offset (O1) 11794.5 Hz (F1) x (F2) 5995.2 Hz with offset (O1) 1976 Hz under 128 transients. Similarly, the receiver gain (RG) 203, acquisition time (AQ) 0.17 sec, and recycle delay (D1) of 1.00 sec.

^{1}H-^{1}H COSY experiment was completed with "*cosygpqf*" pulse program (Bruker library). Whereby, 256 FIDs (F1) and 4 k data points (TD) in F2, equally distributed over spectral width (SW) in both dimensions (F1, F2) 5995.2 Hz with offset (O1) of 1976 Hz, using 8 transients. Similarly, receiver gain (RG) was 181, recycle delay (D1) of 1.5 sec, acquisition time (AQ) was 0.02 (F1), and 0.34 sec (F2).

^{1}H-^{1}H TOCSY experiment was performed with "*mlevetgp*" pulse program (Bruker library). The TOCSY experiment was performed by collecting 128 FIDs (F1) with 4 k data points (TD) over a spectral width (SW) in both dimensions (F1, F2) 5995.2 Hz and offset (O1) 1976 Hz using 16 number of scans (NS). The receiver gain (RG) was 181 and recycle delay (D1) 1.5 sec while, acquisition time (AQ) 0.34 sec (F1) x 0.01 sec (F2). All 2D NMR experiments were finalized when FIDs were zero filled and Fourier transformed into frequency domain as spectra.

5.5 CHEMOMETRIC ANALYSIS

5.5.1 Principal Component Analysis (PCA)

The whole ^{1}H HR-MAS NMR profiles from *Maytenus ilicifolia* and *Maytenus aquifolium* were submitted to the principal component analysis (PCA). ^{1}H HR-MAS NMR spectra were manually referenced TMS signal (δ 0.00) at full width half-height can be small or equal to 1.00 Hz (≤ 1.00 Hz), phases and base lines were corrected in Topspin software package (v. 3.1, Bruker BioSpin GmbH). These HR-MAS NMR spectra were furthermore submitted and pre-processed in AMIX (Analysis of Mixture) software (v. 3.9.12, Bruker BioSpin GmbH).

PCA analysis was performed over δ 8.10-0.67 spectral range in HR-MAS NMR by excluding the noisy region (δ 20.00-8.11 and δ 0.66 to -5.11), residual water (δ 5.18-4.60), acetone (δ 2.18-2.14), and methanol (δ 3.33-3.29). Through preprocessing method, the bin size was estimated to δ 0.03 utilizing δ 0.01-0.05 (Figure 5.12). On one hand, the entire rows (spectra) were mean centered and normalized by "scale to total intensity" using special integration mode. On other hand, the scaling (column-wise) performance was completed via pareto scaling since, "no scale" and "scale to unit variance" were also reviewed.

After data pre-processing, the PCA model of "108 x 262" was achieved, where 108 represented total number of spectra (row-wise) and 262 were net chemical shifts or variables (column-wise). In order to identify samples (abnormal) of different T^2 values, the *influence* and *hotelling's* T^2 (95% confidence level) were implemented.

The conclusion of PCA analysis was consisted *scores* and *loadings* plots. The *scores* plot was responsible to demonstrate samples distribution (groups) by means of colored small spheres (NMR spectra). The *loadings* plot on the other hand was retained all influencing variables (chemical shifts) responsible for groups formation (in *scores*). Both *scores* and *loadings* plots will be viewed in the same direction to understand the relative (influencing) reason behind each cluster or group from the samples. The discriminatory metabolites (variables) for each group (in *scores*) will be observed in the *loadings* plot. The overall performance in PCA was respectively according to the scheme shown in Figure 5.12.

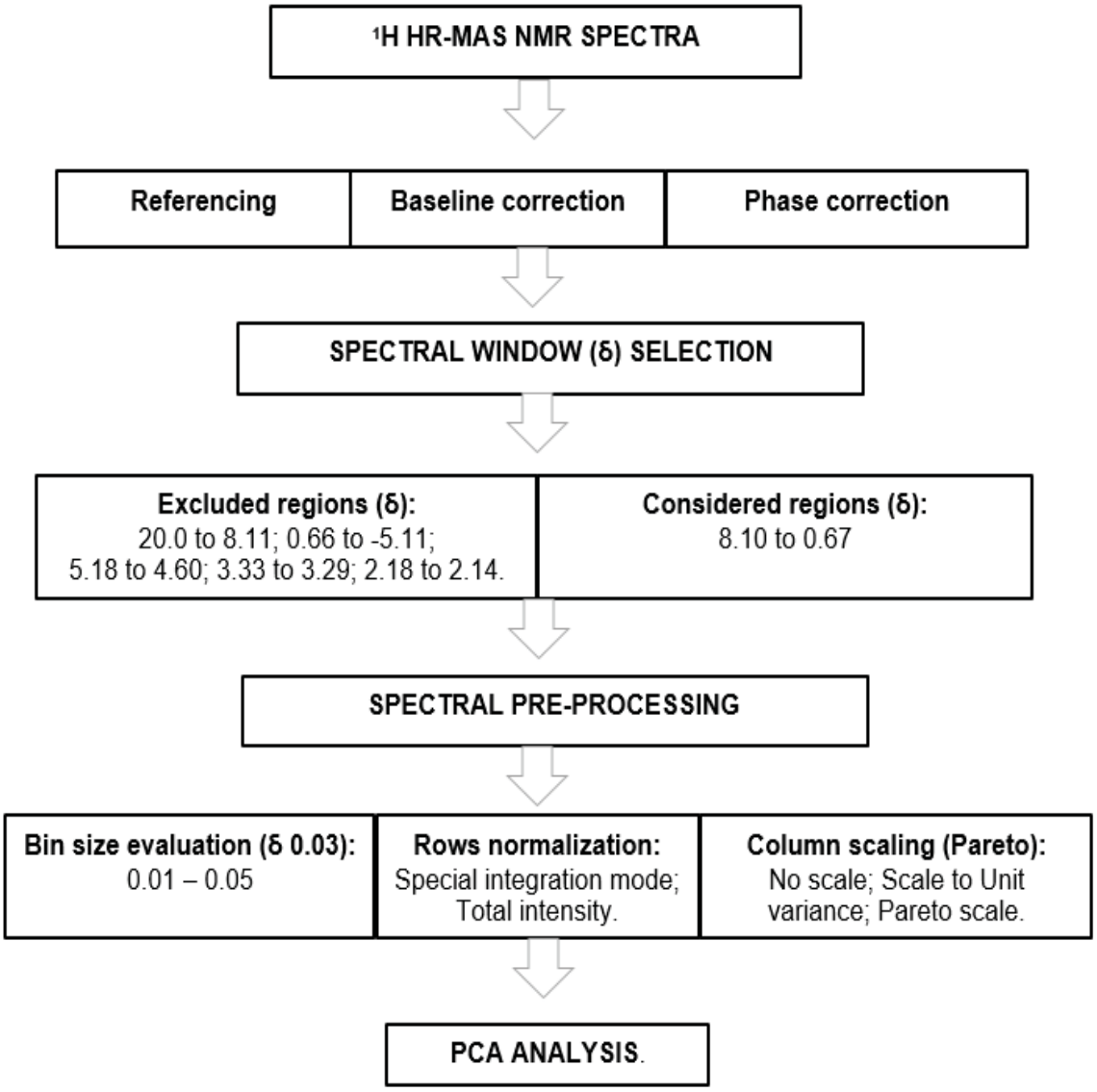

Figure 5.12. Scheme showing optimization method used in the principal component analysis (PCA).

RESULTS AND DISCUSSION

6 RESULTS AND DISCUSSION

6.1 METHODOLOGY EVALUATION AND ^{1}H HR-MAS NMR MEASUREMENTS

6.1.1 Solvent evaluation and selection

The choice of solvent is fundamental feature in ^{1}H (HR-MAS) NMR, to ensure both locking the magnetic field and molecular mobility determination in the sample medium (FAROOQ et al., 2013; ALAM et al., 2012). In this way, individually different deuterated solvents (D_2O, $CDCl_3$ and CD_3OD) were employed to 10 ± 1.0 mg powdered leaves from *Maytenus ilicifolia*. The powdered material was soaked in 40 µL of *d*-solvent for 18 minutes inside MAS rotor and followed by ^{1}H HR-MAS NMR spectra (Figure 6.1). In this way, CD_3OD was chosen and was utilized in overall ^{1}H HR-MAS NMR measurements. Main advantage of CD_3OD was observed with better spectral profile in contrast to D_2O, and $CDCl_3$ (Figure 6.1). On the other hand, CD_3OD provided better mobilities to several polar and non-polar molecules in the samples, CD_3OD over other *d*-solvents has shown several excellent results in previous studies (FLORES et al., 2018).

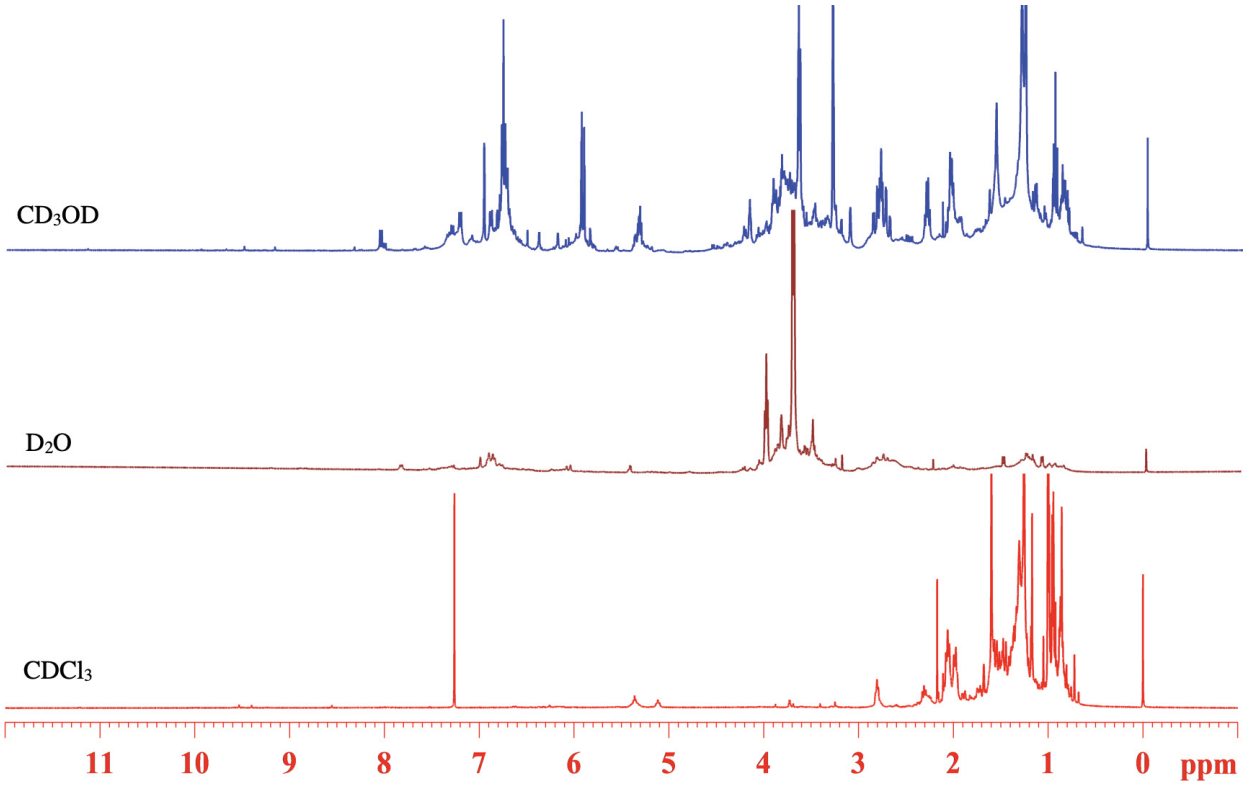

Figure 6.1. ^{1}H HR-MAS NMR spectra (400.13 MHz) showing solvent evaluation in leaf powder (10 ± 1.0 mg) from *Maytenus ilicifolia*.

6.1.2 Botanical samples handlings

In this procedure, the leaves from *Maytenus ilicifolia* and *Maytenus aquifolium* were dried for two days on oven (45 °C) as well as for 28 days at room temperature. In this way, oven and air-dried leaves from both species were grinded into liquid nitrogen, weighed (10 ± 1.0 mg), soaked for 18 min. into 40 µL CD_3OD and submitted to HR-MAS NMR analyses.

6.1.2.1 *Maytenus ilicifolia* Mart. ex Reissek (Celastraceae)

Followed the collection of *Maytenus* leaves, the drying evaluation was achieved. This assessment contained the analyses of fresh leaf directly collected in liquid nitrogen, and leaves dried on room temperature during 28 days and oven temperature two days. In 28 days, seven NMR profiles (each fourth day) were obtained. Based on similiarity between the fresh (in Liq. nitrogen) and oven dried leaf spectrum was used to reference other profiles of the same materials dried over room temperature for 28 days (Figure 6.2).

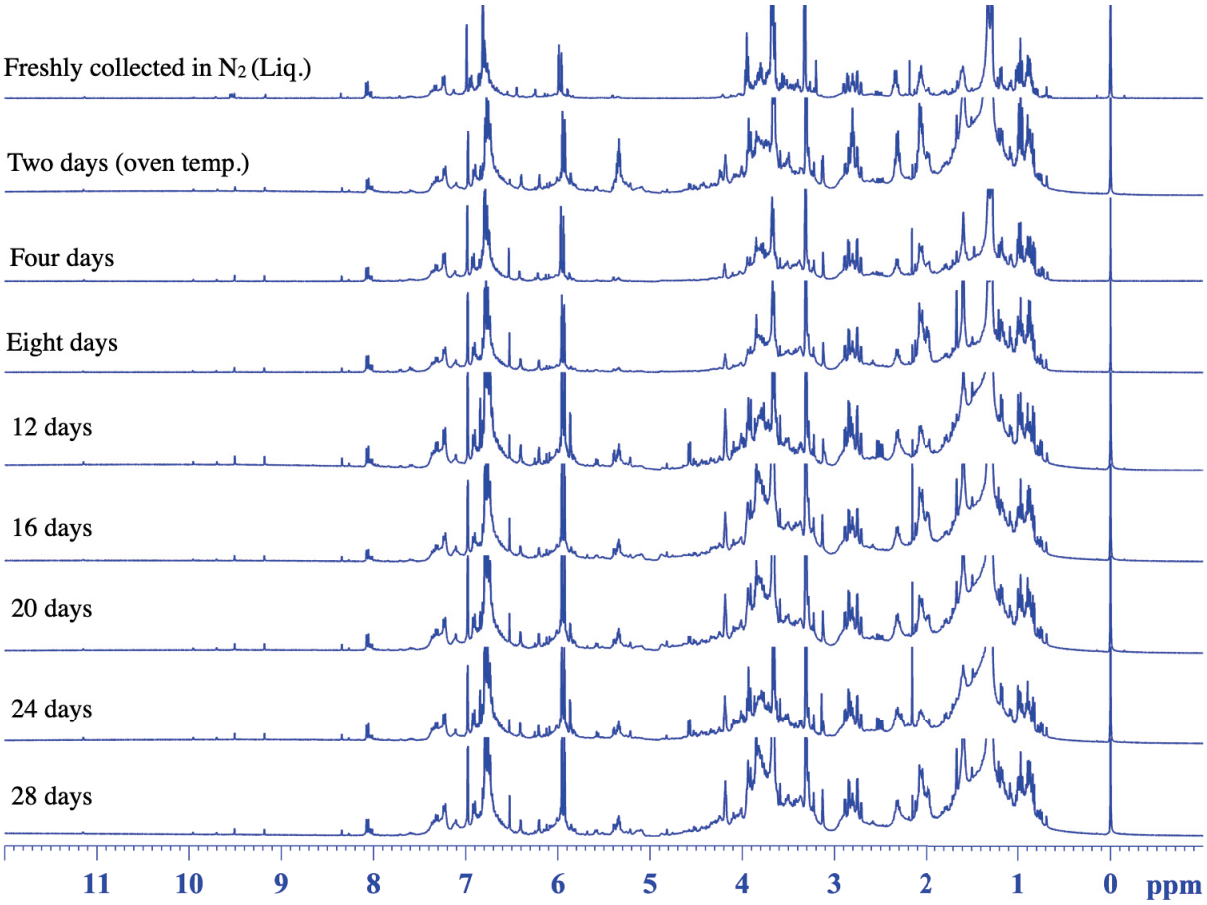

Figure 6.2. ^1H HR-MAS NMR spectra (400.13 MHz) showing drying evaluation in leaf powder (10 ± 1.0 mg: CD_3OD) from *Maytenus ilicifolia*.

The comparative spectra were amplified to better overview the aromatic, carbohydrates, and aliphatic signals (Figure 6.3). In review, the aromatic region showed one singlet signal (δ 6.53: s, shown with red arrow) from fumaric acid with lowest intensity in fresh and oven dried leaf on comparison to other spectra. Similarly, a doublet signal (δ 5.86: d, J = 2.3 Hz marked with green arrow) was appeared intense in the duration of 12, 20, and 24-days.

In the carbohydrate to aliphatic range, few signals from fatty acid (δ 5.34: m; δ 2.81: t, J = 6.0 Hz; δ 2.06, m, with blue arrows) were seen suppressed in the (fresh leaf) period of four and eight days while one triplet signals was observed distorted (δ 0.97, t, J =7.5 Hz) in approximately all days except in the oven dried samples. In order to see the carbohydrate region, a doublet signal from anomeric hydrogen in β-glucose (δ 4.57: d, J = 7.4 Hz, with green arrow) and some unknown intense doublet of doublets signal (δ 2.50: dd, J = 16.1; 8.1 Hz, with red arrow) were intense in two profiles associated to 12 and 24-days duration.

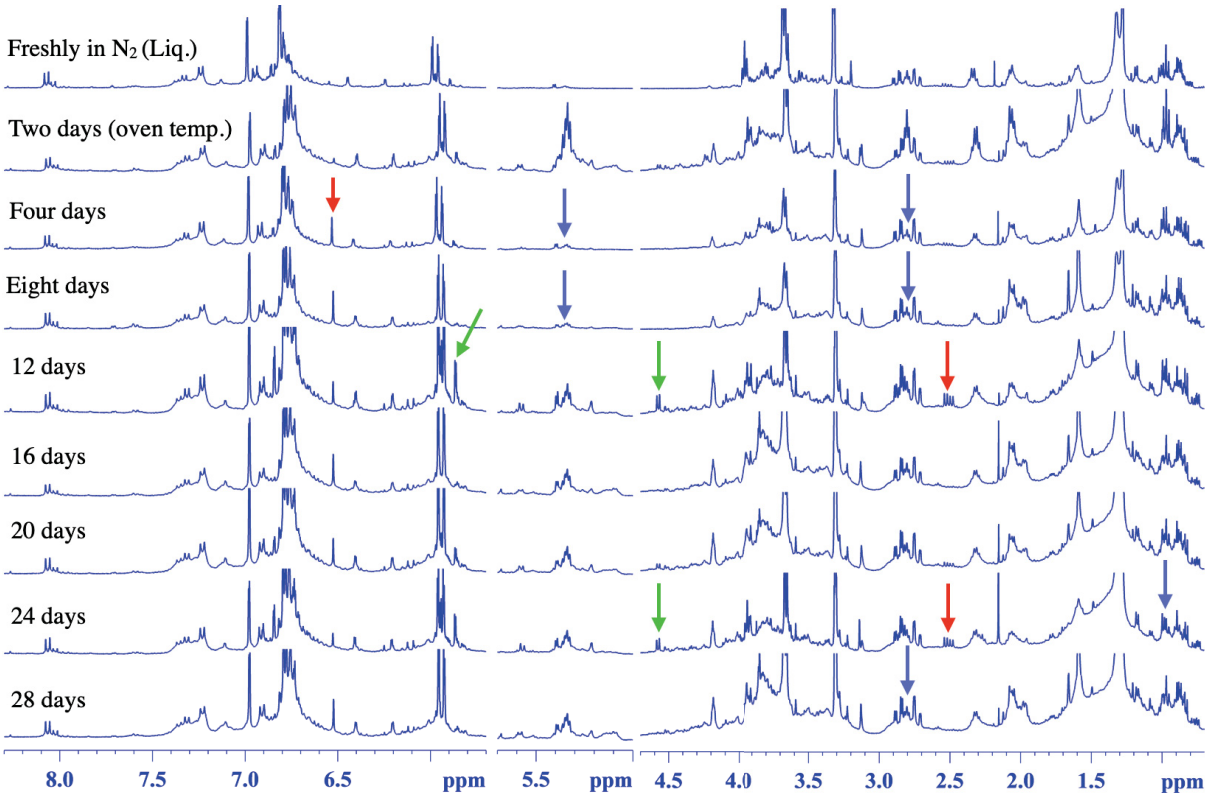

Figure 6.3. Amplified aromatic-aliphatic regions in ^{1}H HR-MAS NMR spectra (400.13 MHz) showing drying evaluation in leaf powder (10 ± 1.0 mg: CD_3OD) from *Maytenus ilicifolia*.

6.1.2.2 *Maytenus aquifolium* Mart. (Celastraceae)

In the same way, leaf samples from *Maytenus aquifolium* were dried on oven and room temperatures, as described for *Maytenus ilicifolia*. Due to the presence of signals similiarities, sequentially eight spectra from air- and oven dried leaves of *Maytenus aquifolium* were referenced to the spectrum obtained from oven dried *Maytenus ilicifolia* (Figure 6.4).

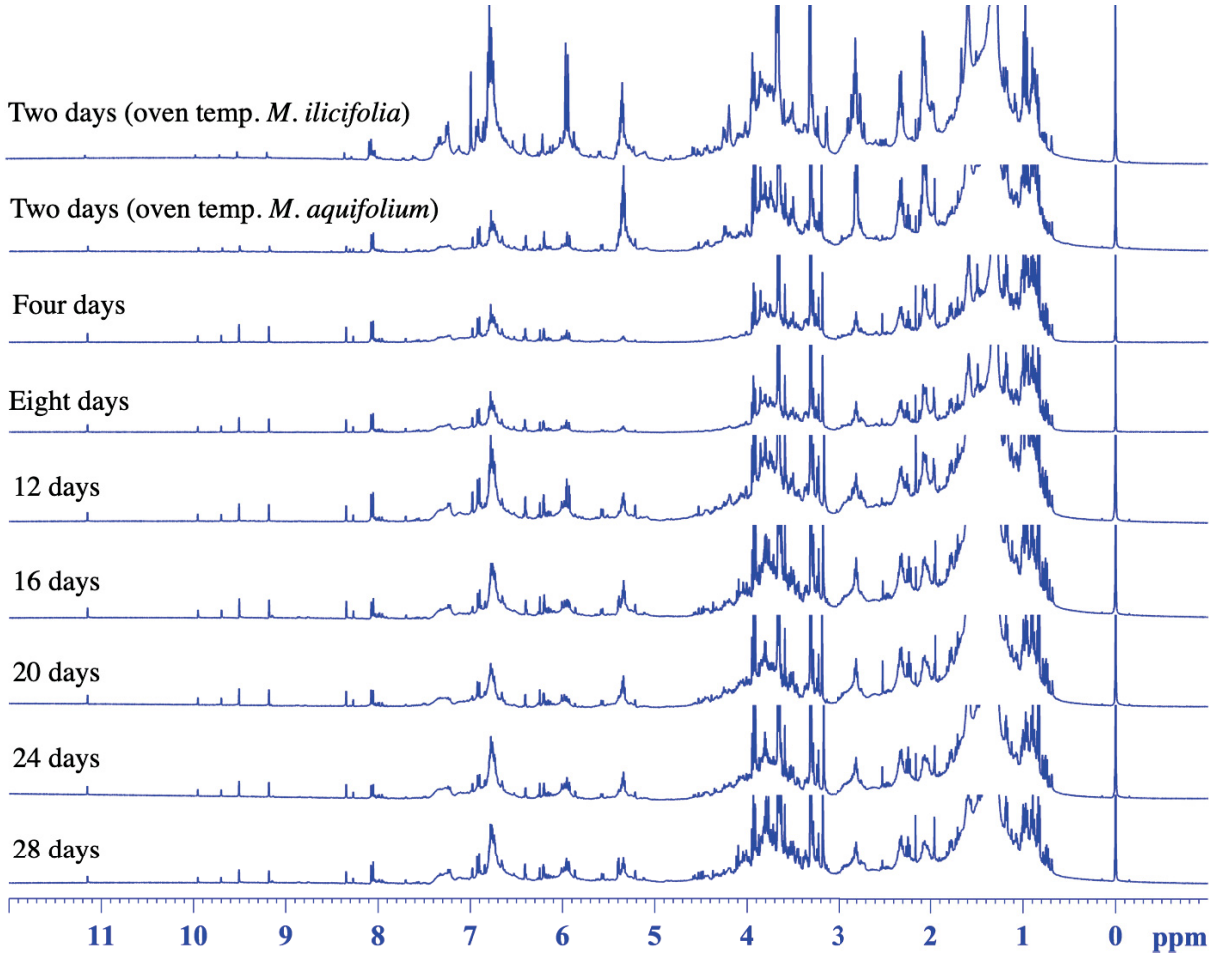

Figure 6.4. Stacked ^{1}H HR-MAS NMR spectra (400.13 MHz) showing drying evaluation in leaf powder (10 ± 1.0 mg: CD_3OD) from *Maytenus aquifolium*.

To overview the amplified aromatic to carbohydrate and aliphatic regions (Figure 6.5) revealed relatively intense signals from (-)-epicatechin (mentioned with blue arrows) in 20-days duration. Moreover, a doublet signal from anomeric hydrogen in sucrose, was found relatively intense during 16 and 28-days, in comparison to other spectra. Similarly, a multiplet signal from fatty acids (δ 5.34, m, red arrows) was almost lost in 4 to 8-days duration. One triplet signal (δ 3.92; t, J = 6.4 Hz, green arrowed) from sugar was relatively intense in entire

days except it was less intense during 4 to 8-days, while one doublet signal (δ 3.66; d, J = 6.4 Hz, green arrowed) was intense and completely leading in overall 28-days. An unknown singlet (δ 3.17, s, orange arrow) was revealed gradually intensified from 4 to 28-days. Several signals of fatty acids (δ 2.81; m, shown with red arrows) were observed downregulated in intensity while, a triplet (δ 0.97; t, J = 7.5 Hz) was completely distorted in 28 days duration.

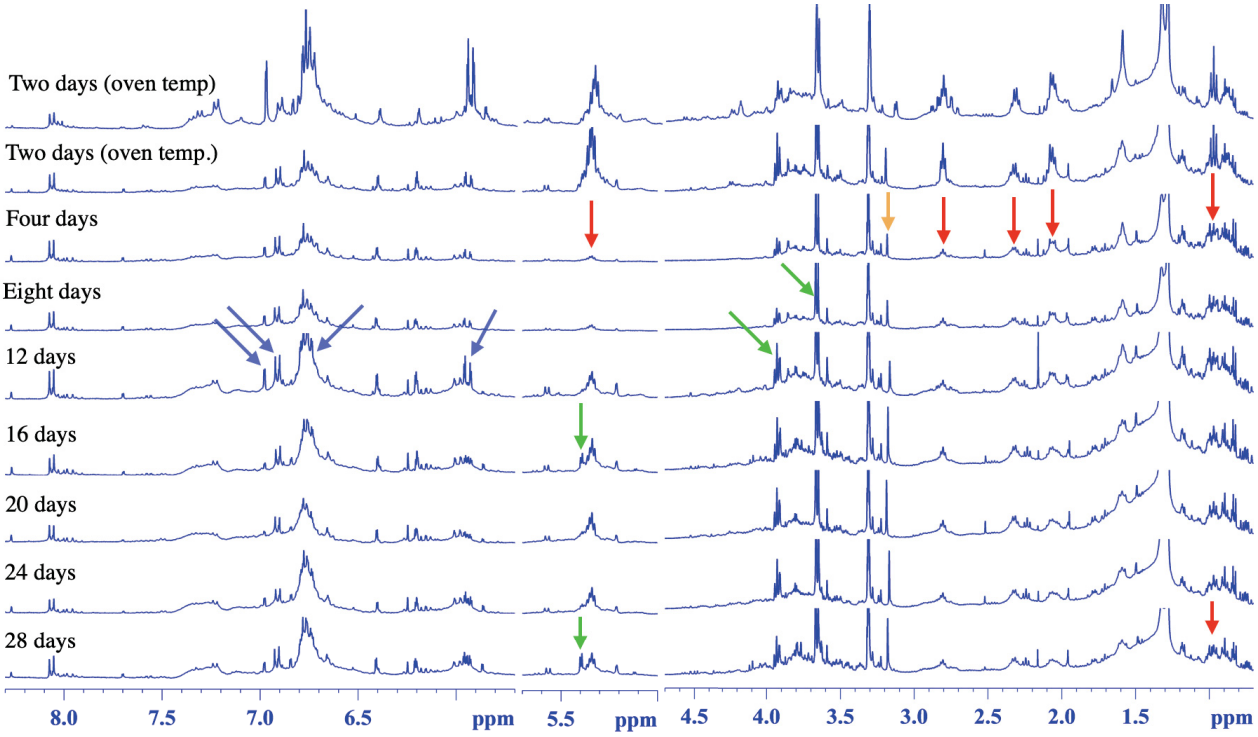

Figure 6.5. Amplified aromatic-aliphatic region in ^{1}H HR-MAS NMR spectra (400.13 MHz) showing drying evaluation in leaf powder (10 ± 1.0 mg: CD_3OD) from *Maytenus aquifolium*.

From signals intensities modifications, it was perceived that uncontrolled condition can cause chemical modification in botanical materials. These variations reflected that the molecules were influenced by microbial enzymatic activities, dehydration and oxidation, and or maturation processes in materials along 28 days. It can be deduced that production or distortion in organic (fumaric and fatty) acids, and carbohydrates (*β*-glucose), and other chemicals contents were affected in these botanical materials were due to the uncontrolled conditions. Moreover, these assumptions represented that oven-based drying method was optimal, and rapid in comparison to other. However, it also means that chemical profile from herbal materials, stored for long time may loss their genuineness or get affected.

6.1.3 Sample preparation and swelling state evaluation

In order to achieve high-resolution NMR spectra with maximum molecular information, the 10 ± 1.0 mg powdered leaves from *Maytenus ilicifolia* were packed in 4-mm (50 µL) MAS rotor followed by soaking in CD_3OD for different intervals of 9,18, and 27-minutes. The swollen or gel-like sample in the MAS rotor was subjected into equipment and followed by ^1H HR-MAS NMR measurements. Out of three NMR profiles, 9-minutes swelling time showed poor signal-to-noise (*S/N* = 1011.22). The *S/N* was seen better and comparable (*S/N* = 1273.50 and 1280.14) after 18- and 27-minutes swell time (Figure 6.6). After the comparasion of *S/N* ratios in different intervals, the 18-minutes time was suitable to soak individual materials prior to perform NMR measurements.

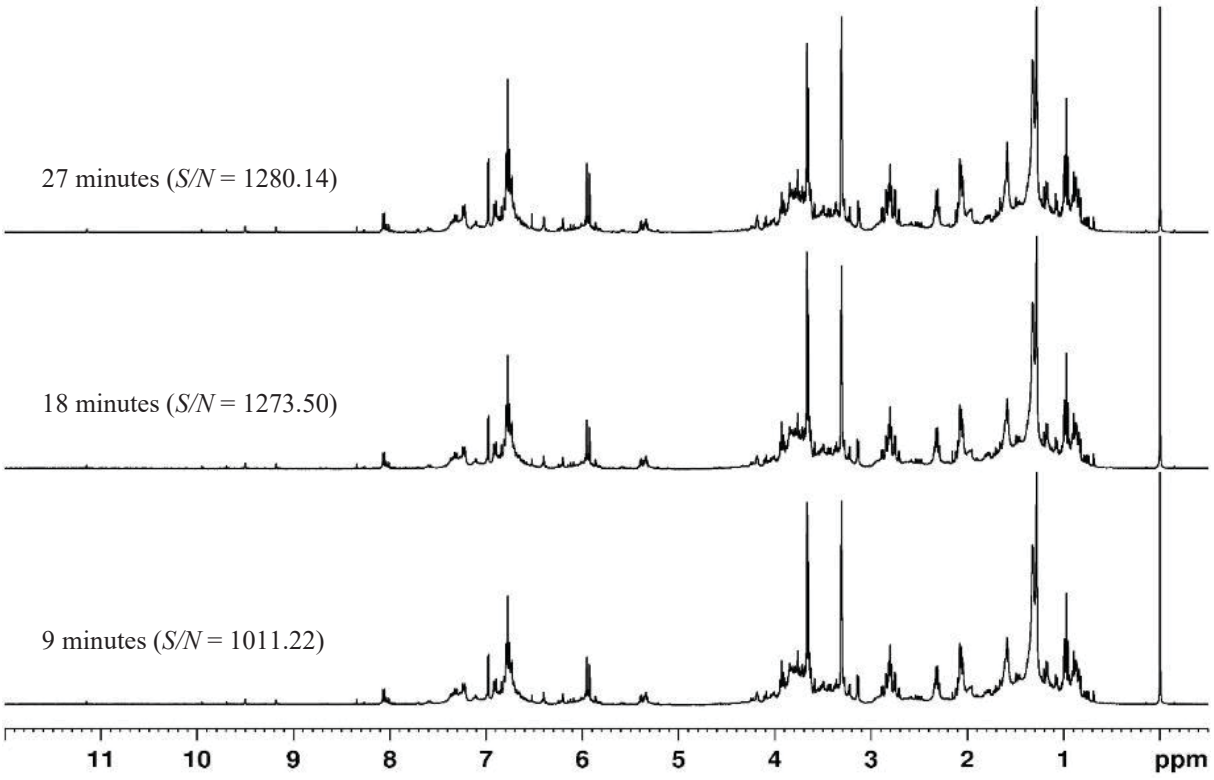

Figure 6.6. ^1H HR-MAS NMR spectra (400.13 MHz) showing sample swelling time evaluation in leaf powder (10 ± 1.0 mg: CD_3OD) from *Maytenus ilicifolia*.

6.1.4 ^1H HR-MAS NMR pulse sequence selection

Plant or other natural materials usually contain high amount of water in comparison to other molecular compositions. In NMR-based plant investigations, experiments begin with conventional *zg* sequence that provide ^1H NMR spectrum wiht intense signal from solvent (HOD) in a specific frequency range (e.g. δ ~5.00 to 4.50). Besides overlapping, the intense

peak from solvent digitized more and effect *S/N* (lower) of signals from interested molecules (TORRES et al., 2016) as well as distort spectrum baseline (GOGIASHVILI et al., 2019). The main goal of metabolomics is to investigate interested organic molecules, hindered from water that needs to remove from the spectra. The removal of solvent in the sample can provide qualitatively high-resolution NMR spectrum which requires to carry out the measurement by some of pre-saturation pulse sequences (ZHENG et al., 2010).

In contrast to *zg*, several solvent suppression pulse sequences: the *zgpr*; *zgcppr*, and *noesypr1d* (OLIVEIRA et al., 2014) were evaluated during NMR measurements. The solvent suppression was performed in pre-saturation followed by 90° pulse in *zgpr* and composite pulses in *zgcppr*, while mixing time period (t_{mix}) was subjected between two consecutive 90° pulses in *noesypr1d* (Figure 6.7 and Figure 5.4; p. 55).

Overviewing spectral profiles (Figure 6.7), the *noesypr1d*-based spectrum was found better with flat baseline and quality saturation of water signal. The signal-to-noise ratios (*S/N*) were calculated in each spectrum. The *zg*, a 1D pulse sequence demonstrated an extraordinarily intense water resonance in the spectrum with poor *S/N* (131.02). When the intense water resonance was removed, the *S/N* ratios were manifold increased for example, *S/N* = 963.03 (*zgpr*), 1420.24 (*zgcppr*), and rspectively *S/N* = 1790.10 (*noesypr1d*). Upon spectral comparions, several other parameters were needed to optimize in *noesypr1d* (also *zgpr* and *zgcppr*). Other than *S/N,* the signals close to the suppression region were efficiently more intense in *noesypr1d* however they were found affected in *zgpr* and *zgcppr.*

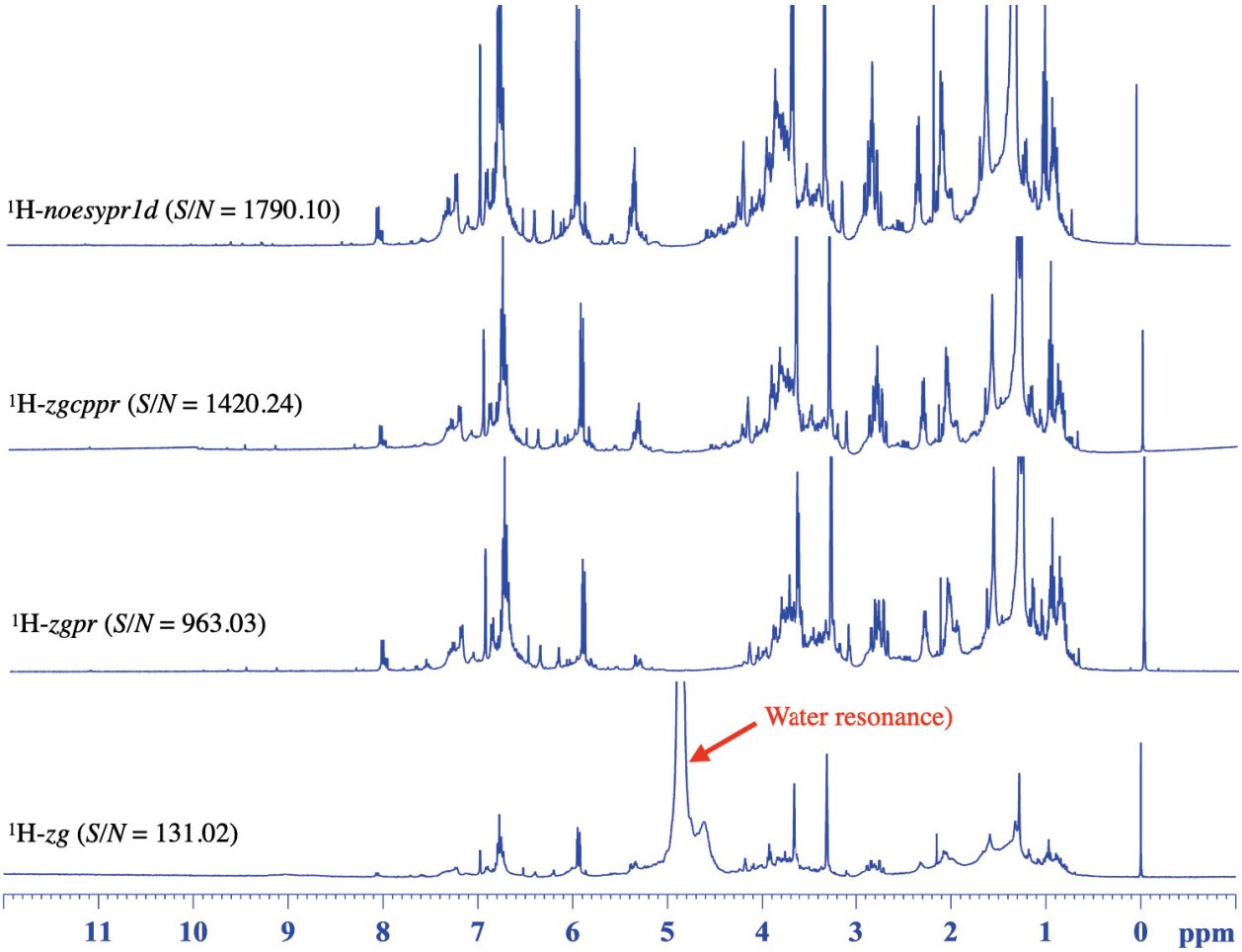

Figure 6.7. ^{1}H HR-MAS NMR spectra (400.13 MHz) showing pulse sequence evaluations in leaf powder (10 ± 1.0 mg: CD_3OD) from *Maytenus ilicifolia*.

6.1.5 ^{1}H HR-MAS NMR *noesypr1d* and additional parameters

The experimental parameters in *noesypr1d* pulse sequence were carefully estimated in the powdered leaf (10 ± 1.0 mg) from *Maytenus ilicifolia* in 40 µL CD_3OD, as locking solvent. These parameters were number of scans (Figure 6.8), rotor spinning frequency (Figure 6.9), mixing time (Figure 6.10), and pre-saturation power level (Figure 6.11).

Usually the numbers of scans (NS) are proportional to experimental time and *S/N* ratio in NMR measurements. It means, maximum scans substantially increase *S/N* utilizing longer experimental time. In order to evaluate NS, HR-MAS NMR measurements were performed in 32, 64, 128, 256 and 512 scans (Figure 6.8). The smaller scans (< 256) showed poor signal-to-noise *S/N* = 534.82 (32 scans), *S/N* = 735.19 (64 scans), and *S/N* = 1057.82 (128 scans). Since, higher scans (> 256) proportionally improved *S/N* in max. experimental time e.g. *S/N* = 1256.50 (256 scans = ~22 min) and *S/N* = 1918.51 (512 scans = ~50 min). In brief, due to experimental time, 256 scans (22 min) were suitable and used against 512 scans.

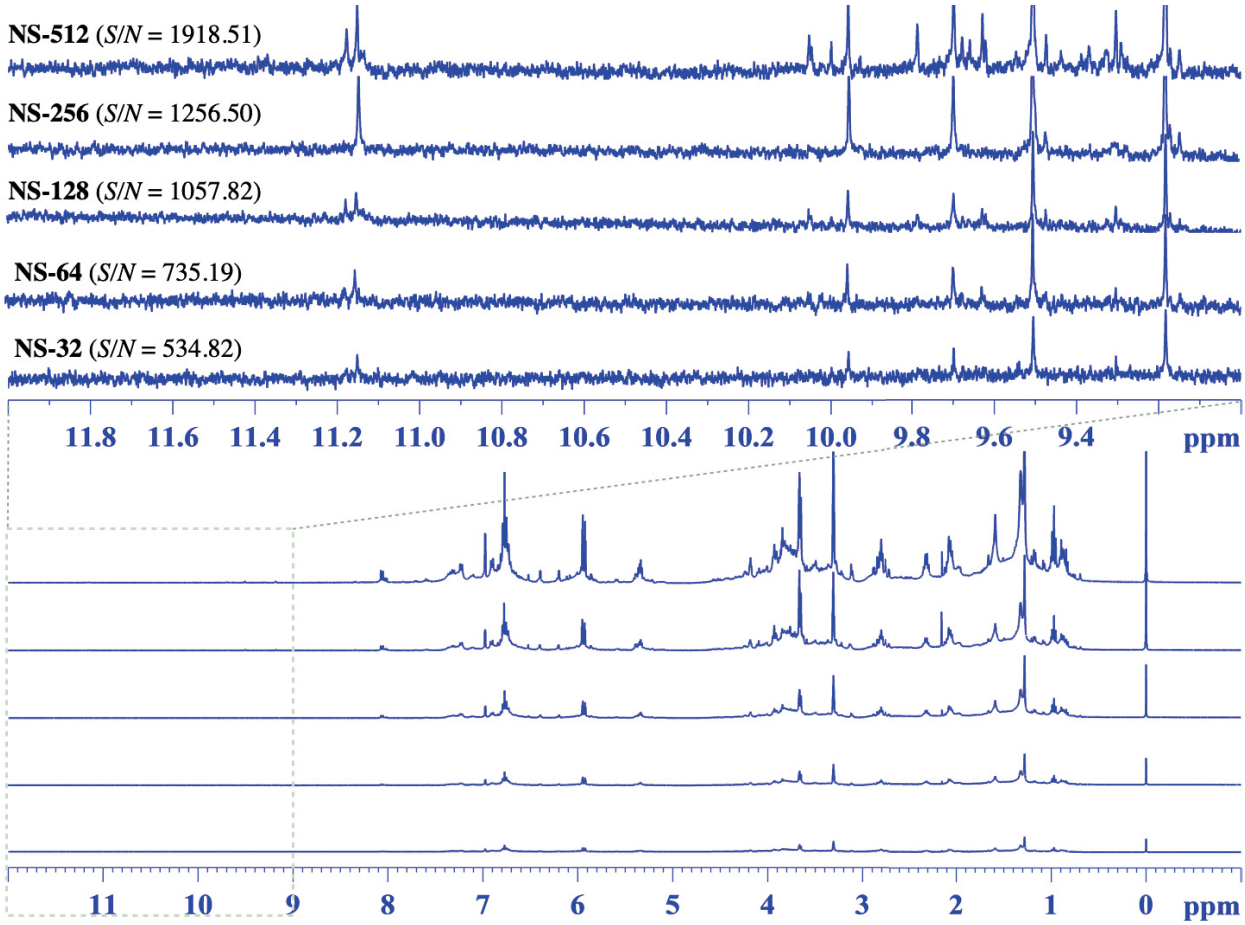

Figure 6.8. ^{1}H HR-MAS NMR *noesypr1d* spectra (400.13 MHz) showing number of scans evaluation in leaf powder (10 ± 1.0 mg: CD_3OD) from *Maytenus ilicifolia*.

The multiorientational atomic interactions in materials were averaged out by an evaluated magnitude of spinning frequency in HR-MAS NMR experiment (RENAULT et al., 2013). It is noteworthy that exceeding moderate spinning speed can increase sample temperature, molecular degradation, and sometime MAS rotor damage (JENSEN et al., 2019). However, lower spinning speed can result spinning side bands (SSBs) (RENAULT et al., 2013). This means, it is of prime importance to establish moderate rotational frequency for MAS rotor (containing sample).

The spinning rate optimization was completed for MAS rotor packed with 10 ± 1.0 mg powdered materials in 40 µL CD_3OD without air bubbles (that resist shimming). In this process five NMR spectra were measured with 2-6 kHz spinning rates (Figure 6.9). When the profiles were mutually compared, several SSBs (pointed with red arrows in Figure 6.9) were observed with lower spinning speed (2-4 kHz). Such SSBs, represented that these spinning rates (< 5 kHz) were probably of insufficient magnitudes to those from anisotropic interactions in the sample. In other words, anisotropic interactions were rather of high degrees

which needed to be averaged out, providing equal or high ordered spinning rates. In order to reduce and or remove these interactions in the sample, spinning rate was increased (5-6 kHz) and related SSBs were disappeared in the spectrum. Similar spectral window (20.00 ppm) was used in spinning rate evaluation, finally 5 kHz spinning rate was found suitable that was used in entire analyses.

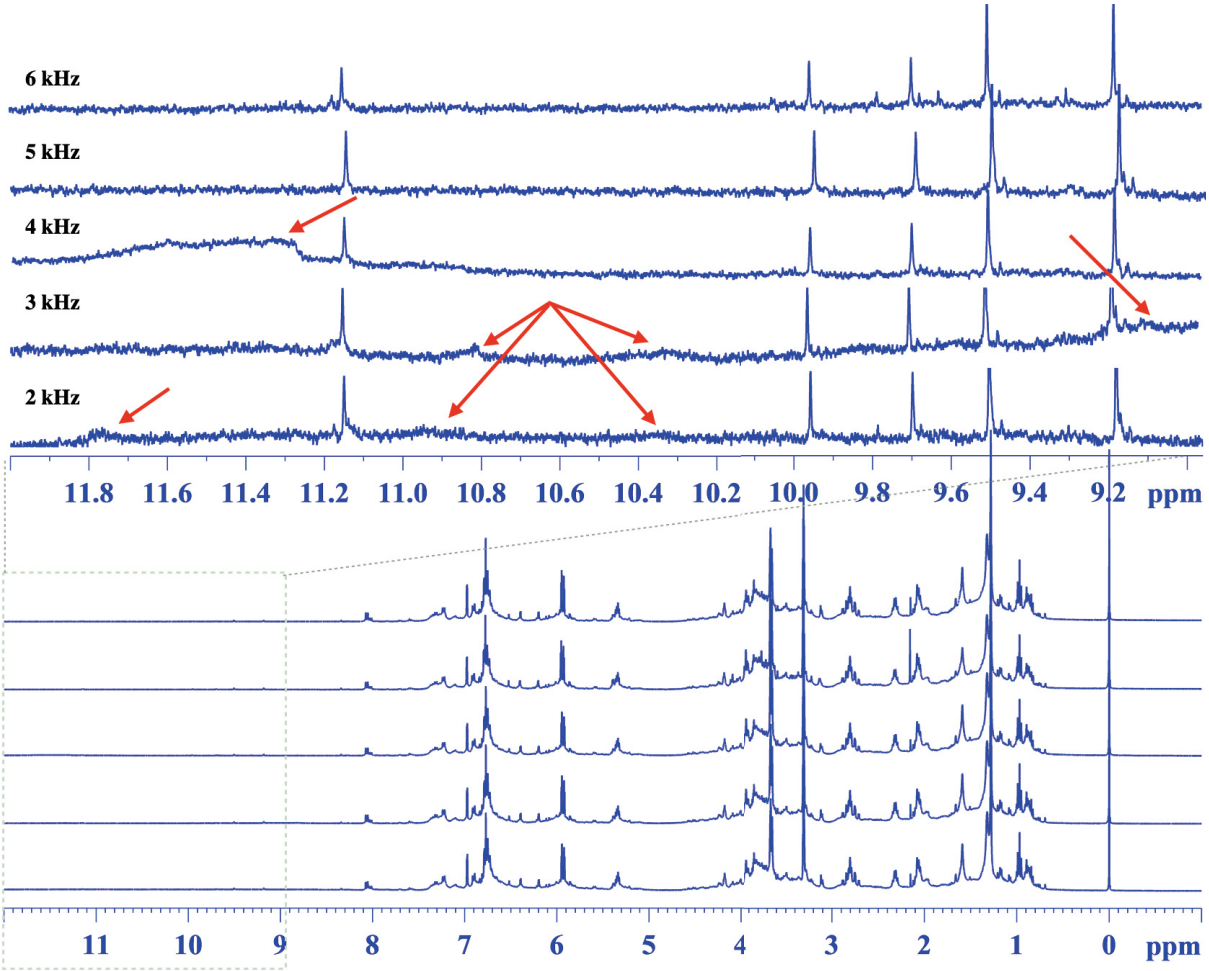

Figure 6.9. ^{1}H HR-MAS NMR *noesypr1d* spectra (400.13 MHz) showing rotor spinning frequency evaluation in leaf powder (10 ± 1.0 mg: CD_3OD) from *Maytenus ilicifolia.*

The (relaxation delay and) mixing time in *noesypr1d* experiment are considered long low power saturation periods that work definitely to saturate intense peak of solvent (water) and avoid other signals unaffected in the spectrum from desired sample (GOGIASHVILI et al., 2019; MCKAY, 2011). In this pulse sequence the intense water signal is irradiated at particular carrier frequency (δ 5.00 – 4.80) to complete suppression mechanism.

In *noesypr1d* (GOGIASHVILI et al., 2019; TENG, 2013), the low power two 90° pulses were applied to convert net magnetizations from solvent and solute spins into "-*z* axis",

generally water spins have different T_1 (spin-lattice) relaxation time (usually longer T_1) than in solutes. These two 90° pulses were followed by a mixing period (ms), time for net magnetization to built equilibrium state back in "+*z*-axis", in this duration spins magnetization vector from solute (with small T_1) were relaxed quicker rather than in solvent. The mixing time (ms) was followed by a third 90° tip angle to once again irradiate the magnetization (to re-saturate the partially relaxed spins of water and) from solute (previously relaxed along +*z* axis) to bring them onto the transverse plane. When the third 90° pulse was switched off, the entire spins restarted to accomplish equilibrium by emitting the priorly absorbed energies that created oscilating fields along *x, y*-plane and finally detected by the electronic coil around the sample inside NMR probe, and sampled as Free Induction Decays (FIDs) in experiment.

In solvent suppression, *noesypr1d* sequence was considered with relaxation delay time of 1 sec, although mixing time (t_{mix}/ D8) period was evaluated by providing several time scales (in millisecond). For instance, variable mixing time (t_{mix}) such as D8 = 100; 150; 200; 250 and 300 milliseconds (ms) were used in the measurements, followed by *S/N* calculations (Figure 6.10). In *S/N* calculations, the signal (δ 7.05-6.95) and noise (δ 12.05-11.95) of equal width (δ 0.10) were considered. In favor of mixing time, satisfactorily higher signal-to-noise ratio (*S/N* = 1423.11) was obtained in D8=100 ms, which were continuously used.

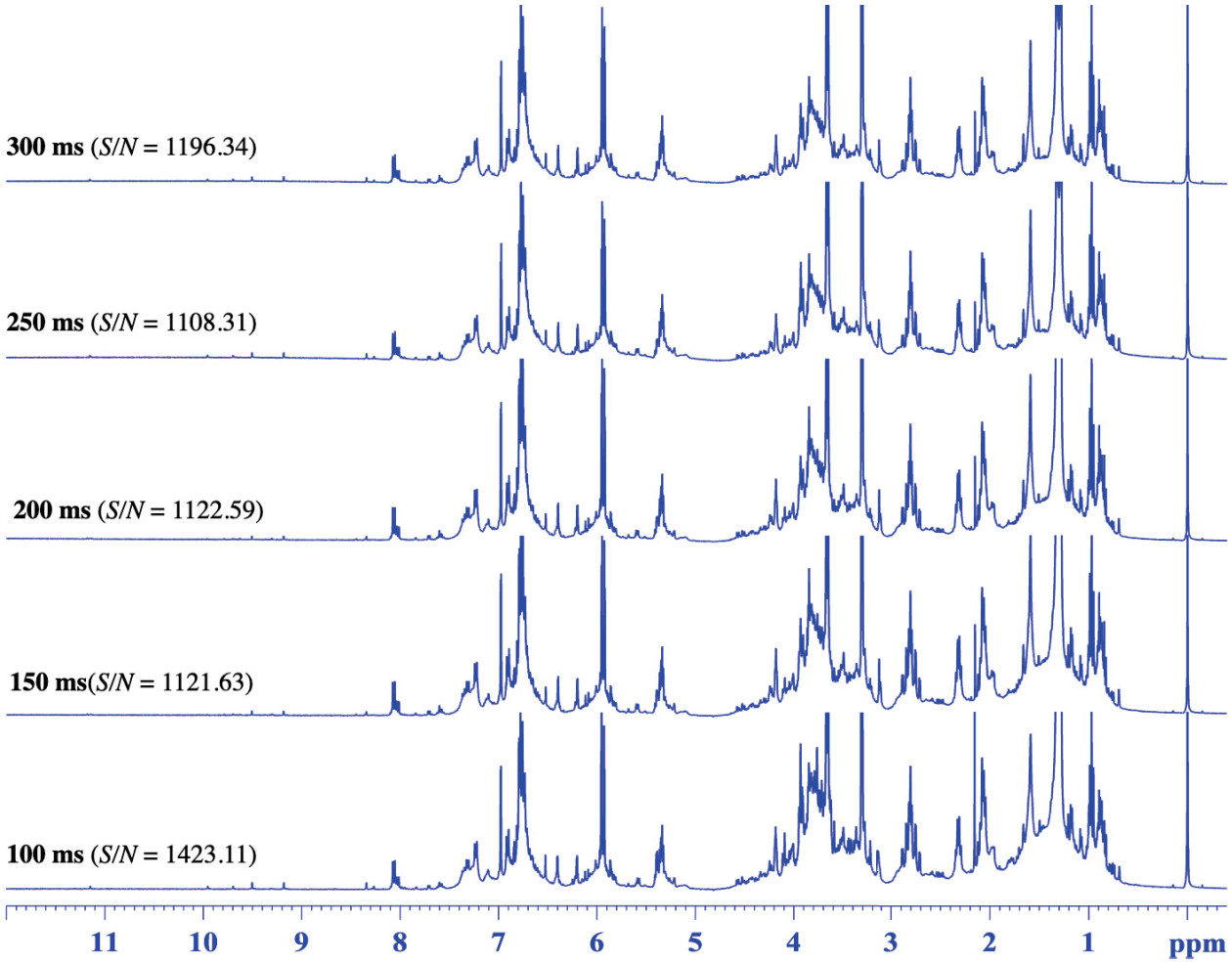

Figure 6.10. ^{1}H HR-MAS NMR *noesypr1d* spectra (400.13 MHz) showing mixing time evaluation in leaf powder (10 ± 1.0 mg: CD_3OD) from *Maytenus ilicifolia*.

In order to eliminate intense water peak in ^{1}H HR-MAS NMR spectra, additionally the power level (pl9 in decibels, dB) was adjusted. In this case, different digital values; 43, 50, 55 and 60 dB were used by irradiating (and overviewing the reappearance of) the water signal in its specific frequency region (δ 5.00-4.80) in successive meaasurements.

The power level evalutaion in *noesypr1d* was helpful that perfectly saturated intense water signal without distracting other spins, as previously observed in the carbohydrates range (under ~43 dB) shown in the amplified spectra (Figure 6.11). On one hand this represents that these resonances were sensitive and suffered when exposed to high power (pl9 = < 55 dB) RF-pulse. Although on the other hand, subjecting low power (pl9 >> 55 dB) RF-pulse the water resonance was returning and causing baseline distortions in the spectrum. To diminish these undesired factors, the RF-pulse was estimated to use a moderate power level (55 dB) that was adequate in achieving high-resolution spectra of better *S/N* (1820.11) (Figure 6.11).

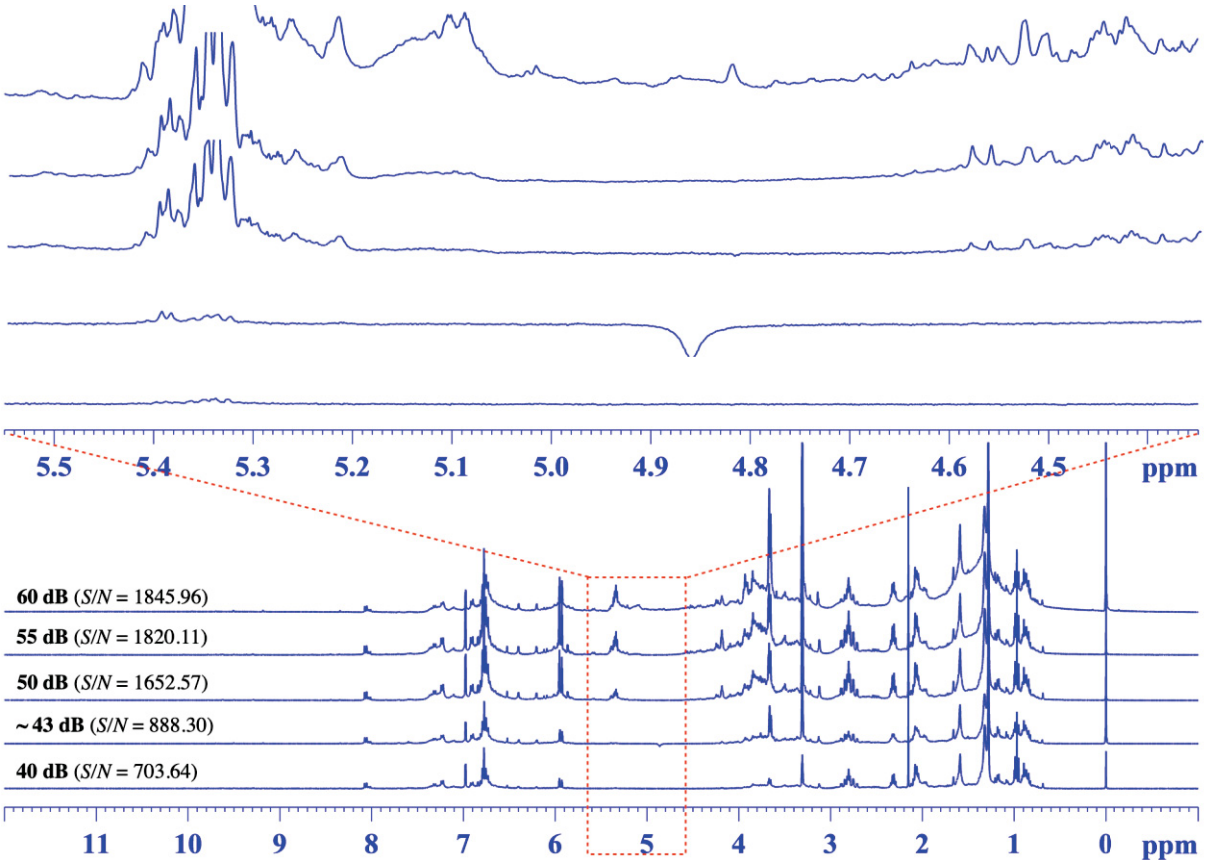

Figure 6.11. ^{1}H HR-MAS NMR *noesypr1d* spectra (400.13 MHz) showing power level (pl9) evaluation in leaf powder (10 ± 1.0 mg: CD_3OD) from *Maytenus ilicifolia*.

Presumably, *noesypr1d* sequence in HR-MAS measurements was assumed sensitive, but robust under controlled pl9, therefore the whole plant matrices were analyzed with a moderate lower pre-saturation power level (55 dB). It is noteworthy that the power level should need to optimize with extreme care, since to surpass a certain limit (here e.g.; pl9 << 43 dB), the pulse sequence turns aggressive that cause technical problem to NMR probehead, temperature increase in the sample, and molecular degradation (TORRES et al., 2016).

Subsequently, overall HR-MAS NMR measurements were performed by *noesypr1d* with 296 K temperature, 256 transients (NS), 1 sec recycle delay (D1), pre-saturation power level (pl9) of 55 dB, mixing time period (D8 = t_{mix}) of 100 ms, pulse duration (p1) of 5.63 µsec, 64 k number of points (TD), spectral window (SW) of 8002.6 MHz and acquisition time (AQ) was 4.09 sec. The *noesypr1d* pulse program was "RD– Π/2- t1– Π/2– t_{mix} – Π/2- AQ". The individual experiment was completed in ~30 minutes including sample preparation, rotor packing, manual tuning-matching and shimming steps.

Throughout HR-MAS NMR experiments, samples were spun with 5 kHz spinning frequency under so-called magic angle (θ_{MAS} = 54.74°). Prior to HR-MAS NMR analyses,

probe tuning-matching, magic angle and shimming adjustment were manually performed. The entire raw Free Induction Decays (FIDs, time domain) were Fourier Transformed (FT) into frequency domain (real spectra) and zero-filled to 64 k data points followed by Lorentzian line broadening function (LB = 0.3 Hz) in Topspin software (v. 3.1, Bruker). All chemical shifts were calibrated to internal reference standard, tetramethylsilane (TMS) signal at δ 0.00.

6.2 NMR-BASED INTER-PLANT SPECIES CORRELATION

The context hereby focused to the identification of similarities and or dissimilarities between *Maytenus* genus (*M. ilicifolia* and *M. aquifolium*) and other plants (*Z. ilicifolia, S. bomplandii, B. laurina,* and *C. gongonha*) that share similar leaf texture (Figure 4.1; p. 30).

According to the same methodology, leaves were harvested in October (2018) from different locations and followed by taxonomical identifications (Table 5.1; p. 51). The leaf materials were prepared according to the protocoled procedure and submitted to HR-MAS NMR analyses. Based on HR-MAS NMR, the spectral profiles from authentic *Maytenus ilicifolia* and further five species were mutually compared (Figure 6.12). The visual assessement of spectra was carried out in order to hypothetically distinguish all plants species based on signals (dis)similarities.

In the initial assessment phase, two spectral profiles (blue in Figure 6.12) from *Maytenus* genus same family (Celastraceae) were very similar. The none matching NMR spectra from remaining plants were separated however, *Maytenus ilicifolia* and *Maytenus aquifolium* were furthermore investigated (Figure 6.13) in detail.

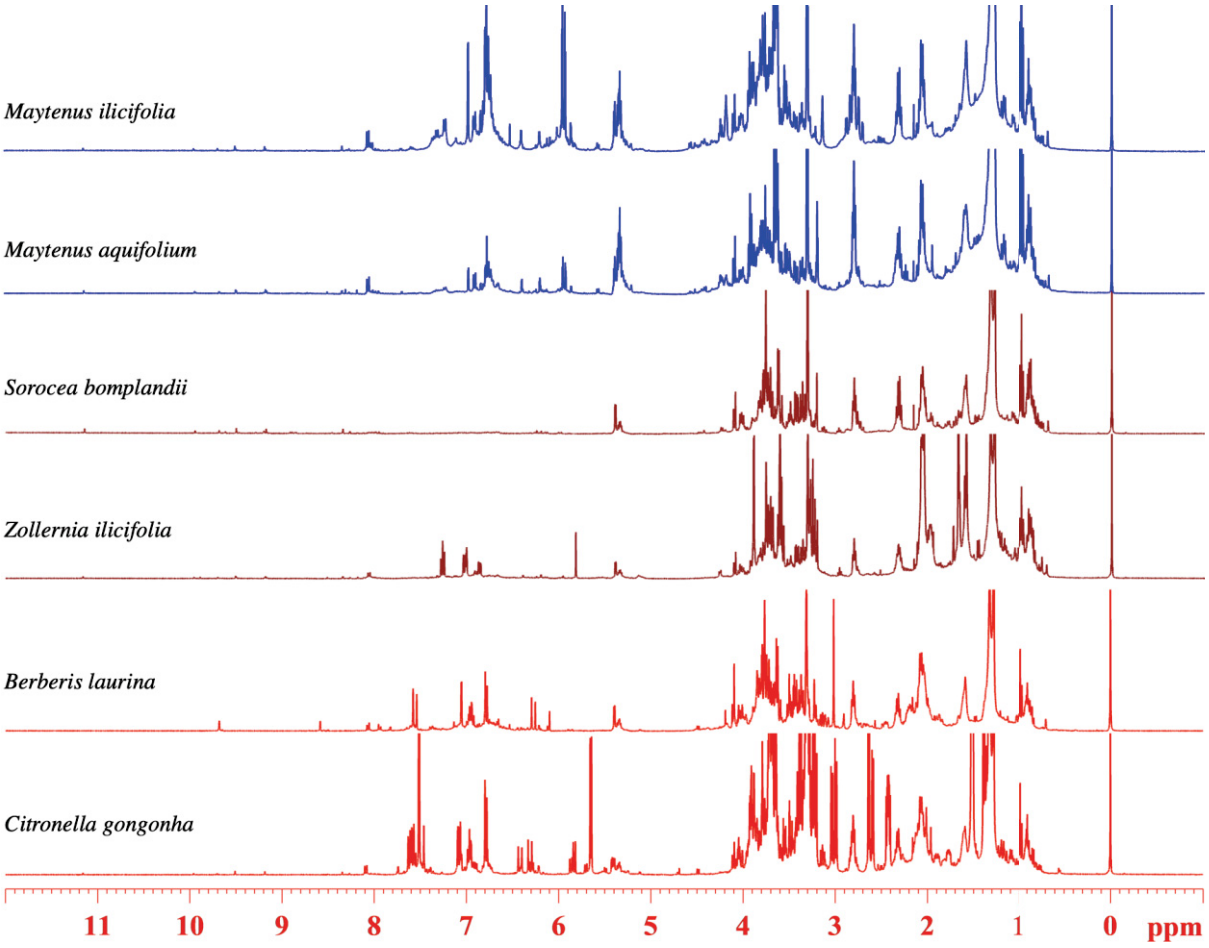

Figure 6.12. Comparative ^{1}H HR-MAS NMR spectra (400.13 MHz) in leaves powder (10 ± 1.0 mg: CD_3OD) from all six individual plant species.

Furthermore, after visualizing similarities between two species of same family were sequentially collected during four seasons (Oct-Dec. 2018; Feb-Aug. 2019). In per harvest time, leaf collection was carried out from three sections (top, middle, bottom) in both allied individuals. The leaf selection from upper to bottom parts in each individual was intended to observe their chemical composition and alterations with respect to their development.

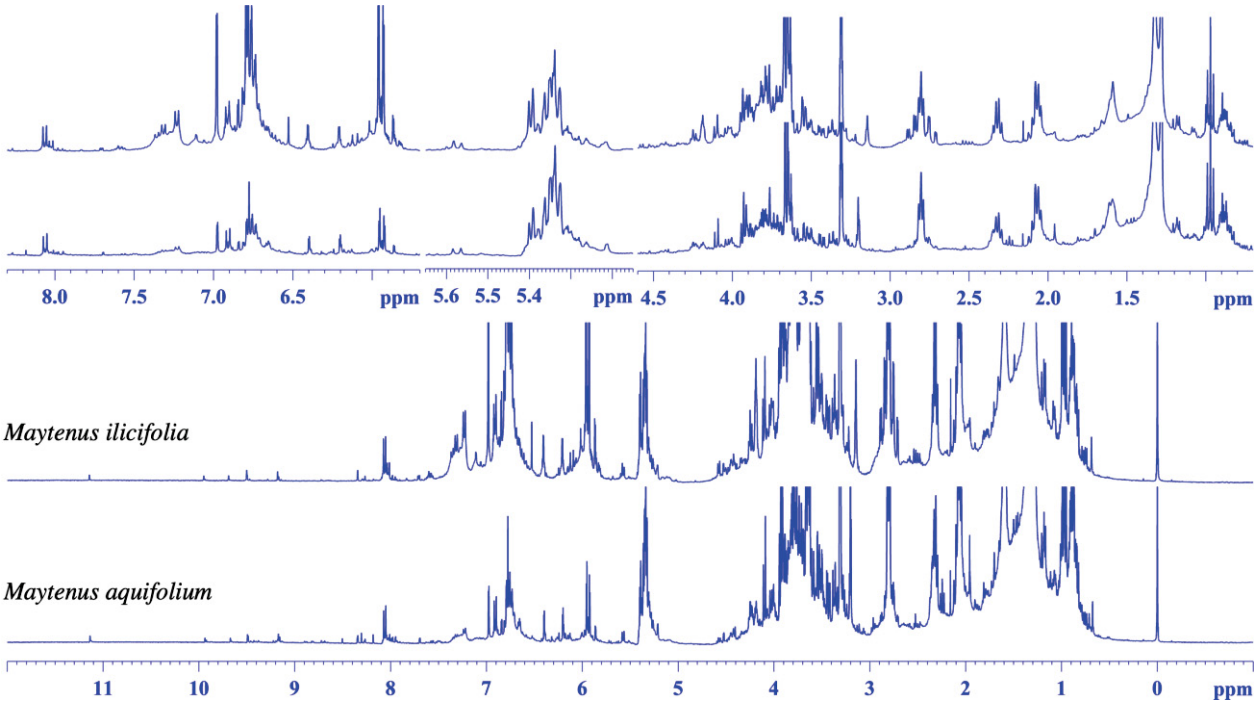

Figure 6.13. Comparative ^{1}H HR-MAS NMR spectra (400.13 MHz) in leaf powder (10 ± 1.0 mg: CD_3OD) from two individual plants species.

This assessment at first was accomplished by comparing signals relative intensities from chemical substance(s) in individual (upper, middle and or lower) part in the plant in accordance to periodic variations. Moreover, to see such differentiation, the spectral data from all upper to lower parts in both idnividuals was then analyzed further through unsupervised principal component analysis (PCA) approach respectively.

6.3 NMR-BASED TOPOLOGY DISCRIMINATION IN *Maytenus ilicifolia* AND *Maytenus aquifoliu*m (CELASTRACEAE)

6.3.1 *Maytenus ilicifolia* Mart. ex Reissek (Celastraceae)

^{1}H HR-MAS NMR measurements were successively carried out to the leaves from top (T), middle (M), and bottom (B) portions in *Maytenus ilicifolia* Mart. Ex Reissek, cultivated in botanical garden of Curitiba-PR. The collection was continued for one-year with a one-month gap (October, O; December, D. 2018: February, F; April, A; June, Jn; August, Aug 2019). After collection, the samples were handled and submitted to HR-MAS NMR analyses in respective time (month). Followed the analyses, spectral profiles (T, M, B) were mutually compared since, T-samples always showed higher spectral intensities (Figure 6.14).

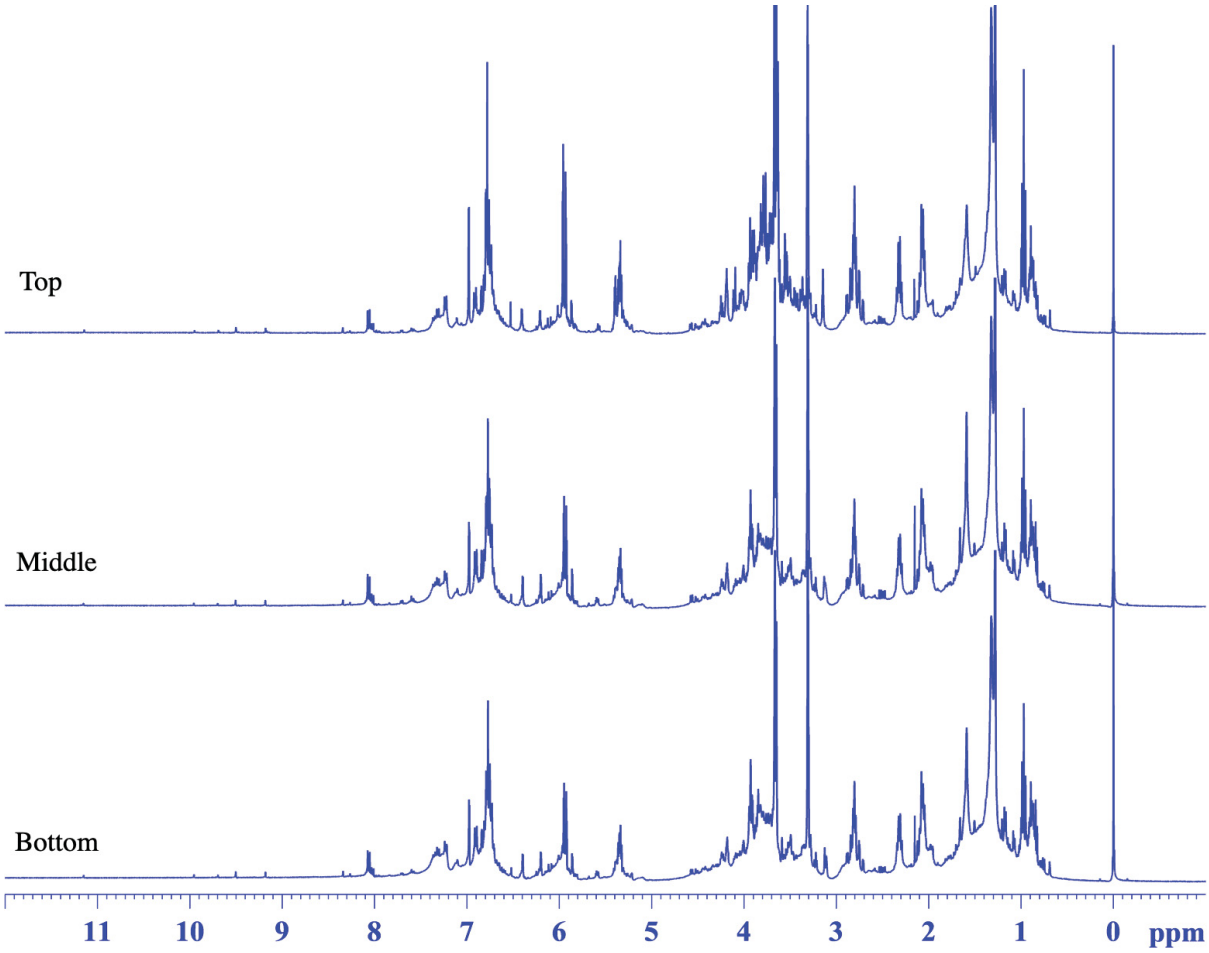

Figure 6.14. ^{1}H HR-MAS NMR spectra (400.13 MHz) in leaf powder (10 ± 1.0 mg: CD_3OD) from three sections in *Maytenus ilicifolia*.

In this way, six ^{1}H HR-MAS NMR profiles (only T-leaf) in different months were additionally compared (Figure 6.15), to determine profile(s) with higher signals relative intensities related to the chemical compound(s). These variations may occure due to the fact of mutual contact between plants and interacting environment or due to the seasonal variations. However, time to time quantitative (de-)stimulation is possible in any of the primary and or specialized metabolites (YANG et al., 2018; SAMPAIO et al., 2016; NCUBE et al., 2012).

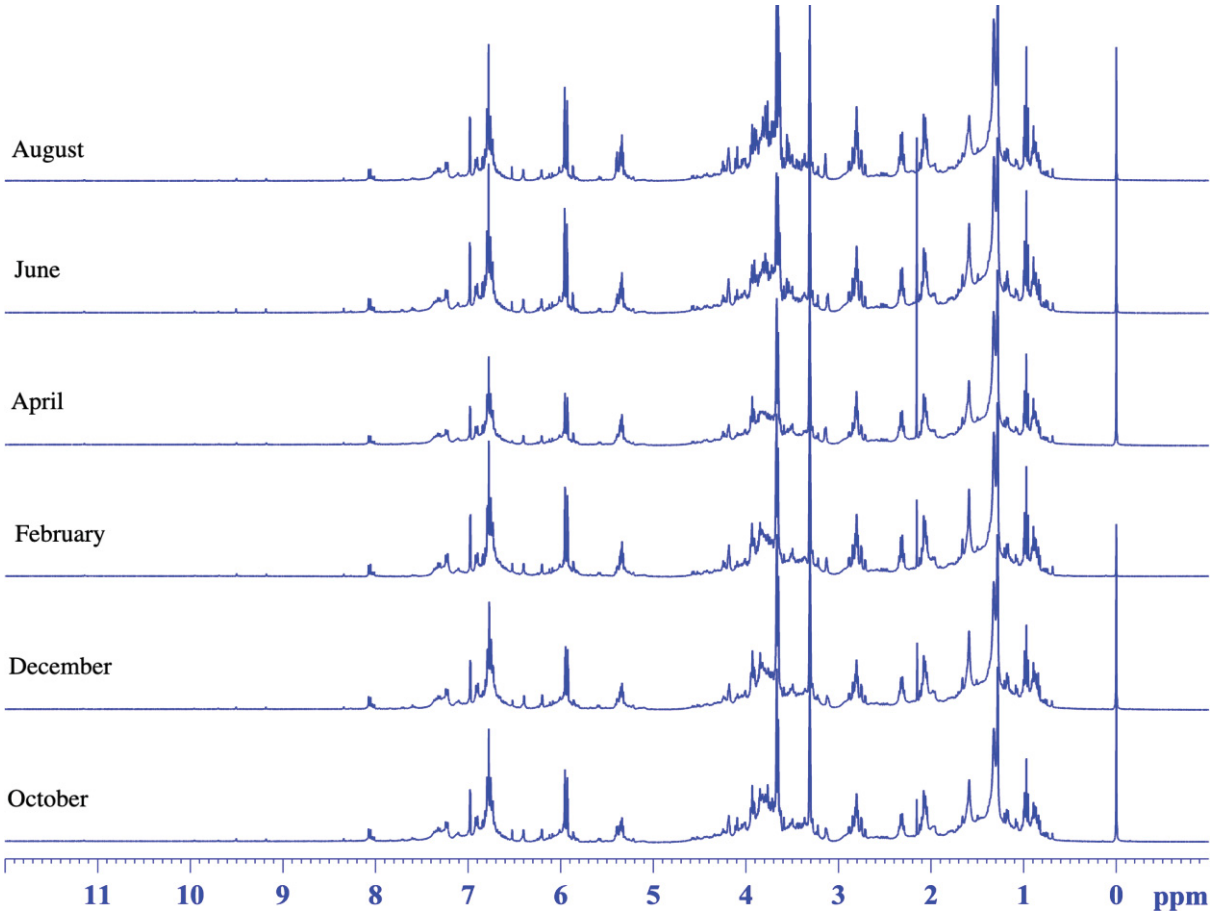

Figure 6.15. ^{1}H HR-MAS NMR spectra (400.13 MHz) in leaf powder (10 ± 1.0 mg: CD_3OD) from top section in *Maytenus ilicifolia* during four seasons (October 2018-August 2019).

Primary metabolites (carbohydrates and others) are mainly concerned to the normal function and growth however, the secondary metabolites (phenolics and several more) serve to protect plants in drastic circumstances that cause variabilities in quantititative chemical status. These fluctuations can be measured in NMR spectroscopy; however, signal intensities proportionally reflect quantitative information from chemical substances in the samples (i.e. plant). To trace the variable chemical states in the samples, their signals relative intensities can be overviewed by colored steric notation (Figure 6.16).

From the aromatic region (Figure 6.16), multiple signals mentioned with blue, green, and red stars, representing (-)-epicatechin (**2**), sucrose (**4**), and respectively fatty acid (**8**). The intensified signals were observed during two months (June-August 2019) from compound **2**, **4**, and **8**. Main chemical shifts (of **2**) were at δ 6.97 (d, $^{4}J_{H\text{-}H}$ = 1.8 Hz, 1H, CH-2'), δ 6.79 (dd, $^{3,4}J_{H\text{-}H}$ = 8.3; 1.8 Hz, 1H, CH-6'), δ 6.75 (d, $^{3}J_{H\text{-}H}$ = 8.3 Hz, 1H, CH-5'), δ 5.94 (d, $^{4}J_{H\text{-}H}$ = 2.3 Hz, 1H, CH-6), and δ 5.91 (d, $^{4}J_{H\text{-}H}$ = 2.3 Hz, 1H, CH-8). The intense doublet signal from sucrose (**4**) was δ 5.38 (d, $^{3}J_{H\text{-}H}$ = 3.8 Hz, 1H, *α*-CH-1). However, intense signals from

unsaturated fatty acid (**8**) were as such δ 5.34 (m, 6H; CH-9,10,12,13,15,16), δ 2.81 (t, $^{3}J_{H\text{-}H}$ = 6.00 Hz, 4H; CH_2-11,14), and δ 0.97 (t, $^{3}J_{H\text{-}H}$ = 7.5 Hz, 3H; CH_3-18).

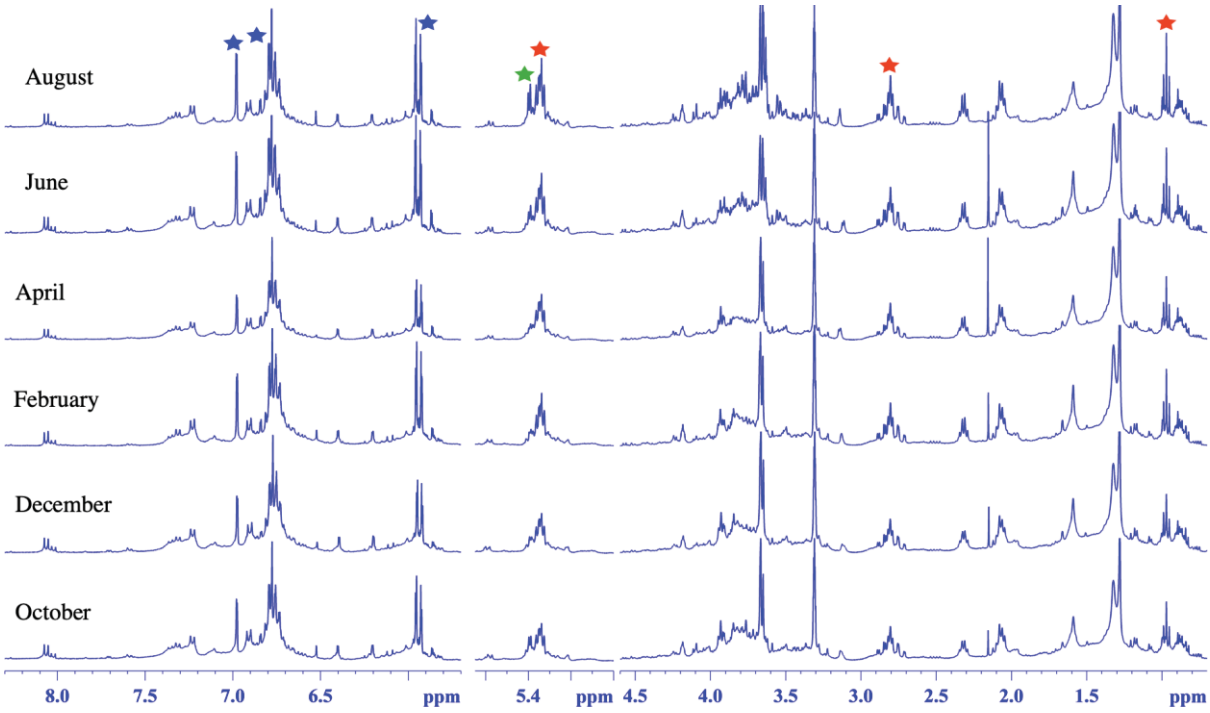

Figure 6.16. ^{1}H HR-MAS NMR spectra (400.13 MHz) in leaf powder (10 ± 1.0 mg: CD_3OD) from top section in *Maytenus ilicifolia* during four seasons (October 2018-August 2019). Signals with blue starrs = (-)-epicatechin, green = sucrose, and red = unsaturated fatty acids.

These chemical improvements were probably due to environmental factors and or seasonal variation as reported in literature (YANG et al., 2018; SAMPAIO et al., 2016; NCUBE et al., 2012). Literally, the months of June and August (2019) were associated to the late autumn and middle of winter in Curitiba-PR, Brazil. (**Spring**: 22 September to 21 December; **Summer**: 21 December to 20 March; **Autumn** (Fall): 20 March to 21 June; **Winter**: 21 June until 23 September).

6.3.2 *Maytenus aquifolium* Mart. (Celastraceae)

The *Maytenus aquifolium* species was non-cultivated naturally grown plant in a shady biome, and completely surrounded by a number of trees with less sunlight availablity. Thus, leaves from *Maytenus aquifolium* Mart. (Celastraceae) were harvested in the same time but different site (Table 5.1; p. 51) in contrast to *Myatenus ilicifolia*. The leaves associated to upper top (T), middle (M), and bottom (B) portions in this individual were continuously collected around one-year with a gap of one month (October 2018- August 2019). After each

collection, the vegetative samples were handled and followed by HR-MAS NMR measurements. A large number of spectral profiles (T, M, B) were obtained and mutually compared (Figure 6.17).

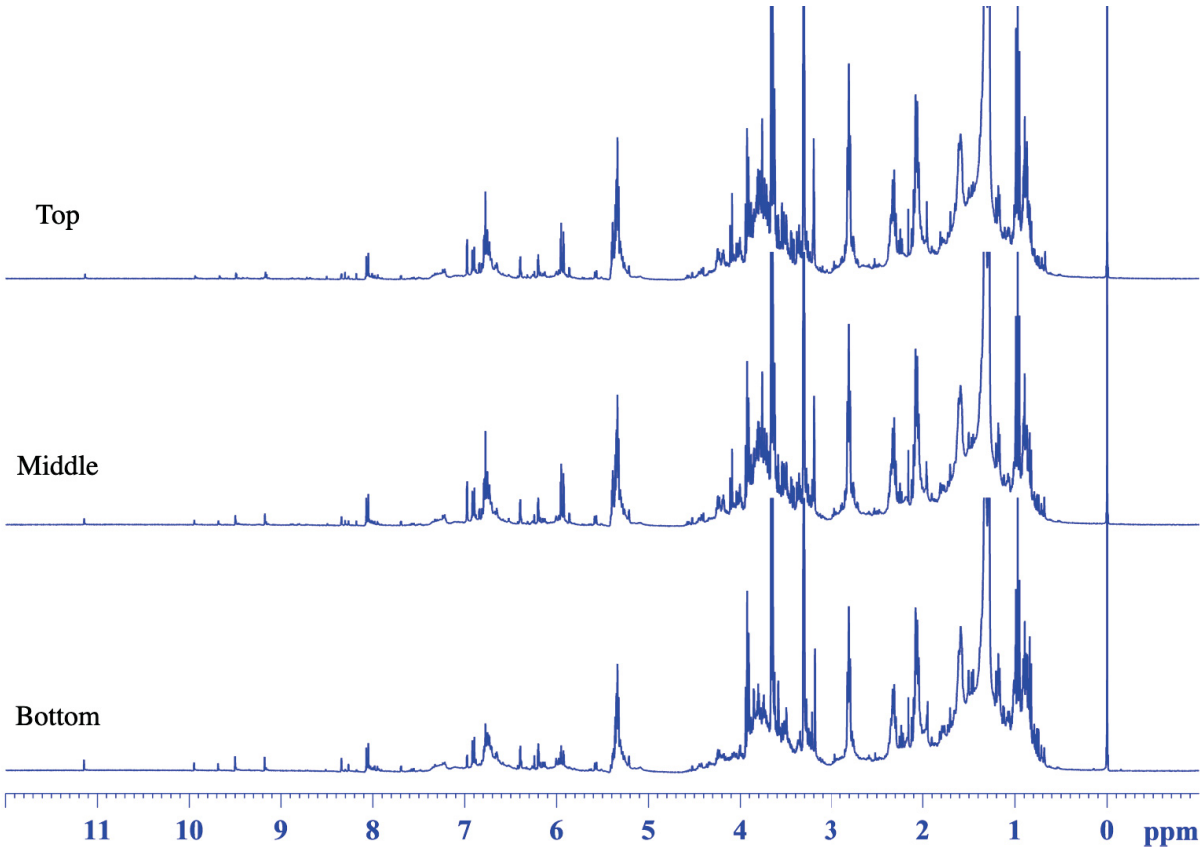

Figure 6.17. ^{1}H HR-MAS NMR spectra (400.13 MHz) in leaf powder (10 ± 1.0 mg: CD_3OD) from three sections in *Maytenus aquifolium*.

Besides, "M and B-leaf samples", the leaf profiles from only top (T) portion were considered (Figure 6.18). In order to recognize the competions among signals intensities, to an extent all (T, M, B) spectra showed downgraded signals from phenolic compounds in comparison to those observed in *Maytenus ilicifolia* (a cultivated species in non-shady environment). In fact, phenolic ingredients play essential role in plant defense mechanisms against critical environmental conditions such as sunlight or other factors. Whenever, the environmental conditions are normal, for example less production or biogenesis of phenolics compounds are expected. These changes can be traced by signals intensities in NMR spectrum. In accordance to developmental process, several T-spectral profiles have been shown in Figure 6.18.

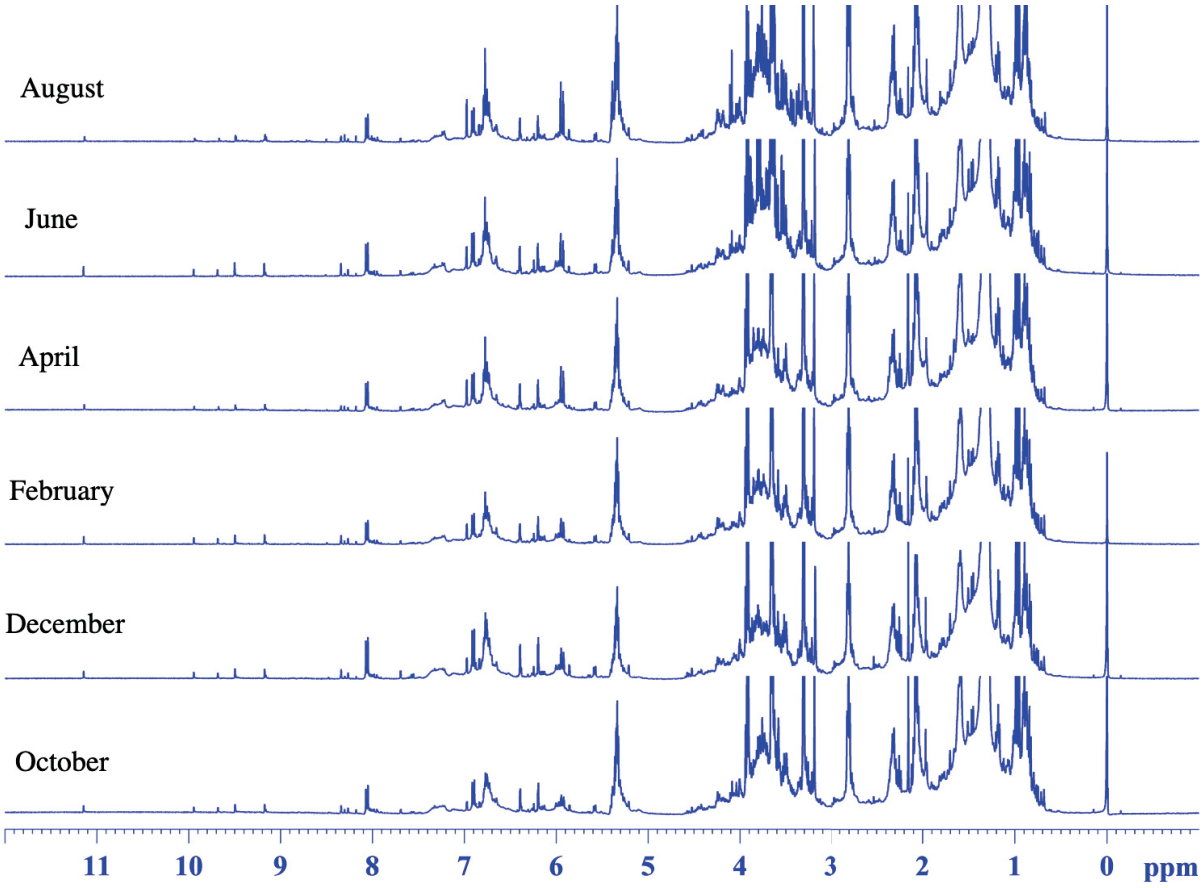

Figure 6.18. ^{1}H HR-MAS NMR spectra (400.13 MHz) in leaf powder (10 ± 1.0 mg: CD_3OD) from top section in *Maytenus aquifolium* during four seasons (October 2018-August 2019).

The Figure 6.19 revealed large number of intensified signals (with stars) from *Maytenus aquifolium,* although these signals were less intense in comparison to *Maytenus ilicifolia*. The relatively increased signals with blue stars were from the phenolics constituents e.g. (-)-epicatechin (**2**) and kaempferol aglycone (**3**), observed in the month of August 2019. The related improved signals from (-)-epicatechin (**2**) were δ 6.97 (d, $^{4}J_{H\text{-}H}$ = 1.8 Hz, 1H, CH-2'), δ 6.79 (dd,$^{3,4}J_{H\text{-}H}$ = 8.3; 1.8 Hz, 1H, CH-6'), δ 5.94 (d, $^{4}J_{H\text{-}H}$ = 2.3 Hz, 1H, CH-6), and δ 5.91 (d, $^{4}J_{H\text{-}H}$ = 2.3 Hz, 1H, CH-8). The kaempferol aglycone (**3**) were δ 8.06 (d, $^{3}J_{H\text{-}H}$ = 8.9 Hz, 1H; CH-2' also CH-6'), δ 6.39 (d, $^{4}J_{H\text{-}H}$ = 2.1 Hz, 1H; CH-8), and δ 6.19 (d, $^{4}J_{H\text{-}H}$ = 2.1 Hz, 1H; CH-6). Similarly, other signals (with red star) at δ 5.34 (m, 6H; CH-9,10,12,13,15,16) of unsaturated component, δ 2.81 (t, $^{3}J_{H\text{-}H}$ = 6.00 Hz, 4H; CH_2-11,14), δ 2.06 (m, 4H; CH_2-8,17) and δ 0.97 (t, $^{3}J_{H\text{-}H}$ = 7.5 Hz, 3H; CH_3-18) in fatty acid (**8**) contents were very intense in all months. The intense doublet signal from sucrose (**4**) was δ 5.38 (d, $^{3}J_{H\text{-}H}$ = 3.8 Hz, 1H, *α*-CH-1), δ 4.09 (d, $^{3}J_{H\text{-}H}$ = 8.4 Hz, 1H; *β*-CH-3') one triplet type signal from sugar at 3.93 (t, J = 6.40 Hz).

.

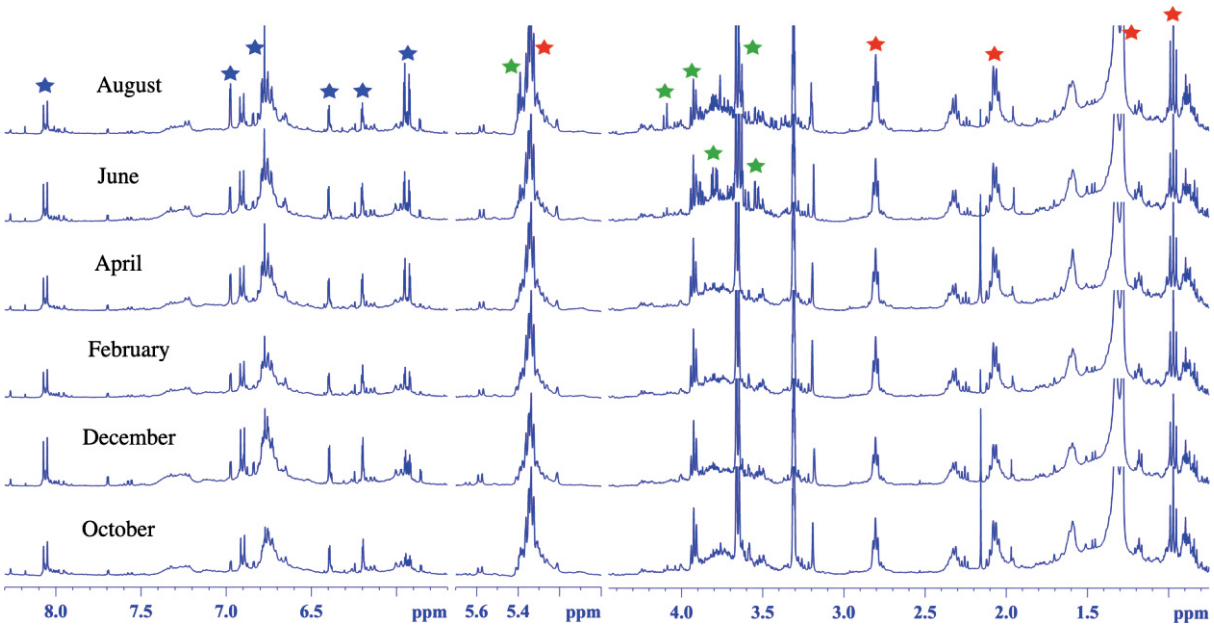

Figure 6.19. ^{1}H HR-MAS NMR spectra (400.13 MHz) in leaf powder (10 ± 1.0 mg: CD_3OD) from top section in *Maytenus aquifolium* during four seasons (October 2018-August 2019). Signals with blue stars = kaempferol and (-)-epicatechin, green = sucrose or other sugars and red = unsaturated fatty acids.

In comparison, the ^{1}H HR-MAS NMR spectra from *Maytenus aquifolium*, showed downgraded signals for phenolics composition, which seemed direct influence from shady environment and or biome on the chemical pattern. The quantitative impact on (primary and or) particularly secondary metabolites could be recognized in plants interacting to the surroundings (NCUBE et al., 2012). As described previously (SAMPAIO et al., 2016), various classes included plant phenolic compounds are natural defenders to overcome the effects from extreme conditions, meaning that maximum temperature, sunlight or other factors are main component tending to disrupt the biosynthetic mechanisms and automatically (de)promote in high (or low) production of phenolic compounds. To compare recent work with literature, the flavan-3-ol, flavonoids, with and without glycosylated flavonol were quantitatively reduced in multiple plants due to shade (XU et al., 2020; YANG et al., 2018). Besides flavonoids and or flavanols (catechins), several organic and phenolic acids, and carbohydrates are reportedly affected from higher sunlight (LI et al., 2020), temperature variabilities, rain fall, humidity, seasonal and geographical orientations (WEN et al., 2020), and herbivores interactions (LI et al., 2020). Some of these factors are reported from Mossi et al. (2009), they demonstrated leaf phenolic profile from *Maytenus ilicifolia* and *Maytenus aquifolium*, and also in the leaves from *Rollinia mucosa* (AFONSO et al., 2019).

According to the discussion above related to both individuals are seeming more effected in two months (June, August). This represented that the June to August phase was probably the drier period of the year and more affective to the plant chemical status especially in *Maytenus ilicifolia* Mart. Other than quantitative properties, the inconvenient ecological conditions may also alters the typical alimentary, neutraceutical and therapeutic values of plants primary and secondary metabolites (KHAN et al., 2019; BAKOYANNIS et al., 2019; FREIRE et al., 2018; PREMALATHA et al., 2018; IMRAN et al., 2018; ALAMGIR., 2017).

In Brazil the four seasons for example, **Spring**: 22 September to 21 December; **Summer**: 21 December to 20 March; **Autumn** (Fall): 20 March to 21 June; **Winter**: 21 June until 23 September.

6.4 CHEMICAL COMPOUNDS IDENTIFICATION IN THE LEAVES FROM *Maytenus ilicifolia* AND *Maytenus aquifolium* MART. (CELASTRACEAE)

Plants are naturally complex matrices of numerous molecules that provide crowded and highly overlapped ^{1}H NMR spectra. These overlapped and or corwded signals requires to be determined with multidimensional NMR approaches. In this study multiple chemical compounds were detected in ^{1}H HR-MAS NMR spectra from *Maytenus ilicifolia* and *Maytenus aquifolium*. These chemical structures were established by multidimensional (2D) NMR approach in the liquid-state. The 2D NMR comprised multiplicity edited HSQC and HMBC mapping that were helpful to investigate heteronuclear assignments (^{1}H-^{13}C). In order to map homonuclear (^{1}H-^{1}H) correlations, the 2D TOCSY and COSY experiments were used.

In following sections, ^{1}H HR-MAS NMR profile of *Maytenus ilicifolia* (Figure 6.20) was divided into three major and amplified regions with signals annotations from individually identified metabolites. Each of the three segments in HR-MAS profiles is directly showed with its matching part from 2D HSQC correlation map. The fundamental purpose to show heteronuclear (^{1}H-^{13}C) HSQC correlation maps were to directly facilitate the distinctions among CH, CH_3 and CH_2 groups in respective molecular structures (GAILLOT et al., 2018). In this discussion the 2D HSQC correlation maps will show two colors (blue and red), the blue colored 2D peaks will suggest CH and CH_3 groups while red colored 2D peaks the CH_2 groups in each molecular structure. The remaining 2D correlation maps (2D HMBC, TOCSY, and COSY) are separately annexed (see Annex 1.1 to Annex 1. 4; p. 135-136).

The three major regions in ^{1}H HR-MAS spectrum are shown with related 2D HSQC NMR correaltion maps, included the aromatic region (δ 8.50 to 6.0: Figure 6.22 and Figure

6.23), carbohydrate region (δ 5.8 to 3.00: Figure 6.27 and Figure 6.28) and respectively the aliphatic region (δ 3.00 to 0.50, Figure 6.30 and Figure 6.31). In ^{1}H HR-MAS NMR analysis, 10 ± 1.0 mg powder leaf materials were used in 40 µL CD_3OD locking solvent, although, in the 2D NMR measurements, 100 ± 1.0 mg powdered materials were extracted, and a total of 600 µL CD_3OD supernatant was used. The comparison between liquid-state (600 µL CD_3OD extract) and HR-MAS NMR (gel-state in 40 µL CD_3OD) measurements can be seen in Figure 6.20, shows almost similar spectra in different states from similar material. In the following discussions, only ^{1}H HR-MAS NMR have been taken respectively.

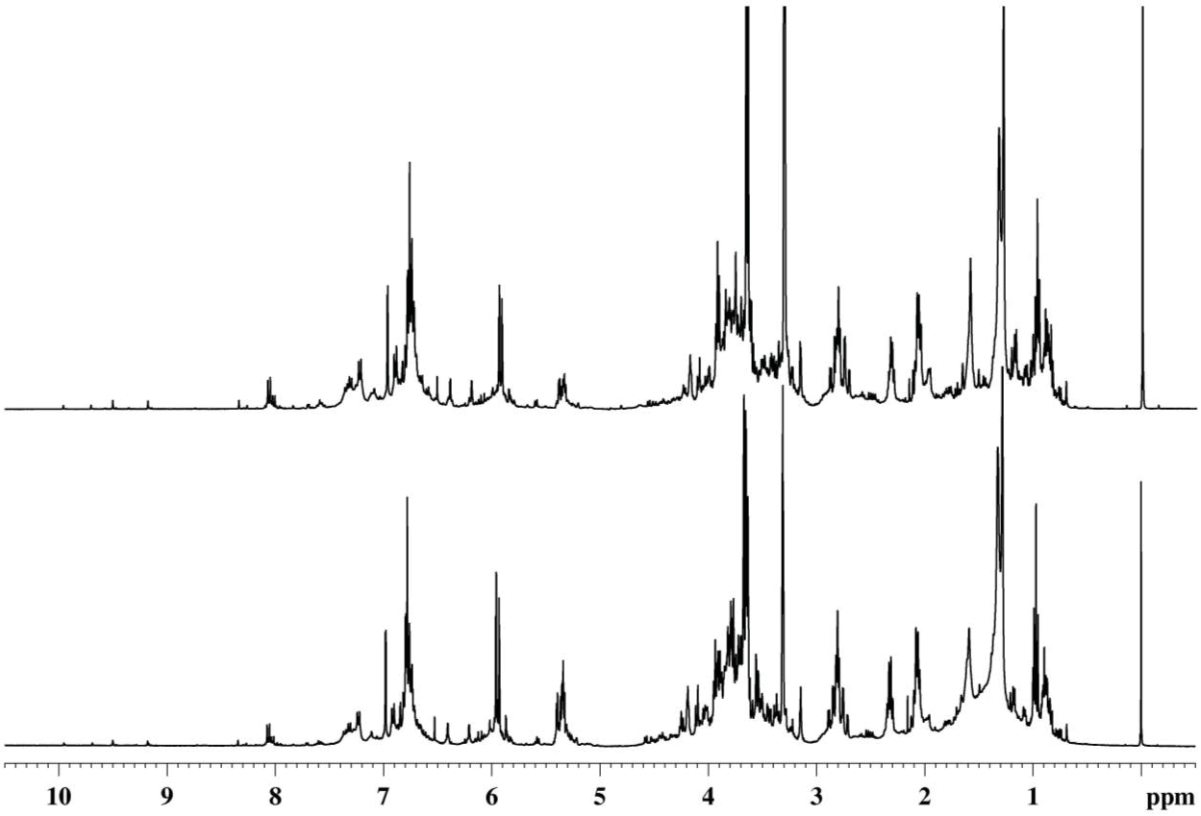

Figure 6.20. ^{1}H HR-MAS NMR spectra (400.13 MHz) in powdered leaf extract (upper spectrum) and gel-state (downward spectrum) from same *Maytenus ilicifolia.*

The ^{1}H HR-MAS NMR spectra demonstrated the presence of eight molecular species for example, kaempferol glycoside (**1**), (-)-epicatechin (**2**), kaempferol aglycone (**3**), sucrose (**4**), fumaric acid (**5**), alanine (**6**), threonine (**7**), and fatty acids (**8**) as shown (Figure 6.21). These molecular structures are explained one-by-one in the following text and the tabular information are given in allied sections.

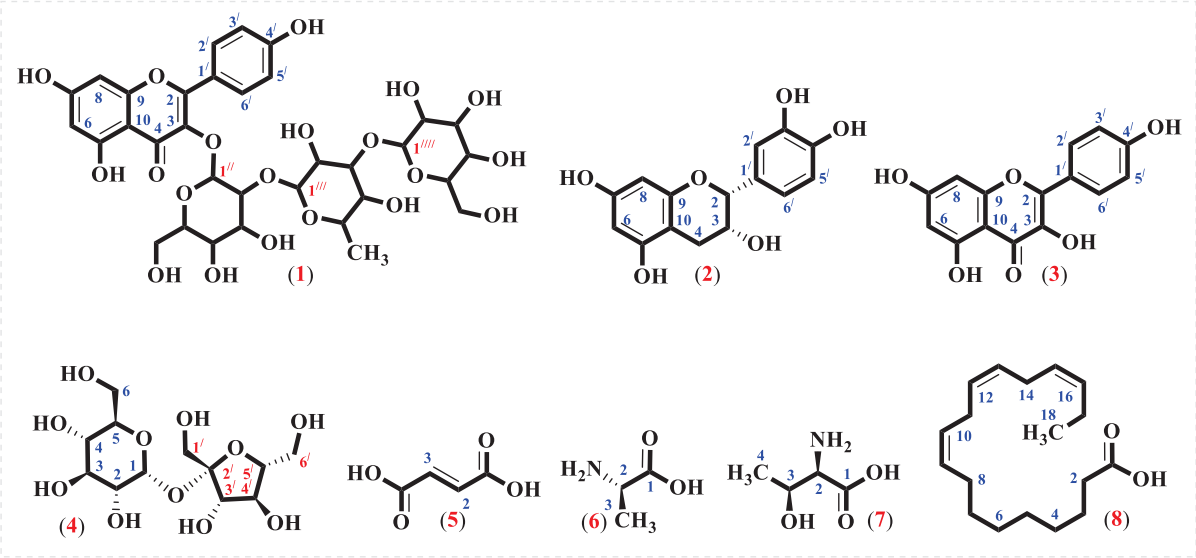

Figure 6.21. The chemical compounds identified in leaves from *Maytenus ilicifolia* and *Maytenus aquifolium* (Celastraceae) were kaempferol glycoside (**1**), (-)-epicatechin (**2**), kaempferol aglycone (**3**), sucrose (**4**), fumaric acid (**5**), alanine (**6**), threonine (**7**), and polyunsaturated fatty acids (**8**).

6.4.1 The aromatic region (δ 8.2-5.7)

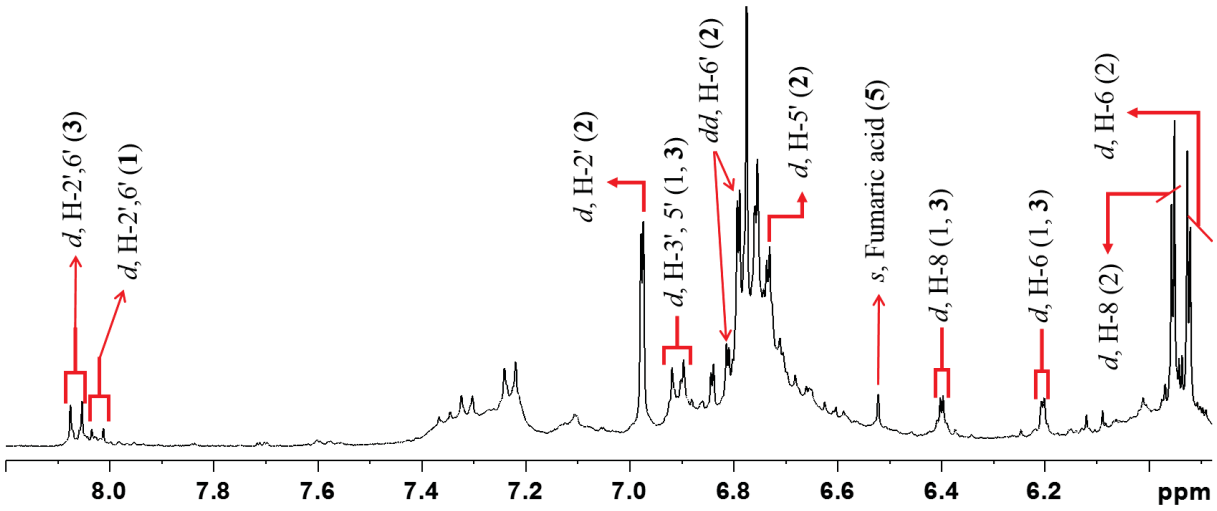

Figure 6.22. Amplified aromatic region (δ 8.20 to 0.07) in ^{1}H HR-MAS NMR spectrum (400.13 MHz) in leaf powder (10 ± 1.0 mg: 40 µL CD_3OD) from *Maytenus ilicifolia.*

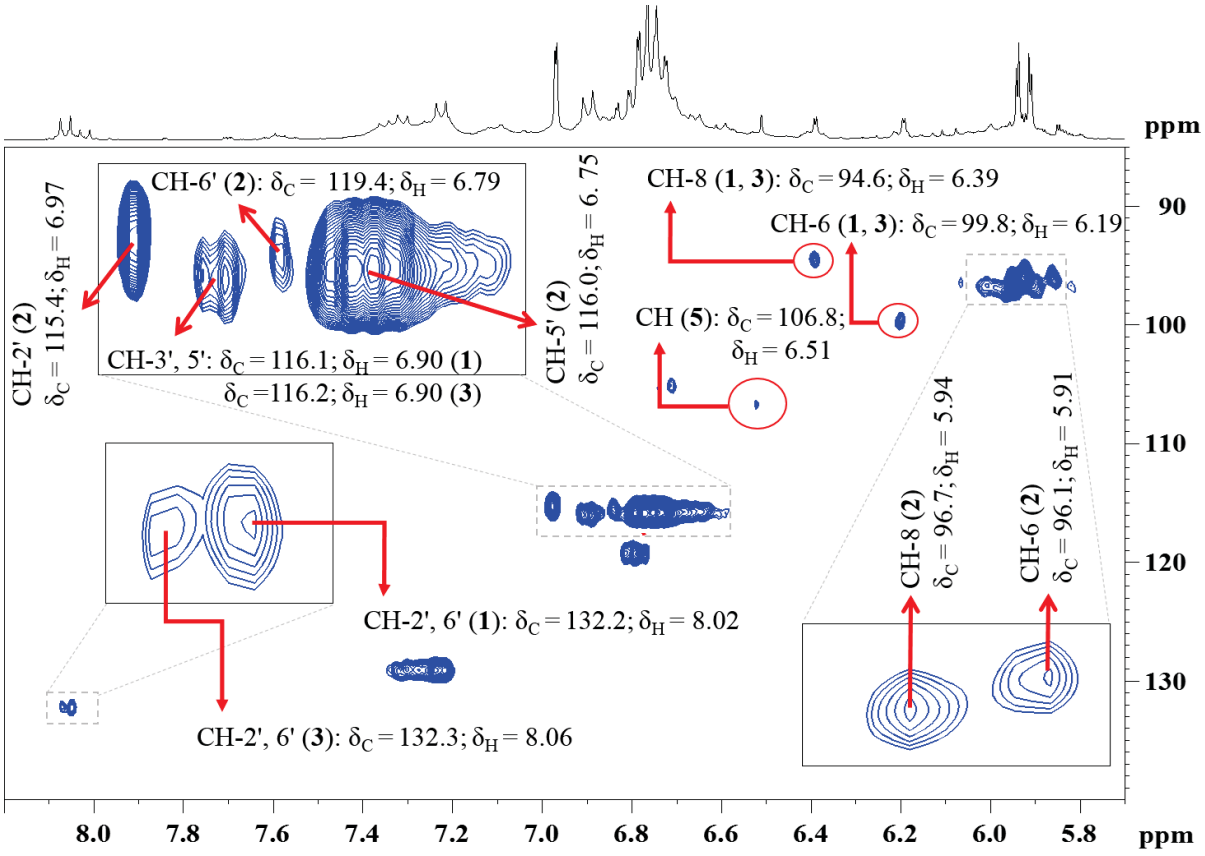

Figure 6.23. Aromatic region (δ 8.2-5.7 *vs.* δ 140.0-85.0) in ^{1}H-^{13}C direct correlation map (400.13-100.62 MHz) from multiplicity edited HSQC experiment performed over powdered leaf from *Maytenus ilicifolia*.

The high frequency range in the spectra (Figure 6.22 to Figure 6.23) presented signal from four metabolites such as kaempferol glycoside (**1**), (-)-epicatechin (**2**), kaempferol aglycone (**3**) and fumaric acid (**5**). The molecule (**5**) is explained later (Sec. 6.4.3.1).

6.4.1.1 The identification and structure elucidation of kaempferol glycoside (**1**)

The main metabolites detected in the leaves from *Maytenus ilicifolia* Mart. included kaempferol glycoside (**1**; Figure 6.24) (VILEGAS et al., 1999). This compound was identified by characteristic doublet signal in δ 6.19 (d, $^{4}J_{H\text{-}H}$ = 2.1 Hz, 1H) attributed to a hydrogen shown direct correlation to the carbon at δ 99.8 in methine group at position-6. The coupling constant of this hydrogen-6 showed that it was *meta*-coupled to another hydrogen represented by a doublet in δ 6.39 (d, $^{4}J_{H\text{-}H}$ = 2.1 Hz, 1H) and correlated to carbon in δ 94.6 of another methine (CH) on position-8 in ring-A (basic skeleton in flavonoid). The doublet signal in δ 8.02 (d, $^{3}J_{H\text{-}H}$ = 8.8 Hz, 1H) attributed to hydrogen at position-2' which was *ortho*-coupled to another hydrogen that showed by a doublet signal in δ 6.90 (d, $^{3}J_{H\text{-}H}$ = 8.8 Hz, 1H) at position-3' in ring-B. These hydrogens (H-2' and H-3') seemed correlated directly to the carbons at δ

132.4 (CH-2') and δ 116.1 (CH-3') in two individual methine groups. These features (δ and *J* values) were equal for other hydrogens and carbons (CH-6'-5') in ring-B in the structure (**1**). In order to see (^{1}H-^{13}C) HMBC map, demonstrated the presence of *β*-D-galactopyranosyl, *α*-L-rhamnopyranosyl, and *β*-D-glucopyranosyl (VILEGAS et al., 1999) sugar components and were possibly detected by their anomeric hydrogens. The anomeric hydrogens such as in the *β*-D-galactopyranosyl was represented by a doublet signal in δ 5.60 (d, $^{3}J_{H\text{-}H}$ = 7.5 Hz, *β*-H) showed direct correlation to the carbon at δ 100.7 (C-1"), other doublet signal at δ 5.21 (brd, *α*-H) correlated to the carbon in δ 102.5 at position-1'" in *α*-L-rhamnopyranosyl while third hydrogen in *β*-D-glucopyranosyl moiety was revealed by doublet signal at δ 4.54 (d, $^{3}J_{H\text{-}H}$ = 7.5 Hz, *β*-H) that showed direct correlation to the carbon at δ 102.0 (COELHO et al., 2003). Further hydrogens in these three sugar units were complex to detect, although the spectral assignments are shown in Table 6.1.

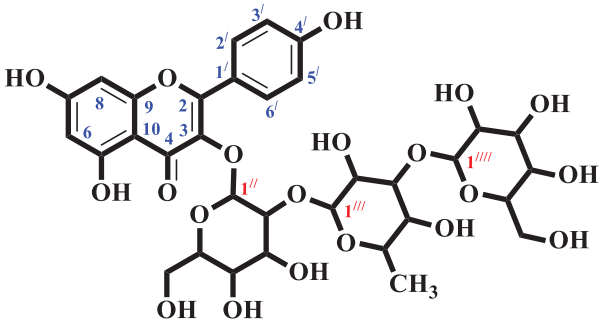

Figure 6.24. Chemical structure of kaempferol glycoside (**1**).

Table 6.1. Spectral assignments of kaempferol glycoside (**1**) detected in the leaves from *Maytenus ilicifolia*.

	kaempferol glycoside **(1)** (Experimental)[a]			kaempferol glycoside **(1)** (VILEGAS et al., 1999) [b]	
Position	**δ ^{1}H (Mult. *J* in Hz)**	**δ ^{13}C**	**(^{1}H-^{13}C) HMBC**	**δ ^{1}H (Mult. *J* in Hz)**	**δ ^{13}C**
1	-	-	-	-	-
2	-	158.4	-	-	158.7
3	-	-	-	-	135.5
4	-	-	-	-	179.4
5	-	-	-	-	163.1
6	6.19 (*d, J* = 2.1)	99.8	105.9; 94.6	6.23 (d, *J* = 1.5)	99.8
7	-	-	-	-	165.8
8	6.39 (*d, J* = 2.1)	94.6	158.4; 99.8	6.42 (d, *J* = 1.5)	94.7
9	-	-	-	-	153.3
10	-	105.9	-	-	105.8
1'	-	123.0	-	-	122.9
2'	8.02 (*d, J* = 8.8)	132.2	161.3	8.07 (d, *J* = 8.4)	132.2
3'	6.90 (*d, J* = 8.8)	116.1	123.0; 116.1	6.93 (d, *J* = 8.4)	116.2
4'	-	161.3	-	-	161.2
5'	6.90 (*d, J* = 8.8)	116.1	123.0; 116.1	6.93 (d, *J* = 8.4)	116.2
6'	8.02 (*d, J* = 8.8)	132.2	161.3	8.07 (d, *J* = 8.4)	132.2
1"	5.60 (*d, J* = 7.5)	100.8	-	5.55 (d, *J* = 7.5)	101.3
2"	-	-	-	3.96 (dd, *J* = 9.7; 7.5)	77.6

3''	-	-	-	3.72 (dd, *J* = 7.5; 3.5)	75.4
4''	-	-	-	3.48 (dd, *J* = 3.5; 1.5)	71.0
5''	-	-	-	3.42 (td, *J* = 7.0; 5.0; 1.5)	75.3
6''	-	-	-	3.47 (dd, *J* = 12.0; 7.0); 3.72 (dd, *J* = 12.0; 5.0)	67.2
1'''	5.21 (br d)	102.5	72.2; 70.0	5.26 (d, *J* = 1.5)	101.9
2'''	-	-	-	4.31 (dd, *J* = 3.5; 1.5)	72.1
3'''	-	-	-	3.96 (dd, *J* = 9.5; 3.5)	83.0
4'''	-	-	-	3.56 (t, *J* = 9.5)	72.8
5'''	-	-	-	4.15 (dq, *J* = 9.5; 6.0)	70.7
6'''	-	-	-	1.03 (d, *J* = 6.0)	17.8
1''''	4.54 (d, *J* = 7.5)	102.0	72.1; 69.6	4.59 (d, *J* = 7.5)	105.8
2''''	-	-	-	3.36 (dd, *J* = 9.5; 7.5)	75.4
3''''	-	-	-	3.42 (t, *J* = 9.5)	77.5
4''''	-	-	-	3.64 (t, *J* = 9.5)	69.8
5''''	-	-	-	3.38 (td, *J* = 9.5; 5.0; 3.5)	77.2
6''''	-	-	-	3.76 (dd *J* = 12.0; 3.5)	62.4

[a] Experiment, acquired with 400.13 MHz for ^{1}H and 100.61 MHz for ^{13}C in CD_3OD included TMS (*v*/*v*, 0.05%) as reference standard. [b] Literature, VILEGAS et al., 1999 (^{1}H 599.19 MHz and ^{13}C 150.85 MHz in CD_3OD). Chemical shifts (δ) in ppm and coupling constants (*J*) are mentioned in Hertz (Hz). Doublet (d), doublet of doublet (dd), double quartet (dq), triplet (t), quartet (q), triple doublet (td), and broaddoublet (brd).

6.4.1.2 The identification and structure elucidation of (-)-epicatechin (**2**)

In comparison to literature (SUN et al., 2006) data (-)-epicatechin (**2**) was detected in the leaves of *Maytenus ilicifolia*. This compound (**2**; Figure 6.25) is a general flavan-3-ol (or a 2,3-*Cis* epimer) monomeric type natural secondary metabolite of flavonoids family.

The compound **2**, was identified by a doublet signal in δ 5.94 (d, $^{4}J_{H\text{-}H}$ = 2.3 Hz, 1H) showing one hydrogen directly correlated to a carbon in fsrequency range of δ 96.7 in methine (CH-6) group. Overviewing the coupling constant, hydrogen-6 appeared *meta*-coupled to another hydrogen characterized by a doublet in δ 5.91 (d, $^{4}J_{H\text{-}H}$ = 2.3 Hz, 1H) that showed direct correlation to carbon in δ 96.1 from another methine (CH-8) group in aromatic A-ring.

Additional doublet signal in δ 6.97 (d, $^{4}J_{H\text{-}H}$ = 1.8 Hz, 1H) attributed to a hydrogen directly connected to the carbon at δ 115.4 from methine (CH-2') group, that was *meta*-coupled to a hydrogen exposed by doublet of sdoublet at δ 6.79 (dd, $^{3,4}J_{H\text{-}H}$ = 8.3; 1.8 Hz, 1H) correlated to the carbon at δ 119.4 from another methine (CH-6') assembly. Rather than *meta*-coupling, this hydrogen-6' was *ortho*-coupled also to its neighbor hydrogen represented by a doublet signal at δ 6.75 (d, $^{3}J_{H\text{-}H}$ = 8.3 Hz, 1H) attributed to the hydrogen correlated to a carbon at δ 116.0 in methine (CH-5') segment of aromatic B-ring in **2**.

The hydrogens in remaining C-ring from molecule (**2**), were established by a broad singlet in δ 4.81 (br*s*, 1H) representting one hydrogen on site-2 and another broad multiplet at

δ 4.17 (br*m*, 1H) attributed to another hydrogen at site-3. These hydrogens (H-2,3) were observed correlated directly to separate carbons in methines at δ 79.9 (CH-2) and 67.6 (CH-3). In order to define the remaining site-4 in C-ring (**2**), two individual doublets of doublets were detected at δ 2.86 and δ 2.73 assigned to two hydrogens correlated directly to a single carbon nucleaus at δ 29.3 represented a methylene (CH_2) group. The observed coupling values for hydrogens-4 (H4a and H4b) were established according to Hemingway (1996), since δ 2.86 (dd, $^{2}J_{H4a\text{-}H4b}$ = 16.8 Hz; $^{3}J_{H3\text{-}H4a}$ = 4.7 Hz, 1H) and respectively in δ 2.73 (dd, $^{2}J_{H4a\text{-}H4b}$ = 16.8 Hz; $^{3}J_{H3\text{-}H4b}$ = 2.8 Hz, 1H). The complete spectral information in addition of (^{1}H-^{13}C) HMBC for molecular structure **2** are tabulated (Table 6.2).

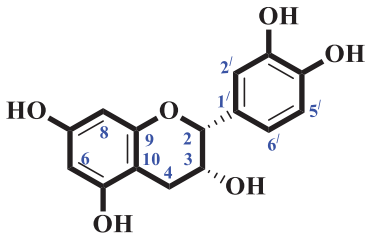

Figure 6.25. Chemical structure of (-)-epicatechin (**2**).

Table 6.2. Spectral assignments of (-)-epicatechin (**2**) detected in the leaves from *Maytenus ilicifolia.*

	(-)-epicatechin **(2)** (Experimental)[a]			(-)-epicatechin **(2)** (SUN et al., 2006) [b]	
Position	**δ ^{1}H (Mult. *J* in Hz)**	**δ ^{13}C**	**(^{1}H-^{13}C) HMBC**	**δ ^{1}H (Mult. *J* in Hz)**	**δ ^{13}C**
1	-	-	-	-	-
2	4.81 (br*s*)	79.9	132.3;119.4;115.4	4.82 (br*s*)	79.8
3	4.17 (*m*)	67.6	-	4.17 (*m*)	67.4
4a	2.86 (*dd, J* = 16.8; 4.7)	29.3	157.2;100.1; 79.9; 67.5	2.85 (*dd, J* = 16.8; 4.8)	29.2
4b	2.73 (*dd, J* = 16.8; 2.8)			2.72 (*dd, J* = 16.8; 2.8)	
5	-	157.2	-	-	157.5
6	5.94 (*d, J* = 2.3)	96.7	157.8; 100.1; 96.1	5.93 (*d, J* = 2.4)	96.4
7	-	157.8	-	-	157.9
8	5.91 (*d, J* = 2.3)	96.1	157.8; 100.1; 96.7	5.91 (*d, J* = 2.4)	95.9
9	-	157.2	-	-	157.3
10	-	100.1	-	-	100.1
1'	-	132.3	-	-	132.3
2'	6.97 (*d, J* = 1.8)	115.4	145.8; 119.4; 79.9	6.96 (*d, J* = 1.6)	115.3
3'	-	145.8	-	-	145.9
4'	-	145.8	-	-	145.7
5'	6.75 (*d, J* = 8.3)	116.0	145.8; 132.3	6.77 (*d, J* = 8.0)	115.9
6'	6.79 (*dd, J* = 8.3; 1.8)	119.4	145.8; 115.4; 79.9	6.81 (*dd, J* = 8.4; 2.0)	119.4

[a] Experiment, acquired with 400.13 MHz for ^{1}H and 100.61 MHz for ^{13}C in CD_3OD included TMS (*v*/*v*, 0.05%) as reference standard. [b] Literature, SUN et al., 2006 (^{1}H 400 MHz and ^{13}C 100 MHz in CD_3OD). Chemical shifts (δ) in ppm and coupling constants (*J*) are mentioned in Hertz (Hz). Doublet (d), doublet of doublet (dd), broadsinglet (brs), and multiplet (m).

6.4.1.3 The identification and structure elucidation of kaempferol aglycone (**3**)

The leaves of *Maytenus ilicifolia* presented kaempferol aglycone (**3**; Figure 6.26) of flavonoids family that was in agreement with literature (SILVA et al., 2017). This metabolite was observed by a doublet signal in frequency region of δ 6.19 (d, $^{4}J_{H\text{-}H}$ = 2.1 Hz, 1H) attributed to site-6 hydrogen, *meta*-coupled to another hydrogen exposed by a doublet in δ 6.39 (d, $^{4}J_{H\text{-}H}$ = 2.1 Hz, 1H) at site-8. These hydrogens (H-6,8) showed direct correlations to methine (CH) carbons in δ 99.8 (CH-6) and δ 94.6 (CH-8) in the A-ring. In the same way, more de-shielded doublet signal in δ 8.06 (d, $^{3}J_{H\text{-}H}$ = 8.9 Hz, 1H) showed hydrogen in methine group at site-2' (equal site-6') and correlated to carbon in δ 132.3 (CH-2' also CH-6'). This hydrogen seemed to be *ortho*-coupled in proximity with less de-shielded hydrogen in methine, appeared at δ 6.90 (d, $^{3}J_{H\text{-}H}$ = 8.9 Hz, 1H) of site-3' (equally site-5') and correlated to a carbon in δ 116.2 (CH-3' equally CH-5') were from B-ring. The structural assignments are given (Table 6.3).

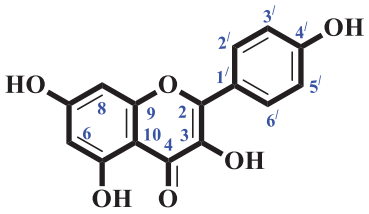

Figure 6.26. Chemical structure of kaempferol aglycone (**3**).

Table 6.3. Spectral assignments of kaempferol **(3)** detected in the leaves from *Maytenus ilicifolia.*

	kaempferol **(3)** (Experimental)[a]			kaempferol **(3)** (SILVA et al., 2017) [b]	
Position	**δ ^{1}H (Mult. *J* in Hz)**	**δ ^{13}C**	**(^{1}H-^{13}C) HMBC**	**δ ^{1}H (Mult. *J* in Hz)**	**δ ^{13}C**
1	-	-	-	-	-
2	-	158.8	-	-	156.3
3	-	-	-	-	133.4
4	-	-	-	-	179.2
5	-	158.5	-	-	161.0
6	6.19 (*d, J* = 2.1)	99.8	105.9; 94.6	6.18 (*d, J* = 1.9)	97.8
7	-	158.5	-	-	164.3
8	6.39 (*d, J* = 2.1)	94.6	158.5; 105.9; 99.8	6.40 (*d, J* = 1.9)	92.8
9	-	158.8	-	-	156.3
10	-	105.9	-	-	103.7
1'	-	123.0	-	-	120.3
2'	8.06 (*d, J* = 8.9)	132.3	158.8;132.3; 161.3	8.09 (*d, J* = 8.9)	129.4
3'	6.90 (*d, J* = 8.9)	116.2	123.0;116.2	6.91 (*d, J* = 8.9)	114.1
4'	-	161.3	-	-	159.1
5'	6.90 (*d, J* = 8.9)	116.2	123.0;116.2	6.91 (*d, J* = 8.9)	114.1
6'	8.06 (*d, J* = 8.9)	132.3	158.8; 32.3; 161.3	8.09 (*d, J* = 8.9)	129.4

[a] Experiment, acquired with 400.13 MHz for ^{1}H and 100.61 MHz for ^{13}C in CD_3OD included TMS (*v*/*v*, 0.05%) as reference standard. [b] Literature, SILVA et al., 2017 (^{1}H 500.13 MHz and ^{13}C 125.76 MHz in CD_3OD

included TMS *v*/*v*, 0.05%). Chemical shifts (δ) in ppm and coupling constants (*J*) are mentioned in Hertz (Hz). Doublet (d).

6.4.2 The carbohydrates region (δ 5.80 to 3.00)

The second segment from ^{1}H HR-MAS NMR (Figure 6.27) revealed numerous signals associated to randomly different sites from kaempferol glycoside (**1**), (-)-epicatechin (**2**), sucrose (**4**), alanine (**6**), threonine (**7**) and fatty acids (**8**). All these chemical structures are explained in the following discussions respectively.

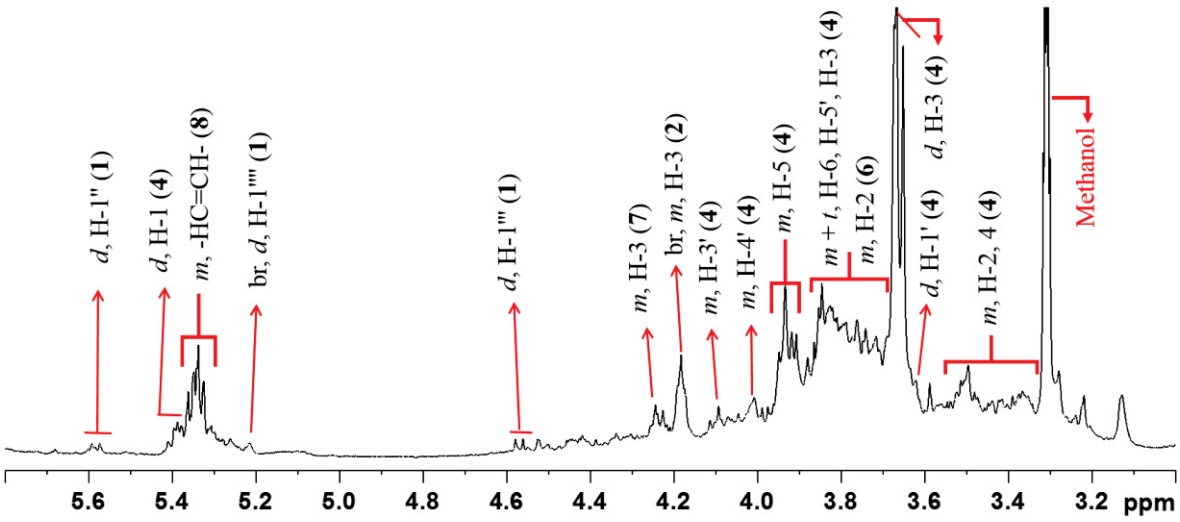

Figure 6.27. Amplified carbohydrates region (δ 5.80 to 3.0) in ^{1}H HR-MAS NMR spectrum (400.13 MHz) in leaf powder (10 ± 1.0 mg: 40 µL CD_3OD) from *Maytenus ilicifolia.*

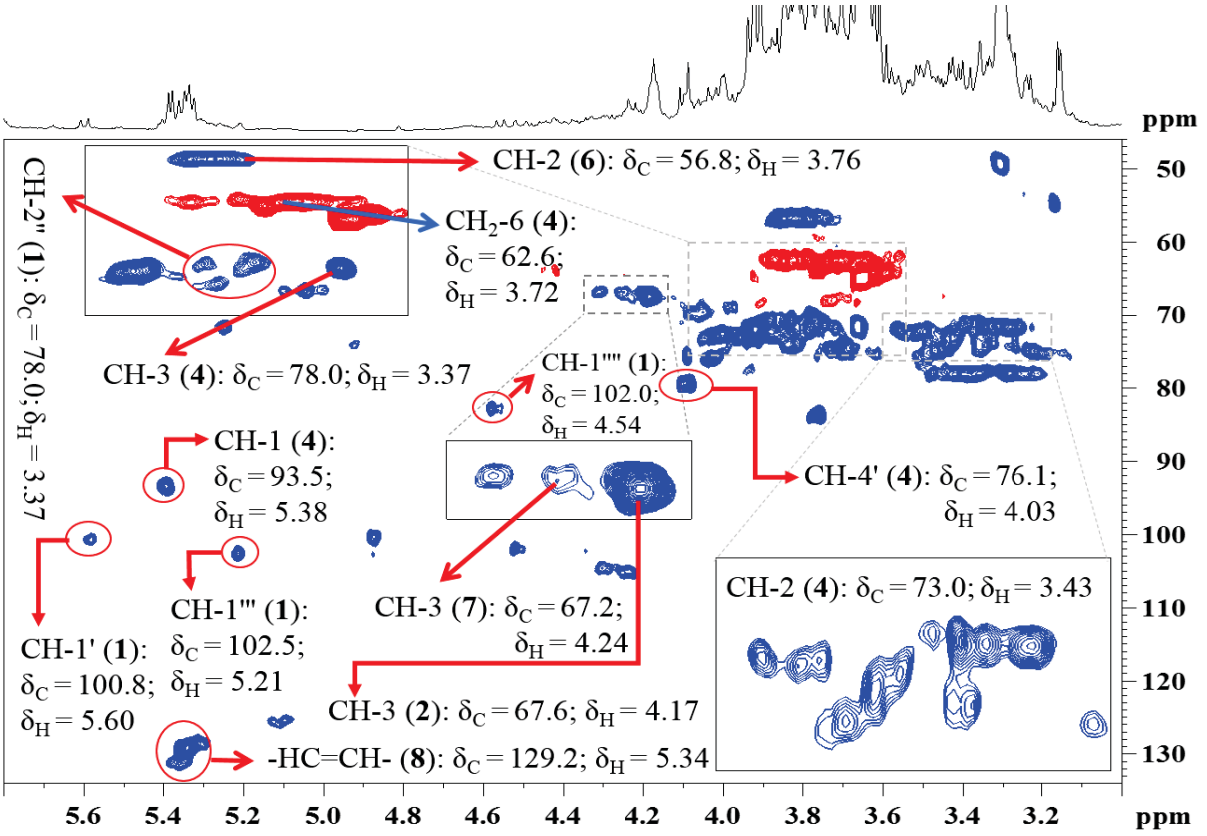

Figure 6.28. Carbohydrates region (δ 5.8-3.0 *vs.* δ 134.0-46.0) in ^{1}H-^{13}C direct correlation map (400.13-100.62 MHz) from multiplicity edited HSQC experiment performed over powdered leaf from *M. ilicifolia*.

6.4.2.1 The identification and structure elucidation of sucrose (**4**)

The leaves from *Maytenus ilicifolia* revealed sucrose (**4**), detected in ^{1}H HR-MAS NMR (Figure 6.27). The entire spectral assignments established for compound (**4**) were in comparison to literature (TSUJIMOTO et al., 2018), although little changes (in δs and or *J*s) were found, perhaps due to difference in magnetic field strengths. The molecular structure (**4**) was detected by typical doublet signal in δ 5.38 (d, $^{3}J_{H\text{-}H}$ = 3.8 Hz, 1H) from anomeric hydrogen in glucose unit (**4**; Figure 6.29) that showed correlation to the carbon in δ 93.5 (*α*-CH-1). The doublet of doublet signal at δ 3.43 (dd, $^{3}J_{H\text{-}H}$ = 9.8; 3.8 Hz, 1H) supposed a hydrogen directly correlated to a carbon in δ 73.0 (CH-2). Another doublet in δ 3.66 (d, *J* = 6.3 Hz, 1H) assigned to a methine hydrogen seeming correlated to the carbon at δ 71.7 (CH-3). One triplet at δ 3.37 (t, $^{3}J_{H\text{-}H}$ = 9.5 Hz, 1H) showed one hydrogen correlated to a carbon at δ 78.0 (CH-4). Due to signals overlaps, hydrogen-5 was not detected since its carbon nucleus appeared in δ 72.0 (CH-5). Similarly, multiplet in δ 3.72 (m, 2H) integrated two hydrogens correlated to same carbon at δ 62.6, seemed a methylene (CH_2-6) group. On the other hand, fructose unit in **4** was completed by a multiplet signal at δ 3.63 (m, 2H) showing two

hydrogens directly associated to a carbon at δ 64.5, appeared to be methylene (CH_2-1') group. On the basis of (^{1}H-^{13}C) HMBC, a carbon (C-2') was found correlated to the carbon in δ 105.4 (C-2'). One doublet signal at δ 4.09 (d, $^3J_{H\text{-}H}$ = 8.4 Hz, 1H) assigned to hydrogen correlated to a carbon in δ 79.3 at position-3'. Similarly, all other hydrogens were appeared multiplets in the frequency ranges of δ 4.0 (m, 1H), δ 3.76 (m, 1H), and δ 3.85(m, 2H) directly correlated to the carbons in δ 76.1, δ 83.7 and δ 62.7 (CH-4', CH-5', CH_2-6'). Th overall signals assignments for this compound (**4**) are tabulated (Table 6.4).

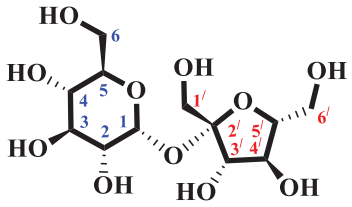

Figure 6.29. Chemical structure of sucrose (**4**).

Table 6.4. Spectral assignments of sucrose **(4)** detected in the leaves from *Maytenus ilicifolia.*

	Sucrose **(4)** (Experimental)[a]		Sucrose **(4)** (TSUJIMOTO et al., 2018) [b]	
Position	**δ ^{1}H (Mult. *J* in Hz)**	**δ ^{13}C**	**δ ^{1}H (Mult. *J* in Hz)**	**δ ^{13}C**
1	5.38 (*d, J* = 3.8)	93.5	5.37 (*d, J* = 3.8)	95.4
2	3.43 (*dd, J* = 9.8; 3.8)	73.0	3.40 (*dd, J* = 9.8; 3.8)	75.0
3	3.66 (*d, J* = 6.3)	78.0	3.68 (*t, J* = 9.6)	76.4
4	3.37 (*t, J* = 9.5)	71.7	3.34 (*t, J* = 9.4)	73.0
5	-	-	-	76.1
6	3.72 (*m*)	62.6	3.70 (*dd, J* = 7.9; 4.0)	63.9
1'	3.63 (*m*)	64.5	3.58 (*d, J* = 12.3)	65.7
2'	-	105.4	-	107.1
3'	4.09 (*d, J* = 8.4)	79.3	4.08 (*d, J* = 8.2)	81.0
4'	4.03 (*m*)	76.1	4.01 (*t, J* = 7.7)	77.4
5'	3.76 (*m*)	83.7	3.83-3.72	85.6
6'	3.85 (*m*)	62.7	3.83-3.72	65.1

[a] Experiment, acquired with 400.13 MHz for ^{1}H and 100.61 MHz for ^{13}C in CD_3OD included TMS (*v*/*v*, 0.05%) as reference standard. [b] Literature, TSUJIMOTO et al., 2018 (800 and 201 MHz for ^{1}H and ^{13}C in CD_3OD). Chemical shifts (δ) in ppm and coupling constants (*J*) are mentioned in Hertz (Hz). Doublet (d), doublet of doublet (dd), triplet (t), and multiplet (m).

6.4.3 The aliphatic region (δ 3.00 to 0.670

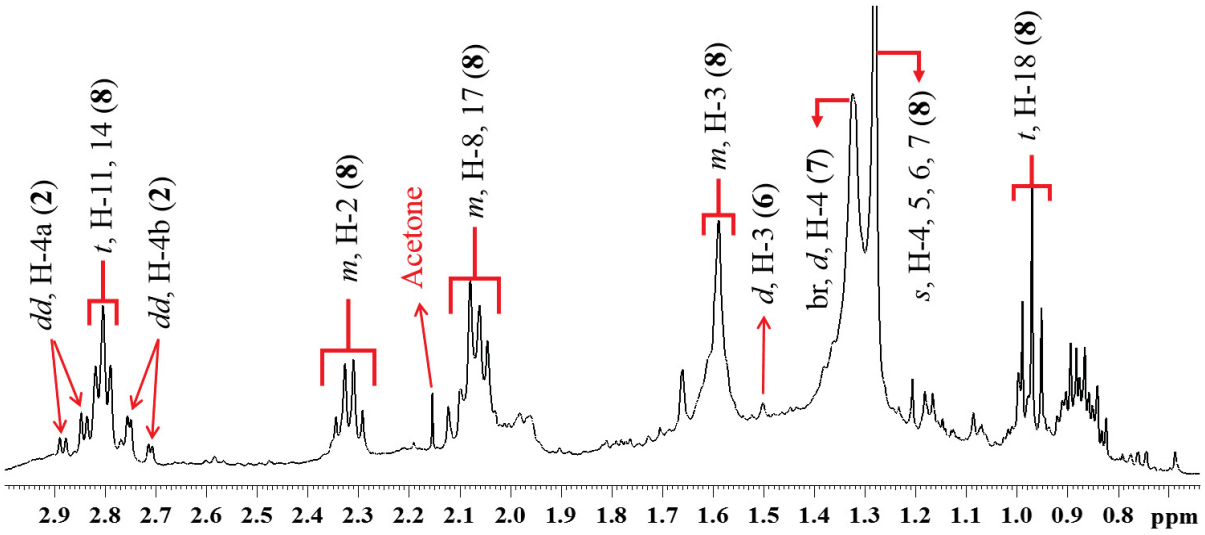

Figure 6.30. Amplified aliphatic region (δ 3.00 to 0.67) in ^{1}H HR-MAS NMR spectrum (400.13 MHz) in leaf powder (10 ± 1.0 mg: 40 µL CD_3OD) from *Maytenus ilicifolia.*

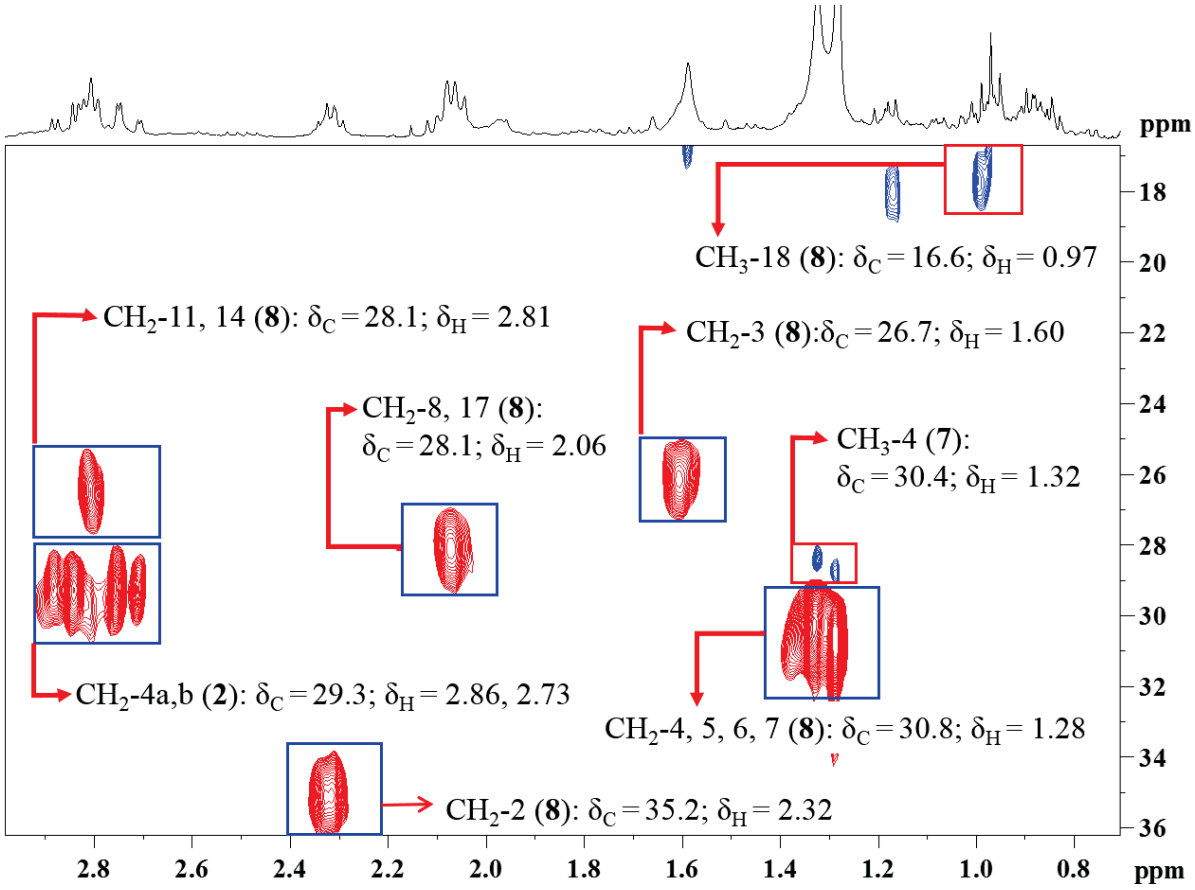

Figure 6.31. Aliphatic region (δ 3.0-0.7 *vs.* δ 36.0-17.0) in ^{1}H-^{13}C direct correlation map (400.13-100.62 MHz) from multiplicity edited HSQC experiment performed over powdered leaf from *Maytenus ilicifolia*.

6.4.3.1 The identification and structure elucidation of fumaric acid (**5**)

The presence of small organic acids was also detected in ^{1}H HR-MAS NMR profile in the leaves from *Maytenus ilicifolia*. This small organic fumaric acid (**6**; Figure 6.32) is more stable and *trans*-isomer of maleic acid which was established in agreement to literature (KIM et al., 2010) and online data sources (MetaboLight, HMBD). The compound **6**, was detected in high freuency region by a singlet signal in δ 6.51 (s, 1H) attributed to two individual hydrogens (position-2,3) and found directly correlated to the carbon resonance in δ 106.82 (CH-2,-3). The spectral attributions of fumaric acid are given in Table 6.5.

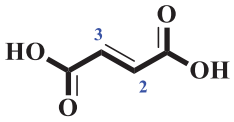

Figure 6.32. Chemical structure of fumaric acid (**5**).

Table 6.5. Spectral assignments of fumaric acid **(5)** detected in the leaves from *Maytenus ilicifolia.*

fumaric acid **(5)** (Experimental)[a]				fumaric acid **(5)** (KIM et al., 2010)[b]	
Position	**δ ^{1}H (Mult. *J* in Hz)**	**δ ^{13}C**	**(^{1}H-^{13}C) HMBC**	**δ ^{1}H (Mult. *J* in Hz)**	**δ ^{13}C**
2,3	6.51 (*s*)	106.82	106.82	6.52 (*s*)	-

[a] Experiment, acquired with 400.13 MHz for ^{1}H and 100.61 MHz for ^{13}C in CD_3OD included TMS (*v*/*v*, 0.05%) as reference standard. [b] Literature, KIM et al., 2010 (^{1}H 500.13 MHz in CD_3OD + Phosphate buffer in D_2O). Chemical shifts (δ) in ppm and coupling constants (*J*) are mentioned in Hertz (Hz). Singlet (s).

6.4.3.2 The identification and structure elucidation of alanine (**6**)

Moreover, some other amino acids were also observed in ^{1}H HR-MAS NMR from the leaves in *Maytenus ilicifolia.* The alanine (**6**) was revealed by a multiplet signal in δ 3.76 (*m*, 1H) that showed one hydrogen directly correlated to the carbon in δ 56.8 was methine group (CH-2). Similarly, another doublet signal in δ 1.48 (d, *J* = 7.20 Hz, 3H) observed to be three hydrogens that showed direct orrelation with carbon resonance in δ 19.1 was reflected the methyl (CH_3-3) group in basic molecular structure (**6**; Figure 6.33). The related signals assignments from this small organic acid (**6**) were compared to the previously published data (KIM et al., 2010) and respectively the available online services (MetaboLight, HMBD). The spectral assignments for alanine are provided in Table 6.6.

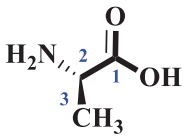

Figure 6.33. Chemical structure of alanine (**6**).

Table 6.6. Spectral assignments of alanine **(6)** detected in the leaves from *Maytenus ilicifolia.*

alanine **(6)** (Experimental)[a]			alanine **(6)** (KIM et al., 2010) [b]	
Position	**δ ^{1}H (Mult. *J* in Hz)**	**δ ^{13}C**	**δ ^{1}H (Mult. *J* in Hz)**	**δ ^{13}C**
1	-	-	-	-
2	3.76 (*m*)	56.8	-	-
3	1.48 (*d, J* = 7.20)	19.1	1.48 (*d, J* = 7.20)	-

[a] Experiment, acquired with 400.13 MHz for ^{1}H and 100.61 MHz for ^{13}C in CD_3OD included TMS (*v*/*v*, 0.05%) as reference standard. [b] Literature, KIM et al., 2010 (^{1}H 500.13 MHz in CD_3OD + Phosphate buffer in D_2O). Chemical shifts (δ) in ppm and coupling constants (*J*) are in Hertz (Hz). Doublet (d), and multiplate (m).

6.4.3.3 The identification and structure elucidation of threonine (**7**)

The spectral attributions from threonine (**7**; Figure 6.34**)** were observed in ^{1}H HR-MAS NMR profile of the leaves from *Maytenus ilicifolia.* The threonine (**7**) was completed with literature (ALI et al., 2009) and online records (MetaboLight, HMBD). This organic acid was revealed by a multiplet signal at δ 3.50 (m, 1H) assigned to a hydrogen correlated to a carbon in δ 72.0 in methine group (CH-2). Similarly, in the range of δ 4.24 (br, m, 1H) a broad multiplet exposing one hydrogen directly linked to a carbon resonance at δ 67.2 in another methine (CH-3) group. In the same way, the broad doublet signal revealed in δ 1.32 (brd, 3H) seemed to be correlated to the carbon resonance in δ 30.4 in methyl (CH_3-4) group in molecule (**7**). The spectral attributions from threonine (**7**) can be viewed in Table 6.7.

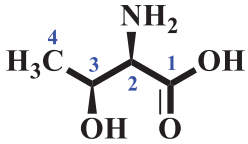

Figure 6.34. Chemical structure of threonine (**7**).

Table 6.7. Spectral assignments of threonine **(7)** detected in the leaves from *Maytenus ilicifolia.*

threonine **(7)** (Experimental)[a]				threonine **(7)** (ALI et al., 2009) [b]	
Position	**δ ^{1}H (Mult. *J* in Hz)**	**δ ^{13}C**	**(^{1}H-^{13}C) HMBC**	**δ ^{1}H (Mult. *J* in Hz)**	**δ ^{13}C**
1	-	-	-	-	-
2	4.24 (br*m*)	67.2	79.0	4.27 (*m*)	-
3	3.50 (*m*)	72.0	67.2	3.51 (*d, J* = 12.0)	-
4	1.32 (br*d*)	30.4	-	1.32 (*d , J* = 7.0)	-

[a] Experiment, acquired with 400.13 MHz for ^{1}H and 100.61 MHz for ^{13}C in CD_3OD included TMS (*v*/*v*, 0.05%) as reference standard. [b] Literature, ALI et al., 2009 (^{1}H 500.13 MHz in CD_3OD, KH_2PO_4 in D_2O, TSP).

Chemical shifts (δ) in ppm and coupling constants (*J*) are mentioned in Hertz (Hz). Doublet (d), broaddoublet (brd), broadmultiplet (brm), and multiplet (m).

6.4.3.4 The identification and structure elucidation of fatty acids (linolenic acid, *omega*-3) (**8**)

The (un)saturated fatty acids are common scaffolds, largely distributed in nature (plants, and or other organisms). There are different types of saturated and mono to polyunsaturated fatty acids of unique biological features, several are classified by White. (2009) as saturated fatty acids: palmitic acid (C_{16}) and stearic acid (C_{18}), monounsaturated fatty acids: oleic acid (C_{18}), Polyunsaturated fatty acids: linoleic acid (C_{18}), linolenic acid (C_{18}), arachidonic acid (C_{20}), eicosapentaenoic acid (C_{20}), and docosahexaenoic acid (C_{22}).

Based on unsaturation, appearing away after C-3 from terminal methyl (CH_3) side, the polyunsaturated linolenic fatty acids are classifed as *omega*-3 (**8**; Figure 6.35). This type polyunsaturated fatty acid (**8**) can easily be observed in ^{1}H HR-MAS NMR spectrum. In this study, the entire spectral assignments for molecule **8** were in agrrement with literature (ALI et al., 2009; BARISON et al., 2010). The experimental results observed for **8**, were almost identical yet little distinctions were seen in resonance shifts comparatively to Barison et al. (2010), in fact they completed NMR measurements in deuterated choloroform ($CDCl_3$).

Followed the literature (ALI et al., 2009; BARISON et al., 2010), compound **8** was confirmed by a multiplet signal in δ 5.34 (m, 6H) showing six hydrogens directly correlated to the carbon at δ 129.35, seemed to be the olefinic unsaturated six methine (CH-9, 10, 12, 13, 15, 16) groups in the molecule (**8**). In order to explore the spectral profile, showed a typical triplet signal particularly in δ 0.97 (t, $^3J_{H\text{-}H}$ = 7.5 Hz, 3H) from three hydrogens directly correlated to the carbon resonance in δ 16.6 appeared to be the terminal methyl (CH_3-18) group. The multiplet signal in δ 2.06 (m, 4H) assigned to four hydrogens directly correlated to the carbon in δ 28.1, represented two methylene groups at position-8,17. Furthermore, a triplet signal in δ 2.81 (t, $^3J_{H\text{-}H}$ = 6.00 Hz, 4H) showed four hydrogens correlated to the carbons in δ 26.7 were respectively from two individual methylene (CH_2) groups at position-11,14. An intense singlet peak in δ 1.28 (*s*, 8H) integrating eight protons directly correlated to the carbon resonances in δ 30.8, represented four methylene groups at position-4,5,6,7 in the molecular chain. The multiplet signal in δ 1.60 (m, 2H) was attributed to the hydrogens showed direct correlations to the carbon resonance appeared in δ 26.7, represented one methylene (CH_2) group at position-3. Some multiplet signals were revealed in the range of δ 2.32 (m, 2H) assigning two hydrogen nuclei and directly correlated to the carbon in δ 35.2, was a

methylene (CH_2) group at position-2. Experimental chemical shifts with relative coupling patterns are mentioned bellow (Table 6.8).

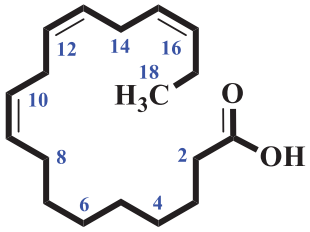

Figure 6.35. Chemical structure of fatty acid (linolenic acid, **8**).

Table 6.8. Spectral assignments of fatty acid (linolenic acid **8)** detected in the leaves from *Maytenus ilicifolia.*

	linolenic acid **(8)** (Experimental) [a]			linolenic acid **(8)** (ALI et al., 2009) [b]	
Position	**δ ^{1}H (Mult. *J* in Hz)**	**δ ^{13}C**	**(^{1}H-^{13}C) HMBC**	**δ ^{1}H (Mult. *J* in Hz)**	**δ ^{13}C**
1	-	174.9	-	-	-
2	2.32 (m)	35.2	174.9; 30.8; 26.7	-	-
3	1.60 (m)	26.7	35.2; 30.8	-	-
4-7	1.28 (brd)	30.8	30.8	-	-
8,17	2.06 (m)	28.1	129.2; 30.8	-	-
HC=CH	5.34 (m)	129.2	28.1; 26.7	-	-
11, 14	2.81 (*t*, *J* = 6.0)	28.1	129.2; 30.8	-	-
18	0.97 (*t*, *J* = 7.5)	16.6	129.2	0.95 (*t* , *J* = 7.5)	-

[a] Experiment, acquired with 400.13 MHz for ^{1}H and 100.61 MHz for ^{13}C in CD_3OD included TMS (*v*/*v*, 0.05%) as reference standard. [b] Literature, ALI et al., 2009 (^{1}H 500.13 MHz in CD_3OD, KH_2PO_4 in D_2O, TSP). Chemical shifts (δ) in ppm, coupling constants (*J*) in Hertz (Hz). Triplet (t), broaddoublet (brd), and multiplet (m).

6.5 CHEMOMETRIC ANALYSIS

6.5.1 ^{1}H HR-MAS NMR spectra from Maytenus ilicifolia and Maytenus aquifolium

In accordance to earlier statements, ^{1}H HR-MAS NMR revealed that only *Maytenus ilicifolia* and *Maytenus aquifolium* were showing equivocal profiles (Figure 6.36). To investigate those ambiguities in the spectra from both palnts species, the entire spectral profiles were submitted to unsupervised principal component analysis (PCA). There were two goals to cover by PCA approach. The initial objective was to simplify ambiguities between resepctive two species and secondly the chemical pattern competitions within each individual in relation to growth, biome, seasonal variations and environmental conditions. In order to investigate these features in *Maytenus ilicifolia* and *aquifolium* spp., the leaf samples (top, middle, and bottom) continuously collected during October (2018) until August (2019). The harvested samples were handled followed by ^{1}H HR-MAS NMR measurements. Similarly,

during the course, total 108 HR-MAS NMR profiles were sequentially obtained, as given in Table 6.9 with a model demonstration of comparative spectra in Figure 6.36.

Table 6.9. Leaf samples from *M. ilicifolia* and *aquifolium* and NMR analyses during six-months.

Maytenus ilicifolia (Celastraceae)				*Maytenus aquifolium* (Celastraceae)			
Plant section with respective NMR spectra				**Plant section with respective NMR spectra**			
Month-Year	**Top (T)**	**Middle (M)**	**Bottom (B)**	**Top (T)**	**Middle (M)**	**Bottom (B)**	**Spectra**
Oct-2018	3	3	3	3	3	3	18
Dec-2018	3	3	3	3	3	3	18
Feb-2019	3	3	3	3	3	3	18
Apr-2019	3	3	3	3	3	3	18
June-2019	3	3	3	3	3	3	18
Aug-2019	3	3	3	3	3	3	18
	18	18	18	18	18	18	**108**

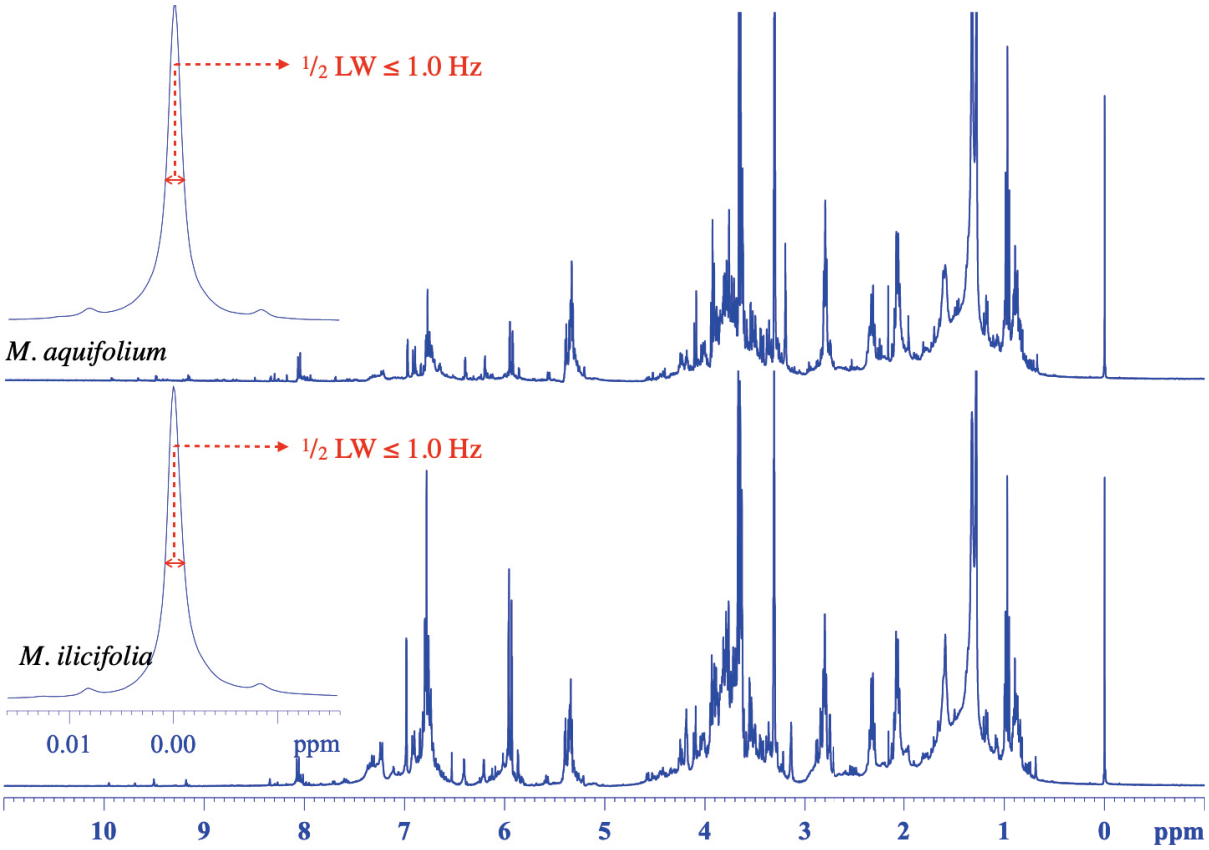

Figure 6.36. Comparative ^{1}H HR-MAS NMR spectra (400.13 MHz) in powdered leaf materials (each 10 ± 1.0 mg: CD_3OD) from both species. The amplified TMS signal shows referencing (δ 0.00) and shimming quality (LW ½; Line Width at half height of TMS signal).

Whole 108 HR-MAS NMR profiles from both individuals were manually referenced to the TMS signal (δ 0.00), baselines and phases were adjusted in Topspin software (v. 3.1,

Bruker) followed up by pre-processing in AMIX (v. 3.9.12, Bruker). The principal component analysis (PCA) was applied in three steps, as described below.

6.5.2 Principal Component Analysis (PCA)

After spectral compatibilities (Sec.6.2; p.75), multivariate principal component analysis (PCA) was executed onto correlated profiles acquired during one-year. The PCA calculation was employed separately to the combined 108 NMR profiles to discriminate (dis)similarity between both species (as showed by NMR). In next step, 54 NMR profiles (per plant) were analyzed to investigate chemical pattern in the leaves (T, M, B) within each individual according to their development and or seasonal variations (month-wise), as discussed in the following sections.

The multivariate exploratory analyses were carried out in AMIX (Analysis of Mixture) software (v. 3.9.12, Bruker). The analyses were performed over specific HR-MAS NMR spectral window (δ 8.10 to 0.67) without δ 20.00 to 8.13 and δ 0.65 to -5.11 (noise region), δ 5.18-4.60 (residual water), δ 3.33-3.29 (methanol) and respectively δ 2.18-2.14 of acetone. Similarly, the entire ^{1}H HR-MAS NMR profiles were pre-processed.

In preprocessing, the spectral profiles were standardized successively, by dividing (or binning) the spectra into small and equal sized ranges (δ) (Figure 6.37). In fact, the binning process supported to reduce signals displacement (due to pH, etc.) from their precise positions. In other words, once the data is binned, it was combined into the (buckets) table to calibrate signals relative intensities of related chemical compounds. The signal mismatches in total spectra were calibrated by using constant δ 0.03 bin size (Figure 6.37) that was found appropriate throughout δ 0.01-0.05 optimization. However, the larger ($\delta > 0.03$) and or smaller ($\delta < 0.03$) bucket sizes were not suitable because they were partitioning the signals (e.g. doublets and multiplets) and taking them away from the variables space. The moderate bucket size of δ 0.03, optimally enclosed all signals dislocation and provided a matrix of "108 (or 54) *versus* 262", where 108 (or 54) represented spectra (rows) and 262 buckets or chemical shifts (columns).

Furthermore, the variations in signals relative intensities along rows in the buckets table were mean centered, normalized and integrated by special integration mode and scaled to total intensities. On the other hand, all signals relative intensity differences along columns were accomplished through pareto scaling, although no scale and scale to unit variance (or autoscaling) methods were also reviewed.

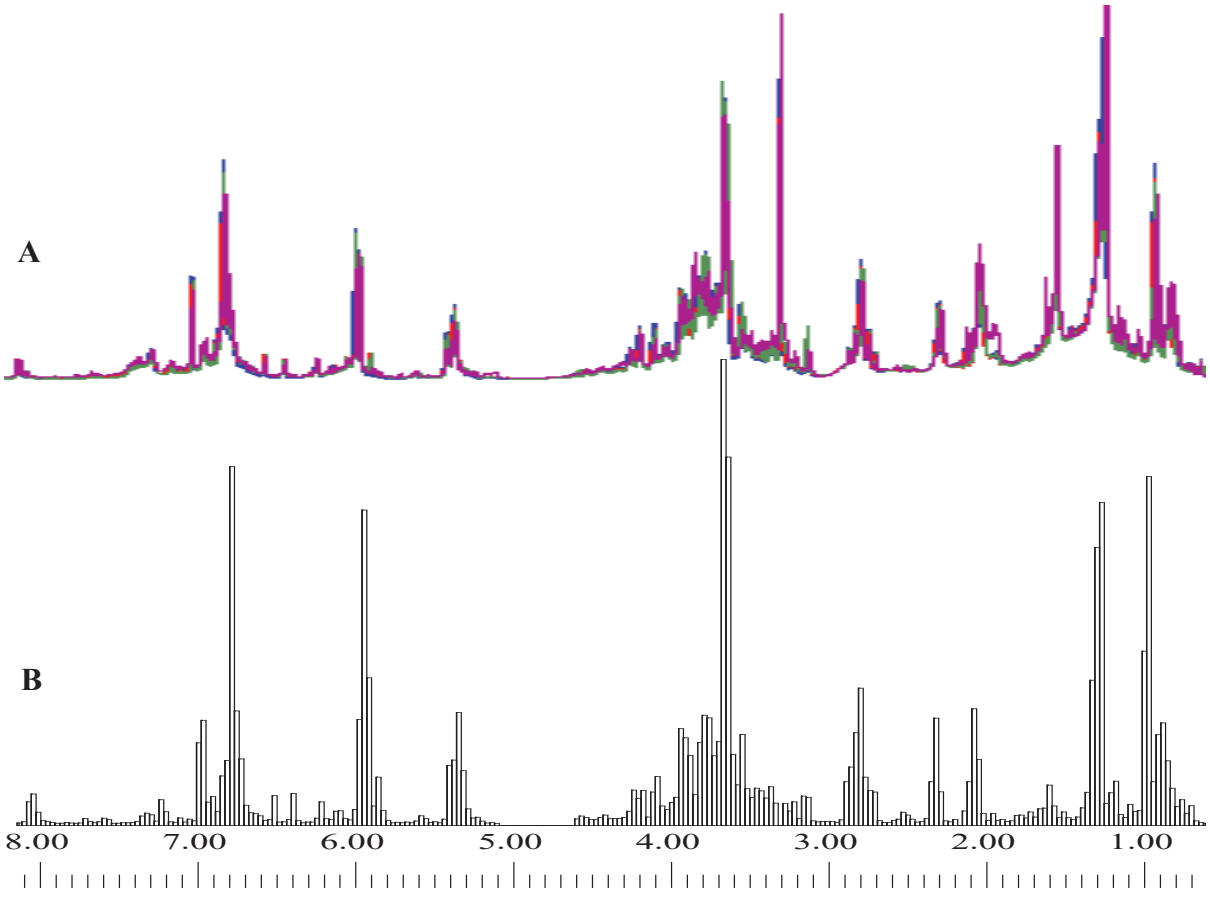

Figure 6.37. General demonstration of original **(A)** ^{1}H HR-MAS NMR profiles (δ 8.10 to 0.67) transformation into binned format **(B)** utilizing bucket length of δ 0.03.

6.5.2.1 PCA-based distinction between *Maytenus ilicifolia* Mart. and *Maytenus aquifolium* Mart. (Celastraceae)

The principal component analysis (PCA) is an unsupervised multivariate data exploratory approach which have the capability to transform multidimensional spectra (of 131072 variables) from x-samples to small amounts of buckets (262) and then into new uncorrelated variables as principal components (PCs). In general, the multidimensional X-size data holding *N*-rows (observations) and *K*-columns (variables). In this study, these observations were NMR spectra while columns represented the chemical shifts (signals).

In discrimination, the matrix that contain 108 NMR spectra from both species was transformed into *scores* and *loadings*. In order to recognize the presence of abnormal samples of different properties, the influence and *hotelling's* T^2 (95% confidence limit) were applied. The influence plot captures information about samples that contribute to or deviate from the model, sample(s) extreme and abnormal or outlying state (KUTZ, 2013). This plot vertically measures that how far apart a spectrum is from the model space (off model distance) while

horizontally represent how far away a spectrum is from the model center. In other words, influence plot combines both the residuals represented by vertical axis and leverages (point far away to the right) by horizontal axis. The abnormal or outlier sample(s) is said to be with high residual, and leverage (T^2) though rather calling them outlier it needs to be confirmed. The leverage is related to the *Hotelling's* T^2, which shows a measure of the distance of a sample from center (T^2 = zero) in the model. The two-lines display is so-called confidence limit (of 95%) which encircle samples spectra contributing to the model with 95% probability (AMIX v. 3.7; 2006). In this measurement, four samples (red rectangle in Figure 6.38) were found isolated away that were considered part of model but with great influence and or higher leverage or T^2 values that showed these samples different from other data. It means that this unique nature (or higher T^2) may be due to some characteristic factors, were explained.

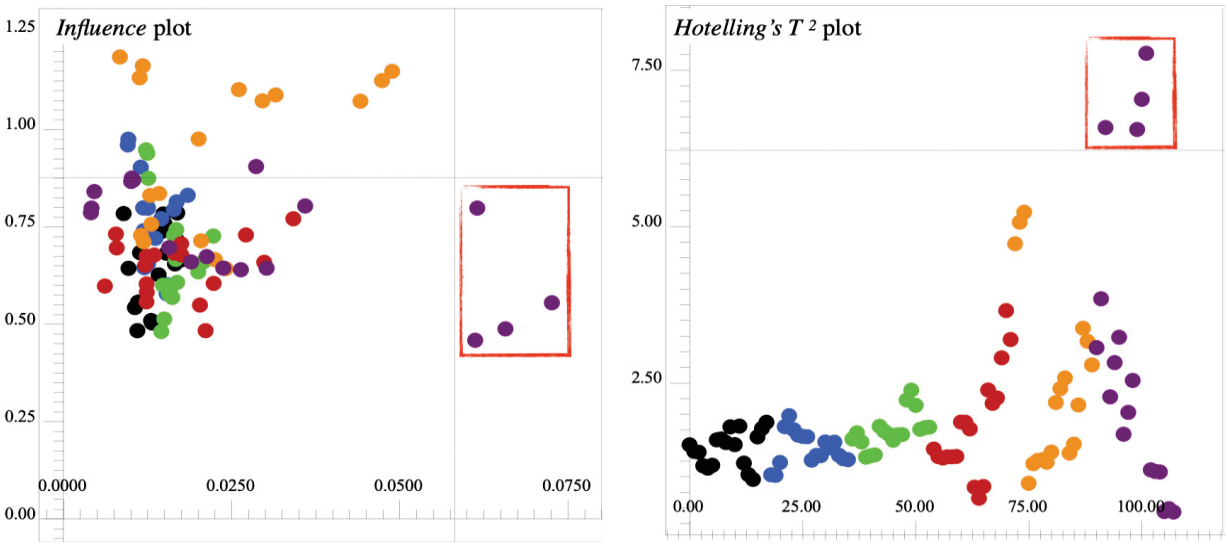

Figure 6.38. The *influence* (left) and *hotelling's* T^2 (right) plot shows an overview of all ^{1}H HR-MAS NMR profiles (108) from leaves (top-bottom sections) of both *Maytenus ilicifolia* and *Maytenus aquifoliums*. All colored spheres represented months as: (●) **October**; (●) **December**; (●) February; (●) **April**; (●) June; and (●) **August** respectively.

These measurements distinguished both *Maytenus ilicifolia* and *Maytenus aquifolium* species. From PCA-calculation, the *scores* plot presented 71.85% two-dimensional spread of 108 NMR observations along two principal components (PC1, PC2). In this way, maximum samples variation was captured by PC1 (59.41%) followed by PC2 (12.44%) since four samples were seen outside of the variables space (see in rectangles, Figure 6.38). However, these four samples were from upper or top leaves in *Maytenus ilicifolia* (three samples) and *Maytenus aquifolium* (one sample) harvested in different places during August 2019. The

corresponding four samples appeared to be due to dfferent chemical nature, biomes and or other factors that are affecting such abnormal behavior.

In samples discriminations, the *scores* plot (Figure 6.39) showed both *Maytenus ilicifolia* and *Maytenus aquifolium* were distributed into two groups along PC1 (59.41%) *vs.* PC2 (12.44%) of net variance 71.85%. Meaning that both species were distinguished by PC1 (59.41%) showing *Maytenus ilicifolia* in the positive although *Maytenus aquifolium* in the negative range. In the meantime, PC2 (12.44%) revealed month-wise distribution in both individuals (Figure 6.39). This later relation was described for both species according to periodic variation overviewing PC2 (12.44%).

In order to explore the *scores*, maximum profiles from *Maytenus ilicifolia* associated to December, February, April, few from June and August can be seen in the positive since other allied to October, June, and few (abnormal) from August were in negative PC2. The distribution of *Maytenus aquifolium* related to the months of October, December, February, April, and few from June were in the positive thus samples from June, and August were in the negative side of PC2 (see Figure 6.39).

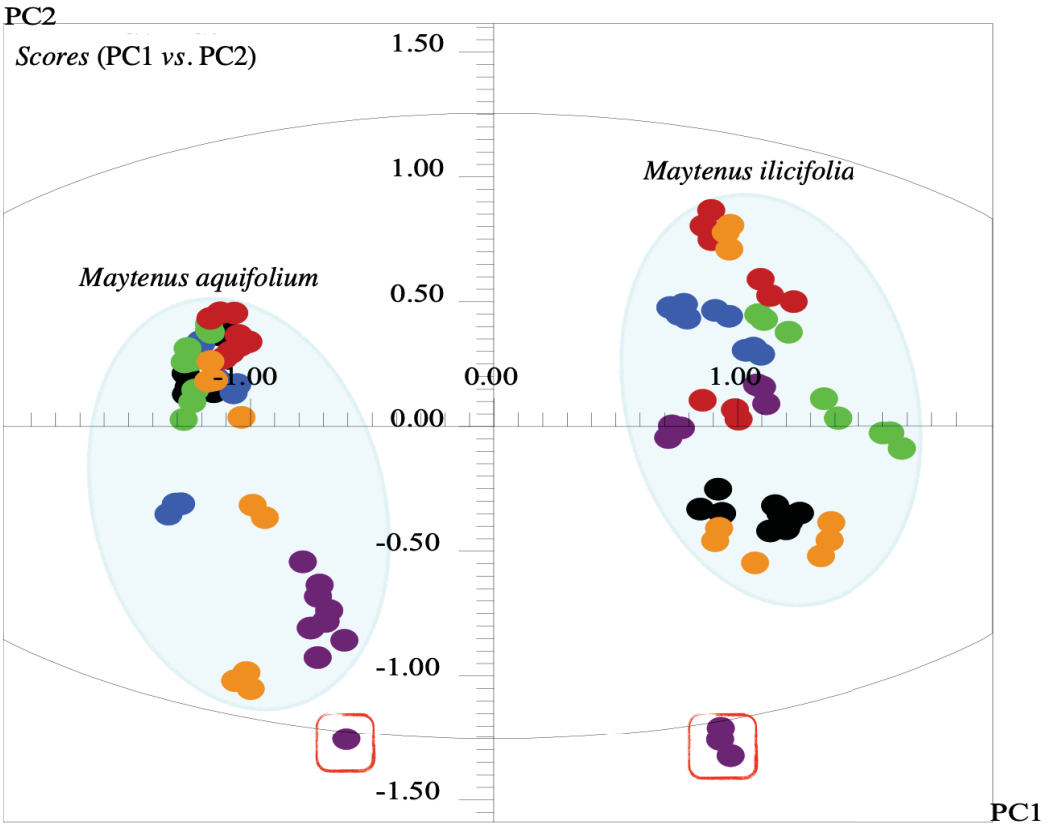

Figure 6.39. The *scores* plot with PC1 (59.41%) *vs* PC2 (12.44%) shows a spread of all ^{1}H HR-MAS NMR profiles (108) from leaves (top-bottom sections) of both *Maytenus ilicifolia* and *Maytenus aquifolium*. Total used buckets were 262 (bin width = δ 0.03) and pareto scaled. All colored spheres represented months as: (●) **October**; (●) **December**; (●) February; (●) **April**; (●) June; and (●) **August**.

Samples groups discrimination with respect to time intervals was withdrawn from *loadings* plot comparitively with ^{1}H HR-MAS NMR profiles mentioned with those signals equivalent to the discriminatory variables in *loadings* graph (Figure 6.40).

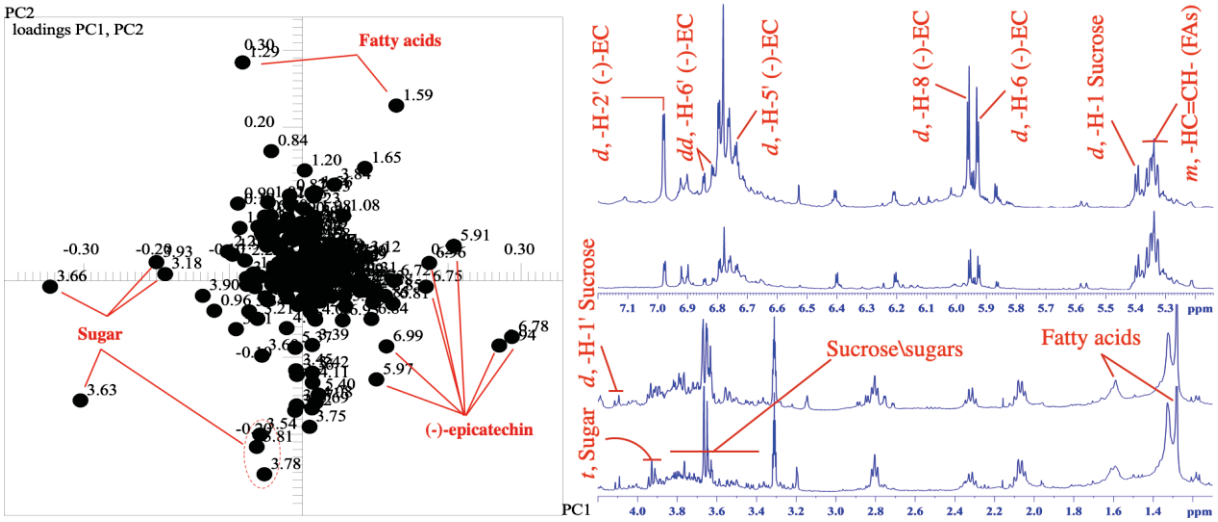

Figure 6.40. The loadings plot (left) with PC1 (59.41%) vs PC2 (12.44%) that discriminated two groups mentioned in the *scores* plot with δ 0.03 sized and pareto scaled, and to the right is given two ^{1}H HR-MAS NMR spectra (In spectral components, top is *Maytenus ilicifolia* and bottom one *Maytenus aquifolium*) shows only the discriminatory peaks associated to the groups (in *scores* plot) and simultaneous to *loadings* (left). (-)-EC = (-)-epicatechin, FAs = Fatty acids.

The overview of *loadings verses scores* resepsented three main chemical compounds were discriminating *Maytenus ilicifolia*. These chemical compounds were (-)-epicatechin (**2**), polyunsaturated fatty acids (**8**), and respectively the sucroses (**4**). In order to comparatively see the *loadings* and ^{1}H HR-MAS NMR profiles, the chemical shifts associated to (-)-epicatechin (**2**) were in the δ 6.98\6.97 (d, $^{4}J_{H\text{-}H}$ = 1.8 Hz, 1H, CH-2'), 6.80\6.79 (dd, $^{3,4}J_{H\text{-}H}$ = 8.3; 1.8 Hz, 1H, CH-6'), 6.77-6.74 (d, $^{3}J_{H\text{-}H}$ = 8.3 Hz, 1H, CH-5'), 5.96\5.94 (d, $^{4}J_{H\text{-}H}$ = 2.3 Hz, 1H, CH-6), and 5.93\5.91 (d, $^{4}J_{H\text{-}H}$ = 2.3 Hz, 1H, CH-8). The signals from polyunsaturated fatty acids (**8**) were in δ 1.58\1.60 (m, 2H, CH_2-3), and δ 1.28\1.28 (*s*, 8H, CH_2-4,5,6,7), since sucrose (**4**) were δ 5.39\5.38 (d, $^{3}J_{H\text{-}H}$ = 3.8 Hz, 1H, α-CH-1), 4.10\4.09 (d, $^{3}J_{H\text{-}H}$ = 8.4 Hz, 1H, CH-3'), 3.77, 3.68\3.66 (d, *J* = 6.3 Hz, 1H, CH-3), and 3.62\3.63 (m, 2H, CH_2-1'). Moreover, *Maytenus aquifolium* was seen totally discriminated by sugar composition due to the chemical shifts of δ 3.92, 3.80, 3.77, and 3.65-3.62.

This association obtained from PC2 (12.44%) exposed seasonal relationship reciprocally affecting the chemical ingredients in particular sugars. The appearance of four abnormal samples (see Figure 6.39) from both *Maytenus ilicifolia* (three-samples) and *Maytenus aquifolium* (one-sample) were may be due to high amount of sugars in related

month(s) of (June and) August 2019. In other words, June and August are the middle of winter and are driest months in Curitiba-PR, Brazil. In the dry seasons, due to less availability of water, plants concentrate their sugars to complete their basic needs, therefore the outlying behavior is mostly because of the increased amount of sugar in the samples. This showed that these months (June and August) were responsible factors to enlarge sugar amounts reciprocally increased T^2 values. In Brazil the **Spring**: 22 September to 21 December; **Summer**: 21 December to 20 March; **Autumn** (Fall): 20 March to 21 June; **Winter**: 21 June until 23 September.

6.5.2.2 PCA-based topology discrimination within *Maytenus ilicifolia* Mart. (Celastraceae)

In order to investigate topological chemical pattern within *Maytenus ilicifolia*, the leaves from this species were harvested from upper top (T), middle (M), and lower (B) sections around one year (October 2018-August 2019). All botanical samples were handled and followed by ^{1}H HR-MAS NMR analyses. In this case, 54 NMR profiles were recorded and submitted to PCA calculations.

In these measurements, the entire (54) spectra were transformed into *scores* and *loadings,* holding two uncorrelated principal components (PC1, PC2). In addition to *scores* and *loadings*, the *influence* and *hotelling's* T^2 (95% confidence limit) were used to confirm the presence of abnormal samples (not observed) in net observations (Figure 6.41).

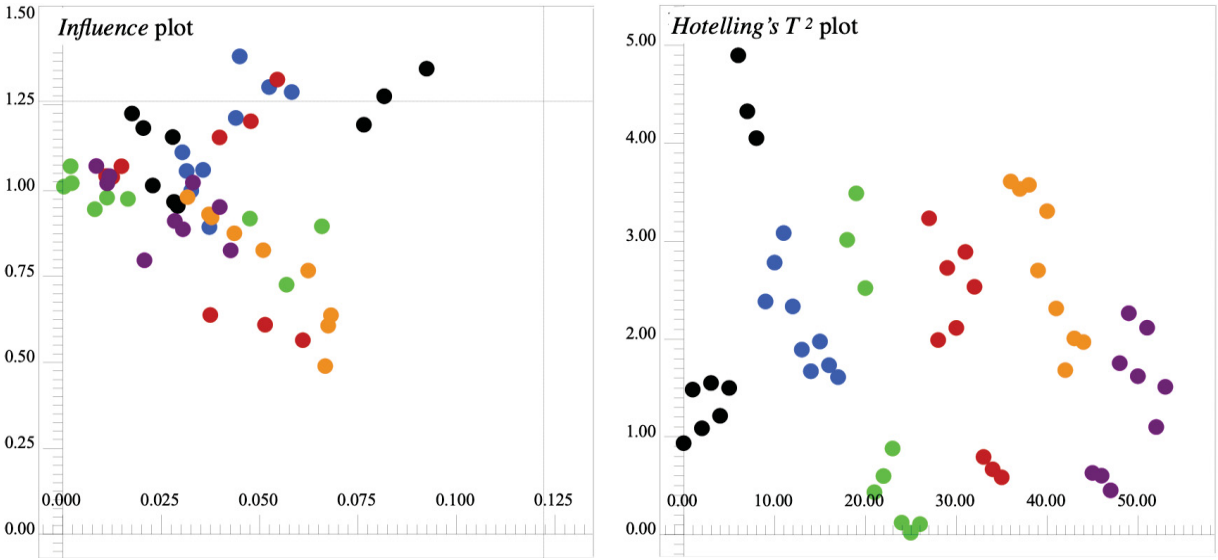

Figure 6.41. The *influence* (left) and *hotelling's* T^2 (right) plot shows an overview of all NMR spectra (54) recorded for the leaf samples from top (T), middle (M), and bottom (B) sections only in *Maytenus ilicifolia.* All colored spheres represented months as: (●) **October**; (●) **December**; (●) **February**; (●) **April**; (●) **June**; and (●) **August** respectively.

From *scores* (Figure 6.42) all 54 NMR leaf (TMB) profiles were scattered around the mean or central position in PCA. These spectra (TMB) were distributed over PC1 (31.45%) and PC2 (20.73%) in the variables space. The distribution was perceived and discriminated the topological profiles and their one-to-one comparative relationship to periodic variabilities.

Overviewing the spectral distribution however, in average maximum number of leaf profiles from top with 3M spectra were found in positive range though bottom samples with few TM were appeared in the negative region of PC1 (31.45%). On the other hand, PC2 (20.73%) possibly described spectral distributions according to seasonal flux (October 2018-August 2019). The relation between these profiles and periodic variation was obtained from *scores*. This showed large number of profiles related to February (April at center and June dispersed), and August 2019 were in the positive range, although those from October and December 2018 were present in the negative region in PC2 (see Figure 6.42).

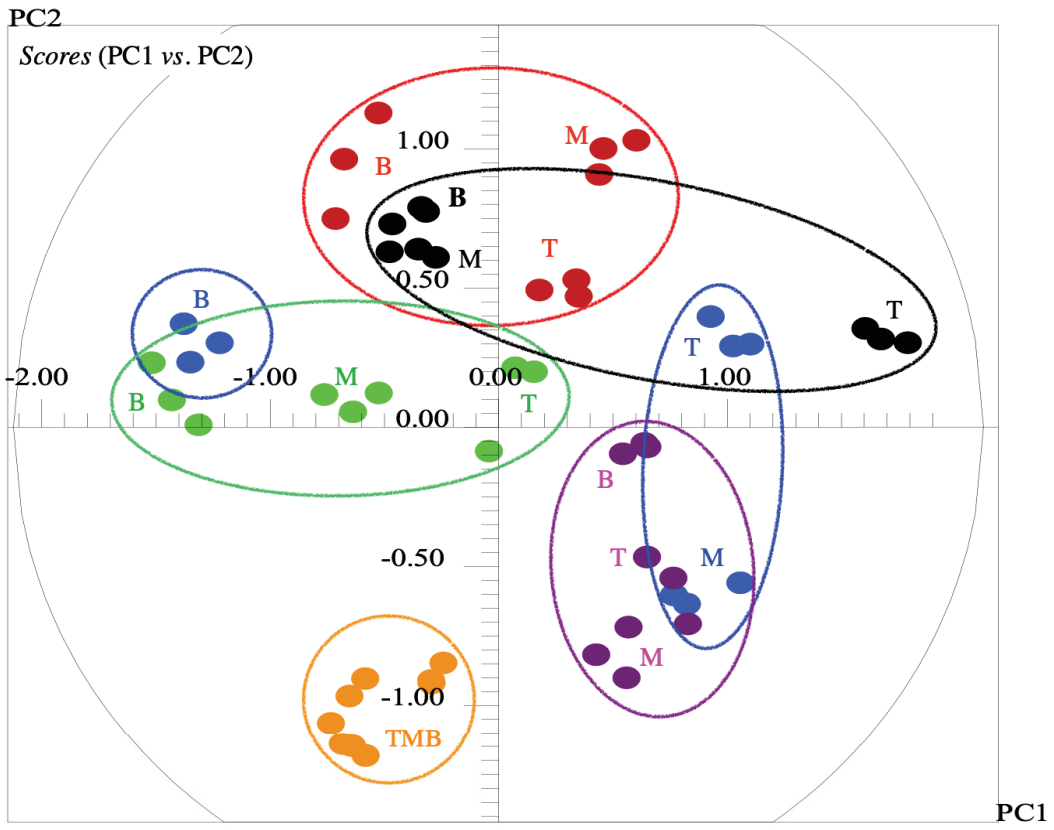

Figure 6.42. The *scores* plot with PC1 (31.97%) *vs* PC2 (19.28%) shows a spread of all NMR spectra (54) recorded for the leaf samples from top (T), middle (M), and bottom (B) sections only in *Maytenus ilicifolia.* All colored spheres represented months as: (●) **October**; (●) **December**; (●) **February**; (●) **April**; (●) **June**; and (●) **August**. Total used buckets were 233 out of 262, the data was divided into equal sized regions of δ 0.03 and pareto scaled.

The abovementioned spectral dispersals were due to several variables, observed from *loadings* and ^{1}H HR-MAS NMR spectrum of related plant species (Figure 6.43).

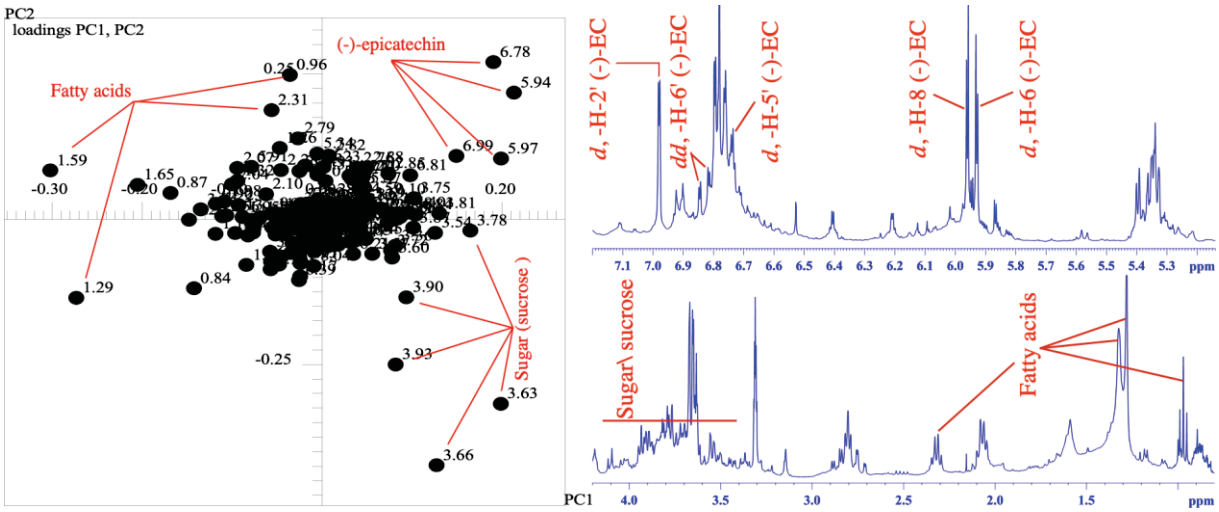

Figure 6.43. The *loadings* plot (left) with PC1 (31.45%) vs PC2 (20.73%) that discriminated topology mentioned in the *scores* plot with bin size of δ 0.03 and pareto scaled, and to the right is given a ^{1}H HR-MAS NMR spectrum (*Maytenus ilicifolia*) shows only the discriminatory peaks associated to the spectral dispersion (in *scores* plot) and appeared in the *loadings* (left).

Overall topological and spectral profiles distributions were detected by means of (-)-epicatechin (**2**), sucrose (**4**) or other sugars, and polyunsaturated fatty acids (**8**) in related samples. This chemical overview was described combinedly with seasonal variation as shown below. In discussion the numbers; 3, 6, or 9 expresses total number of samples profiles.

From *loadings* together with ^{1}H HR-MAS NMR spectrum, the (-)-epicatechin (**2**) on the basis of δ 6.99\6.97 (d, $^{4}J_{H\text{-}H}$ = 1.8 Hz, 1H, CH-2'), 6.81\6.79 (dd, $^{3,4}J_{H\text{-}H}$ = 8.3; 1.8 Hz, 1H, CH-6'), 6.78\6.77-6.74 (d, $^{3}J_{H\text{-}H}$ = 8.3 Hz, 1H, CH-5'), 5.97\5.94 (d, $^{4}J_{H\text{-}H}$ = 2.3 Hz, 1H, CH-6), and 5.94\5.91 (d, $^{4}J_{H\text{-}H}$ = 2.3 Hz, 1H, CH-8) responsibly discriminated typical leaf profiles from top (6TM) in February, and June and August (6T). This was noticed that compound (**2**) was in maximum amount particularly in the top section of *Maytenus* spp. during middle- of summer (February), autumn (June), and winter (August). It means these months seemed to be of extreme sunlight where the secondary metabolites (e.g. **2**) become active and serve to protect plant against intense sunlight radiations.

Moreover, δ 3.93 to δ 3.54 from sugar were main chemical shifts that discriminated maximum leaf profiles from middle section (9TMB) in October and June (3M). In this case, sugar compositions were higher during middle- of spring (October-December), and autumn (June). It reflected that this was drier period around the year, where plants accumulate more sugar to retaliate unfeasible conditions and continue to survive.

Similarly, the polyunsaturated fatty acids (**8**) due to the δ 2.33\2.32 (m, 2H, CH_2-2), 0.96 (t, 7.5 Hz, 3H, CH-18), 1.59\1.60 (m, 2H, CH_2-3), and 1.29\1.28 (*s*, 8H, CH_2-4,5,6,7)

discriminated large number of leaf profiles from bottom section in *Maytenus ilicifolia* during February (3B), August (6MB), June (3B), and April (9TMB). The accumulation of polyunsaturated fatty acids (**8**) in the bottom leaves was found during middle- of summer (February), autumn (April-June), and winter (August). Fatty acids play vital role in different mechansims including plant defense in extreme conditions, since the fatty acid accumulation may be due to seasonal variation (HARRAT et al., 2020) and or other ecological interactions.

6.5.2.3 PCA-based topology discrimination within *Maytenus aquifolium* Mart. (Celastraceae)

In the same way, the leaves harvested from different section (TMB) in *Maytenus aquifolium* in the four seasons (October 2018-August 2019) and investigated by NMR. Total 54 NMR profiles were deferred to PCA to measure chemical profile topologogically in relation to the seasonal flux (months). The spectral data was converted into *scores* and *loadings* plots by applying *influence* and *hotelling's* T^2 (95% confidence limit) that showed three abnormal samples associated to the month of June (red rectangles in Figure 6.44).

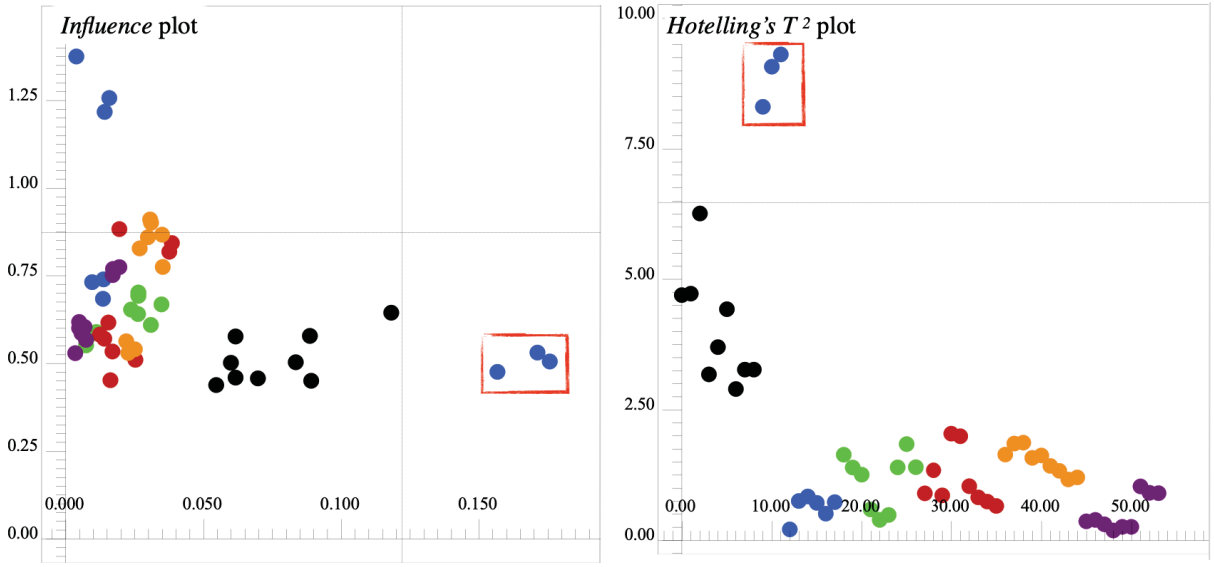

Figure 6.44. The *influence* (left) and *hotelling's* T^2 plot (right) shows an overview of all NMR spectra (54) recorded for the leaf samples from top (T), middle (M), and bottom (B) sections only in *Maytenus aquifolium.* All colored spheres represented months as: (●) **October**; (●) **December**; (●) **February**; (●) **April**; (●) **June**; and (●) **August** respectively.

Based on the *scores* (Figure 6.45), overall spectral profiles were appeared more controlled and less dispersed in comparison to other species (see Sec.6.5.2.2). However maximum samples (42TMB) associated to overall months (October 2018 to June 2019) were clustered around and close to the mean in *scores* towards positive side in contrast to few (9TMB, August-2019) in negative PC1 (35.83%). Samples in the big cluster appeared

comparable in all aspects in exception of those combined in the small group (9TMB). Furthermore, few profiles (3T-June; Figure 6.45) were farthest away in the spectral space showing maximum influence and T^2, probably due to the different chemical nature, seasonal variation and or environmental conditions impacting these samples isolating into the negative range of PC2 (19.35%).

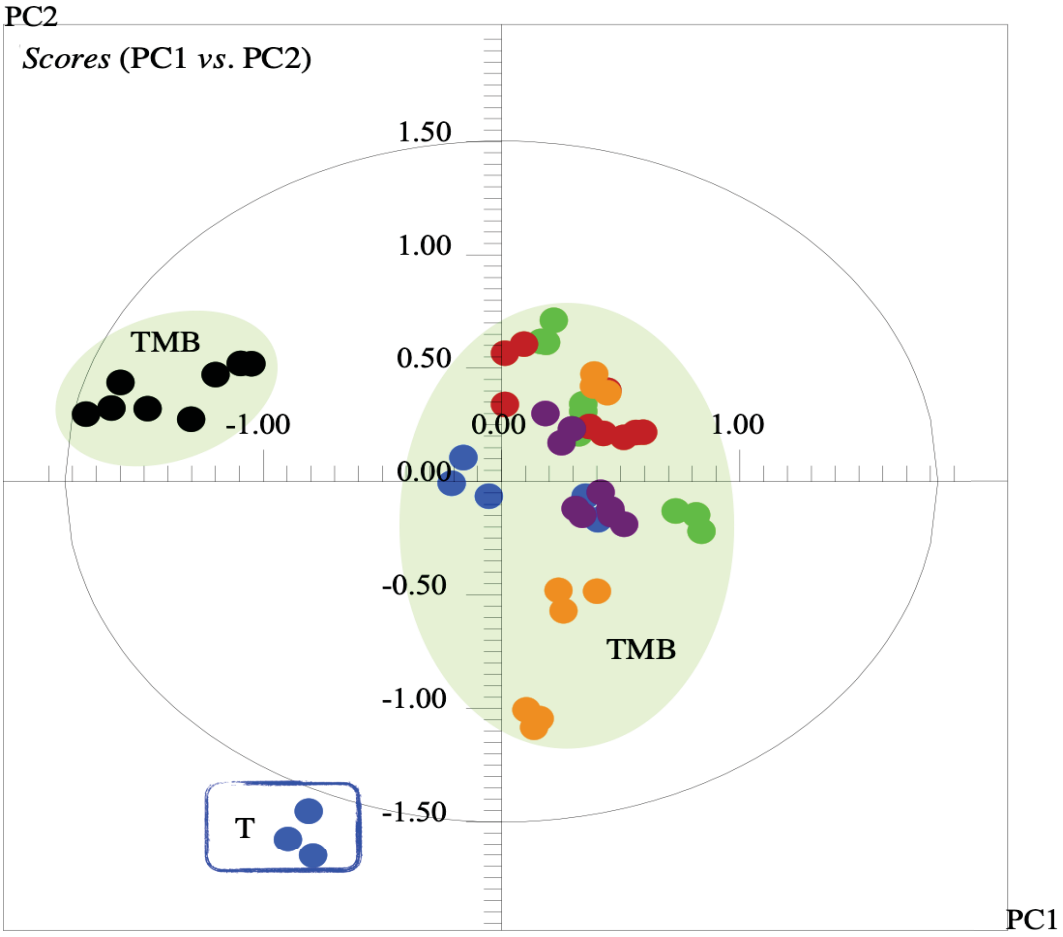

Figure 6.45. The *scores* plot (PC1 35.83% *vs* PC2 19.36%) shows a spread of all NMR spectra (54) from from top (T), middle (M), and bottom (B) leaves in *Maytenus aquifolium*. All colored spheres represented months as: (●) **October**; (●) **December**; (●) **February**; (●) **April**; (●) **June**; and (●) **August**. Total used buckets were 231 out of 262, the data was divided into equal sized regions of δ 0.03 and pareto scaled.

Analyzing samples grouping and dispersal was studied together with *loadings* and supplementary ^{1}H HR-MAS NMR spectrum (Figure 6.46) to identify significant variables.

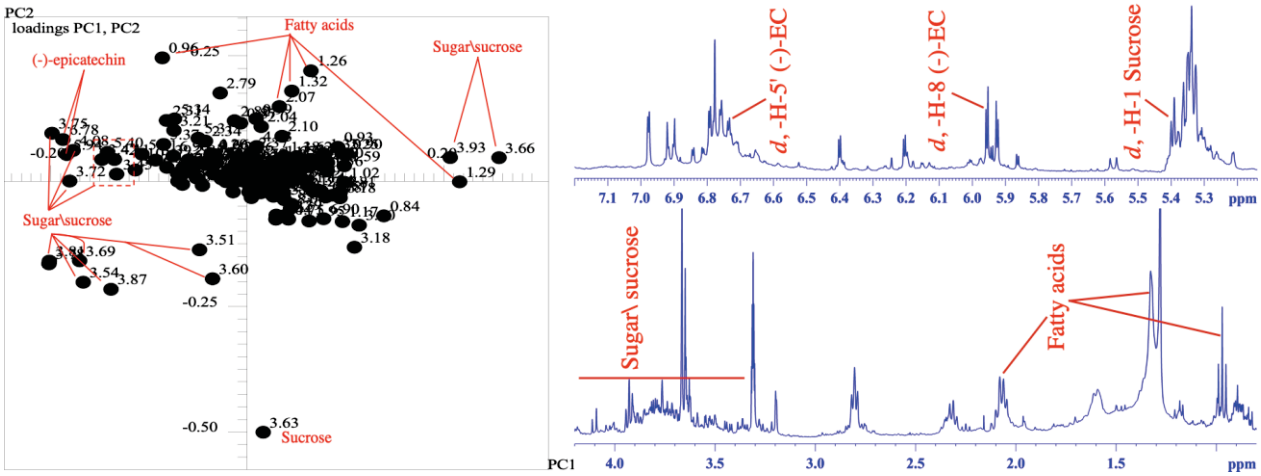

Figure 6.46. The *loadings* plot (left) with PC1 (35.83%) *vs* PC2 (19.36%) that discriminated topology mentioned in the *scores* plot with bin size of δ 0.03 and pareto scaled, and to the right is given a ^{1}H HR-MAS NMR spectrum (*Maytenus aquifolium*) shows only the discriminatory peaks associated to the spectral dispersion (in *scores* plot) and appeared in the *loadings* (left).

The *loadings* together with ^{1}H HR-MAS NMR profile from *M. aquifolium* (Figure 6.46) showed sugar or sucrose, unsaturated fatty acids, and probably (-)-epicatechins were contributing to samples dispersals. Since, several variables as δ 3.93, and 3.66 (d, J = 6.3 Hz, 1H, CH-3), and fatty acids at δ 2.06\2.06 (m, 4H, CH_2-8,17), and 1.32-1.29\1.28 (*s*, 8H, CH_2-4,5,6,7) from sugar or sucrose and fatty acids were responsibly linked a range leaf profiles (42TMB) into big cluster. This may represent that these metabolites were more accumulated in the plant leaves during one year (October 2018-June 2019).

Furthermore, it was noted that (-)-epicatechin due to δ 6.77 (d, $^{3}J_{H\text{-}H}$ = 8.3 Hz, 1H, CH-5'), and 5.94 (d, $^{4}J_{H\text{-}H}$ = 2.3 Hz, 1H, CH-6) whereas fatty acids δ 0.96\0.97 (t, 7.5 Hz, 3H, CH-18), and sucrose or sugars in δ 5.40\5.39 (d, $^{3}J_{H\text{-}H}$ = 3.8 Hz, 1H, *α*-CH-1), 4.08\4.09 (d, $^{3}J_{H\text{-}H}$ = 8.4 Hz, 1H, CH-3'), 3.87-3.75 (m, 4H, CH-4', CH-5', CH_2-6'), 3.72 (m, 2H, CH_2-6), 3.69-3.54 and respectively 3.43 (dd, $^{3}J_{H\text{-}H}$ = 9.8; 3.8 Hz, 1H) were responsible for the discrimination of few samples (9TMB) into one single small group during middle of winter (August).

There were three more samples (3T, June) isolated (Figure 6.45), due to a δ 3.63 (m, 2H, CH_2-1') from sucrose. This typical signal (δ 3.63) was intense in the NMR profiles (shown by red arrow) from top portion in *M. aquifolium* harvested in June. However, such characteristic signal was less intense and usually missing in the remaining profiles during other months (Figure 6.47). This unique signal (δ 3.63) from sucrose was contributing to isolate three top samples (in June) away from other groups respectively.

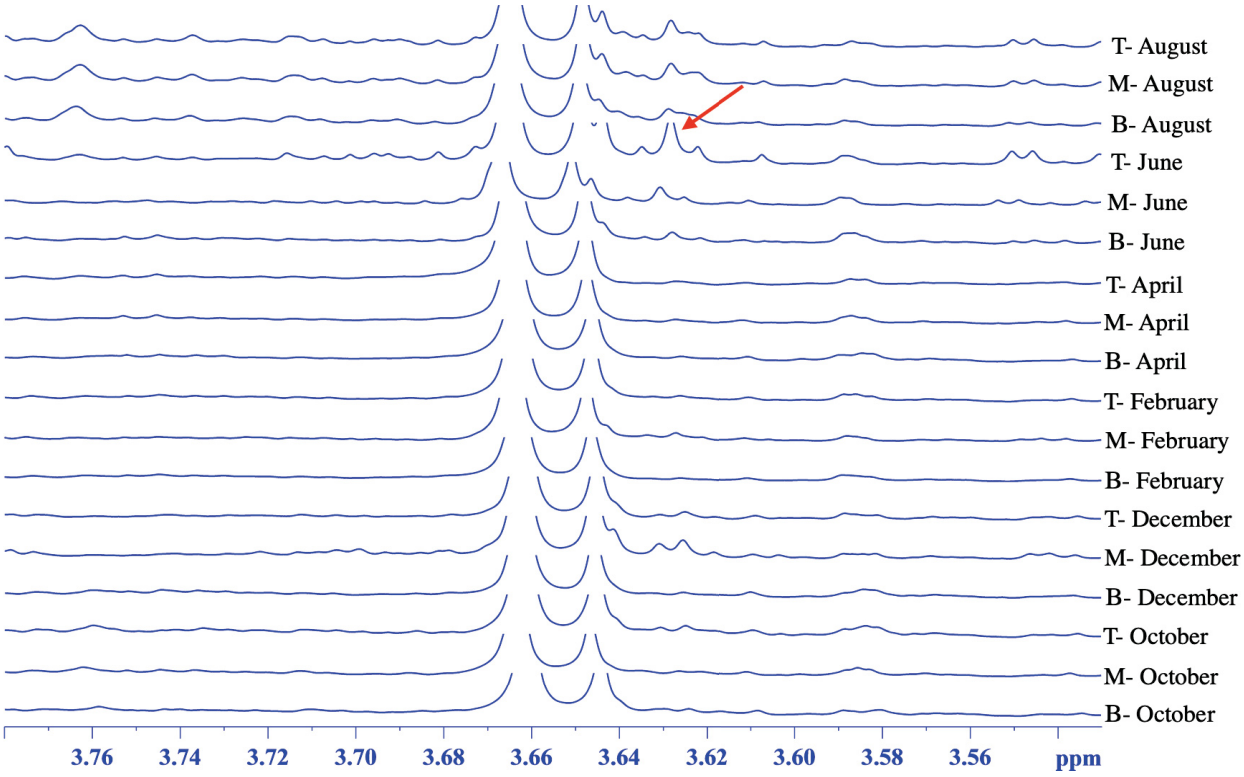

Figure 6.47. The representative carbohydrate region showing characteristic signal (δ 3.63) in ^{1}H HR-MAS NMR profiles from different (TMB) sections in *Maytenus aquifolium* in relation to months (Oct-August).

The compatibilities in *Maytenus ilicifolia* and *Maytenus aquifolium* were investigated by considering their topology, chemical compositions, and seasonal variation. Initially, both species were seen different on the basis of their chemical compositions. The topological profiles in both species were perceived affected against seasonal variablities.

The overall topological leaf profiles from *Maytenus ilicifolia* were dispersed more with respect to months whereas less distribution was revealed in *Maytenus aquifolium* except several T-samples (August). In other words, the chemical composition in *Maytenus ilicifolia* appeared as (-)-epicatechin was representative ingredient in average top leaf during middle- of summer (February), autumn (June), and winter (August). The fatty acid was characteristic component in average bottom leaf during middle- of summer (February), autumn (April-June), and winter (August). Since, sugars mostly represented the middle leaf during middle- of spring (October-December), and autumn (June). On the other hand, sugar composition was usually distributed in entire leaves from *Maytenus aquifolium* around four seasons even though maximum amount together with little (-)-epicatechin and fatty acids were seen in the upper to lower leaves only in the middle of winter (August). In general, the *aquifolium* spp. was observed over dominated by high amount of sugar as observed in NMR analyses (see Sec. 6.3.2; p. 80).

In this way, the month of August (mid-winter) was realized more influential to the leaf fingerprints in *Maytenus aquifolium.* The leading amounts of sugar revealed to be due to some additional factors affecting *aquifolium* species. For instance, as previously reported that both primary and secondary metabolites (NCUBE et al., 2012) such as, organic and phenolic acids, carbohydrates, flavan-3-ol (catechins) and (non)glycosylated flavonoids can cause from shades or scarce light (XU et al., 2020; YANG et al., 2018) and high sunlight (LI et al., 2020), herbivore interactions (LI et al., 2020), different biome, deviating temperature, rain fall, humidity, and season (WEN et al., 2020).

The discussion about relationship between plant topology and seasonal fluctuation represented that these trends may affect chemical pattern. In other words, it represents plant adaptation against season and biome however chemical status does not remain uniform against time-to-time seasonal variations. It is important to note that ecological conditions may alter typical alimentary, nutraceutical and therapeutic values of plants primary and secondary metabolites (KHAN et al., 2019; BAKOYANNIS et al., 2019; FREIRE et al., 2018; PREMALATHA et al., 2018; IMRAN et al., 2018; ALAMGIR., 2017).

6.6 AUTHENTICITY DISCRIMINATION OF COMMERCIAL *Maytenus ilicifolia* MART. (ESPINHEIRA-SANTA)

In light of therapeutic attributes, the medicinal plants attained great attention in folk medicines, herbal formulations and raw materials. The direct intake of plant products lack of understanding, classification, and or labeling may be unfavorable to health, however they can contain (non)toxic chemical substance, foreign matter or some harmful mixed material. Hence, this require authenticity evaluation, which is important factor in cataloging herbal materials to assure public health security and meet customers expectations.

This study have been focused to the commercial *Maytenus ilicifolia* Mart. (Espinheira-Santa), procured as chopped leaves, tea sachets, and capsules (Table 5.2; p. 52). Similarly, several herbal samples branded as *Maytenus ilicifolia* and or Espinheira-Santa from different fabricators (not shown) were collected and investigated. Moreover these herbal products were assigned usual codes (Table 5.2; p. 52) and directly stored under freezing temperature until ^{1}H HR-MAS NMR analyses.

Following the previous results, NMR spectra from commercial *Maytenus ilicifolia* Mart. were competed with authentic species (SA016) as mentioned in Figure 6.48. The comparison

between authentic and commercial products of Espinheira-Santa was made on the availability of main discriminatory metabolite in the commercial materials.

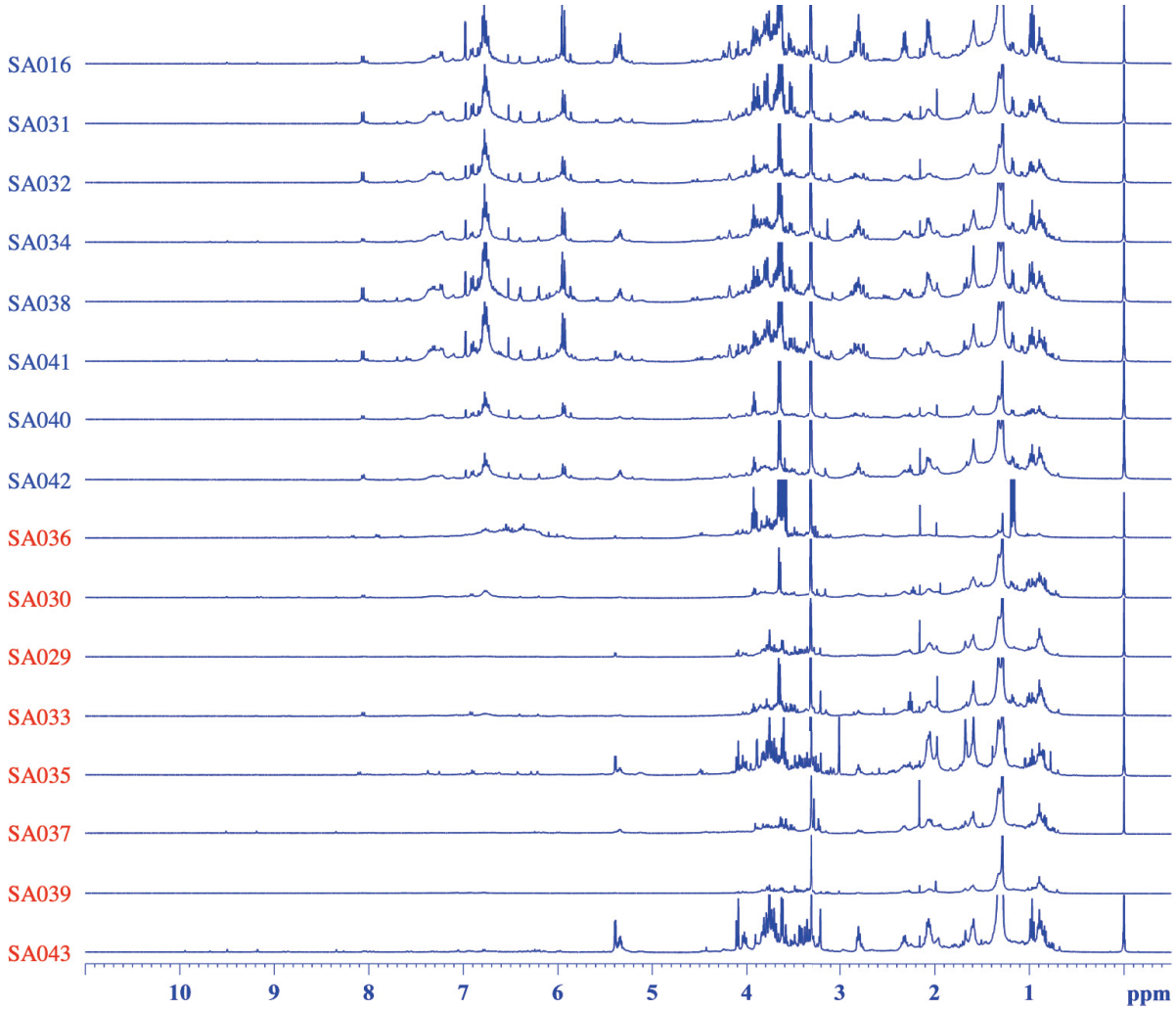

Figure 6.48. ^{1}H HR-MAS NMR spectra (400.13 MHz) in powdered materials (each 10 ± 1.0 mg: CD_3OD) from authentic (SA016) and commercial *Maytenus ilicifolia*.

The visual inspection of NMR profiles (Figure 6.48) revealed very few commercial materials (SA031, SA032, SA034, SA038, SA041, SA040, SA042) similar to the original *Maytenus ilicifolia* (SA016). NMR profiles from maximum commercial products were not discriminated as real Espinheira-Santa. The better assay regarded to (dis)similarities was observed from amplified profiles (Figure 6.50). To remind earlier statements (Sec. 6.5.2.1, p. 102), *Maytenus ilicifolia* (SA016) was discriminated by (-)-epicatechin metabolite (**2**; Figure 6.49) that was supplemental to furthermore authenticate commercial products. In context, only the characteristic signals from (-)-epicatechin compound (**2**) were addressed to compete all commercial and none commercial Espinheira-Santa.

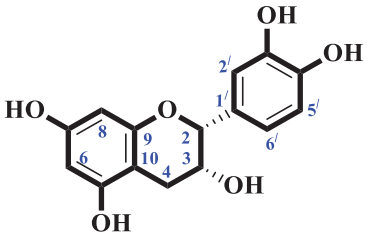

Figure 6.49. The chemical structure of (-)-epicatechin (**2**).

In investigation, the spectra (Figure 6.50) presented several doublet signals in frequency range of δ 6.97 (d, $^{4}J_{H\text{-}H}$ = 2.8 Hz, 1H; H-2'), δ 6.79 (dd, $^{3,4}J_{H\text{-}H}$ = 8.3; 1.8 Hz, 1H; H-5') and δ 6.75 (d, $^{3}J_{H\text{-}H}$ = 8.3 Hz, 1H; H-6') which showed all hydrogen nuclei in the B-ring in molecular structure (**2**). Similarly, two mutually coupled hydrogens appeared by individual doublets at δ 5.91 (d, $^{4}J_{H\text{-}H}$ = 2.3 Hz, 1H; H-6) and δ 5.94 (d, $^{4}J_{H\text{-}H}$ = 2.3 Hz, 1H; H-8) from A-ring in **2**. The presence of C-ring was confirmed by means of two individual doublets of doublet in δ 2.86 (dd, $^{2}J_{H4a\text{-}H4b}$ = 16.8 Hz; $^{3}J_{H3\text{-}H4a}$ = 4.7 Hz, 1H, H-4a) and correspondingly at δ 2.73 (dd, $^{2}J_{H4a\text{-}H4b}$ = 16.8 Hz; $^{3}J_{H3\text{-}H4b}$ = 2.8 Hz, 1H, H-4b). ^{1}H HR-MAS NMR-based study showed maximum commercial *Maytenus ilicifolia* were missing these characteristic signals.

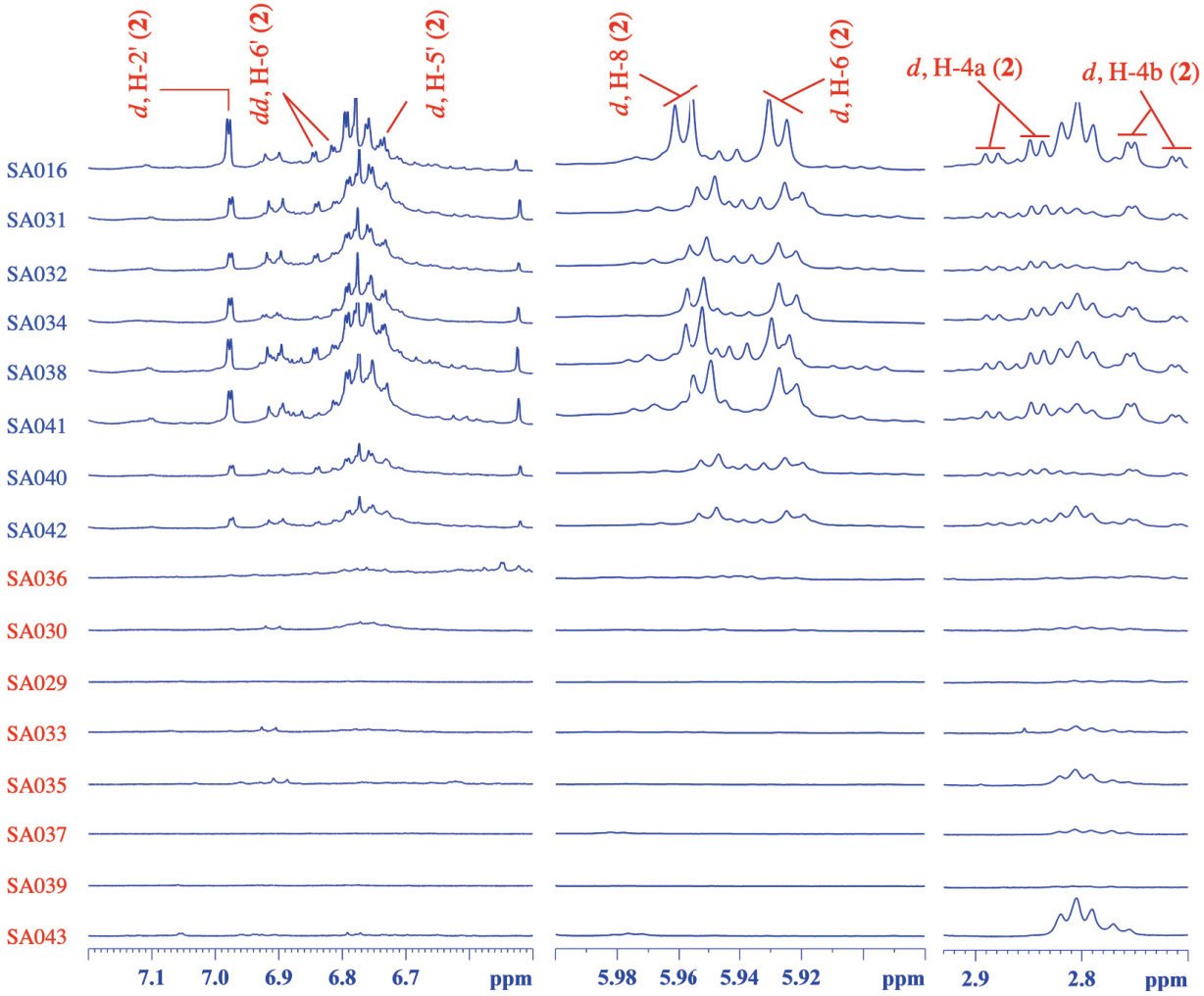

Figure 6.50. Amplified ^{1}H HR-MAS NMR spectra (400.13 MHz) in powdered materials (each 10 ± 1.0 mg: CD_3OD) from authentic (SA016) and commercial *Maytenus ilicifolia*.

Since, these products were furthermore analyzed and confirmed alternatively by multivariate principal component analysis (PCA). In such calculation, the *scores*, *loadings, influence* and *hotelling's* T^2 (95% confidence limit) were attained. The *influence* and *hotelling's* T^2 showed maximum samples were far away as outliers in the model space exposing higher residuals and T^2 values (Figure 6.51).

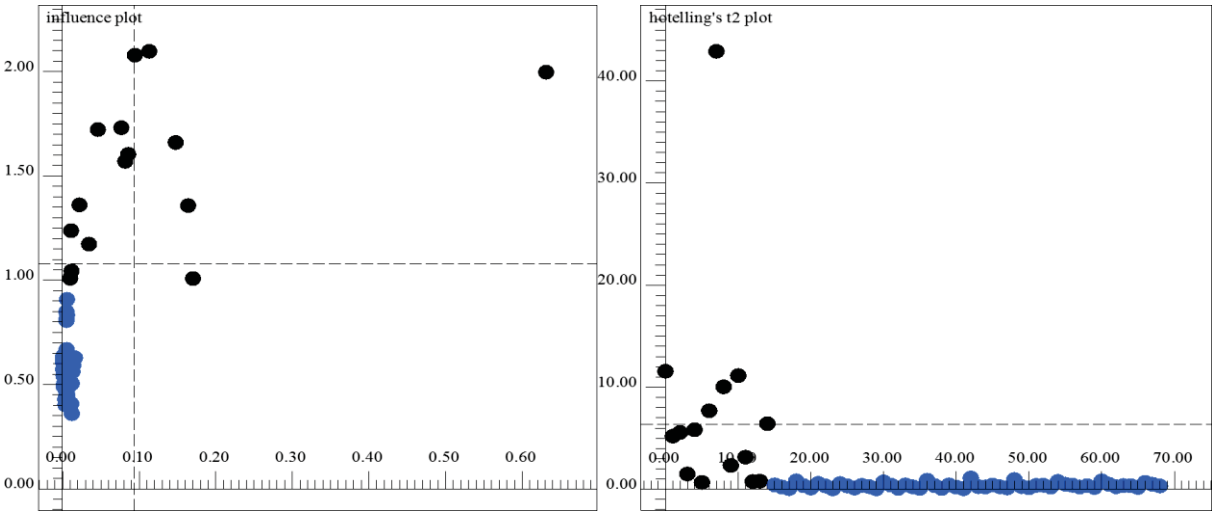

Figure 6.51. The *influence* (left) *vs. hotelling's* T^2 (right) plot from 69 NMR profiles of commercial (15 = ●) and real *Maytenus ilicifolia* (54 = ●).

In order to review the *scores* and *loadings* (Figure 6.52), exposed only few samples (SA031, SA032, SA034, SA038, SA040, SA041, SA042) were compatibly similar.

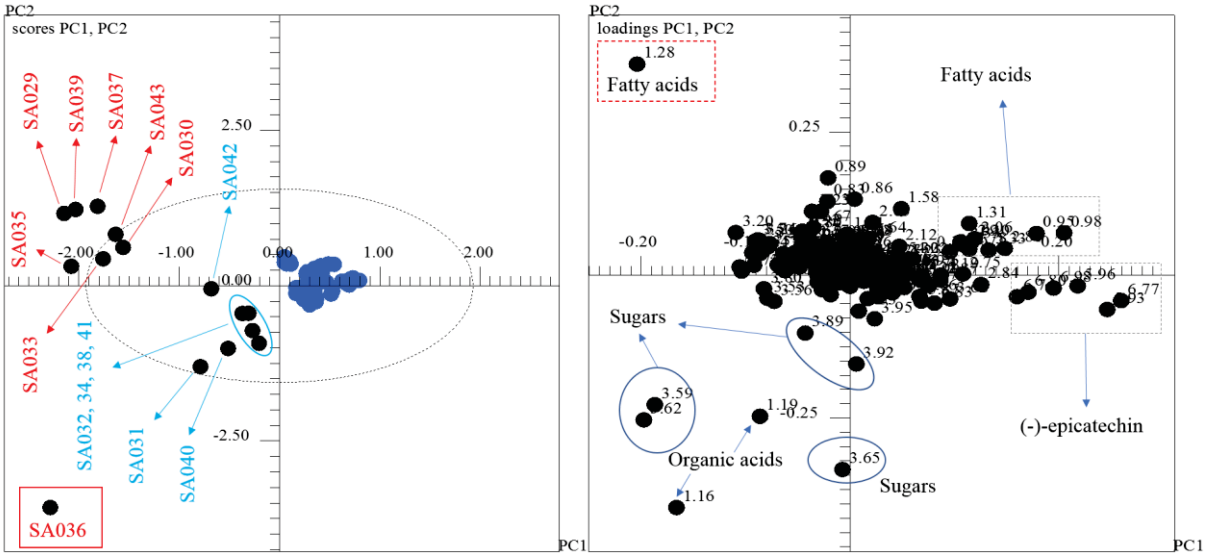

Figure 6.52. The *scores* (left) and *loadings* (right) plot with PC1 (32.85%) *vs* PC2 (21.35%) from 69 NMR profiles of commercial (15 = ●) and real *Maytenus ilicifolia* (54 = ●). Total used buckets 295 out of 314, equally binned (δ 0.03) and pareto scaled.

In outline the analogous profiles (SA031, SA032, SA034, SA038, SA040, SA041, SA042) were appeared in opposite side next to the group from real *Maytenus ilicifolia* shown in the positive region in PC1. The equivalent profiles were discriminated by the presence of (-)-epicatechin and sugar in the materials. However, the none matching samples (SA029, SA030, SA033, SA035, SA037, SA039, SA043) were not grouped and found away from real

species although outside of the variables space (95%) in PCA (Figure 6.52). Since, this effect was observed due to the fatty acids though one SA036 sample was based on organic acid, and sugar variables that boosted into the residuals and T^2 value, that's why the relevant samples were dispersed and completely different. The dissimilarities might be due to several reasons for example; lack of information, unintended mishandling during processing and packing, or adulteration of other plants parts to increase product volume etc. or either loss of the chemical ingredients over long time on the (none)local markets, pharmacies and natural products stores.

The conclusion made by ^{1}H HR-MAS NMR combined to PCA, revealed that limited commercial samples were found similar to the original *Maytenus ilicifolia*. In findings, maximum products labelled as *Maytenus ilicifolia* and or Espinheira-Santa were not real, which means they represented lack of quality management. In this way, it needs more strict quality control measurements to stop further falsification, adulteration in the future.

CONCLUSION

7 CONCLUSION

The intent of this work was to develop ^{1}H HR-MAS NMR fingerprinting coupled to principal component analysis (PCA) method to achieve quality control for *Maytenus ilicifolia* Mart. (Espinheira-Santa). The utility of this tool was to examine multiple metabolites in non-altered state of botanicals with little efforts.

In this analytical method, the entire botanical materials were distinguished on the basis of their spectral profiles and chemical fingerprints. The fingerprints overview showed that two *Maytenus* species were ambiguously similar but chemically different from other plants (*Sorocea bomplandii*, *Zollernia ilicifolia*, *Berberis laurina* Bilb., *Citronella gongonha* etc.).

To realized main contributing biomarker(s) in quality control, possibly a range of primary and specialized metabolites (organic and fatty acids, carbohydrates, flavonoids, flavanols) were investigated in HR-MAS NMR-fingerprinting from leaves in *Maytenus* species. Prospecting little differences in the spectra, the correlated plants were taken in account and continuously studied.

Beyond fingerprints characterization, the topological leaf chemical pattern *verses* seasonal variabilities or ecological interactions was investigated by HR-MAS NMR and PCA. The relationship was observed in a way that major fingerprints (epicatechin, sugar, fatty acids) were more accumulated in the upper leaves from *Maytenus ilicifolia* during mid-autumn and winter (June-August 2019) seasons. Since, overall topological leaves from *Maytenus aquifolium* showed high sugar contents in all seasons (October 2018-August 2019).

PCA calculation initially showed that *Maytenus ilicifolia* was different on the basis of (-)-epicatechin from *Maytenus aquifolium* (sugar composition). This means that (-)-epicatechin was main contributor to authenticity determination in *Maytenus ilicifolia* which is in agreement with ANVISA (ANVISA, 2018). The NMR spectrum from *Maytenus aquifolium* represented similar but less intense signals from this chemical component, which seemed environmentally affected. In order to trace leaf (upper-lower section) chemical patterns in both correlated species *versus* seasonal or environmental interactions, were investigated during four seasons (October 2018 to August 2019). In PCA measurements, the metabolic pattern in *Maytenus ilicifolia* was affected with seasonal change as well as *Maytenus aquifolium* was seen influenced by seasonal and other factors (biome, shades, pathogens, etc.). In general, most of the top leaves from *Maytenus ilicifolia* accumulated (-)-epicatechin in the middle of summer and winter, and late autumn. The middle leaves represent the accumulation of sugar during mid-spring and late autumn while bottom leaves the unsaturated fatty acids in

the mid-summer, winter, and autumn. *Maytenus aquifolium* was seen with controversial findings, representing that this spp. may be interrupted from different biome, pathogen attack, high shades or some other factors. For example, reviewing topological patterns except mid-winter (August) that was effective to the accumulation of sugar with additional (-)-epicatechin, and fatty acids in several leaves however, this spp. was completely dominated by sugar in entire four seasons. The leading amount of sugar in *M. aquifolium* represented that this was due to different biome, shady environment, and probably pathogens. From entire discussion, it was perceived that late autumn and mid-winter were more impacting seasons to the chemical and topological patterns in both species. In addition to seasonal flux, further environmental trends can highly affect quantitative levels of approximately all metabolites in the plants (YANG et al., 2018; SAMPAIO et al., 2016; NCUBE et al., 2012).

Both HR-MAS NMR coupled to PCA was found helpful approach in the characterization of all herbal species included the commercial *Maytenus ilicifolia,* procured from (non)local markets, stores and pharmacies. The study suggested maximum Espinheira-Santa sold on commercial points, had not shared similar results as those from real plant species. Based on NMR approach, it was concluded that maximum products (chopped leaves, tea sachets, extracts, capsuls) labled as Espinheira-Santa were not real which showed lack of quality control. It means that miss labeled or false products can be risky to health, however, such materials can contain lethal ingredients. Hence, this work advised further authenticity and correct cataloging of these products in order to assure efficacy of the products and health security.

In conclusions it can be suggested that inter- and intra-plant metabolic patterns in relation to seasonal changes and ecological interactions can help to understand novel insights such as nascent molecular discovery, growth gradient, genetic to molecular configuration, adaptation, metabolic pathwyas, and so on. These findings may be helpful and adaptable in further researches associated to health safety, quality control of plants and food products, agronomic as well as other plant policies.

REFERENCES

8 REFERENCES

ABBAS, O.; ZADRAVEC, M.; BAETEN, V.; MIKUŠ, T.; LEŠIĆ, T.; VULIĆ, A.; PRPIĆE, J.; JEMERŠIĆ, L.; PLEADIN, J. Analytical methods used for the authentication of food of animal origin. **Food Chemistry**, v. 246: p. 6-17, 2018.

AFONSO, S.; SILVA, F. B.; MARCHEAFAVE, G. G.; HATUMURA, P. H.; BRUNS, R. E.; SCARMINIO, I. S. Influence of seasonality and sunlight effects on *Rollinia mucosa* leaves fingerprint. **Journal of the Brazilian Chemical Society**, v. 30, n. 5: p. 968-977, 2019.

AGATONOVIC-KUSTRIN, S.; KUSTRIN, E.; GEGECHKORI, V.; MORTON, D. W. High-performance thin-layer chromatography hyphenated with microchemical and biochemical derivatizations in bioactivity profiling of marine species. **Marine drugs**, v. 17, n. 3: p. 148, 2019.

AGRA, M. F.; FREITAS, P. F.; BARBOSA-FILHO, J. M. Synopsis of the plants known as medicinal and poisonous in Northeast of Brazil. **Brazilian Journal of Pharmacology**, v. 17, n. 1: p. 114-140, 2007.

AKILAN, S.; HALIMA, T. H.; SASI, S.; KAPPACHERY, S.; BANIEKAL-HIREMATH, G.; VENKATESH, J.; GURURANI, M. A. Evaluation of osmotic stress tolerance in transgenic *Arabidopsis* plants expressing *Solanum tuberosum* D200 gene. **Journal of Plant Interactions**, v. 14, n. 1: p. 79-86, 2019.

ALAMGIR, A. N. M. **Therapeutic use of medicinal plants and their extracts**: Pharmacognosy, Cham: Springer International Publishing: Imprint: Springer, v.1: 2017.

ALAM, T. M.; JENKINS, J. E. HR-MAS NMR spectroscopy in material science. In FARRUKH, M. A, Editor. **Advance Aspects of Spectroscopy**, Intech Open, p. 279-306, 2012.

ALI, K. MALTESE, F.; ZYPRIAN, E.; REX, M.; CHOI, Y. H.; VERPOORTE, R. NMR Metabolic fingerprinting-based identification of grapevine metabolites associated with downy mildew resistance. **Journal of Agricultural and Food Chemistry**, v. 57, n.20: p. 9599-9606, 2009.

ALVES, T. B.; SOUZA-MOREIRRA, T. M.; VALENTINI, S. R.; ZANELLI, C. F.; FURLAN, M. Friedelin in *Maytenus ilicifolia* is produced by friedelin synthase isoforms. **Molecules**, v. 23, n.3: p. 700-700, 2018.

ANVISA. AGÊNCIA NACIONAL DE VIGILÂNCIA SANITÁRIA. **Primeiro Suplemento do Formulário de Fitoterápicos da Farmacopeia Brasileira**, 1ª edição, Brasília, 2018.

BAKHMUTOV, V. I. **Practical Nuclear Magnetic Resonance relaxation for chemists**, Chapt. 2. John Wiley & Sons, p. 19-29, 2005.

BAKOYANNIS, I.; DASKALOPOULOU, A.; PERGIALIOTIS, V.; PERREA, D. Phytochemicals and cognitive health: Are flavonoids doing the trick? **Biomedicine & Pharmacotherapy**, v. 109: p. 1488-1497, 2019.

BALLIN, N. Z.; LAURSEN, K. H. To target or not to target? Definitions and nomenclature for targeted versus non-targeted analytical food authentication. **Trends in Food Science & Technology**, v.86: p.537-543, 2019.

BARISON, A.; PEREIRA DA SILVA, C. W.; CAMPOS, F. R.; SIMONELLI, F.; LENZ, C. A.; FERREIRA, A. G. A simple methodology for the determination of fatty acid composition in edible oils through ^{1}H NMR spectroscopy. **Magnetic Resonance in Chemistry**, v. 48, n. 8: p. 642-650, 2010.

BAZAZ, R. D.; FARSHID, F.; ZARE, Z.; HAMEDANI, M.; RABIEI, M.; KHOSHAYAND, M. R.; VOGEL, H. J. Detection of adulteration in the Iranian saffron samples by ^{1}H NMR spectroscopy and multivariate data analysis techniques. **Metabolomics**, v. 13, n. 2: p. 1-19, 2017.

BHARDWAJ, D.; KAUSHIK, N. Phytochemical and pharmacological studies in genus Berberis. **Phytochemistry reviews**, v. 11: p. 523-542, 2012.

BRASIL. Ministério da Saúde. Resolução da Diretoria Colegiada–RDC nº 18, de 03 de abril de 2013. **Boas práticas de processamento e armazenamento de plantas medcinais.** Brasília, DF, 3 de abril de 2013.

BRASIL. Ministério da Saúde. DAF/SCTIE/MS–**Relação Nacional de Plantas Medicinais de Interesse ao SUS**-RENISUS, Brasília–DF, fevereiro, 2009.

CAGLIANI, L. R.; SCANO, P.; CONSONNI, R. NMR-based metabolomics: quality and authenticity of plant-based foods. **Modern Magnetic Resonance**, Chap.1 (Ed, G. A. Webb) Springer, Cham, p. 1-20, 2017.

CALDAS, D. K. D.; DE MATOS, W. R. Identificação das espécies comercializadas como "Espinheira-Santa" em comércios populares do Grande Rio e Baixada Fluminense–RJ, Brasil. **UNICIÊNCIAS**, v. 23, n. 1: p.57-59, 2019.

CARVALHO, A. C. B.; LANA, T. N.; PERFEITO, J. P. S.; SILVEIRA, D. The Brazilian market of herbal medicinal products and the impacts of the new legislation on traditional medicine. **Journal of Ethnopharmacology**, v. 212: p. 29-35, 2018.

CARVALHO, A. C. B.; RAMALHO, L. S.; DE OLIVEIRA MARQUES, R. F.; PERFEITO, J. P. S. Regulation of herbal medicines in Brazil. **Journal of Ethnopharmacology**, v. 158 (Part B): p.503- 506, 2014.

CHEN, H.; YAO, J.; WANG, F.; ZHOU, Y.; CHEN, K.; ZHUANG, R.; CHOI, M. M. F.; ZARAY, G. Toxicity of three phenolic compounds and their mixtures on the gram-positive bacteria *Bacillus subtilis* in the aquatic environment. **Science of The Total Environment**, v. 408, n.5: p. 1043-1049, 2010.

CICERO, N.; CORSARO, C.; SALVO, A.; VASI, S.; GIOFRÉ, S. V.; FERRANTELLI, V.; DUGO, G. The metabolic profile of lemon juice by proton HR-MAS NMR: the case of the PGI Interdonato Lemon of Messina. **Natural product research**, v. 29, n. 20: p. 1894-1902, 2015.

CIPRIANI, T. R.; MELLINGER, C. G.; DE SOUZA, L. M.; BAGGIO, C. H.; FREITAS, C. S.; MARQUES, M. C. A.; GORIN, P. A. J.; SASSAKI, G. L.; IACOMINI, M. A polysaccharide from a tea (infusion) of *Maytenus ilicifolia* leaves with anti-ulcer protective effects. **Journal of Natural Products**, v. 69: p. 1018-1021, 2006.

CLARIDGE, T. D. W. **High-resolution NMR techniques in organic chemistry**. Chapt. 2, Ed. 3. United Kingdom: Elsevier, v. 27: p. 11-59, 2016.

COELHO, R. G.; STASI, L. C. D.; VILEGAS, W. Chemical constituents from the infusion of *Zollernia ilicifolia* Vog. and comparison with *Maytenus* species. **Z. Naturforsch**, v. 58, n. 1-2: p. 47-52, 2003.

CONSONNI, R.; RUTH C. L.; COGLIATI, C. NMR based geographical characterization of roasted coffee. **Talanta**, v. *88*: p. 420-426, 2012.

CORADIN, L.; SIMINSKI, A.; REIS, A. Espécies nativas da flora brasileira de valor econômico atual ou potencial: plantas para o futuro-região sul. **Brasilia:** *Sorocea bonplandii*, *Zollernia ilicifolia*, *Jodina rhobifolia*: falsas Espinheiras-Santas. Chapt.5, 2nd ed., **Ministério do Meio Ambiente**, p. 701-708, 2011.

CRAIG, A.; CLOAREC, O.; HOLMES, E.; NICHOLSON, J. K.; LINDON, J. C. Scaling and normalization effects in NMR spectroscopic metabonomic data sets. **Analytical chemistry**, v. 78, n. 7: p. 2262-2267, 2006.

DEBORDE, C.; FONTAINE, J. X.; JACOB, D.; BOTANA, A.; NICAISE, V.; RICHARD-FORGET, F.; LECOMTE, S.; DECOURTIL, C.; HAMADE, K.; MESNARD, F.; MOING, A.; MOLINIÉ, R. "Optimizing 1D 1 H-NMR profiling of plant samples for high throughput analysis: extract preparation, standardization, automation and spectra processing. **Metabolomics**, v. 15, n. 3: p. 28-28, 2019.

DEBORDE, C.; MOING, A.; ROCH, L.; JACOB, D.; ROLIN, D.; GIRAUDEAU, P. Plant metabolism as studied by NMR spectroscopy. **Progress in Nuclear Magnetic Resonance Spectroscopy**, v. 102: p. 61-97, 2017.

DIAGONE, C. A.; COLOMBO, R.; LANÇAS, F. M., YARIWAKE, J. H. CZE/PAD and HPLC-UV/PAD profile of flavonoids from *Maytenus aquifolium* and *Maytenus ilicifolia* "Espinheira-Santa" leaves extracts. **Chromatography Research International**, 2012.

DJINGOVA, R.; KULEFF, I.; MARKERT, B. Chemical fingerprinting of plants. **Ecological Research**, v. 9: p. 3-11, 2004.

EBRAHIMI, P.; VIERECK, N.; BRO, R.; ENGELSEN, S. B. Chemometric analysis of NMR spectra. **Springer: Cham, Switzerland**: p.1-20, 2017.

EMWAS, A. H.; EDOARDO, S.; XIN G.; RYAN, T. M.; VITOR, A. P. M. D. S.; RAJA, R.; DAVID, S. W. Recommended strategies for spectral processing and post-processing of 1D ^{1}H-NMR data of biofluids with a particular focus on urine." **Metabolomics,** v. 14, n. 3: p. 31-31, 2018.

EUCEDA, L. R.; GISKEØDEGÅRD, G. F.; BATHEN, T. F. Preprocessing of NMR metabolomics data. **Scandinavian journal of clinical and laboratory investigation**, v. 75, n. 3: p. 193-203, 2015.

FANG, C.; ALISDAIR, R. F.; JIE, L. Exploring the diversity of plant metabolism. **Trends in plant science**, v. 24, n. 1: p. 83-98, 2019.

FAROOQ, H.; COURTIER-MURIAS, D.; SOONG, R.; BERMEL, W.; KINGERY, W. M.; SIMPSON, A. J. HR-MAS NMR spectroscopy: a practical guide for natural samples. **Current Organic Chemistry**, v. 17, n. 24: p. 3013-3031, 2013.

FISCHER, S. Z.; STUMPF, E. R. T.; MARIOT, M. P. *Maytenus ilicifolia*- a plant with many possibilities. **Acta Horticulture,** v. 1104, n. 1104: p. 517-520, 2015.

FLORES, I. S.; MARTINELLI, B. C. B.; PINTO, V. S.; QUEIROZ JR, L. H. K.; LIAO, L. M. Important issues in plant tissues analyses by HR-MAS NMR. **Phytochemical Analysis**, v. 30, n. 1: p. 5-13, 2018.

FREIRE, C. J.; BARBOSA, L. R. S.; COSTA, J. G.; SANTOS, R. G. A.; SANTOS, A. F. Phytotherapy in pediatrics: the production of knowledge and practices in primary care. **Revista Brasileira de Enfermagem**, v.71: p. 637-645, 2018.

GAILLOT, A. R. C.; BEZERRA, I. D. L.; PALHARES, L. C. G. F.; SANTANA-FILHO, A. P.; CHAVANTE, S. F.; SASSAKI, G. L. Structural characterization of blackberry wine polysaccharides and immunomodulatory effects on LPS-activated RAW 264.7 macrophages. **Food Chemistry**, v. 257: p. 143-149, 2018.

GARCIA, M. G. D.; BRITEZ, L.; GONZALEZ, Y.; ARRUA, R. D. D. Comparative morphoanatomy of *Genipa americana L.* (Rubiaceae) and *Sorocea bonplandii* (Baill.) W. C. Burger, Lanj. & Wess. Boer (Moraceae) marketed in San Lorenzo's market. **Rojasiana**, v. 10, n. 1: p. 93-101, 2011.

GIULIANI, A. The application of principal component analysis to drug discovery and biomedical data. **Drug discovery today**, v. 22, n 7: p. 1069-1076, 2017.

GOGIASHVILI, M.; NOWACKI, J.; HERGENRÖDER, R.; HENGSTLER, J. G.; LAMBERT, J.; EDLUND, K. HR-MAS NMR based quantitative metabolomics in breast cancer. **Metabolites**, v. 9, n. 2: p. 19-19, 2019.

GONZALEZ, F. G.; PORTELA, T. Y.; STIPP, E. J.; DI-STASI, L. C. Antiulcerogenic and analgesic effect of *Maytenus aquifolium, Sorocea bomplandii* and *Zollernia ilicifolia*. **Journal of Ethnopharmacology**, v. 77, n.1: p.41-47, 2001.

HARDING, S. A. Condensed tannins: arbiters of abiotic stress tolerance?. **Tree physiology**, v. 39, n. 3: p.341-344, 2019.

HARRAT, M.; GOURINE, N.; VÁLEGA, N.; SILVA, A. M. S.; YOUSFI, M. Seasonal variability of chemical composition and antioxidant activity of lipids (fatty acids and tocopherols) from the leaves of Pistacia lentiscus L. **Food Measure**, v. 14: p. 1939-1956, 2020.

HEMINGWAY, R. W.; TOBIASON, F. L.; MCGRAW, G. W.; STEYNBERG, J. P. Conformation and complexation of tannins: NMR spectra and molecular search modeling of flavan-3-ols. **Magnetic Resonance in Chemistry**, v. 34, n. 6: p. 424-433, 1996.

HORNING, E. C.; HORNING, M. G. Metabolic profiles: gas-phase methods for analysis of metabolites. **Clinical Chemistry**, v. 17, n. 8: p. 802–809, 1971.

HOTELLING, H. Analysis of a complex of statistical variables into principal components. **Journal of educational psychology**, v. 24, n. 6: p. 417-417, 1933.

IACCARINO, N.; AMATO, J.; PAGANO, B.; PAGANO, A.; D'ORIANO, L.; PELLICCIA, S.; GIUSTINIANO, M.; BRANCACCIO, D.; MERLINO, F.; NOVELLINO, E.; ALVIGGI, C. ^{1}H NMR-based metabolomics study on follicular fluid from patients with Polycystic Ovary Syndrome. **Biochimica Clinica**, v. 42, n. 1: p.26-31, 2018.

IMRAN, M.; RAUF, A.; SHAH, Z. A.; SAEED, F.; IMRAN, A.; ARSHAD, M. U.; AHMAD, B.; BAWAZEER, S.; ATIF, M.; PETERS, D. G.; MUBARAK, M. S. Chemo-preventive and therapeutic effect of the dietary flavonoid kaempferol: a comprehensive review. **Phytotherapy Research**, v. 33, n. 2: p. 263-275, 2018.

JAHANGIR, M.; NURINGTYAS, T. R.; ALI, K.; WILSON, E. G.; CHOI, Y. H.; VERPOORTE, R. NMR-based metabolomics: Understanding plant chemistry and

identification of biologically active compounds. **NMR-based Metabolomics**, p. 246-263, 2018.

JENSEN, H. M.; BERTRAM, H. C. The magic angle view to food: magic-angle spinning (MAS) NMR spectroscopy in food science. **Metabolomics**, v. 15, n. 3: p. 44-44, 2019.

JESUS, W. M. D. M.; CUNHA, T. N. D. Estudo das propriedades farmacológicas da Espinheira-Santa (*Maytenus ilicifolia* Mart. ex Reissek) e de duas espécies adulterantes. **Revista Saúde e Desenvolvimento**, v. 2, n. 1: p.20-46, 2012.

KHALID, N.; AQEEL, M.; NOMAN, A. System biology of metal tolerance in plants: An integrated view of genomics, transcriptomics, metabolomics, and phenomics. **Plant Metabolomics and Functional Omics***,* Springer, Cham, p. 107-144, 2019.

KHAN, M. S. A.; AHMAD, I. Herbal Medicines: Current trends and future prospects. **New Look to Phytomedicine: Advancements in Herbal Products as Novel Drugs Leads**, p. 3-13, 2019.

KHARBACH, M.; MARMOUZI, I.; JEMLI, M. E.; BOUKLOUZE, A.; HEYDEN, Y. V. Recent advances in untargeted and targeted approaches applied in herbal-extracts and essential-oils fingerprinting-A review. **Journal of Pharmaceutical and Biomedical Analysis**, v. 177: p. 112849-112849, 2020.

KIM, H. K.; CHOI, Y. H.; VERPOORTE, R. NMR-based plant metabolomics: where do we stand, where do we go? **Trends in Biotechnology**, v. 29, n. 6: p. 267-275, 2011.

KIM, H. K.; CHOI, Y. H.; VERPOORTE, R. NMR-based Metabolomic analysis of plants. **Nature Protocol**, v. 5, n. 3: p. 536-549, 2010.

KOKOVA, D.; MAYBORODA, O. A. Twenty years on: Metabolomics in Helminth research. **Trends in Parasitology**, v. 35, n. 4: p.282-288, 2019.

KOOY, F.V. D.; MALTESA, F.; CHOI, Y. H.; KIM, H. K.; VERPOORTE, R. Quality control of herbal material and phytopharmaceuticals with MS and NMR based metabolic fingerprinting. **Planta Medica**, v. 75, n. 7: p. 763-775, 2009.

KUTZ, M. **Handbook of measurement in science and engineering**. Chapt. 65, Ed. 1. **Wiley**, v. 3: p.2309-2403, 2013.

KRISHNAN, P.; KRUGER, N. J.; RATCLIFFE, R. G. Metabolite fingerprinting and profiling in plants using NMR. **Journal of experimental botany**, v. 56, n. 410: p. 255-265, 2004.

KUBALLA, T.; BRUNNER, T. S.; THONGPANCHANG, T.; WALCH, S. G.; LACHENMEIER, D. W. Application of NMR for authentication of honey, beer and spices. **Current Opinion in Food Science**, v. 19: p. 57-62, 2018.

KUJAWSKA, M. Yerba Mate (*Ilex paraguariensis*) beverages: Nutraceutical ingredients or conveyor for the intake of medicinal plants? Evidence from Paraguayan folk medicine. **Evidence-based Complementary and Alternative Medicine**, p. 6849317-6849317, 2018.

KUMAR, S.; PANDEY, A. K. Chemistry and biological activities of flavonoids: an overview**.** **The Scientific World Journal**, p. 162750-162750, 2013.

LANDRUM, L. R. Revision of *Berberis* (Berberidaceae) in Chile and adjacent southern Argentina. **Annals of the Missouri Botanical Garden**, p. 793-834, 1999.

LEE, K. M.; JEON, J. Y.; LEE, B. J.; LEE, H.; CHOI, H. K. Application of metabolomics to quality control of natural product derived medicines. **Biomolecules and Therapeutics**, v. 25, n. 6: p. 559-568, 2017.

LEITE, J. P. V.; RASTRELLI, L.; ROMUSSI, G.; OLIVEIRA, A. B.; VILEGAS, J. H. Y.; VILEGAS, W.; PIZZA, C. Isolation and HPLC quantitative analysis of Flavonoid glycosides from Brazilian beverages (*Maytenus ilicifolia* and *M. aquifolium*). **Journal of Agriculture and Food Chemistry**, v. 49, n. 8: p. 3796-3801, 2001.

LEVITT, M. H. Nuclear spin relaxation. **Resonance**, v. 20, n. 11: p. 986-994, 2015.

LI, L.; TINGTING, L.; YUANYUAN, J.; YUNQIU, Y.; LIANG, Z.; ZONGDE, J.; Chaoling, W.; Xiaochun W.; Hua, Y. Alteration of local and systemic amino acids metabolism for the inducible defense in tea plant (*Camellia sinensis*) in response to leaf herbivory by Ectropis oblique. **Archives of Biochemistry and Biophysics**, v. 683: p. 108301-108301, 2020.

LI, X.; ZHANG, L.; AHAMMED, G. J.; LI, Z. X.; WEI, J. P.; SHEN, C.; YAN, P.; ZHANG, L. P.; HAN, W. Y. Stimulation in primary and secondary metabolism by elevated carbon dioxide alters green tea quality in *Camellia sinensis* L. **Scientific Reports**, v. 7, n.1: p. 7937-7937, 2017.

LIEBEKE, M.; PUSKÁS, E. Drying enhances signal intensities for global GC–MS metabolomics. **Molecule**, v. 9, n. 4: p.68, 2019.

LORENZI, H. In; Arvores brasileiras: manual de identificação e cultivo de plantas arbóreas nativas do Brasil. **Nova odessa SP: Instituto Plantarum**., Chapter **3** (Ed.1): p. 384, 2009.

LUAN, H.; WANG, X.; CAI, Z. Mass spectrometric-based metabolomics: Targeting the crosstalk between gut microbiota and brain in neurodegenerative disorders. **Mass Spectrometry Review**, v. 38: p. 22-33, 2017.

MAHOMOODALLY, F.; SUROOWAN, S.; SREEKEESSOON, U. Adverse reactions of herbal medicine- A quantitative assessment of severity in Mauritius. **Journal of Herbal Medicine**, v.12: p. 49-65, 2018.

MANSANO, V. D. F.; TUCKER, S. C.; TOZZI, A. M. G. D. A. Floral ontogeny *Lecointea*, *Zollernia*, *Exostyles* and *Harleyodendron* (Leguminosae: Papilionoideae: Swartzieae S. L). **American Journal of Botany**, v. 89, n. 10: p. 1553-1569, 2002.

MATICH, E. K.; SORIA, N. G. C.; AGA, D. S.; ATILLA-GOKCUMEN, G. E. Applications of metabolomics in assesing ecological effects of emerging contaminants and pollutants on plants. **Journal of Hazardous Materials**, v. 373, n. 5: p. 527-535, 2019.

MAZZA, M. C. M.; SANTOS, J. E. D.; MAZZA, C. A. D.S. Reproductive phenology of *Maytenus ilicifolia* (Celastraceae) in the Irati National Forest Paraná Brazil. **Brazilian Journal of Botany**, v. 34, n.4: p. 1-12, 2011.

MAZZEI, P.; COZZOLINO, V.; PICCOLO, A. High-Resolution magic-angle spinning NMR and magnetic resonance imaging spectroscopies distinguish metabolome and structural properties of maize seeds from plants treated with different fertilizers

and arbuscular mycorrhizal fungi. **Journal of agricultural and food chemistry**, v. 66, n. 11: p. 2580-2588, 2018.

MAZZEI, P.; PICCOLO, A.; VALENTINI, M. Intact food analysis by means of HRMAS-NMR spectroscopy. **Modern magnetic resonance**, p.1-16, 2017.

MBAVENG, A. T.; QIAOLI Z.; VICTOR K. "Harmful and protective effects of phenolic compounds from African medicinal plants." **Toxicological Survey of African Medicinal Plants**, p. 577-609, 2014.

MCKAY, R. T. How the 1D-NOESY suppresses solvent signal in metabonomics NMR spectroscopy: An examination of the pulse sequence components and evolution. **Concepts in Magnetic Resonance Part A**, v. 38, n. 5: p. 197-220, 2011.

MOSCHEN, S.; MARINO, J.; NICOSIA, S.; HIGGINS, J.; ALSEEKH, S.; ASTIGUETA, F.; LANGLADE, N. B. Exploring gene networks in two sunflower lines with contrasting leaf senescence phenotype using a system biology approach. **BMC plant biology**, v. 19, n. 1: p. 1-15, 2019.

MOSSI, A.; MAZUTTI, M.; PAROUL, N.; CORAZZA, M. L.; DARIVA, C.; CANSIAN, R. L.; OLIVEIRA, J. V. Chemical variation of tannins and triterpenoids in Brazilian populations of *Maytenus ilicifolia* Mart. ex Reiss. **Brazilian Journal of Biology**, v. 69, n. 2: p. 339-345, 2009.

MUHAMMAD, U.; ZHU, X.; LU, Z.; HAN, J.; SUN, J.; TAYYABA, S.; ABBASI, B.; SIYAL, F. A.; DHAMA, K.; SAQIB, J. Effects of extraction variables on pharmacological activities of vine tea extract (*Ampelopsis grossedentata*). **International Journal of Pharmacology**, v. 14, n. 4: p.495-505, 2018.

NICHOLSON, J. K.; LINDON, J. C.; HOLMES, E. Metabonomics: understanding the metabolic responses of living systems to pathophysiological stimuli via multivariate statistical analysis of biological NMR spectroscopic data. **Xenobiotica**, v. 29, n. 11: p. 1181-1189, 1999.

NCUBE, B.; FINNIE, J. F.; STADEN, J. V. Quality from the field: the impact of environmental factors as quality determinants in medicinal plants**. South African Journal of Botany**, v. 82: p.11-20, 2012.

OLIVEIRA, A. L.; MARTINELLI, B. C. B.; LIÃO, L. M.; PEREIRA, F. C.; LACERDAC, E. P. S.; ALCANTARA, G. B. ^{1}H HR-MAS NMR and S180 Cells: Metabolite Assignment and Evaluation of Pulse Sequence. **Journal of Brazilian Chemical Society**, v. 25, n. 6: p. 1135-1142, 2014.

OLIVER, S. G.; WINSON, M. K.; KELL, D. B.; BAGANZ, F. Systematic functional analysis of the yeast genome. *Trends in biotechnology*, v. 16, n. 9: p. 373-378, 1998.

PAGTER, M.; YDE, C. C.; KJÆR, K. H. Metabolic fingerprinting of dormant and active flower primordia of *Ribes nigrum* using high-resolution magic angle spinning NMR. **Journal of agricultural and food chemistry**, v. 65, n. 46: p. 10123-10130, 2017.

PALHARES, R. M.; DRUMMOND, M. G.; BRASIL, B. S. A. F.; BRANDÃO, M. G. L.; OLIVEIRA, G. Medicinal Plants Recommended by the World Health Organization: DNA Barcode Identification Associated with Chemical Analyses Guarantees their Quality. **Public Library of Sciences (PLOS ONE)**, v. 10, n. 5: p. 1-29, 2015.

PATHAK, S.; AGARWAL, A. V.; AGARWAL, P.; RIVEDI, P. K. Secondary Metabolite Pathways in Medicinal Plants: Approaches in Reconstruction and Analysis. **Molecular Approaches in Plant Biology and Environmental Challenges**, Springer, Singapore, p. 339-364, 2019.

PATTI, G. J.; YANES, O.; SIUZDAK, G. Innovation: Metabolomics: the apogee of the omics trilogy. **Nature Reviews Molecular Cell Biology**, v. 13, n. 4: p. 263-269, 2012.

PAULING, L.; ROBINSON, A. B.; TERANISHI, R.; CARY, P. Quantitative analysis of urine vapor and breath by gas-liquid partition chromatography. **Proceedings of the National Academy of Sciences**, v. 68, n. 10: p. 2374-2376, 1971.

PEARSON, K. LIII. On lines and planes of closest fit to systems of points in space. **The London, Edinburgh, and Dublin Philosophical Magazine and Journal of Scienc**e, v. 2, n.11: p. 559-572, 1901.

PELKONEN, O.; XU, Q.; FAN, T. P. Why is Research on Herbal Medicinal Products Important and How Can We Improve Its Quality? **Journal of Traditional and Complimentary Medicine**, v. 4, n. 1: p. 1-7, 2014.

PÉRICO, L. L.; RODRIGUES, V. P.; ALMEIDA, L. F. R.; FORTUNA-PEREZ, A. P.; VILEGAS, W.; HIRUMA-LIMA, C. A. *Maytenus ilicifolia* Mart. ex Reissek. **Medicinal and Aromatic Plants of South America** Springer, Dordrecht, v. 5: p. 323-335, 2018.

PINTO, G. H. T.; PEREIRA, A. M. S.; SILVA, L. L.; ALVARES, N. D. C.; BERTONI, D. W.; PINA, E. S. Introdução *in vitro* de *Maytenus aquifolium*. **Ciência & Tecnologia Fatec- JB**, v. 10, n. 2: p. 47-52, 2018.

PREMALATHA, T.; RAMYA, K. B. Nutraceuticals: The medicine. **Pharma Science Monitor, v.** 9, n. 1: p. 203-216, 2018.

QIAN, Y.; ZHAO, X.; ZHAO, L.; CUI, L.; LIU, L.; JIANG, X.; LIU, Y.; GAO, L.; XIA, T. Analysis of stereochemistry and biosynthesis of epicatechin in tea plants by chiral phase high performance liquid chromatography. **Journal of Chromatography B**, 1006: p.1-7, 2015.

QIAO, R.; SHENG, C.; LU, Y.; ZHANG, Y.; REN, H.; LEOMOS, B. Microplastic induce intestinal inflammation, oxidative stress, and disorders of metabolome and microbiome in zebrafish. **Science of the Total Environment**, v. 662: p. 246-253, 2019.

QIAO, D.; YANG, C.; CHEN, J.; GUO, Y.; LI, Y.; NIU, S.; CAO, K.; CHEN, Z. Comprehensive identification of the full-length transcripts and alternative splicing related to the secondary metabolism pathways in the tea plant (*Camellia sinensis*). **Scientific Reports**, v. 9, n. 1: p.2709-2709, 2019.

RAYMUNDO, T. M.; FAVILLA, M.; NIERO, R.; ANDRADE, S. F.; MAISTRO, E. L. Genotoxicity of the medicinal plant *Maytenus robusta* in mammalian cells *in vitro*. **Genetic and Molecular Research**, v. 11, n. 3: p. 2847-2854, 2012.

RENAULT, M.; LAETITIA S.; MARTIAL, P.; STEFANO, C. Slow-spinning low-sideband HR-MAS NMR spectroscopy: delicate analysis of biological samples**. Scientific reports**, v. 3, n. 1: p. 1-5, 2013.

RIACHI, L. G.; SIMAS, D. L. R.; COELHO, G. C.; MARCELLINI, P. S.; DA SILVA, A. J. R.; DE MARIA, C. A. B. Effect of light intensity and processing conditions on

bioactive compounds in *maté* extracted from *yerba mate* (*Ilex paraguariensis* A. St.-Hil.). **Food Chemistry**. v. 266, n. 15: p.317-322, 2018.

RODRIGUES, V. E. G.; CARVALHO, D. A. D. Florista de plantas medicinais nativas de floresta estacional semidecidual na região do Alto Rio Grande-Minas Gerais. **Cerne-lavras**, v. 14, n. 2: p. 93-112, 2008.

RUSCHEL, A. R.; NODARI, R. O.; MOERSCHBACHER, B. M. The genetic structure of *Sorocea bonplandii* in Southern Brazilian forest fragments: AFLP diversity. **Silvae Genetica**, v. 56, n. 2: p. 51-58, 2007.

SÁ, R. R.; MATOS, R. A.; SILVA, V. C.; CALDAS, J. D. C.; SAUTHIER, M. C. D. S.; SANTOS, W. N. L. D.; Magalhães, H. I. F.; Júnior, A. D. F. S. Determination of bioactive phenolics in herbal medicines containing *Cynara scolymus*, *Maytenus ilicifolia* Mart ex Reiss and *Ptychopetalumuncinatum* by HPLC-DAD. **Microchemical Journal**, v. 135, n. 1: p. 10-15, 2017.

SAAD, B.; DAKWAR, S.; SAID, O.; ABU-HIJLEH, G.; AL-BATTAH, F.; KMEEL, A.; AZIAZEH, H.; Evaluation of Medicinal plant hepatotoxicity in co-cultures of hepatocytes and monocytes. **Evidence-based Complementary and Alternative Medicine**, v. 3, n. 1: p. 93-98, 2006.

SAIJO, Y.; ELIZA P. I. L. Plant immunity in signal integration between biotic and abiotic stress responses. **New Phytologist**, v. 225, no 1: p. 87-104, 2020.

SAMPAIO, B. L.; EDRADA-EBEL, R.; DA COSTA, F. B. Effect of the environment on the secondary metabolic profile of Tithonia diversifolia: a model for environmental metabolomics of plants. **Scientific Reports**, v. 6: p. 29265, 2016.

SAUERSCHNIG, C.; DOPPLER, M.; BUESCHL, C.; SCHUHMACHER, R. Methanol generates numerous artifacts during sample extraction and storage of extracts in metabolomics research. **Metabolites**, v. 8, n. 1: p. 1-1, 2018.

SAVORANI, F.; TOMASI, G.; ENGELSEN, S. B. icoshift: A versatile tool for the rapid alignment of 1D NMR spectra. **Journal of magnetic resonance**, v. 202, n. 2: p. 190-202, 2010.

SERKOVA, N. J.; DAVIS, D. M.; STEINER, J.; AGARWAL, R. Quantitative NMR-based metabolomics on tissue biomarkers and its translation into *In Vivo* magnetic resonance spectroscopy. **High-Throughput Metabolomics**. Humana, New York, NY: p. 369-387, 2019.

SEUKEP, A. J.; NOUMEDEM, J. A. K.; DJEUSSI, D. E.; KUETE, K. Genotoxicity and teratogenicity of African medicinal plants. **Toxicological Survey of African Medicinal Plants**, p. 235-275, 2014.

SHEN, J.; WANG, Y.; DING, Z.; DING, S.; WANG, H.; BI, C.; WANG, L. Metabolic analysis reveal growth characteristics of young tea shoots in spring. **Scientia Horticulturae**, v. 246: p. 478-489, 2019.

SILVA, F. A.; PAULA, J. A. M.; SANTOS, P. A.; OLIVEIRA, L. A. R.; OLIVEIRA, G. A. R.; LIAO, L. M.; PAULA, J. R.; SILVA, M. R. R. Phytichemical analysis and antimicrobial activity of *Myrcia tomentosa* (Aubl.) DC. Leaves. **Molecules**, v. 22, n. 7: p. 1100-1100, 2017.

SILVA, A. D.; SALEM, V.; MATTHEWS, P. M.; DHILLO, W. S. The use of functional MRI to study appetite control in the CNS. **Experimental Diabetes Research**, v. 2012: p. 764017-764017, 2012.

SINGH, A. K.; SAHA, S. Chemistry, therapeutic attribute and biological activities of *Dillenia indica* Linn. **Environmental Biotechnology: For Sustainable Future,** p. 237-260, 2019.

SIMMLER, C.; GRAHAM, J. G.; CHEN, S. N.; PAULI, G. F. Integrated analytical assets aid botanical authenticity and adulteration management. **Fitoterapia**, v. 129: p. 401-414, 2018.

SONI, U.; BRAR, S.; GAUTTAM, V. K. Effects of seasonal variation on secondary metabolites of medicinal plants. **International Journal of Pharmaceutical Sciences and Research**, v. 6, n. 9: p. 3654-3662, 2015.

SOUZA, L. F.; VIEIRA, T. S.; ALCANTARA, G. B.; LIÃO, L. M. HR-MAS NMR for rapid identification of illicit substances in tablets and blotter papers seized by police department. **Journal of the Brazilian Chemical Society**, v. 27, n. 11: p. 2141-2148, 2016.

SPANAKIS, M.; SFAKIANAKIS, S.; SAKKALIS, V.; SPANAKIS, E. G. PharmActa: Empowering patients to avoid clinically significant drug-herb interactions. **Medicines**, v. 6, n.1: p. 26, 2019.

SUN, J.; JIANG, Y.; WEI, X.; SHI, J.; YOU, Y.; LIU, H.; KAKUDA, Y.; ZHAO, M. Identification of (−)-epicatechin as the direct substrate for polyphenol oxidase isolated from litchi pericarp. **Food Research International**, v. 39, n. 8: p. 864-870, 2006.

TAKIS, P. G.; LEONARDO, T; ENRICO, R; CLAUDIO, L. Gelified biofluids for High-Resolution Magic Angle Spinning ^{1}H NMR analysis: the case of urine. **Analytical chemistry**, v. 89, n. 2: p. 1054-1058, 2017.

TENG, Q. **Structural biology**: practical NMR applications, Chapt. 9, Ed. 2. Springer Science & Business Media, p. 311-392, 2013.

TRIMIGNO, A.; MARINCOLA, F. C.; DELLAROSA, N.; PICONE, G.; LAGHI, L. Definition of food quality by NMR-based foodomics. **Current Opinion in Food Science**, v. 4: p. 99-104, 2015.

TSAO, R. Chemistry and biochemistry of dietary polyphenols. **Nutrients**, v. 2, n. 12: p. 1231-1246, 2010.

TSUJIMOTO, T.; YOSHITOMI, T.; MARUYAMA, T.; YAMAMOTO, Y.; HAKAMATSUKA, T.; UCHIYAMA, N. ^{13}C-NMR-based metabolic fingerprinting of *Citrus*-type crude drugs. **Journal of Pharmaceutical and Biomedical Analysis**, v.161: p. 305-312, 2018.

TOCI, A. T.; RIBEIRO, M. V.; TOLEDO, P. R. A. B.; BORALLE, N.; PEZZA, H. R.; PEZZA, L. Fingerprint and authenticity roasted coffees by ^{1}H-NMR: the Brazilian coffee case. **Food Science and Biotechnology**, v. 27, n. 1: p. 19-26, 2018.

TORRES, A. M.; PRICE, W. S. Common problems and artifacts encountered in solution-state NMR experiments. **Concepts in Magnetic Resonance Part A,** v. 45, n.2: p. e21387-e21387, 2016.

TURCHETTO, F.; ARAUJO, M. M.; BERGHETTI, A. L. P.; GRIEBELER, A. M.; RORATO, D. G. Phytosociology of floristic groups in subtropical seasonal forests in the south extreme of the Atlantic Forests Biome. **Advances in Forestry Science**, v. 5, n. 2: p. 357-362, 2018.

VELOSO, C. C.; FERREIRA, R. C. M.; RODRIGUES, V. G.; DUARTE, L. P.; KLEIN, A.; DUARTE, I. D.; ROMERO, T. R. L.; PEREZ, A. C.; Tingenone, a pentacyclic triterpene, induces peripheral antinociception due to cannabinoid receptors activation in mice. **Inflammopharmacology**, v. 26, n. 1: p. 227-233, 2018.

VELOSO, C. C.; SOARES, G. L.; PEREZ, A. C.; RODRIGUES, V. G.; SILVA, F. C. Pharmacological potential of *Maytenus* species and isolated constituents, especially tingenone for treatment of painful inflammatory diseases, **Revista Brasileira de Farmacognosia**, v. 17, n. 4: p. 533-540, 2017.

VERHOEVEN, A.; SLAGBOOM, E.; MUHRER, M.; GIERA, M.; MAYBORODA, O. A. Automated quantification of metabolites in blood-derived samples by NMR. **Analytica Chimica Acta**, v. 976: p. 52-62, 2017.

VIANI, R. A. G.; VIEIRA, A. O. S. Flora arbórea da bacia do rio Tibagi (Paraná, Brasil): Celastrales sensu Cronquist. **Acta Botanica Brasilica**, v. 21, n. 2: p. 457-472, 2007.

VILEGAS, W.; SANOMMIYA, M.; RASTRELLI, L.; PIZZA, C. Isolation and structure elucidation of two new flavonoid glycosides from the infusion of *Maytenus aquifolium* leaves. Evaluation of the antiulcer activity of the infusion. **Journal of agricultural and food chemistry**, v. 47, n. 2: pp.403-406, 1999.

VILEGAS, J. H. Y.; FERNANDO M. L.; JEAN-NOËL W.; LUC A. Characterization of adulteration of Espinheira-Santa (*Maytenus ilicifolia* and *Maytenus aquifolium*, Celastraceae) hydroalcoholic extracts with *Sorocea bomplandii* (Moraceae) by high-performance thin layer chromatography. **Phytochemical Analysis: An International Journal of Plant Chemical and Biochemical Techniques**, v. 9, n. 6: p. 263-266, 1998.

VINICIUS, L. C. M.; FERNANDA, T. S.; CAIO, B.; LUIS, F. U. D. S.; DE SOUZA, A. L. Avaliação da qualidade das plantas medicinais comercializadas no Mercado Municipal de Campos dos Goytacazes-RJ, **Revista Fitos**. **Rio de Janeiro**, v. 12, n. 2: p. 127-134, 2018.

WANG, D.; FAN, W.; GUO, X.; WU, K.; ZHOU, S.; CHEN, Z.; ZHOU, Y. MaGenDB: a functional genomics hub for Malvaceae plants. **Nucleic acids research**, v. 48, n. 1: p. 1076-1084, 2020.

WEN, B.; SHUANG, R.; YANYUAN, Z.; YU, D.; JIAZHI, S.; XUJUN, Z.; YUHUA, W.; YUANCHUN, M.; ZHONGWEI, Z.; WANPING, F. Effects of geographic locations and topographical factors on secondary metabolites distribution in green tea at a regional scale. **Food Control**, v. 110: p. 106979-106979, 2020.

WHITE, B. Dietary fatty acids. **American family physician**, v. 80, n. 4: p. 345-350, 2009.

WINK, M. Mode of action and toxicology of plant toxins and poisonous plants. **Julius-Kühn-Archiv**, n.421: p. 93-112, 2010.

WISHART, D. S. Metabolomics: applications to food science and nutrition research. **Trends in Food Science & Technology**, v. 19, n. 9: p. 482-493, 2008.

WONG, A.; LUCAS-TORRES, C. High-resolution magic angle spinning (HR-MAS) NMR spectroscopy. **The Royal Society of Chemistry**, Chapter 5: p. 133-150, 2018.

XIA, E. H.; TONG, W.; WU, Q.; WEI, S.; ZHAO, J.; ZHANG, Z. Z.; WAN, X. C. Tea plant genomics: achievements, challenges and perspectives. **Horticulture Research**, v. 7, n. 1: p. 1-19, 2020.

XIE, P.; CHEN, S; LIANG, Y. Z.; WANG, X.; TIAN, R.; UPTON, R. Chromatographic fingerprint analysis—a rational approach for quality assessment of traditional Chinese herbal medicine. **Journal of chromatography A**, v. 1112, n. 1-2: p. 171-180, 2006.

XU, P.; HUI, S.; RONG, J.; YUXIAO, M.; ANAN, X.; HAIYAN, C.; YUEFEI, W.; QING, M. Shading effects on leaf color conversion and biosynthesis of the major secondary metabolites in the Albino tea cultivar "Yujinxiang". **Journal of Agricultural and Food Chemistry**, v. 68, n. 8: p. 2528-2538, 2020.

YANG, Q.; ZHANG, A. H.; MIAO, J. H; SUN, H.; HAN, Y.; YAN, G. L.; WU, F. F.; WANG, X. J. Metabolomics biotechnology, applications, and future trends: a systematic review. **RSC Advances**, v. 9, n. 64: p. 37245-37257, 2019.

YANG, L.; WEN, K. S.; RUAN, X.; ZHAO, Y. X.; WEI, F.; WANG, Q. Response of plant secondary metabolites to environmental factors. **Molecules**, v.23, n.4: p. 762-762, 2018.

YUAN, Y.; ZHAO, Y.; YANG, J.; JIAN, Y.; LU, F.; JIA, Y.; YANG, B. Metabolomic analyses of banana during postharvest senescence by ^{1}H-high resolution-NMR. **Food Chemistry**, v. 218: p. 406-412, 2017.

YUN, D. Y.; KANG, Y. G.; KIM, E. H.; KIM, M.; PARK, N. H.; CHOI, H. T.; GO, G. H.; LEE, J. H.; PARK, J. S.; HONG, Y. S. Metabolomics approach for understanding geographical dependence of soybean leaf metabolome. **Food Research International**, v. 106: p.842-852, 2018.

ZACHARIAS, H. U.; ALTENBUCHINGER, M.; GROWNWALD, W. Statistical analysis of NMR-based metabolic fingerprints: Established methods and recent advances. **Metabolites**, v. 8, n. 3: p. 47, 2018.

ZHENG, G.; PRICE, W. S. Solvent signal suppression in NMR. **Progress in nuclear magnetic resonance spectroscopy**, v. 56, n. 3: p. 267-288, 2010.

ZHI, H. J.; QIN, X. M.; SUN, H. F.; ZHANG, L. Z.; GUO, X. Q.; LI, Z. Y. Metabolic fingerprinting of *Tussilagofarfara* L. using ^{1}H-NMR spectroscopy and multivariate data analysis. **Phytochemical Analysis**, v. 23, n. 5: p. 492-501, 2012.

ZHOU, W.; WANG, Y.; YANG, F.; DONG, Q.; WANG, H.; HU, N. Rapid determination of amino acids of *Nitraria tangutorum* Bobr. from the Qinghai-Tibet Plateau using HPLC-FLD-MS/MS and a highly selective and sensitive pre-column derivatization method. **Molecule**, v. 24, n. 9: p. 1665, 2019.

ANNEX 1 –2D NMR correlation maps (COSY, TOCSY, HSQC and HMBC)

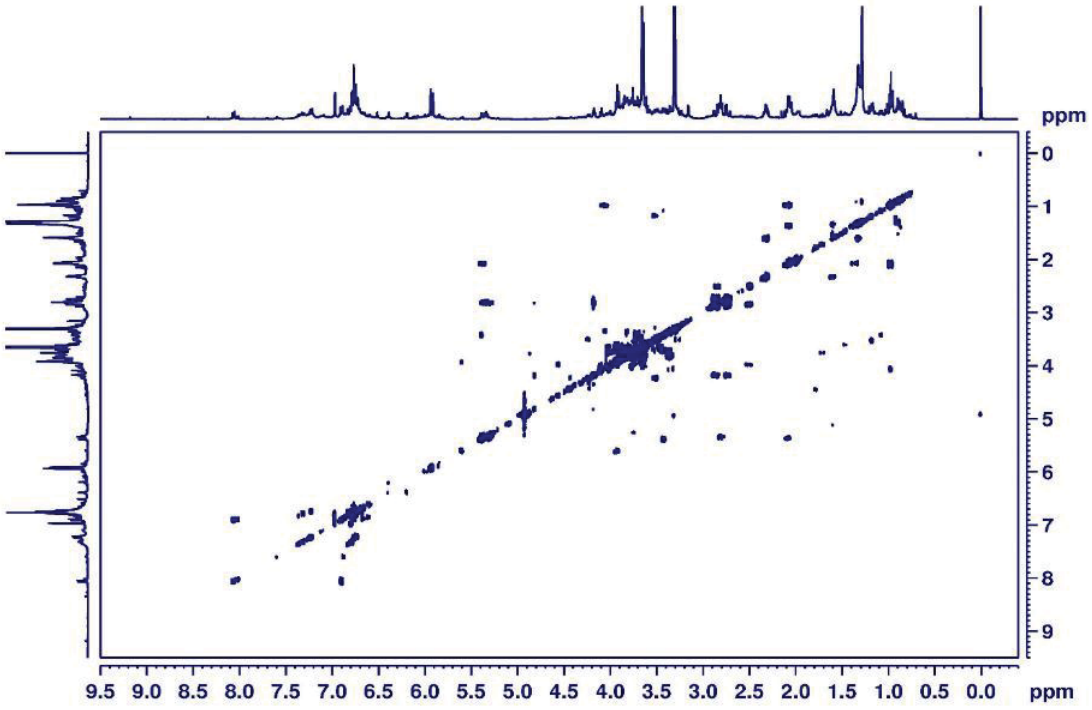

Annex 1.1. ^{1}H-^{1}H correlation map (400.13 MHz) from 2D COSY experiment performed over powdered leaf from *Maytenus ilicifolia*.

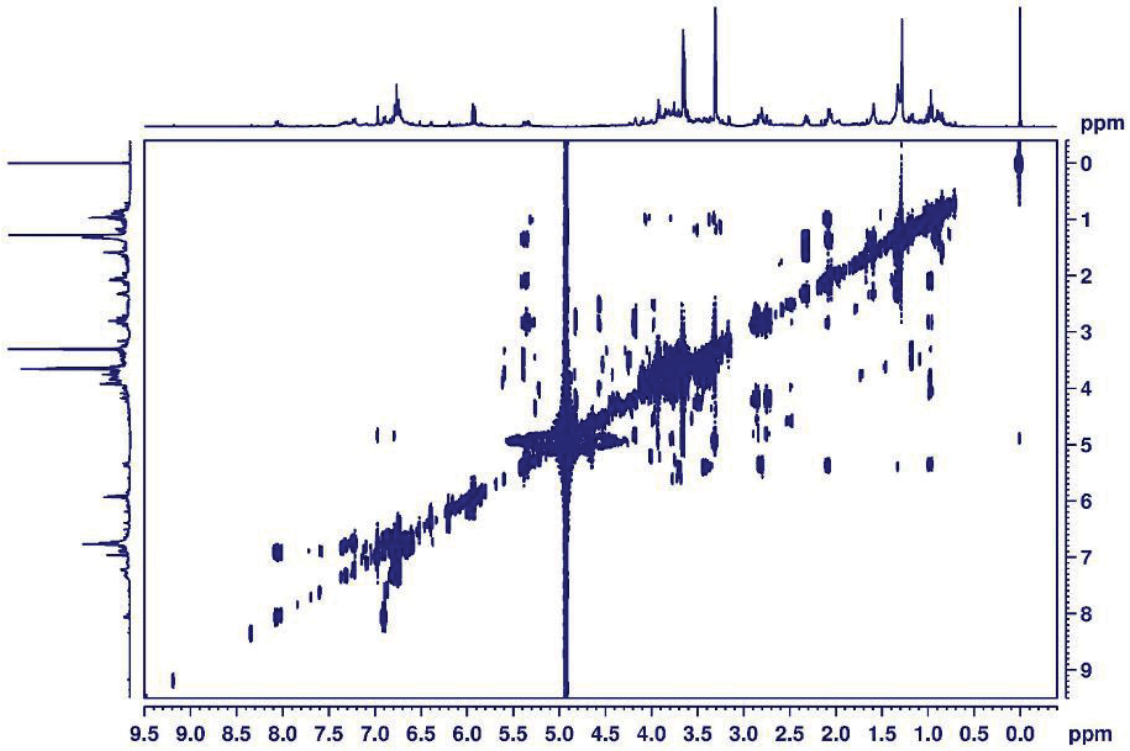

Annex 1. 2. ^{1}H-^{1}H total correlation map (400.13 MHz) from 2D TOCSY experiment performed over powdered leaf from *Maytenus ilicifolia*.

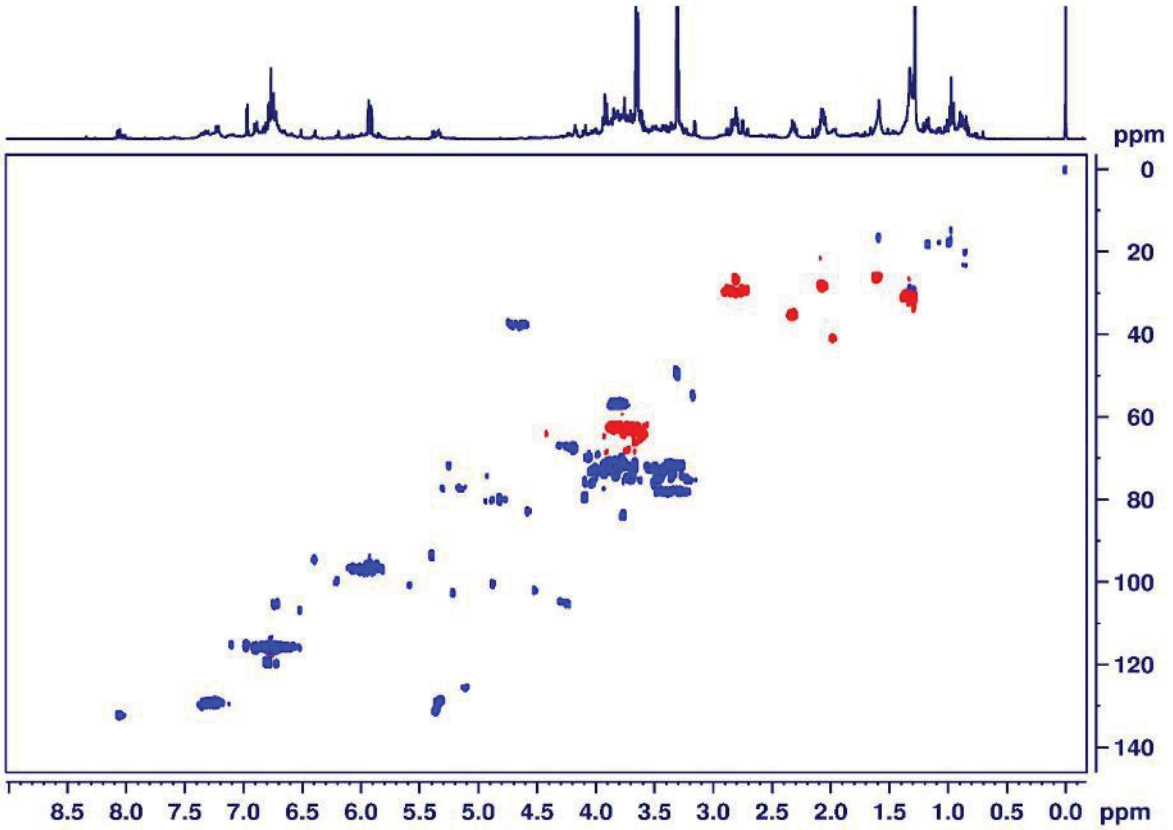

Annex 1. 3. ^{1}H-^{13}C direct correlation map (400.13-100.62 MHz) from multiplicity edited HSQC experiment performed over powdered leaf from *Maytenus ilicifolia*.

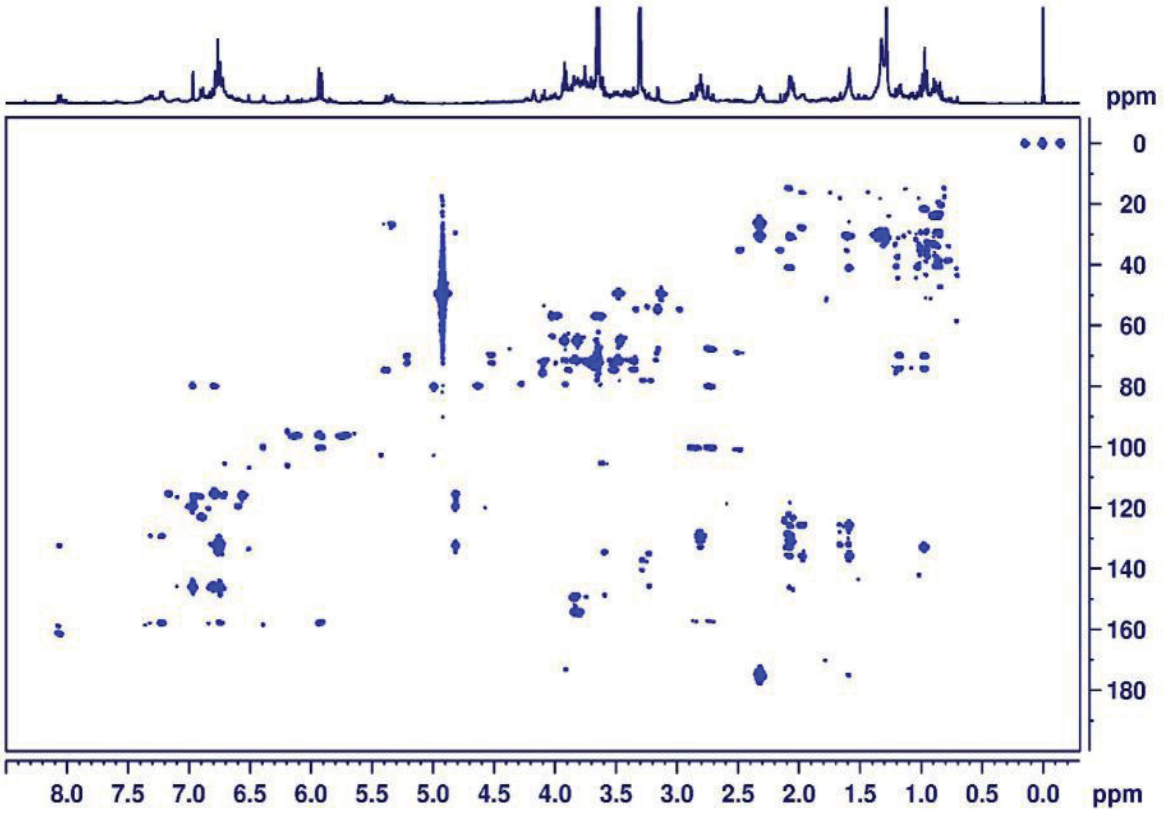

Annex 1. 4. ^{1}H-^{13}C long range correlation map (400.13-100.62 MHz) from HMBC experiment performed over powdered leaf from *Maytenus ilicifolia*.